ABSTRACT

Title of Dissertation:	MODELING FLOOD STAGE-DURATION-FREQUENCY: A RISK ASSESSMENT OF CRITICAL INFRASTRUCTURE IN THE TIDAL POTOMAC
	Yilu Feng, Doctor of Philosophy, 2016
Dissertation directed by:	Dr. Kaye L. Brubaker, Department of Civil and Environmental Engineering

The service of a critical infrastructure, such as a municipal wastewater treatment plant (MWWTP), is taken for granted until a flood or another low frequency, high consequence crisis brings its fragility to attention. The unique aspects of the MWWTP call for a method to quantify the flood stage-duration-frequency relationship. By developing a bivariate joint distribution model of flood stage and duration, this study adds a second dimension, time, into flood risk studies. A new parameter, inter-event time, is developed to further illustrate the effect of event separation on the frequency assessment. The method is tested on riverine, estuary and tidal sites in the Mid-Atlantic region.

Equipment damage functions are characterized by linear and step damage models. The Expected Annual Damage (EAD) of the underground equipment is further estimated by the parametric joint distribution model, which is a function of both flood stage and duration, demonstrating the application of the bivariate model in risk assessment.

Flood likelihood may alter due to climate change. A sensitivity analysis method is developed to assess future flood risk by estimating flood frequency under conditions of higher sea level and stream flow response to increased precipitation intensity. Scenarios based on steady and unsteady flow analysis are generated for current climate, future climate within this century, and future climate beyond this century, consistent with the WWTP planning horizons. The spatial extent of flood risk is visualized by inundation mapping and GIS-Assisted Risk Register (GARR). This research will help the stakeholders of the critical infrastructure be aware of the flood risk, vulnerability, and the inherent uncertainty.

MODELING FLOOD STAGE-DURATION-FREQUENCY: A RISK ASSESSMENT OF CRITICAL INFRASTRUCTURE IN THE TIDAL POTOMAC

by

Yilu Feng

Dissertation submitted to the Faculty of the Graduate School of the
University of Maryland, College Park, in partial fulfillment
of the requirements for the degree of
Doctor of Philosophy
2016

Advisory Committee:

Dr. Kaye L. Brubaker, Chair
Dr. M. Sherif Aggour
Dr. Gregory B. Baecher
Dr. Barton A. Forman
Dr. Richard H. McCuen
Dr. Karen L. Prestegaard

Acknowledgements

I am deeply grateful to my academic advisor, Dr. Kaye Brubaker, for her mentorship for these early steps in my career in water resources research and engineering. She planted my interest of learning, watered my learning curve with patience, encouragement and technical guidance, and fertilized my growth with numerous workshop and collaboration opportunity.

I appreciate the members of my dissertation research committee, Dr. Richard McCuen, for his guidance on statistical modeling, hydrologic modeling, technical writing, and encouragement to pursue graduate research, Dr. Barton Forman, for his classes and comments on hydrologic modeling, Dr. Gregory Baecher, for his classes and insights on risk assessment, Dr. M. Sherif Aggour, for his time and effort in reviewing my manuscript, and Dr. Karen Prestegaard, for those wonderful field trips and demonstration of data manipulation techniques.

I thank my supervisors and colleagues at DC Water, Salil Kharkar, Mark Ramirez, Lawrence Bastian, Bohdan Bodniewicz, Aklile Tesfaye, Nick Passarelli, Ryu Suzuki and Walter Bailey, for their insights on plant infrastructure planning. I am grateful for Hassan Mashriqui, James Halgren, and Seann Reed (NOAA, Mid-Atlantic River Forecast Center)'s generosity for sharing their Potomac River model. I would also like to thank Dr. Glenn Molgen of Virginia Tech., for his elicitation of climate change related data and literature.

I have been fortunate to have my 'committee of friends and colleagues' at University of Maryland, Chalida U-Tapao, Jiayu Liu, Yang Wen, Yezhou Yang, Yan Wang, Seksun Moryadee, Yu Mo, Feng Zhao, Qianli Deng, Misty Joshi, Garrett Hughes, Yuan Xue, Jennifer Olszewski, Jing Wang, Elizabeth Ryan, Ruiqian Fan, Dustin DeHaven, Jian Gao, Jacob Schaperow, Rachel Moglen, Nick Lucchesi, Chiaki Aita and Nazre Batool. They inspired me with diverse ideas of fun facts, inside or outside work.

I would like to express my gratitude to my parents, Lan Chen and Weimin Feng, for their endless love and support. Many thanks to my grandpa, Tingtao Chen, my auntie, Yingwen Li, and my cousin, Mengli Zhang. My family is my source of positive energy.

I gratefully acknowledge the support of DC Water (Grant No. 120809). The findings and recommendations in this dissertation research are those of the author and do not represent the policy or planning views of DC Water unless designated by other documentation.

Table of Contents

List of Figures

List of Tables

1 INTRODUCTION

1.1 Problem Statement

Flooding is the most widespread natural hazard. Around 60% of the world's population lives within 60 km of the coast. In the United States, around 10% of the population lives within 100-year flood plains. Two-thirds of all federally-declared disasters are floods (Smith & Ward, 1998). Flood losses exceed 7 billion dollars each year according to a 30-year average (NWS, 2016).

Floods influence many aspects of human life and can cause catastrophic damage. Despite the increasing attention to flood damages to residential properties, the serviceability of a critical infrastructure element is taken for granted until a low frequency, high consequence crisis, such as a major flood, brings its fragility to attention. Low lying critical civil infrastructure, such as a wastewater treatment plant (WWTP), is especially vulnerable to flooding. When an authority needs to estimate the investment of flood mitigation or damage recovery, broad assumptions must be made. Risk contingency plans may be copied from other localities with little thought given to their applicability at the current location. Therefore, a systematic flood risk assessment approach is needed for a specific type of infrastructure with unique characteristics.

The traditional engineering design paradigm has paid considerable attention to quantifying flood magnitudes, both discharge rates and stages. Hewlett (1982) stated that it is not the peak discharge in the headwaters that produces the downstream flood, but rather the volume of stormflow released by the headwater areas. Civil infrastructures commonly refer to base flood elevation (100-year flood) and 500-year flood elevation reported by Federal Emergency Management Agency (FEMA) Flood Insurance Study (FIS) for decisions associated with extreme wet weather events. It remains a question whether this approach provides sufficient information for civil infrastructure design and flood mitigation. Underground transportation, utility, and service systems have increased with urbanization. Only a limited number of studies address the

issue of subsurface flooding. Probabilistic assessments of flood stage and discharge are essential for some analyses but insufficient for others. To many of those subjected to flooding, the duration of flooding, not only the depth, is critical. For example, those responsible for managing water treatment infrastructure are concerned with the duration that a facility will be offline. Even after floodwaters recede, the time required to restore the facility to full function is essentially part of the flood duration. The traditional univariate, stage-dependent approach to flood evaluation needs to be broadened to include duration as a critical variable, thus better connecting the probabilistic behavior of flooding to damages and service disruptions. If this time dimension is introduced to flood risk assessment, the 100-year flood and the expected annual damage need to be redefined as the flood stage-duration-frequency relationships, thus providing information to quantify the subsurface flooding risk and out-of-service time.

Statistical analyses of flooding are mostly based on the assumption of stationarity. However, as the images of melting glaciers and reports of sea level rise indicate, climate change is underway. Difficulties often arise when designing or retrofitting a local civil infrastructure to withstand the impact of climate change. For a micro-scale, agency- based flood risk assessment, applying the public available hydrologic and hydraulic tools in innovative manners may yield great potential in solving the computationally intensive problem, and address the climate change impact with the best available data.

1.2 Research Questions

Given these problems, this research addresses the following questions using quantitative analyses. Qualitative justification in sections 1.2.1 to 1.2.2 supports the rationality of these research questions and this approach.

1.2.1 Why Is Flood Duration Critical for Flood Risk Assessment?

Based on the perceptions of 289 building surveyors, flood duration ranked the fourth most important flood characteristic, after sewage content, contaminant content, and flood depth (Soetanto and Proverbs, 2004). The extent of flood damage is a function of flood depth, duration, velocity of water flow, the quantity of debris carried by the water and the silt load deposited, and any contaminants carried by the water (Penning-Rowsell & Fordham, 1994). Flood duration analysis measures the severity of flooding in terms of timing. It is vital for characterizing many hydraulic and hydrological phenomena.

Recent flood disasters have highlighted the effects of flood duration on urban infrastructure damage. In October 2012, Hurricane Sandy caused one of the most destructive flooding events in recorded history on the northeast coast of the U.S.A. In addition to visible surface damage, flood waters intruded into and filled the underground tunnels that house essential equipment in wastewater treatment plants. Millions of gallons of untreated sewage were discharged into receiving waters (Kenward, Yawitz, & Raja, 2013).

Flood duration is a critical factor for transportation disruption (Dutta, Herath, & Musiake, 2003; Penning-Rowsell & Wilson, 2003; Pfurtscheller & Schwarze, 2008). Hurricane Sandy inundated the New York subway tunnels, significantly disrupting the daily commute. A July 2013 flash flood resulted in the closure of Toronto Subway stations, another storage related transportation disaster (Nirupama, Armenakis, & Montpetit, 2014). Longer durations of flooding may bring greater volumes of debris and sediment, which can increase the costs and duration of clean-up.

Flood duration is an essential consideration for structural damage. The risk of material damage increases with the duration of flood inundation, since corrosion and fungus growth are more severe when a structure is exposed to water (Wagenaar, 2012). It has been reported that

the damage to a variety of building materials and construction, such as mortar, drains, and stud partition walls, increases with the flood duration (Penning-Rowsell & Wilson, 2003).

Duration has been identified as a factor in flood management policies. The U.S. Army Corps of Engineers (USACE, 1995) suggested that sump pumps and other standby generating equipment should be operable for a period of 125 percent of the anticipated duration of the design flood, and that holding tanks in sanitary sewer systems should be able to store 150 percent of the anticipated demand for the duration of a design flood. Flood duration is also an essential predictor in modeling levee breaching, seepage through dikes, and the erosion of sand cores (Allsop et al., 2007; Jaffe & Sanders, 2001; Messner & Meyer, 2006).

Knowledge of potential flood durations can also assist agricultural and ecosystem planning and management. Flood duration affects soy bean and lowland rice weed growth (Griffin & Saxton, 1988; Kent & Johnson, 2001; Scott, DeAngulo, Daniels, & Wood, 1989), as well as the species richness, diversity, and plant distribution patterns in floodplain forests (Ferreira & Stohlgren, 1999).

Socio-economic assessments of flood consequences, such as anxiety damage (Lekuthai & Vongvisessomjai, 2001), and mortality/fatality (Jonkman, 2007) also depend on flood duration. Downtime damages, both to production facilities subjected to flooding and unemployment of people inside and outside of the flood zone, are also closely related to flood duration (Wagenaar, 2012).

Flood duration affects both the natural and built environments. It matters for the various aspects of social and economic consequences, ranging from civil infrastructure, transportation facilities, and building structure integrity, to agricultural field inundation and wildlife habitat quality. For any storage related system, the length of the flood event determines the volume of

intruding water, which directly affects flood damages. This urges the research to quantify the time dimension of floods.

1.2.2 What Are the Unique Aspects of WWTP Vulnerability to Flooding?

The water and wastewater system sector is one of the 16 sectors of critical infrastructure system defined by US Departmen of Homeland Security (2016). Municipal wastewater treatment plants (MWWTPs) are located downstream of the wastewater collection system. They are usually close to the receiving water body. Their geographical locations are a significant factor in their potential vulnerability to flood hazards.

The majority of WWTP essential equipment is located inside underground galleries and tunnels. Traditional flood depth-damage relationship is not applicable to subsurface flooding and damage prediction. Regression equations that are reported for a region are usually not site-specific. A municipal wastewater treatment plant differs from a residential building in that its main function is significantly affected by wet weather events (Locke et al., 2006). The treatment capacity and biological process stability are affected by the magnitude of receiving wastewater influent, which is highly correlated to the severity of a flood event. Although hydro-economic models, such as Hazus-MH (FEMA, 2009), include a damage module for WWTPs, they do not elaborate the uniqueness of each WWTP and characterize the damage in detail.

Existing hydro-economic models are not adequate for the critical infrastructure (such as WWTP) for the following reasons:

1. For accurate quantification of flood risk, depth-damage curves must be developed for a specific facility.

2. The depth-damage curves developed for surface flooding do not adequately capture damage to underground infrastructure.
3. The location of the WWTP on a tidal estuary makes it particularly susceptible to changes in downstream sea level and upstream freshwater input.

This research addresses the above concerns for the principal study site, proposes quantitative models, and discusses the potential application to similar infrastructure.

1.2.3 How Can Climate Change Impact be Considered in a Micro-scale Site-specific Study?

Growing awareness of climate change has attracted increasing attention on wise decision making based on future climate. The stakeholder's preference on site-specific study indicates that micro-scale analysis with acceptable accuracy and complexity is critical for civil infrastructure planning, design, and resources allocation. Translating these needs to the study of flood risk, the question will be how to quantify the likelihood of flood damage in the future climate, considering the tradeoff of model scale, accuracy and complexity.

Global and regional scale climate change research provides estimates of future temperature, precipitation, etc. Those projected outcomes provide valuable estimates of the impact of climate change. However, the resolution is too coarse for most basin-scale studies. For example, the regional climate models of the North American Regional Climate Change Assessment Program (nested within multiple atmosphere-ocean general circulation models) calculated future precipitation and other variables at a 50-km spatial resolution (Mearns et al., 2007, updated 2014), which is considerably larger than most of the study basins for the micro-scale flood risk study.

Assume that a future precipitation estimate is available and the scale is suitable for a basin wise study, a calibrated hydrologic/watershed model is needed to convert the precipitation to

runoff, thus estimating the flood stage and likelihood. If projected future-climate based information are available for the upstream and downstream boundary conditions, a hydraulic model is applicable to estimate the water surface elevation profile along the reach. The flood stage-frequency information can then be extracted from the model output. For both the hydrologic and hydraulic models, stream gauge and tidal gauge information is particularly helpful for providing model input and for model calibration.

The following preliminary steps are recommended for considering climate change impact on the micro-scale flood risk analysis:

1. Study the literature on the climate change projections of precipitation, runoff, and sea-level rise. Sources of information include government reports, journal publications, news items and reports from the web. The studies for a region that is geographically close to the study site, or have the similar hydroclimate characteristics, generally provide the most valuable information.
2. Obtain the best measurement for precipitation, runoff and sea-level rise, including stream/tidal gauge measurements and remote sensing measurements, and record the sample size of the data (data length and record interval).
3. Identify the applicable model, hydrologic and hydraulic, based on the available data to quantify the impact of climate change on flood stage and discharge at the study site.

1.3 Research Goal and Objectives

Given the research questions identified in section 1.2, the goal of this research is to provide a quantitative method of developing a flood magnitude-duration risk assessment, with the method illustrated using a municipal WWTP. The goal of this study reflects three major tasks: (1) Develop a sensitivity analysis framework to estimate current and future flood stage of the tidal Potomac;

(2) Incorporate flood duration into flood risk model; (3) Demonstrate the application of the new flood risk model by assessing the flood risk of critical infrastructure based on various model scenarios.

The objectives for the first task are:

- Develop a model to estimate the frequency distribution of flood stage.
- Create a sensitivity analysis method to assess future flood risk by estimating flood frequency under conditions of higher sea level and stream flow responses to increased precipitation intensities.

The objectives for the second task are:

- Develop a bivariate joint distribution model to assess flood stage-duration-frequency relationship.
- Test the model on riverine, estuary, and tidal sites.

The objective for the third task are:

- Develop a GIS database for the essential equipment inside the underground tunnels and galleries for the study site.
- Develop a method to generate underground equipment depth-duration-damage curves.
- Integrate the flood stage-duration-frequency model with the flood damage model to estimate the expected annual damage of the essential equipment.
- Estimate building percent damage, service disruption loss and evacuation risk, and develop multidimensional vulnerability curves.
- Visualize flood risk by flood inundation mapping and GIS-Assisted Risk Register (GARR).

The methods developed for the objectives will be implemented on a principal study site, a municipal wastewater treatment plant on the tidal Potomac, which will be introduced in section 3.2.

2 LITERATURE REVIEW

2.1 Flood Risk Assessment Framework

A flood system encompasses all physical and organizational systems that influence or are influenced by flooding, including (1) the physical attributes of the earth's surface involved in the water cycle, e.g., processes of rainfall and runoff; (2) the artificially created systems of drainage, storage, and flood defense structures; (3) the economic, social, and environmental assets that are located in the floodplains; (4) the organizations that are responsible for managing flood risk, insurers who provide cover for flood risks, and broader stakeholder groups that have an interest in flood risk management (Hall, Meadowcroft, Sayers, & Bramley, 2003; Thorne, Evans, & Penning-Rowsell, 2007). Growing awareness of the criticality of flood risk assessment has been developed along with the knowledge of climate change, rural land cover change, intensive grazing, arable farming, and urbanization (Ashkar, 2008; Thorne et al., 2007). Flood risk analyses combines the hydrological information about event frequency, hydraulic knowledge about inundation behavior, and economic information on damage assessment. In a public policy view, flood risk analysis supports decisions of allocation of tax monies, project appraisal, and accountability (Messner et al., 2007).

Penning-Rowsell and Fordham (1994) described the flood vulnerability by its general form,

$$Vulnerability = f\,(Physical\ Characteristics + Human\ Characteristics) \quad (2\text{-}1)$$

The indicators for flood vulnerability analysis consist of elements at risk, exposure and susceptibility, as summarized in Figure 2-1 (Messner & Meyer, 2006). To assess the consequences of floods, a conceptual framework should be established before detailed modeling and analysis to define the scope of the flood risk assessment.

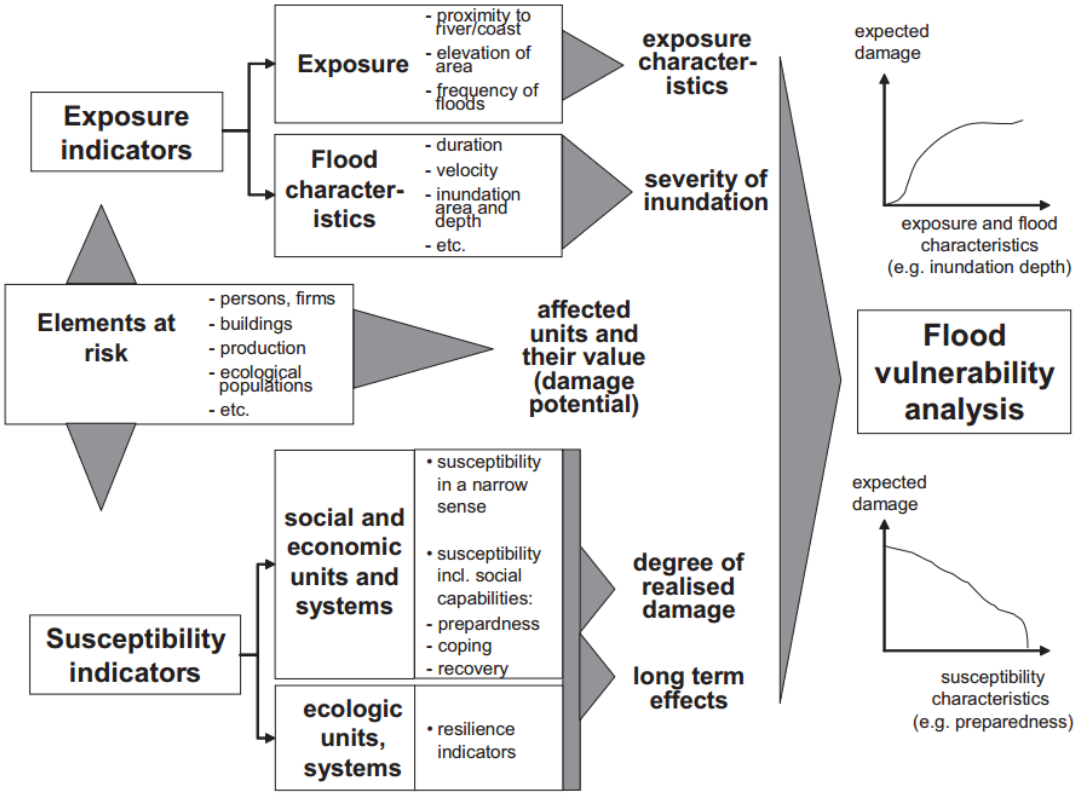

Figure 2-1. Indicators in flood vulnerability analysis (Messner & Meyer, 2006)

The source-pathway-receptor (SPR) model is a well-established framework for environmental risk assessment, where source is the weather events or sequences of events that may result in flooding; pathways are the mechanisms that convey floodwaters to places where they may impact the receptors, e.g., fluvial flows, overland flows, failure of flood defense structures; and receptors are the people, industries, and built or natural environment that may be affected by the flood (Gormley, Pollard, Rocks, & Black, 2011; Thorne et al., 2007). The pressure-state-impact-response (PSIR) model conceptualizes the change in the flood system. It deals with the change in the system state with the direction indicated by the arrow (Thorne et al., 2007; Turner et al., 1998):

Socio-economic drivers → environmental pressures → changes in environmental state → environmental and socio-economic impacts → stakeholder gains/losses → policy responses. Based on the sources-pathway-receptor-consequence model, flood risk can be expressed by

$$\text{Flood risk} = f([p,m,w,t]_{\text{source}}, [i,a,c]_{\text{pathway}}, [s,r]_{\text{receptor}}, [v,d]_{\text{consequence}}) \quad (2\text{-}2)$$

where *p* is the probability of flood events with magnitude (m); *w* is early warning; *t* is the retention capacity of the source area of inland flood; *i* is the inundation with attributes (*a*) and flood control (*c*); *s* is the susceptibility with interventions to strengthen resilience and resistance (*r*); *v* is the value of damage with interventions to decrease or to compensate them (*d*) (Schanze, 2006).

Figure 2-2 illustrates a basic framework for flood management. Risk analysis is a process to provide information on past, current, and future flood risk, including hazard determination, vulnerability determination, and risk determination. Risk assessments deal with risk perception and evaluation. The ultimate goal is risk reduction, which consists of pre-reduction, flood event reduction, and post-flood reduction (Schanze, 2006).

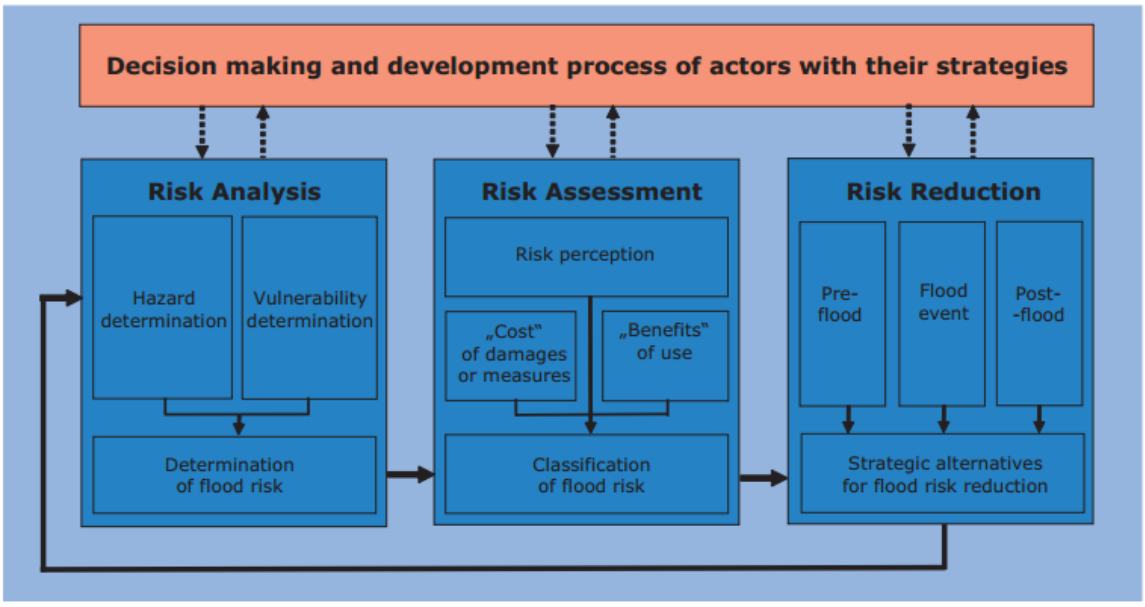

Figure 2-2. Basic framework of flood risk management (Schanze, 2006)

DEFRA (2009) described the stages in the strategic framework for flood and coastal erosion risk management (Figure 2-3), outlining strategies from national to local level. High level plans are expected to inform and influence local options and choices for project appraisal (DEFRA, 2009).

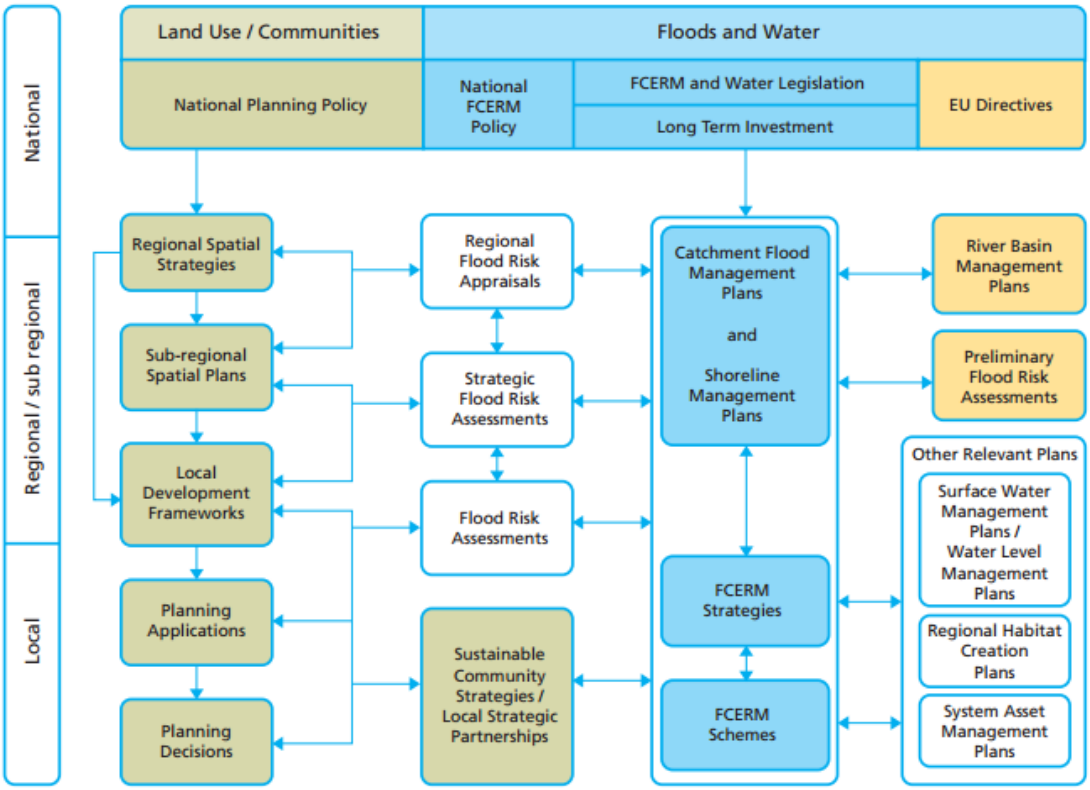

Figure 2-3. An indicative illustration of the relationship between high level plans, strategies, schemes and other planning initiatives (DEFRA, 2009)

Flood assessment models can be categorized into four types: (1) flood behavior model, (2) flood hazard estimation model, (3) flood loss estimation model, and (4) flood mitigation model. The categorization of each model and its focus are summarized in Table 2-1 (Hansson, Larsson, Danielson, & Ekenberg, 2011).

Table 2-1. Types of flood assessment models (Hansson et al., 2011)

Type of model	Flood behavior model	Flood hazard estimation model	Flood loss estimation model	Mitigation model
Focus	Understanding how floods occur, predictions, frequencies	Vulnerability assessment, likelihood assessment, flood characterization	Assessing losses given a location	Assessing costs/benefits from mitigation strategies

A modern flood risk assessment framework is an integrated approach that encompasses geospatial data (including hydrology, climate, topography, vegetation and soils) and multi-criteria decision making (Chen et al., 2015). Winsemius, Van Beek, Jongman, Ward, and Bouwman (2013) proposed a global framework for risk assessment of river floods. In their framework, hazard is evaluated at ~1km^2 resolution using global forcing datasets of the current or future climate, a global hydrological model, a global flood-routing model, and an inundation downscaling routine. Müller (2013) developed a flood risk assessment framework at the scale of the administrative unit of an urban building block using geo-data based approach. Under the spatial risk evaluation framework, Chen et al. (2015) weighted the spatial indices using analytical hierarchy process (AHP) and integrated the indices into an suitability assessment model. Based on a GIS platform, Jiang, Wang, Lung, Guo, and Li (2012) developed a generic framework to delineate warning areas and perform real-time risk assessments for chemical spills in river.

The scope of flood risk management and the scale of flood models are widely debated by policy maker, stakeholders and the communities involved. The flood damage evaluation method can be categorized as micro-, meso- and macro-scale. The micro-scale methods apply to single properties, such as a local building. The meso-scale methods are designed for regional analysis, such as residential or industrial areas. The macro-scale methods are national or international level assessments, which consider the whole administrative unit, such as a nation (Messner & Meyer, 2006; Messner et al., 2007). For modern flood project appraisal, Penning-Rowsell et al. (2014)

suggested catchment and coastal cell-based approaches and risk management to consider multiple benefits, including economic, environmental and social aspects. Community focus and partnership working are recommended. All aspects and the whole-life costs of investments should be considered, including adaption to climate change and future potential risks (Penning-Rowsell et al., 2014).

2.2 Type of Floods

The National Weather Service Hydrologic Glossary defines flood as “any high flow, overflow or inundation by water which causes or threatens damage” (NWS, 2015). Chow (1956) defines flood as “a relatively high flow which overtaxes the natural channel provided for runoff”. The major causes of floods are excessively heavy or prolonged precipitation, snowmelt, flood defense structure failure, coastal storm surge, earthquake, landslide, and storm drain surcharge. Floods can be intensified by factors associated with catchment or drainage networks, as well as funneling effects of estuary shape and coastal configurations. Water storage in the soil, basin shape, pattern of the drainage network, channel slope, and offshore slope of the seabed also affect flood magnitude and timing. The absolute flood magnitude generally increases with basin area and the specific magnitude, such as discharge per unit area, generally decreases with basin size (Smith & Ward, 1998).

The major types of flood are

- **Coastal flood:** occurs in low-lying coastal area, including estuaries where flood is a consequences of large freshwater input upstream and storm-surge downstream (Smith & Ward, 1998). When high tide is coincident with low atmospheric pressure, a tidal surge may occur and result in flooding (Penning-Rowsell et al., 2014).

- **Riverine/fluvial flood:** occurs when water draining from the surrounding land exceeds the capacity of the stream or river channel. River flood results from overspill and surface ponding in natural banks or artificial embankment (Smith & Ward, 1998).
- **Surface/pluvial flood:** occurs when surface water accumulated from heavy rainfall and ponding occurs more rapidly than the flood water can drain to the nearest waterbody.
- **Groundwater flood**: occurs when ground water level rises above the surface level (Penning-Rowsell et al., 2014).
- **Structure failure flood**: occurs when structures, such as a sewer network, dam, or detention pond, are overwhelmed by heavy rainfall, stream flow, or tidal wave, or are blocked by sediments.

Perry (2000) summarized the most devastating floods in the U.S. in the 20th century. The map (Figure 2-4) shows the location of the floods listed in Table 2-2.

In terms of timing and duration, flash flood has the greatest potential for loss of life and local damage. A flash flood is "a flood that rises and falls quite rapidly with little or no advance warning, usually as the result of intense rainfall over a relatively small area" (AMS, 2015). Flash floods are localized phenomena that usually occur in small and medium size watersheds of 10,000 km^2 or less. Rapid basin response to intense precipitation due to steep basin and channel slope, saturated soils and impermeable surface as a result of urbanization may cause flash floods. Six hours is an approximate threshold to distinguish a flash flood from a slow-rising flood (National Research Council, 2005).

Table 2-2. Significant floods in the U.S. during the 20th century (Perry, 2000)

Flood type	Map no.	Date	Area or stream with flooding	Reported deaths	Approximate cost (uninflated)	Comments
Regional flood	1	Mar.–Apr. 1913	Ohio, statewide	467	$143M	Excessive regional rain.
	2	Apr.–May 1927	Mississippi River from Missouri to Louisiana	unknown	$230M	Record discharge downstream from Cairo, Illinois.
	3	Mar. 1936	New England	150+	$300M	Excessive rainfall on snow.
	4	July 1951	Kansas and Neosho River Basins in Kansas	15	$800M	Excessive regional rain.
	5	Dec. 1964–Jan. 1965	Pacific Northwest	47	$430M	Excessive rainfall on snow.
	6	June 1965	South Platte and Arkansas Rivers in Colorado	24	$570M	14 inches of rain in a few hours in eastern Colorado.
	7	June 1972	Northeastern United States	117	$3.2B	Extratropical remnants of Hurricane Agnes.
	8	Apr.–June 1983 June 1983–1986	Shoreline of Great Salt Lake, Utah	unknown	$621M	In June 1986, the Great Salt Lake reached its highest elevation and caused $268M more in property damage.
	9	May 1983	Central and northeast Mississippi	1	$500M	Excessive regional rain.
	10	Nov. 1985	Shenandoah, James, and Roanoke Rivers in Virginia and West Virginia	69	$1.25B	Excessive regional rain.
	11	Apr. 1990	Trinity, Arkansas, and Red Rivers in Texas, Arkansas, and Oklahoma	17	$1B	Recurring intense thunderstorms.
	12	Jan. 1993	Gila, Salt, and Santa Cruz Rivers in Arizona	unknown	$400M	Persistent winter precipitation.
	13	May–Sept. 1993	Mississippi River Basin in central United States	48	$20B	Long period of excessive rainfall.
	14	May 1995	South-central United States	32	$5-6B	Rain from recurring thunderstorms.
	15	Jan.–Mar. 1995	California	27	$3B	Frequent winter storms.
	16	Feb. 1996	Pacific Northwest and western Montana	9	$1B	Torrential rains and snowmelt.
	17	Dec. 1996–Jan. 1997	Pacific Northwest and Montana	36	$2-3B	Torrential rains and snowmelt.
	18	Mar. 1997	Ohio River and tributaries	50+	$500M	Slow-moving frontal system.
	19	Apr.–May 1997	Red River of the North in North Dakota and Minnesota	8	$2B	Very rapid snowmelt.
	20	Sept. 1999	Eastern North Carolina	42	$6B	Slow-moving Hurricane Floyd.
Flash flood	21	June 14, 1903	Willow Creek in Oregon	225	unknown	City of Heppner, Oregon, destroyed.
	22	June 9–10, 1972	Rapid City, South Dakota	237	$160M	15 inches of rain in 5 hours.
	23	July 31, 1976	Big Thompson and Cache la Poudre Rivers in Colorado	144	$39M	Flash flood in canyon after excessive rainfall.
	24	July 19–20, 1977	Conemaugh River in Pennsylvania	78	$300M	12 inches of rain in 6-8 hours.
Ice-jam flood	25	May 1992	Yukon River in Alaska	0	unknown	100-year flood on Yukon River.
Storm-surge flood	26	Sept. 1900	Galveston, Texas	6,000+	unknown	Hurricane.
	27	Sept. 1938	Northeast United States	494	$306M	Hurricane.
	28	Aug. 1969	Gulf Coast, Mississippi and Louisiana	259	$1.4B	Hurricane Camille.
Dam-failure flood	29	Feb. 2, 1972	Buffalo Creek in West Virginia	125	$60M	Dam failure after excessive rainfall.
	30	June 5, 1976	Teton River in Idaho	11	$400M	Earthen dam breached.
	31	Nov. 8, 1977	Toccoa Creek in Georgia	39	$2.8M	Dam failure after excessive rainfall.
Mudflow flood	32	May 18, 1980	Toutle and lower Cowlitz Rivers in Washington	60	unknown	Result of eruption of Mt. St. Helens.

Note: M=Million;B=Billion

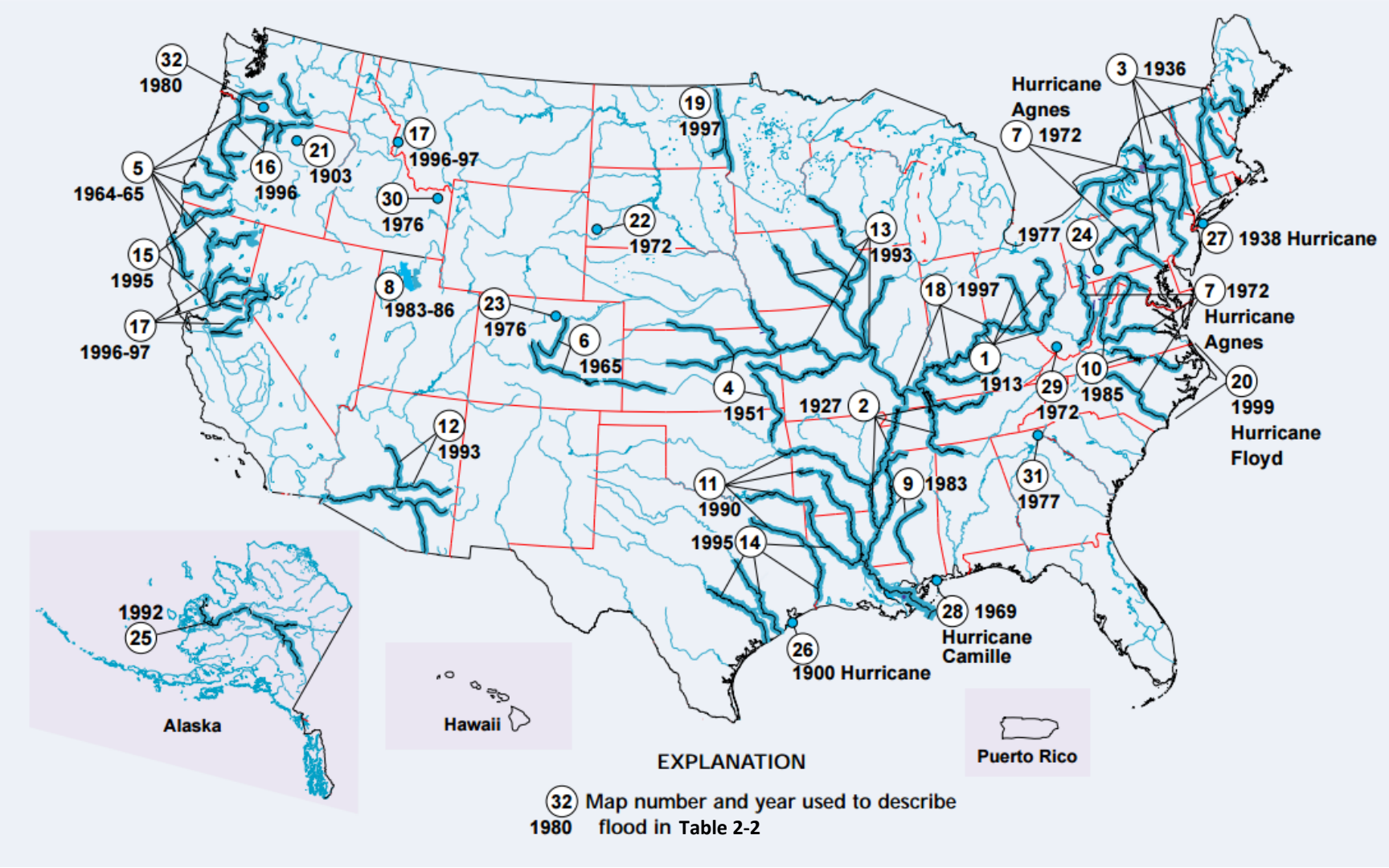

Figure 2-4. Map of the significant floods in the U.S. during the 20th century (Perry, 2000)

2.3 Flood Frequency

Flood frequency is a statistical measurement of the probable occurrence of a flood of a given magnitude (Smith & Ward, 1998). It is frequently used in flood risk assessment, as well as in the concept of design flood when sizing civil structures.

The 100-year flood is typically used for describing a flood that has 1 percent chance of being equal or exceeded in any given year, which can also be referred to as the base flood. The 100-year flood plain is another concept – the land area surrounding a river or water body whose outer edge has an annual probability of 1 percent of being inundated (Platt, 1995). Generally, in terms of level of protection, the concept of the T-year reflects a particular flood flow with a 1 in T change of being exceeded in any year (Platt, 1995). An expected probability, or expected exceedance probability, is a concept to incorporate hydrologic uncertainty, first introduced by Beard (1960). Beard (1960) defined the expected exceedance probability of a given magnitude as the average of the true exceedance probabilities of an infinite number of magnitudes that might be determined in the same manner from random samples of the same size derived from the same parent population.

Flood frequency is generally characterized by a parametric distribution or probability function. Gumbel was a pioneer in studying the theoretical basis of extreme value distribution of flood frequency analysis (Gumbel & Lieblein, 1954). His early work includes flood discharge plotting position (Gumbel, 1943), theory of largest values, flood return period and distribution (Gumbel, 1941), and the extreme value distribution of flood discharge (Gumbel & Lieblein, 1954). The Gumbel (Type I), Frechet (Type II), and Weibull (Type III) distributions are three special cases of the generalized extreme value distribution (GEV). The GEV is commonly used for annual peak time series. It is parameterized with location (mu), scale (sigma) and shape (k) parameters. When k>0, the distribution has heavy tail (Type II); when k=0, the distribution has light tail (Type I); when

k<0, the upper tail is bounded (Type III). Type I extreme value distribution (Gumbel) is frequently applied in flood frequency analysis (Jam & Singh, 1987). Smith (1987) applied the extreme value distribution to estimate the upper tail of the flood frequency distributions, which is the flood quantiles of 10-20% of the flood peaks. Tawn (1992) applied the extreme value distribution (Gumbel) to estimate the probability of annual maximum hourly sea-levels.

The logarithmic Pearson type III (LPIII) distribution, with parameters of mean, standard deviation, and skew, is recommended to fit the annual maximum stream flows for gauged sites (Interagency Advisory Committee on Water Data [IACWD], 1982). It is a shifted gamma distribution [Eq.(2-3)]. The procedure of fitting the sample data with the LPIII distribution is well documented in Bulletin 17B (IACWD, 1982).

$$f(y) = \frac{1}{|\beta|\Gamma(\alpha)}\left[\frac{(y-c)}{\beta}\right]^{\alpha-1}\exp\left[-\frac{(y-c)}{\beta}\right] \qquad (2\text{-}3)$$

where y is the logarithm (base 10) of stream flow, α is the shape parameter, β is the scale parameter and c is the location/shift parameter (Arora & Singh, 1989).

Adjustments may be needed if the dataset is not homogeneous due to mixed populations, location differences, missing events, climate cycles, or the effect of basin development. To make a homogeneous dataset from the mixed populations, the IACWD (1982) recommends separating hurricane events from the non-hurricane events. A conditional probability adjustment may be needed for incomplete records for high floods, low floods, or zero- flood years. If records exist but are not long enough for the frequency analysis, the mean and standard deviation of a short-record station can be adjusted using cross-correlation with a long-record station using the two-station comparison method. It should be noted that equations are available for the direct adjustment of the mean and standard deviation, but not the skew coefficient. A weighted skew coefficient can be estimated using the generalized skew coefficient and the computed station skew coefficient.

The equivalent record length is also estimated for the short-record station. Non-stationary peak discharges can be adjusted to form a stationary series following procedures suggested in IACWD (1982).

Other statistical models are used in addition to the two commonly used distributions (Gumbel and LPIII). Hermanson and Johnson (1966) used the log-normal distribution to model flood flow. Weibull plotting position is used to model annual flood extremes (Zhang, 1982). A regional Weibull model is used to estimate annual flood quantiles (Boes, Heo, & Salas, 1989). The binomial distribution can be applied for estimating the probability of the exact number of flood events occurring over a period of several years; using the exceedance probability of the annual events (USACE, 1993).

Annual peak event analysis generally ensures event independence, but may not cover all of the significant extreme events. The second largest flood event in a year may be much larger than the largest flood in another year. When modeling extreme or rare events, the modeler may chooses either the Annual Maximum (AM) series or the Peaks above Threshold (PoT) series. The generalized Pareto distribution can be used to model the PoT time series or the upper tail distribution (Coles, Bawa, Trenner, & Dorazio, 2001; Dupuis, 2007; Smith, 1987).

For an ungauged location, regression equations can be applied to estimate peak flood discharges when a flood hydrograph is not required. Regional regression equations are obtained by regression analysis of various gages in the region for estimating flood flows with 2-, 5-, 10-, 50-, 100-, and 500-year recurrence-interval (Maryland Hydrology Panel, 2010). For example, the fixed region regression equation for the 100-year flood of the Western Coastal Plain of Maryland is:

$$Q_{100} = 143.56 DA^{0.586} (IA+1)^{0.260} (S_D+1)^{0.469} \quad (2\text{-}4)$$

where DA is the drainage area in mi^2, IA is the impervious area in percent, S_D is the percentage of Group D soil. Sauer, Thomas Jr, Stricker, and Wilson (1983) provided techniques to adjust the

flood discharge values computed with rural equations for urban conditions. If significant land use change has occurred, the regression equations developed before the change would not be applicable (Sauer et al., 1983). If a gage with a data record is located inside the study site or on the same stream stem, and the drainage area of the study site is within 50% to 150% of the drainage area of the gage, the flood discharge of the study site could be estimated by weighting the single station record and the regional regression estimates (Maryland Hydrology Panel, 2010).

If a nearby stream or tidal gage is available on the same stream of a ungauged location, the transposition of the discharges can be made using the drainage area ratio method and Sauer's weighting-function method (McCuen and Levy, 2000). When a calibrated rainfall-runoff model is available, the model can be used instead of the regional regression equation or transposition. TR-20 is a deterministic rainfall-runoff model recommended by the Maryland Hydrology Panel (2010). FEMA (2013b) recommended the use of the rainfall-runoff models under the list of the Numerical Models Meeting the Minimum Requirements for the National Flood Insurance Program. The model results should be compared to other hydrologic estimates, such as USGS regression equations or the gaged site near the studied site (FEMA, 2013b).

2.4 Flood Damage

2.4.1 Types of Flood Damage

Flood damage is a consequence of physical exposure and system vulnerability. Physical exposure accounts for the type of flood and its magnitude and location, while system vulnerably reflects the population and assets subjected to flood damage, as well as the state of the flood defense structures (Smith & Ward, 1998).

Flood damage can be classified as direct or indirect. Direct damage is the physical damage caused by contact between flood water and humans or property. Indirect damage includes the

loss of business and production, emergency response and preparedness costs. Flood loss can also be categorized as tangible and intangible. Tangible loss can be directly quantified by a monetary value, such as damage to buildings and contents. Intangible loss cannot be quantified by a price, such as loss of an archaeological site (Penning-Rowsell & Wilson, 2003; Smith & Ward, 1998; Soetanto & Proverbs, 2004). Jonkman, Bočkarjova, Kok, and Bernardini (2008) listed the examples for each category (Table 2-3).

Table 2-3. Classification of flood damages

	Tangible and priced	Intangible and unpriced
Direct	Residences	Fatalities
	Capital Assets and inventory	Injuries
	Business interruption (inside the flooded area)	Inconvenience and moral damages
	Vehicles	Utilities and communication
	Agricultural land and cattle	Historical and cultural losses
	Roads, utility and communication infrastructure	Environmental losses
	Evacuation and rescue operations	
	Reconstruction of flood defenses	
	Cleanup costs	
Indirect	Damage for companies outside the flooded area	Societal disruption
	Adjustments in production and consumption patterns outside the flooded area	Psychological traumas
	Temporary housing of evacuees	Undermined trust in public authorities

Source: Jonkman et al. (2008)

Flood losses can also be grouped into primary and secondary losses. Smith and Ward (1998) explained the primary and secondary losses for the 3 combinations of flood damage types (Table 2-4).

Table 2-4. Primary and secondary flood losses

	Primary	Secondary
Direct, tangible losses	Direct physical damage to property	Restoration of the direct damage
Direct, intangible losses	Mortality - Enhanced rates of death caused by disaster	Morbidity - Physical and mental illness result from injury and disease
Indirect, tangible losses	Disruption of economy and social activities	Long-term effects such as reduced tourism income at the flooded area

Source: Smith and Ward (1998)

2.4.2 Flood Damage Valuation and Decision Criteria

Flood damage valuation is a critical step for hydro-economic flood risk assessment. In general, damage can be calculated by the simplified function:

$$Damage = \sum_{i=1}^{n}\sum_{j=1}^{m} value_{i,j} \times susceptibility_{i,j} \tag{2-5}$$

$$Susceptibility_{i,j} = f(entity\ characteristics_{i,j}, inundation\ characteristics_{k}, socioeconomic\ characteristics_{l}) \tag{2-6}$$

where i is category of tangible elements at risk (n categories possible); j is entity in an elements-at-risk category (m entities possible); k is flood type/specific flood scenario; l is type of socio-economic system. Susceptibility is measured in percent (Messner et al., 2007).

The total economic value is defined as the summation of use value and non-use value (Pearce & Turner, 1990). The use-value is the value an individual gains from consuming or accessing some quantity of a good. The non-use value is the value given to a good over and above the use value the consumer attaches to that good (Penning-Rowsell et al., 1992). The use-value includes all values related to the physical conjunction of individual and asset (Penning-Rowsell et al., 2014), while the non-use or passive-use value is frequently used for natural resources valuation, e.g. damage of oil spill (Carson et al., 1992), annual recreation, and amenity benefits

(Penning-Rowsell & Wilson, 2003). Individuals who make no active use of particular natural resources may derive satisfaction from their existence (Arrow & Solow, 1993).

In terms of the scale of the damage valuation, Penning-Rowsell and Fordham (1994) distinguished the economic and financial losses from flood events. The economic analysis considers the total net change in resources and consumption across the nation in consequence of a decision or change. The financial analysis only deal with the changes that affect the organization for which the analysis is being undertaken (Penning-Rowsell et al., 1992). The government may be more concerned with the economic analysis; however, the insurance companies are interested in the financial losses. Financial loss per property can be significantly higher than the economic loss per property (Penning-Rowsell & Wilson, 2003).

Penning-Rowsell et al. (2014) summarized the following four strategies for deriving values: (1) using market prices, which is also referred to as the revealed preference technique; (2) using inferential methods, in which statistical analysis infers the value of a non-observable price, such as travel cost method (Clawson, 1959) and hedonic price technique (Rosen, 1974); (3) Using expressed-preference methods, such as conjoint analysis (Green & Srinivasan, 1978) or contingent valuation method (Arrow & Solow, 1993); and (4) Benefit transfer. Market Prices assuming equilibrium prices is the simplest method. Travel Cost is an indirect method to value public good based on the distance traveled and costs of visiting a particular site. It involves the regression analysis of visitor rates to the site and visitor origin and is often used for recreational benefit evaluation. Hedonic Price, also an indirect method, infers the value of one good by evaluating the consumption of another good which is associated with the good of interest. It is often used to evaluate amenity benefits. The Contingent Valuation method evaluates goods using social survey. It is a direct method applicable to all goods (Penning-Rowsell et al., 1992). Benefit

Transfer is a method to derive unit value of some benefit or cost using another context, standard or average value, or site-specific value with a predictive equation (Penning-Rowsell et al., 2014).

A damage function is the most common practice to quantify flood damage for a specific damage category. Damage is quantitatively predicted as a function of some flood property, usually depth. Flood damage functions can be developed using survey data and synthetic data (Messner et al., 2007). Specialized assessors, e.g., insurance loss adjusters, can estimate the loss of a particular property in a flood of a given magnitude. Choi and Fisher (2003) used insured catastrophe data of Mid-Atlantic region and event-by-event hurricane losses data for North Carolina to develop regression equations to estimate catastrophe losses. However, surveys are costly since the sample size required is large.

A synthetic approach is to assess the losses that would be experienced by a specific property type. It is independent of a particular flood experience. Market research data can be used for this method (Penning-Rowsell & Chatterton, 1977; Penning-Rowsell & Fordham, 1994). An early study of flood damage estimate is an analysis of 90,000 urban properties in the Susquehanna River Basin based on synthetic depth/damage data (US Department of Agriculture Soil Conservation Service, 1970). Stage-damage curves are developed for combinations of residential property type, age, and social class of occupants (Penning-Rowsell & Chatterton, 1977). Damage can be quantified by absolute value or percent damage. A dimensionless damage axis can be used to enable comparison between different damage measurements. For example, Higgins and Robinson (1981) plotted relative damage against flood stage, with damage expressed as a proportion of a baseline damage.

With standard datasets, flood damage can also be estimated by unit loss approaches (Penning-Rowsell & Fordham, 1994). The unit loss approach estimates the loss as a proportion of the value at risk, which is applicable for a system with a reliable database of building and contents,

e.g., a taxation database. The disadvantage of the method is that the database may not have information on the vertical distribution of the building and contents. An areal depth-damage curve can be used when the database is not available. Site surveys are usually required for the floor levels (Penning-Rowsell & Fordham, 1994).

Willingness to pay (WTP) measures losses by eliciting the public's preference and the value they put on maintenance or enhancement of recreational and environmental activities (Penning-Rowsell et al., 2014). According to a study of WTP by survey, DEFRA (2005) recommend a value of £200 per household per year to represent the benefits of reduced health impacts as a consequence of a reduced flooding risk. Veronesi, Chawla, Maurer, and Lienert (2014) concluded from a discrete choice experiment on a representative Swiss population sample that about 71% of the respondents are willing to pay a higher annual local tax to reduce the risk of sewer overflowing in rivers and lakes, while about 54% are willing to pay to reduce the risk of flooding in streets. Based on the contingent valuation method, Palanca-Tan (2015) estimated a WTP of US$0.17-0.29/$m^3$ of water use for improved sewage and sanitation service in reduction of waterborne diseases in Metro Manila, Philippines. Genius et al. (2005) found that WTP for wastewater treatment facility is 44 € (to be paid as an additional charge on the water bill) based on 326 households interviews in northwest Crete. Hensher, Shore, and Train (2005) defined the marginal willingness to pay (MWTP) for an attribute as the derivative of utility with respect to the attribute divided by the (negative of the) derivative of utility with respect to price. The residential customers of Canberra, Australia's MWTP for wastewater service attributes are summarized in Table 2-5. The study further concluded that the customers' willingness to pay decreases with the increment of interruption they face per year (Hensher et al., 2005).

Table 2-5. Residential customers' marginal willingness to pay for wastewater service attributes (Hensher et al., 2005)

Frequency	Mean	Std. Dev.	25tile	Median	75tile
Panel A: To reduce the frequency of overflows. Expressed as share of water and sewerage bill					
Once in 10 years	0.2794	0.3406	0.0504	0.2794	0.5076
Every other year	0.2049	0.2498	0.0370	0.2049	0.3722
Once a year	0.1537	0.1873	0.0277	0.1537	0.2792
Twice a year	0.1025	0.1249	0.0185	0.1025	0.1861
In Australian dollars					
Once in 10 years	212.32	273.90	35.59	197.96	373.73
Every other year	155.70	200.86	26.10	145.17	274.07
Once a year	116.77	150.64	19.58	108.88	205.55
Twice a year	77.85	100.43	13.05	72.59	137.03
Expressed as share of bill:					
Time until fixed	Mean	Std. Dev.	25tile	Median	75tile
Panel B: To reduce repair times					
1 hour	0.1232	0.0916	0.0625	0.1232	0.1857
2 hours	0.0821	0.0611	0.0416	0.0821	0.1238
4 hours	0.0493	0.0367	0.0250	0.0493	0.0743
8 hours	0.0274	0.0204	0.0139	0.0274	0.0413
12 hours	0.0190	0.0141	0.0096	0.0190	0.0286
24 hours	0.0099	0.0073	0.0050	0.0099	0.0149
In Australian dollars:					
1 hour	94.06	75.87	43.72	87.88	137.81
2 hours	62.71	50.58	29.15	58.59	91.87
4 hours	37.63	30.35	17.49	35.15	55.12
8 hours	20.90	16.86	9.72	19.53	30.62
12 hours	14.47	11.67	6.73	13.52	21.20
24 hours	7.53	6.07	3.50	7.03	11.02

In terms of project appraisal, Penning-Rowsell and Wilson (2003) suggested the following two criteria to compare options: (1) benefit-cost ratio; (2) net present values. The benefit-cost ratio (B/C) is the ratio of the present value of all of the streams of benefits over the present value of all of the streams of cost. The net present value is the difference between the present value of all of the streams of benefits and the present value of all of the streams of costs (Penning-Rowsell et al., 2014). The desirable project is usually the one with the higher overall benefit-cost ratio, the marginal benefit-cost ratio above unity, or higher net present value. The best risk reduction alternative maximizes the probability of the target benefit (Ayyub, McGill, & Kaminskiy, 2007):

$$\Pr\left(\frac{B}{C} \geq \alpha\right) = 1 - \Pr(B - \alpha\, C \leq 0) \tag{2-7}$$

where benefit B is the difference between the risk before and after implementation; cost C is the equivalent annual cost to implement the risk mitigation solution over a specified time domain; and α is a target benefit cost ratio (Ayyub et al., 2007).

The benefit or cost in future year can be expressed in terms of the present value by applying the discount rate (Penning-Rowsell & Wilson, 2003). The cost/benefit that occurs in one year's time is treated as having a lower real value now, which is an opposite concept of interest (Penning-Rowsell et al., 1992).

$$PV = \sum_{t=1}^{t=T} \frac{x_t}{(1+r)^t} \tag{2-8}$$

where PV is the present value of the benefit or cost occurring in a future year; r is the discount rate, t is the number of years into the future the benefit or cost occurs after the base date of analysis ; X_t is benefit or cost in year t, T is the projected life of the scheme (Penning-Rowsell et al., 1992).

In the National Economic Development (NED) benefit evaluation study (Water Resources Council, 1983), benefits associated with the urban flood hazard reduction features of water resource plans and projects are defined for the following three categories:

(1) Inundation reduction benefit: If floodplain use is the same with and without the plan, the benefit is the increased net income generated by that use. If an activity is removed from the floodplain, this benefit is realized only to the extent that removal of the activity increases the net income of other activities in the economy.

(2) Intensification benefit: If the type of floodplain use is unchanged but the method of operation is modified because of the plan, the benefit is the increased net income generated by the floodplain activity.

(3) Location benefit: If an activity is added to the floodplain because of a plan, the benefit is the difference between aggregate net incomes (including economic rent) in the economically affected area with and without the plan.

The following ten steps are recommended to compute the NED benefits (1) Delineate affected area; (2) Determine floodplain characteristics; (3) Project activities in affected area; (4) Estimate potential land use; (5) Project land use; (6) Determine existing flood damages; (7) Project future flood damages; (8) Determine other costs of using the floodplain; (9) Collect land market value and related data; (10) Compute NED benefits. When historical damage data is not sufficient, the existing flood damage can be estimated by standard damage-frequency integration technique, with historical hydrological flood variables as inputs. Future flood damages can be assessed by the projection of future hydrological, economic and demographic changes (Water Resources Council, 1983).

2.4.3 Damage-Frequency Integration Technique and Expected Annual Damage

The standard damage-frequency integration technique, also known as the classical four-part diagram (Penning-Rowsell & Wilson, 2003), is a commonly used method to assess the likelihood of flood damage. The classical risk based approach to flood impact analysis is to conjoin the relationships between flow, probability, stage, and damage, as illustrated in Figure 2-5 (Davis, Faber, & Stedinger, 2008). By plotting flood loss against exceedance probability, the average annual flood damage can be estimated by the area under the curve.

This method can be used for project appraisal of flood defense structures. The Above Design Standard (ADS) benefits can be derived using the flood damage-exceedance probability curve (Penning-Rowsell & Wilson, 2003). To determine the optimal capacity of a flood control structure, Leclerc and Schaake (1972) calculated the expected annual flood damage and net national income benefits:

$$\bar{d} = \int_0^\infty d(x) f(x) dx \tag{2-9}$$

$$\pi(x) = \bar{d} - [c(x) + \int_x^\infty f(x) d(x) dx] \tag{2-10}$$

where $\bar{d}$ is expected annual flood damage; x is the flood magnitude of annual flood at a given location; $\pi(x)$ is net national income benefits; $c(x)$ is the cost of flood control. The integral of Eq. (2-10) removes the contribution to the expected annual flood damage due to depth exceeding x.

USACE Hydrologic Engineering Center (1989) stated that damage can be computed in three modes: (1) The damage associated with a specific flood event, e.g., the estimated damage when the standard project flood occur. (2) The expected annual damage associated with a specific year or several selected years. (3) The equivalent annual flood damage associated with a particular discount rate and period of analysis.

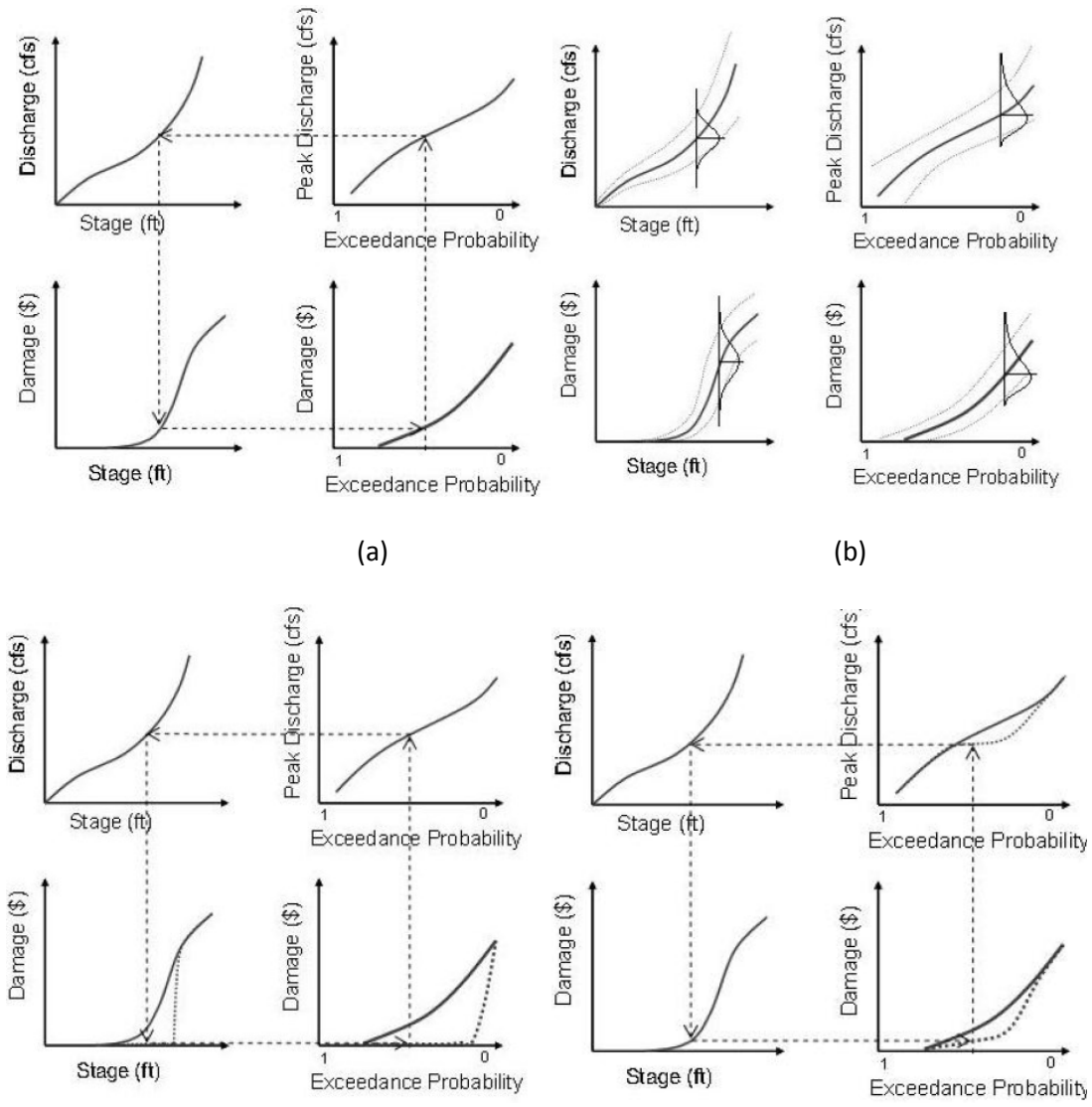

Figure 2-5. Conjoining of relationships between flow, probability, stage and damage
(a) Deterministic solution (b) solution considering uncertainty (c) relationships altered by a levee (d) relationships altered by a reservoir (Davis et al., 2008)

Expected (Average) Annual Damage (EAD) is a concept for evaluating project risk. It is the frequency weighted sum of damage for the full range of possible damaging flood events and can be viewed as what might be expected to occur in the present or any future year (USACE Hydrologic

Engineering Center, 1989). It can be computed by the integral approach based on the classic four-part diagram (Figure 2-5). This concept can also be understood as existing flood damages, which is the potential average annual dollar damages to activities affected by flooding at the time of the study (Water Resources Council, 1983).

Whether the expected annual damage changes over time depends on whether the damage and frequency change each year. Damage is usually treated as a singular value. There are several different concepts involved, such as event damage, equivalent annual damage, and expected annual damage. The equivalent value assumed a uniform distribution (over each year) of annual value and is calculated by discounting and amortizing each year's expected annual damage value over the period of analysis. It is commonly used to compare alternative plans or compare cost with the damage (USACE Hydrologic Engineering Center, 1989).

The expected annual damage $E(D)$ can be calculated by

$$E(D \mid q_c^*) = \int_{q_c^*}^{\infty} D(q) f(q) dq \tag{2-11}$$

where q_c^* is the flow capacity of hydraulic structure with a probability density function $f(q)$. $D(q)$ is the damage function corresponding to the flood magnitude of q (Bao, Tung, & Hasfurther, 1987). Eq. (2-11) is the commonly used function for expected annual damage.

Bao et al. (1987) also proposed a way to consider hydrological uncertainty. The expected damage for a flood magnitude of return period T can be computed by

$$E(D_T \mid q_c^*) = \int_{q_c^*}^{\infty} D(q_T) h(q_T) dq_T \tag{2-12}$$

where $E(D_T|q_c^*)$ is the expected damage corresponding to a T year flood; $h(q_T)$ is the sample probability density function of flood magnitude of a given return period T; q_T is the dummy argument of T year flood (Bao et al., 1987).

The annual expected damage can then be expressed as Eq. (2-13) by considering the hydrological uncertainty represented by $f(q)$ and the hydrologic parameter uncertainty, represented by $h(q_T)$ (Bao et al., 1987).

$$E(D \mid q_c^*) = \int_{q_c^*}^{\infty} [\int_{q_c^*}^{\infty} D(q_T) h(q_T) dq_T] f(q) dq \tag{2-13}$$

Equation. (2-11) is an asymptotic solution when sample size of Eq. (2-12) and Eq. (2-13) approaches infinity.

When considering design cost, the annual total expected cost ($ATEC$) is computed by

$$ATEC = FC * CRF + E(D) \tag{2-14}$$

where FC is the total installation cost and CRF is the capital recovery factor to convert the present worth of the installation cost to an annual basis (Bao et al., 1987).

One early application of the expected annual damage concept is Arnell (1986)'s zonal average annual damage computation. It is indexed by flood hazard factor, defined as the depth difference between the 10 year and 100 year flood. The sum of damage of the individual property is close to the aggregate of the annual damage. Arnell (1986) selected the Gumbul distribution to represent the stage-frequency relationship for 10 gaging stations in Britain. Pingel and Watkins Jr (2009) studied the possible approach to estimate EAD based on multiple flood sources.

Merz, Elmer, and Thieken (2009) concluded from three case studies in German riverine flood-prone area that high probability/low damage flood events dominate the EAD, while the low probability/high damage floods have minor contribution. Approximately 80% of the flood protection benefits results from the reduced damage due to events with return period of up to 100-year. This result is not in agreement with the general perception of flood risk in the societal view. This leads to the quantification of risk aversion into the evaluation process (Merz et al., 2009).

Expected probability is another concept to address the flood damage (Beard, 1997). This theory is extensively compared with the expected annual damage concept. The controversy centers on whether the expected probability is a biased estimate. The National Research Council prefers the expected damage approach considering hydrologic uncertainty while the USACE recommends the expected probability approach (Beard, 1990, 1997; Platt, 1995; Stedinger, 1997).

2.4.4 Model Flood Damage in a Interdependent System

When predicting flood damage in a complex system, the cascading effect and system response to a major flood event are vital for flood risk assessment. The system can be as big as a nation (macro-scale flood model) or as small as a process plant (micro-scale flood model). The complexity of the model depends on the details required to accurately describe the system.

Tree or diagram based analyses are helpful for structuring the cascading effect and probability propagation, thus assisting the selection of the systematic risk strategy. Fault tree, event tree, decision trees, fishbone diagram, bow-tie diagrams, and influence diagram are commonly used methods (Rausand & Høyland, 2004). Inoperability Input-output models (Crowther, Haimes, & Taub, 2007) and Bayesian network (Li, Wang, Leung, & Jiang, 2010) are also applicable for assessing the flood impact propagation in a system. Experts may have difficulty deciding whether to assign a 10^{-4} or 10^{-8} probability to a rare event; fault tree and event tree helps decompose the problem (Goodwin & Wright, 2007).

Risk indicators are frequently used for system-based risk assessment to provide a standard of measurement for network interdependency. Zimmerman (2004) constructed a set of indicators to assess critical infrastructure interdependency. Zimmerman (2004) defined the Effect Ratio (ER), as the ratio of (being a cause of failure) to (being affected by failure) to assess the role of one infrastructure sector among the system (Zimmerman, 2004):

$$ER = \frac{number\ of\ times\ infrastructure\ caused\ failure\ of\ other\ infrastructure}{number\ of\ times\ infrastructure\ was\ affected\ by\ other\ infrastructure\ failures} \quad (2\text{-}15)$$

LaRocca and Guikema (2011) conducted a survey of network theoretic approaches for risk analyses of complex infrastructure systems and examined approaches for assessing both the robustness and resilience of infrastructure systems. They characterized the structure of a network by the average path length, the clustering coefficient, the degree distribution, and the betweenness. Network performance was measured by

$$S = \frac{NS'}{NS} \quad (2\text{-}16)$$

where NS is the number of nodes in the largest connected component of the network before the failure and NS' is the number of nodes in the largest connected component of the network after the failure. Cascading failures were simulated by network efficiency (*E*), defined as:

$$E = \frac{1}{N(N-1)} \sum_{i,j} \frac{1}{d_{i,j}} \quad (2\text{-}17)$$

where N is the number of nodes in the network and $d_{i,j}$ is the distance of the shortest path between *i* and *j*. For example, the performance of electric power grids can be measured by connectivity loss (CL), defined as:

$$CL = 1 - \frac{1}{N_d \sum_i^{Nd} \frac{N_g^i}{N_g}} \quad (2\text{-}18)$$

where N_g is the total number of generators, N_d is the total number of distribution substations, and N_g^i is the number of generators connected to substation *i* (LaRocca & Guikema, 2011) .

Zio and Sansavini (2011) characterized the criticality of components in a power network system by the following specific indicators:

$$f_i = \frac{number\ of\ failures\ of\ component\ i}{number\ of\ \ cascades\ simulated} \tag{2-19}$$

$$t_i = \frac{time\ when\ component\ i\ enters\ the\ cascade}{total\ number\ of\ cascades\ simulated} \tag{2-20}$$

$$s_i = \frac{final\ size\ of\ a\ cascade\ following\ the\ failure\ of\ component\ i}{total\ number\ of\ cascades\ simulated} \tag{2-21}$$

where f_i is a measurement of importance of a component in the buildup of a cascade, t_i is an indicator of how early in time a component gets involved in a cascade process, and s_i indicates the criticality of a component in the network in terms of the subsequent failure of other component as a result of the failure of component i (Zio & Sansavini, 2011).

A system flood damage model requires appropriate application of statistical inference to characterize failure and damage beyond the distribution of flood stage and discharge (introduced in Section 2.3). This involves the probabilistic estimation of system behavior. A triangular distribution is commonly used in decision and uncertainty analysis software, such as Crystal Balls and @risk, for subjective estimates that use lower and upper bounds along with the mode. A standard, two-sided power family of distributions is appropriate for fitting peaked histograms. A four parameter, two-sided power distribution could be used for expert elicitation of extreme event consequences, as well as the risk and uncertainty problem that involves activity duration, such as "Project Evaluation and Review Technique" (PERT) (Barker & Haimes, 2009). An uneven, two-sided power distribution would treat the type of distribution that is asymmetric, with a jump discontinuity at a single point (Kotz & Van Dorp, 2004). Uncertainties of probabilities of human error are frequently described by the rectangular distribution (Hauptmanns, 2010). The failure rate distribution can be characterized by a bathtub curve (Rausand & Høyland, 2004).

The Dormant-Weibull Formula is selected for predicting probabilities of dam failure due to its components and systems [U.S. Bureau of Reclamation (USBR) & U.S. Army Corps of

Engineers (USACE), 2012]; it may also be adopted to characterize the failure probability of equipment in a MWWTP. It is a modification of the Weibull formula to consider the durations of time when a product is not in use:

$$P_n = 1 - \exp\left(\frac{(n-1)\tau - \gamma}{\eta}\right)^{\beta} \times \exp\left[-\left(\frac{n\tau - \gamma}{\eta}\right)^{\beta}\right] \quad (2\text{-}22)$$

where n is the number of times the component operated in its life; P_n is the probability of failure over the entire interval n; η is the characteristic life parameter, that is, is the point in time when 63.2% of the components under study are expected to have failed (e.g., if the characteristic life of a component is 50 years, 63 out of 100 components would be expected to fail by that time in history); η is derived by expert elicitation; β is the shape parameter, which is derived for the failure modes that equipment experienced (e.g., β=2.0 for clogging, β =3.0 for cavitation); γ is the location parameter, which is the difference in years between when the component was originally installed and when it was replaced; τ (year) is the inspection interval or time since last operated. The log-normal distribution is used to represent uncertainties of failure rates of technical components in the framework for flood protection decisions of process plants (Hauptmanns, 2010):

$$f(x) = \frac{1}{\lambda\sqrt{2\pi}S} exp(\frac{-(ln\lambda - \mu)^2}{2S^2}) \quad (\lambda > 0) \quad (2\text{-}23)$$

where λ is the failure rate; μ is the mean value of its logarithms; S is the corresponding standard deviation of the logarithms.

Bier, Haimes, Lambert, Matalas, and Zimmerman (1999) states that the probability of an extreme event may be viewed as the tail probability distribution of another distribution. For example, the probability of a failure mode of the dam could be represented as the tail probability of the flood height distribution. A threshold value may play a critical role in the probability distribution. For example, flood damage may be characterized as a function of wave heights that

exceed a threshold, regardless of the number of waves that occur below the threshold (Bier et al., 1999).

When the weight of evidence is involved, one could update the prior probability distribution by Bayes' rule. Li et al. (2010) constructed a Bayesian Network to predict flood losses when domain knowledge and spatial data are available. Catastrophic risk was modeled by the following (Li et al., 2010):

$$R = \iint C(V)P(V \mid A)P(A)dVdA \tag{2-24}$$

where $P(A)$ is the probability of the disaster event A; $P(V|A)$ is the probability of vulnerability for a certain individual V given event A; $C(V)$ is the damage potential of V.

If the distribution cannot be derived directly using an analytical approach, a first-order second-moment approximation, point estimate method and Monte Carlo simulation can be applied (Christian & Baecher, 1999; Kortenhaus, 2007; Rosenblueth, 1975) .

2.4.5 Contemporary Flood Damage Assessment Tools

The acceptance and popularity of a flood risk modeling tool vary with geographical location and the purpose of the study. Several tools developed or partially developed in the U.S. and the multi-colored manual developed by the Flood Hazard Research Centre at Middlesex University, UK (Penning-Rowsell et al., 2014), are introduced in this section.

Hazus-MH is the Federal Emergency Management Agency's (FEMA's) methodology for estimating potential losses from earthquakes, floods, and hurricanes. Hazus-MH Flood Model is designed to provide flood loss estimates for risk mitigation, emergency preparedness, response and recovery (FEMA, 2009). It is capable of characterizing riverine and coastal flood hazard (Scawthorn, Blais, et al., 2006). The Hazus Flood Model uses depth-damage functions to estimate

damage for general building stock, essential facilities, lifeline systems, vehicles, and agriculture (Scawthorn, Flores, et al., 2006).

The Hazus-MH Flood Model is composed of five components: inventory data, flood hazard, direct physical damage, induced physical damage, and economic and social impact. They are interrelated and supported by Geographic Information System (GIS) to handle spatial data. Hazus-MH supports both the default and the user-specified inventory data and damage curves (FEMA, 2009).

Three levels of analysis are available in Hazus-MH Flood Model. Level 1 is based on input built into the modeling program. Level 2 is based on the Level 1 analysis with addition of user supplied data; the Flood Information Tool (FIT) is used to handle the user specified data. Level 3 requires extensive user-developed information compared to Levels 1 and 2. The major difference of the analysis levels lies in the amount of user defined input, including parameters, inventory data, hydrology and hydraulic analysis to define flood elevations, etc. (FEMA, 2009). In the Level 1 analysis, riverine flood hazard is characterized by regional regression equations and rating curves. The velocity effects are considered in velocity-specific damage curves. The coastal flood hazard is modeled by base flood elevation or wave crest elevations along shore-perpendicular transects. Dune erosion and wave effects are also considered (Scawthorn, Blais, et al., 2006).

Hazus-MH Flood model can be extended to assist flood vulnerability study in a broader range than estimating dollar damage. Cummings, Todhunter, and Rundquist (2012) examined lakeshore flood hazards and evaluated community relocation as a flood mitigation response. Remo, Pinter, and Mahgoub (2015) developed a flood vulnerability index using Hazus-MH coupled with a parametric social vulnerability index.

In terms of uncertainty and application scale, Tate, Muñoz, and Suchan (2014) studied the global sensitivity of the Hazus-MH Flood Model and concluded that DEM model component has

the greatest influence on model uncertainty, compared to river hydraulics, residential buildings and depth-damage functions. Banks, Camp, and Abkowitz (2014) concluded from a study of May 2010 Davidson County (Nashville), Tennessee flood that Hazus-HM is useful in predicting county-level flood damage, but limited at the subcounty level.

In the flood module, Hazus-MH values the wastewater sectors as shown in Table 2-6 (FEMA, 2009). Flood vulnerability to inundation, erosion and scour, debris impact and hydraulic pressure are summarized by the risk matrix (Table 2-7).

Table 2-6. Hazus valuation of wastewater system (FEMA, 2009)

Occupancy	Thousands of dollars
Sewer & interceptors	1
Small WWTPs	60000
Medium WWTPs	200000
Large WWTPs	720000
Control vaults and control stations	50
Small lift stations with wet well/dry well	300
Medium/large lift stations with wet well/dry well	1050
Small submerged lift stations	300
Medium/large submerged lift stations	1050

Table 2-7. Hazus flood sub-hazard vulnerability (FEMA, 2009)

	Inundation	Scour/Erosion	Debris impact/ Hydraulic pressure
Treatment plants	high	low	low
Pump/Lift stations	high	none	none
Pipelines-Bridge crossings	low	none	medium
Pipelines-Buried river crossings	none	high	low
Collection systems	high	none	none
Control vaults (meter pits, control valves)	high	low	low

In Hazus, the study site of this research can be classified as a large wastewater treatment. The large wastewater treatment plant is worth 720 million dollar Hazus value. The Hazus model evaluates the percent damage by depth of flooding (see Figure 2-6).

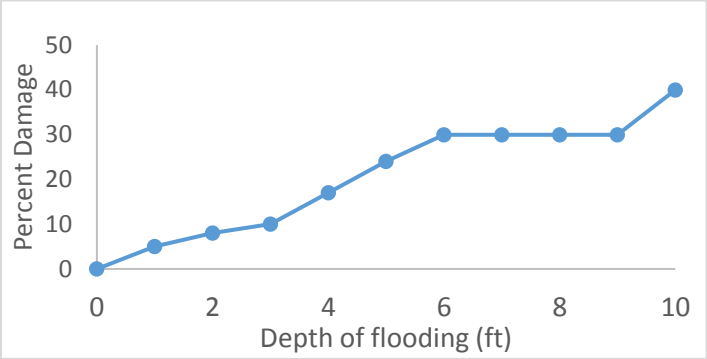

Figure 2-6. Percent damage of large wastewater treatment plant

Source: FEMA (2009)

The Hazus flood model estimates the percent equipment damage of the wastewater treatment facility by Eq. (2-25) and Eq.(2-26). The percent damage is based on the function showed in Figure 2-6 (FEMA, 2009).

$$\%\ Damage = Damage\ at\ (depth\ of\ water - equipment\ height) \quad (2\text{-}25)$$

$$(\$\ Loss) = (\%\ Damage) * (Inventory\ \$\ value) \quad (2\text{-}26)$$

When dealing with site specific loss estimates, such as a municipal wastewater treatment plant, Hazus may not be able to consider the uniqueness of the sector in great detail. It only deals with the ground level damage. In a municipal wastewater treatment plant, most equipment above ground are designed to be wet.

Another tool that provides the guidelines of damage assessment of water and wastewater sector is the Flood Hazard Research Centre at Middlesex University, UK's multi-colored manual (Penning-Rowsell et al., 2014). It is a widely adopted manual and handbook on the benefits of

flood and coastal risk management, which is developed in the form of Blue (Penning-Rowsell & Chatterton, 1977), Red (Parker, Green, & Thompson, 1987), and Yellow (Penning-Rowsell et al., 1992) manuals. A range of data and techniques are provided for various practical aspects of flood risk management, including flood damage assessment of residential and non-residential properties, utility services, schools, hospitals, transportation networks and agriculture. Multi-criteria analysis is used to broaden the criteria involved in the flood risk study (Penning-Rowsell et al., 2014).

Based on Penning-Rowsell et al. (2014), the total flood damage of wastewater treatment plant is summarized in Table 2-8, and the cost of service disruption can be estimated as

$$Estimated\ cost\ of\ disruption = N \times U \times WTP \times D \tag{2-27}$$

where N is the number of households affected by the service, U is the hourly usage/consumption, WTP is willingness to pay value per hour to avoid the outage, D is the estimated length of disruption to supply.

Table 2-8. Average damages per square meter expected from different depths of flooding for a sewage treatment works (Penning-Rowsell et al., 2014)

Depth (cm)		-50	0	25	50	100	150	200
Total damage (£/m^2)	Short duration floods (<12 hour)	0	5	30	40	70	100	145
	Long duration floods (<12 hour)	0	10	45	70	110	145	180

The Flood Damage Reduction Analysis (HEC-FDA) is developed by the USACE Hydrologic Engineering Center (HEC) to perform an integrated hydrologic engineering and economic analysis (USACE Hydrologic Engineering Center, 2008). HEC-FDA requires study configuration data, water surface profiles, exceedance probability functions, regulation inflow-outflow functions, stage-discharge functions, levee data, damage categories, structure modules, structure inventory data

and stage-damage functions. The risk analysis procedures are consistent with USACE (1996). The classical four part diagram and damage-frequency integration technique are the theoretical basis of the HEC-FDA damage assessment.

HEC-FDA's damage assessment is limited to structure and content damage. Hazus-MH has a greater breadth of damage functions in terms of occupancy. HEC-FDA is more powerful in hydrologic analyses, including stream and reach creation and modification, stage-discharge relationship development, and levee impact assessment.

To meet the requirements of the National Flood Insurance Program (NFIP), FEMA Substantial Damage Estimator (SDE) is a tool to assist Federal, State and local officials to assess substantial damage for residential and non-residential structures. Before using this tool, it is necessary to determine if the structural damage within a mapped Special Flood Hazard Area (SFHA) meets the criteria for Substantial Damage. SFHA is defined as the land in the floodplain within a community subject to the 1 percent or greater chance of flooding in any given year (i.e., the 100-year flood). NFIP regulations defines Substantial Damage as "Damage of any origin sustained by a structure whereby the cost of restoring the structure to its before-damaged condition would equal or exceed 50 percent of the market value of the structure before the damage occurred." (FEMA, 2014). Table 2-9 shows one example of the percent damage threshold.

Table 2-9. Foundation damage threshold and description (FEMA, 2013a)

Foundation			Damage Threshold			
			0- 25%	25-50%	50-75%	Over 75%
Description	Continuous perimeter foundations, footings, and piers for internal beams and floor loads. Materials include masonry or concrete masonry units (CMUs) or piles.	Threshold Markers	Water level rises just above first floor level.	Water level is 4-7 feet against the outside of the building.	Water level is 7-10 feet against the outside of the building.	Water level is more than 10 feet against the outside of the building.
			No scouring around foundation.	Limited scouring around foundation.	Limited scouring around foundation.	Limited scouring around foundation.
			Some undermining but no visible cracking at concrete slab.	Soils are saturated.	Soils are saturated and unstable.	Foundation is notably cracked and/or displaced. Structure has been knocked off its foundation.
				Undermining of the foundation, especially at corners - hairline cracks only.	Cracks noted on or along the foundation walls.	Portions of the foundation are damaged or missing.
					Significant undermining of the foundation - significant cracking is visible.	Significant undermining of the foundation - major cracking and separation of the foundation.
		Common Damages	Short-term inundation to limited heights. Limited scouring and erosion - low-flow and low velocity floodwaters. No noticeable cracking of the masonry or displacement of the foundation walls.	Short-term inundation - foundation is inundated with flood waters but for a limited duration. Limited scouring or undermining of the foundation or footings is found. Minor cracking from some settlement but no displacement, heaving, or discontinuities of the structural support systems.	Floodwaters extend over the top of the foundation system - significant inundation for over 12 hours. Some cracking of the masonry/concrete foundation walls. Some damages to the foundation wall from debris or settlement noted.	Settlement noted at the footings due to erosion or unstable soils. Foundation wall damage - sections of the walls cracking, displaced, and missing, causing an inherent instability to the support for the building. Use caution when approaching or entering the building.
	Special Considerations for Coastal/High Velocity Floods		Coastal floods may have more evidence of scouring at the supports - the foundation system may be better designed to resist this scouring action. High-velocity floodwaters may create erosion/scouring that the building has not been designed to resist.			

2.5 Impact of Climate Change on Flood

Climate change may affect the magnitude and timing of floods. In a flood risk study, peak flow and sea level are the major concerns, either as deterministic boundary conditions for hydrology and hydraulic models or described as random variables to derive expected value over a given time.

In order to estimate the peak flow and sea level, precipitation and temperature are considered the two major climate change drivers. Precipitation is the main driver of riverine flood. Temperature is usually considered when modeling evapotranspiration, ice/snow melting and thermal expansion of oceans; ocean expansion is a less significant contributor for the regional water balance. The effect of individual components on sea-level rise can be assessed by the expected change in global temperature (Penning-Rowsell & Fordham, 1994).

Precipitation has increased by about 10% across the contiguous United States since 1910. Positive trends in the upper 10 percentiles of the precipitation distribution are responsible for over half (53%) of the total increase of precipitation. An increase in the intensity of the precipitation events is also significantly contributing (about half) to the precipitation increase (Karl & Knight, 1998).

Thorne et al. (2007) stated that decreases in average rainfall could also increase flood probability if the mean decrease is coupled with an increase in intensity or clustering of events. Based on a regression analysis, Choi and Fisher (2003) estimated that 1% increase in annual precipitation will cause 6.5% increase in annual flood loss in U.S. Based on the global scale analysis with grid resolution of 0.5 × 0.5°, Arnell and Gosling (2014) found that approximately 450 million people would be exposed to a doubling of flood frequency in 2050, based on one climate model pattern (HadCM3) and future scenario (A1b). The percentage change in the magnitude of the 100-year flood based on seven climate models (Figure 2-7) indicated consistent increases in flood magnitude in high latitude North America (Arnell & Gosling, 2014).

The general assumption for calibrating climate model is that if the model parameters and forcing are appropriate for the current climate, the model output should be close to the observed climate. The parameters can then be used to predict the climate change due to changes in the forcing (Penning-Rowsell & Fordham, 1994). Future climate projections are commonly used as input to hydrologic models to simulate future flows in the watershed. The use of a rainfall-runoff model assumes that the relationship between the rainfall and runoff captured by the model will be preserved in the future. By inputting a future precipitation scenario, the model predicted runoff is the best estimate of future floods. Therefore, the key to future flood assessment is to quantify the future precipitation.

For most regional rainfall-runoff models, the Regional Climate Models (RCMs) are the preferable input due to their higher spatial and temporal resolutions. The GCM projections must be downscaled to finer resolution for hydrological modeling. Statistical downscaling and dynamic downscaling can both serve this purpose (Fowler, Blenkinsop, & Tebaldi, 2007). Trinh et al. (2016) used bias corrected downscaled future precipitation data as the input to the hydro-climate model, WEHY, to simulate hourly flow along the main Cache Creek brank for 2010-2099. An increasing trend of flow was observed for the study period. Moglen and Rios Vidal (2014) explored the detention basin response to downscaled future precipitation. Greater uncontrolled peak discharge, controlled peak discharge were projected under future climate (Moglen & Rios Vidal, 2014). Lu, Qin, and Xie (2016) used a hybrid model based on automated regression-based statistical downscaling tool and K-nearest neighbor to downscale rainfall. Conditional Density Estimate Network was applied for downscaling minimum temperature and relative humidity from global circulation models (GCMs) to local weather stations. The projected weather information can then be used for flood risk study (Lu et al., 2016).

Climate change can also be characterized by change of the parameters of the frequency distribution of a physical variable such as precipitation or flood stage. Kharin and Zwiers (2005) treated the GEV parameters as a time dependent variable for annual extreme of precipitation and temperature. Gilroy and McCuen (2012) vary the GEV parameters to estimate the distribution of future precipitation. Boettle, Rybski, and Kropp (2013) assumed that increasing the location parameter of the GEV distribution of flood level reflects the sea level rise. In their study, the damage function is approximated by power laws; the expected damage of the case study site is derived as a function of varying location and scale parameters.

When discussing sea level rise, the difference between the two concepts, global mean sea level (GSL) and relative sea level rise (RSLR), sometimes causes confusion. GSL is the elevation of the ocean as an effect of large-scale warming, as reported in the Intergovernmental Panel on climate Change (ICPP)'s reports. RSLR describes the ocean relative to the land surface at a defined location, which combines the global effect and local factors such as local vertical land motion. Due to oceanographic and geophysical drivers, large spatial and temporal variability of RSLR is observed. Relative sea level is more applicable for local planning and flood risk assessment (Williams, 2013).

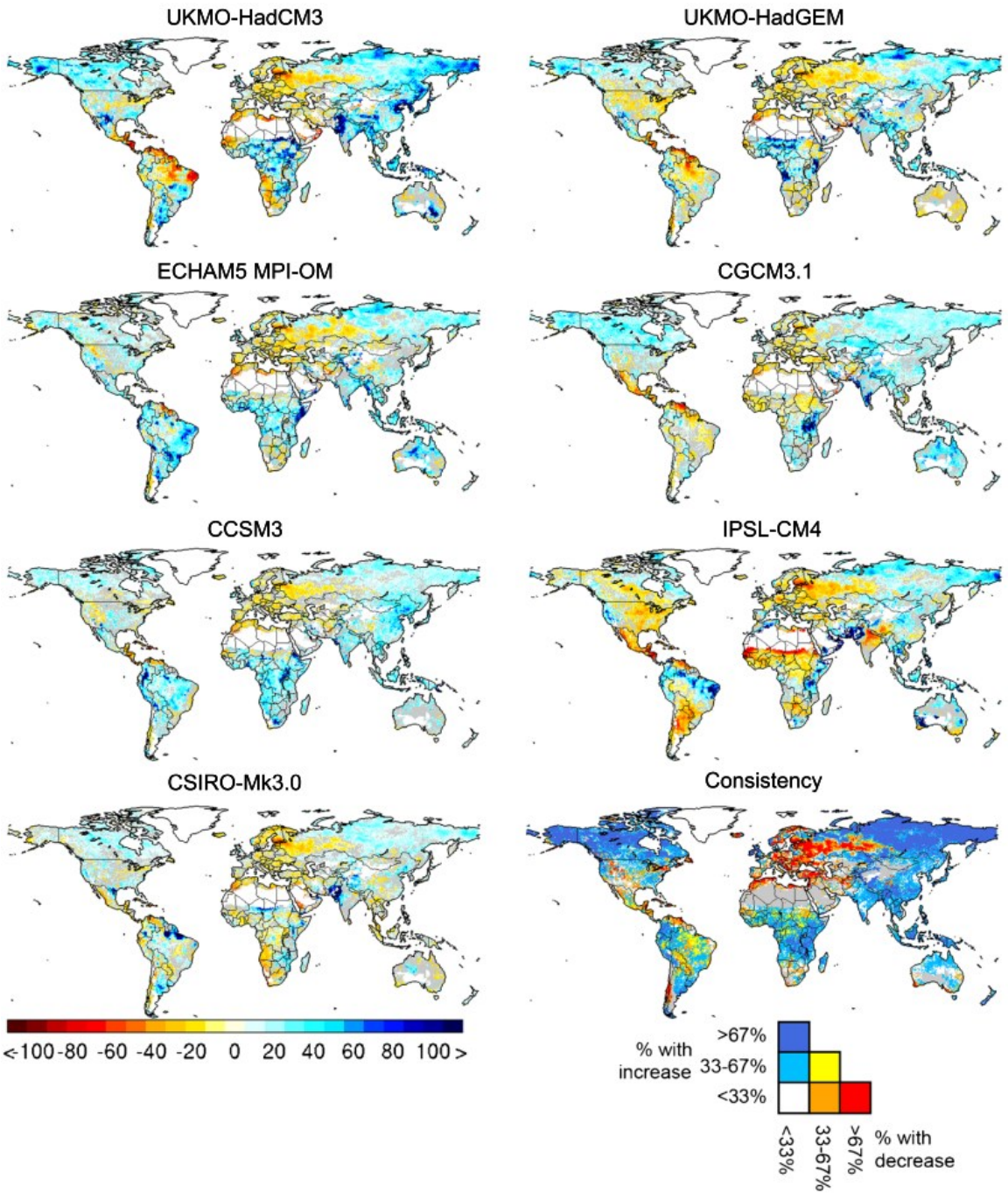

Figure 2-7. Percentage change of estimated 100-year flood under SRES A1b emissions in 2050 (Arnell & Gosling, 2014)

Note: Consistency is expressed as a percentage of the total number of models in projected change across 21 climate models (Arnell & Gosling, 2014).

For the Mid-Atlantic Region in the U.S., sea-level, temperature and stream flow are projected to increase due to higher level of atmospheric CO_2 (Najjar et al., 2000). As indicated by Najjar et al. (2000)'s summary in Table 2-10, the prediction of the stream flow is less certain due to the combined uncertainty of temperature, precipitation, CO_2 and their contribution to modeled streamflow (Najjar et al., 2000). For the Chesapeake Bay, Najjar et al. (2010) reviewed and synthesized the scientific literature on climate change and reported increases in sea level, CO_2 concentrations, and water temperature of 0.7–1.6 m, 50–160%, and 2–6 ^{o}C, respectively. The highest stream flow projection for the Northeast U.S. is around 30% (Najjar et al., 2010). Barros, Duan, Brun, and Medina Jr (2013) detected positive trends in annual maximum stream flow for the Atlantic Coastal Plain using the two-tail Mann-Kendall test. According to Armstrong, Collins, and Snyder (2014)'s Mann-Kendall trend test at p=0.05 level, 71% of study gauges in Mid-Atlantic region (53 out of 75) show increasing trends in annual maximum discharge; 75% of the study gauges (50 out of 67) show increasing trends in the occurrence of peak over threshold in a water year (POT/WY).

Table 2-10. Mid-Atlantic coastal region climate projections for 2030 and 2095 with respect to 1990 (Najjar et al., 2000)

Parameter	2030		2095		Reliability of mean prediction
	Mean	Range	Mean	Range	
CO_2 (%)[a]	+25	+20 to +30	+92	+52 to +118	Very high
(ppm)	+90	+70 to +105	+325	+185 to +420	
Sea level (cm)[b]	+19	+11 to +31	+66	+39 to +102	High
Temperature (°C)[c]	+1.3	+1.0 to +1.5	+4.0	+2.7 to +5.3	High
Precipitation (%)[c]	+4	−1 to +8	+15	+6 to +24	Medium
Streamflow (%)[d]	+2	−2 to +6	+11	−4 to +27	Low

[a]Mean reflects IS92a and range reflects IS92d and IS92f CO_2 emission scenarios; see Fig. 5b from technical summary of Houghton et al. (1996). 1990 CO_2 concentration was 355 ppm

[b]Low, middle and high projections of Warrick et al. (1996) for IS92a scenario with varying aerosols (see their Fig. 7.7), plus a local component of 2 mm yr^{-1}

[c]Range is given by Hadley Centre and Canadian Climate Centre (CCC) models for the mid-Atlantic region (Polsky et al. 2000). Mean is average of 2 models. Changes are with respect to 1983–1994 model output

[d]For the Susquehanna River Basin, using a water balance model forced with the CCC and Hadley output (Neff et al. 2000)

For the operating authorities in the United Kingdom, DEFRA (2006) proposed the regional net sea level rise allowance (Table 2-11) and indicative sensitivity ranges (Table 2-12) as guidance for sea level rise, rainfall, peak river flow, offshore wind speed and wave height change due to climate change. The uncertainty of DEFRA (2006)'s 20% adjustment is discussed by Kuklicke and Demeritt (2016).

Table 2-11. Regional net sea level rise allowance (DEFRA, 2006)

Administrative or Devolved Region	***Assumed Vertical Land Movement (mm/yr)***	***Net Sea-Level Rise (mm/yr)***				***Previous allowances***
		1990-2025	***2025-2055***	***2055-2085***	***2085-2115***	
East of England, East Midlands, London, SE England (south of Flamborough Head)	-0.8	4.0	8.5	12.0	15.0	6mm/yr* constant
South West and Wales	-0.5	3.5	8.0	11.5	14.5	5 mm/yr* constant
NW England, NE England, Scotland (north of Flamborough Head)	+0.8	2.5	7.0	10.0	13.0	4 mm/yr* constant

Table 2-12. Indicative sensitivity ranges (DEFRA, 2006)

Parameter	***1990-2025***	***2025-2055***	***2055-2085***	***2085-2115***
Peak rainfall intensity (preferably for small catchments)	*+5%*	**+10%**	*+20%*	*+30%*
Peak river flow volume (preferably for larger catchments)	+10%	**+20%**		
Offshore wind speed	*+5%*		**+10%**	*+10%*
Extreme wave height	*+5%*		**+10%**	*+10%*

2.6 Uncertainty

To avoid the 'garbage in, garbage out' situation in flood risk assessment, quantifying uncertainty is an important factor for flood risk analysis. The uncertainty imported into the flood damage estimate will be exported to the decision domain and affect the allocation of resources and project appraisal (Messner et al., 2007). USACE (1992) defined uncertainty as the situations in which the probability of potential outcomes and their results cannot be described by objectively known probability distributions, or the outcomes themselves, or the results of those outcomes are indeterminate.

The generic sources of uncertainty are lack of knowledge, statistical variation, measurement error and subjective judgement (Thorne et al., 2007). For hydrological flood damage modeling, the sources of uncertainty can be limited knowledge of system processes and the lack of accuracy when specifying model parameters to describe the natural processes (Platt, 1995). For example, the flow rate time series maybe too short to represent the historical flood record. Change may have occurred over time such that the historical data does not represent the natural regime. A statistical distribution inferred from a small sample may not adequately capture the tails of the distribution, representing possible extreme values.

Hall and Solomatine (2008) proposed a framework for uncertainty analysis in flood risk management (Figure 2-8). The major steps are (1) Establish purpose and scope of uncertainty analysis; (2) Identify and define uncertainties; (3) Assemble evidence about uncertainties; (4) Construct appropriate functions quantifying uncertainties; (5) Propagate uncertainties through to outputs of interest; (6) Store the results in a database; (7) Perform uncertainty-based sensitivity analysis; (8) Examine the effects of uncertainties on option choices; and (9) Report and discuss results (Hall & Solomatine, 2008).

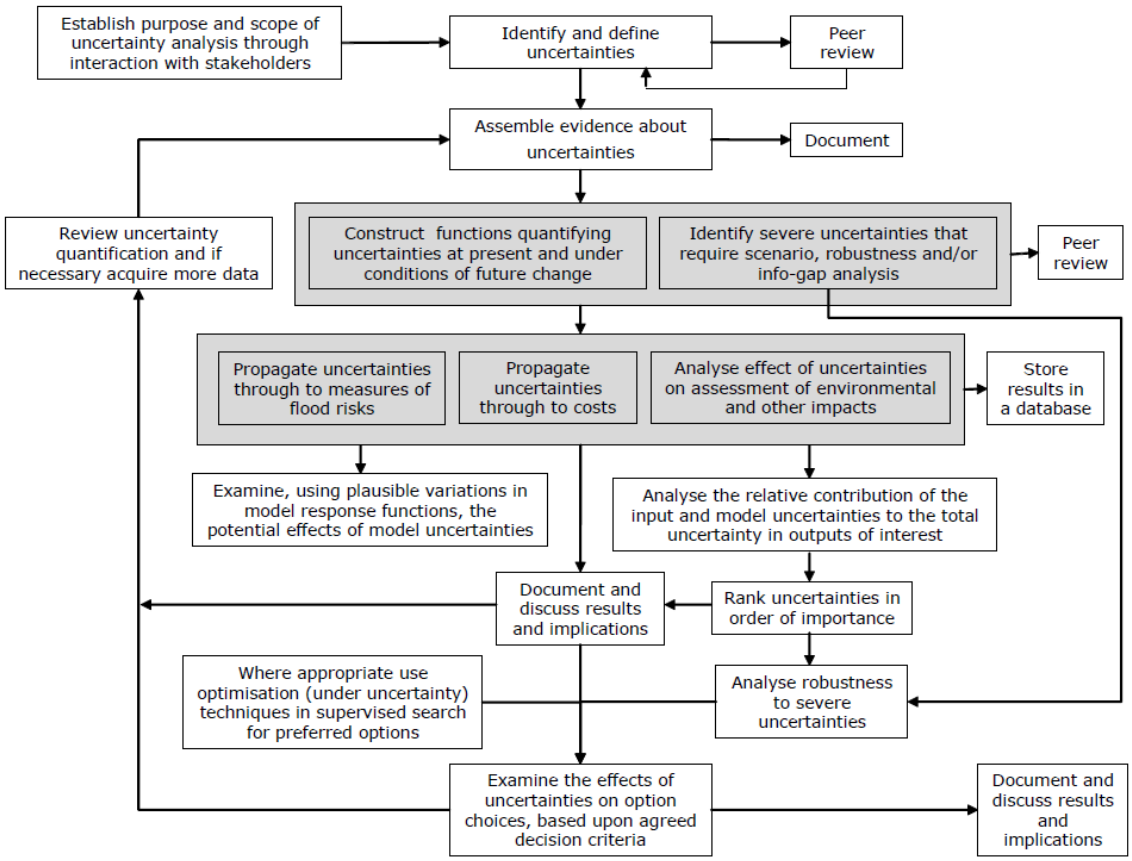

Figure 2-8. Uncertainty analysis framework (Hall & Solomatine, 2008)

With the development of quantitative computing tools and big data approach, researchers explored and documented uncertainty with diverse methods. Sensitivity analysis can be used to describe differences among alternatives, thus examine the uncertainty (Platt, 1995). It is one way to report the uncertainty, which is especially applicable when the truth is unknown or unknowable. Saint-Geours, Grelot, Bailly, and Lavergne (2015) developed a variance-based global sensitivity analysis method that considered the uncertainty propagation using Monte Carlo simulation. The digital elevation model uncertainties are modeled by Gaussian noise without spatial correlation; the uncertainties in annual maximum discharge data (short time series) are modeled by the confidence interval of the fitted discharge-frequency relationship; the uncertainty

of depth-damage curve is modeled by random multiplicative coefficients ranging from 0.5 to 1.5; and the project cost uncertainty is modeled by triangular distribution based on expert opinion (Saint-Geours et al., 2015). Info-gap theory starts from the best estimate of the future. As the actual conditions depart from expectation, alternative decisions are evaluated (Hall & Solomatine, 2008). This approach is applicable for the robust decision making in flood and climate change related decision analysis (Hall et al., 2012; Matrosov, Woods, & Harou, 2013). Fontanazza, Freni, and Notaro (2012) applied Bayesian uncertainty analysis to flood damage analysis and demonstrated that this approach is effective in defining model uncertainty. The model can be updated when new data are available and the uncertainty can then be reduced. In cases when the best model structure is unknown, Notaro, Fontanazza, Freni, and La Loggia (2014) applied the Bayesian model-averaging technique to flood damage models; the Bayesian model-average prediction performs better than the best single model. Su and Tung (2013) developed a framework for evaluating a flood-damage-mitigation project by considering epistemic uncertainty due to sampling error. In this study, the standard error of the Gumbel flood quantile was estimated by three parameter estimation methods. Uncertainty of the project net benefit was then evaluated. Hauptmanns (2010) treated the uncertainty of component failure rates as a log-normal distribution and propagated the uncertainty through a process plant flooding fault tree analysis. When the uncertainty of parameter is considered in a system, Monte Carlo simulation is often used to assess the uncertainty propagation (Jonkman, Van Gelder, & Vrijling, 2003).

Risk register is a table that records the risk number, risk type, description, likelihood, interdependencies, expected consequences, risk owner and risk status [Figure 2-9(a), HM Treasury (2003)]. The service disruption chart of Yu (2010) is an application of risk matrix to flood risk analysis. Five levels of service disruption are developed for wastewater and other six major infrastructure sectors for four flood events (Yu, 2010).

Consistent terminology on uncertainty is expected when preparing journal articles and research reports. Consistency in the usage of terms to describe probability estimates is necessary for a risk analysis project to avoid ambiguity (Kent, 1964). Manning (2006) suggested the treatment of uncertainties as risk matrix in the 'ICPP Uncertainty Guidance Note', which is adopted by Najjar et al. (2010), Mastrandrea et al. (2010), and many climate change studies. An example summary matrix is shown in Figure 2-9 (Mastrandrea et al., 2010).

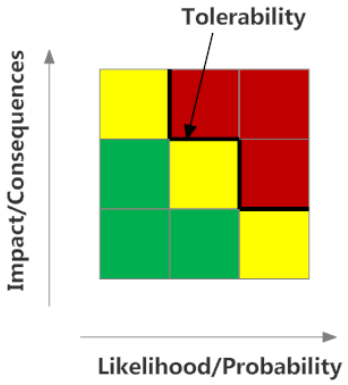

(a)

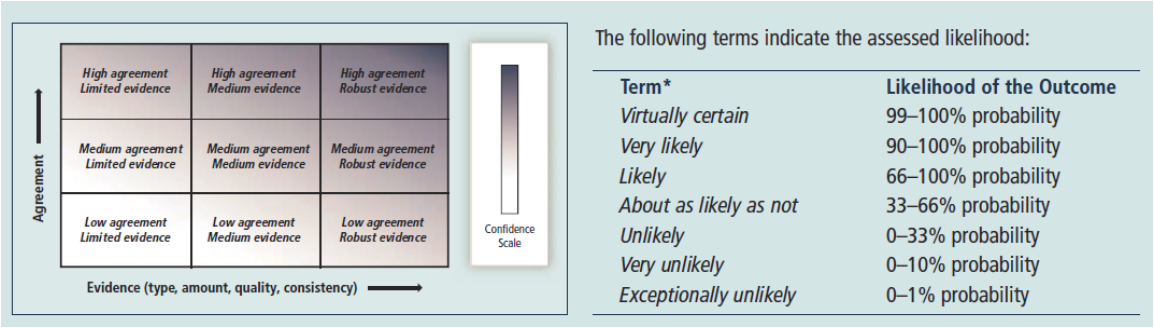

(b)

Figure 2-9. Risk matrix
(a) Risk register (HM Treasury, 2003); (b)Summary matrix of agreement, evidence and likelihood (Mastrandrea et al., 2010)

2.7 Flood Duration

2.7.1 Current Approaches to Quantifying Flood Duration

Flood duration is affected by hydro-meteorological factors, such as river size, morphological peculiarities of the valley, and formation of the riverbed (Kukharchyk, 2006). Only a limited number of studies have tried to quantify the likelihood of flood duration. This deficiency is partly due to the lack of a precise definition of flood duration.

Duration is sometimes defined as the fraction of time in a year that the water level is above a particular elevation. For example, Law (2002) developed a water-level duration curve for lowlands, sinkholes, caves, and wells by computing the percentage of time each water level is equaled or exceeded in a given year. A linear shape of an inundation curve indicates slow and constant drainage rates, while the commonly assumed exponential shape indicates fast and variable drainage rates.

Duration can also be defined as a fixed time interval that is applied to filter a stage time series. The duration filter method applies a moving window of a specified length of time and extracts the associated depth, discharge, or volume information. Variables such as maximum stage, average stage, total volume and average discharge are calculated within the moving time window, and analyzed statistically, analogous to depth- or intensity-duration-frequency (DDF or IDF) analysis of precipitation. For example, Javelle, Ouarda, and Bobée (2003) used the flood discharge-duration-frequency (QdF) study of Javelle et al. (2002), which involves a moving average window, to extract a new time series of the maximum stream flow for catchments in Quebec and Ontario, Canada. By using the time dependent parameters, Cunderlik and Ouarda (2006) tested the moving window concept and the QdF approach to a changing environment.

Finally, duration can be defined as the actual time that a flood event lasts. This definition requires identifying the points in time at which the flood event begins and ends. The methods

used to separate flood events and extract flood duration information can be grouped into the following two categories: (1) the rise-recession-method, which detects the time between the abrupt rise and flattening of the recession limb of the hydrograph; and (2) the threshold method, which extracts a time series of duration above or below a specified threshold. The first method is an event-based separation method. Yue (2001) applied the rise-recession method to the flood time series in Madawask Basin in Quebec, Canada. However, due to the irregular and asymmetric shape stage hydrographs, this method is hard to apply in a robust manner. The threshold method is a hydrological application of Theory of Runs, which is commonly used in drought likelihood analysis (Guerrero-Salazar & Yevjevich, 1975; Mishra & Singh, 2011; Shiau & Shen, 2001; Yevjevich, 1967). A run is a sequence of observation of one variable succeeded and preceded by values of another variable (Rodriguez-Iturbe, 1969). A time-run, which is a time-sequence of observations, provides a method to treat the hydrological data for frequency analysis (Yevjevich, 1967). A truncation level (Chang, 1990) is used to separate the time series positive and negative run-lengths (Guerrero-Salazar & Yevjevich, 1975), or upcrossings and downcrossings (Rodriguez-Iturbe, 1969). Because it can be implemented without manual analysis of event hydrographs, the threshold method holds great potential for frequency analyses associated with the actual flood event duration distribution.

Joint distribution functions are an approach to quantifying the association of flood duration and depth or volume. Javelle et al. (2002) used a Generalized Extreme Value (GEV) distribution to fit the T-year quantiles of discharge as a function of –ln(-ln(1-1/T)) for a set of defined durations. Yue, Ouarda, Bobée, Legendre, and Bruneau (1999) proposed a bivariate extreme value distribution with Gumbel marginals for the joint distribution of flood duration and volume. Yue (2001) characterized the joint distribution of flood volume and duration by a

bivariate gamma distribution. Copula functions have also been applied to estimate the bivariate joint distribution of flood duration and discharge (Bačová Mitková & Halmová, 2014).

The growing awareness of the importance of the time dimension in assessing flood risk, coupled with the limited body of literature on robust flood duration assessment urges the research needs on modeling the time dimension of the floods. Models that completely describe the flood duration characteristic and likelihood are needed. Such models would be especially valuable to those responsible for returning flooded facilities to full-scale operation.

2.7.2 Flood Duration Database

Flood duration sample data can be obtained by observations, reported by the local witnesses of a flood event, or recorded by instrumentation, such as stream gauges. Analogous to the high water mark in flood depth observation, duration of flood can be determined by visual inspection, local information/witness, bulletin issued by environment agency, environment agency, water authority, public health of local authority (Soetanto & Proverbs, 2004).

Databases can be developed for recording the flood observations. The U.S. Flash Flood Observation Database records the start time, end time, and peak time based on USGS stream gauge data and the National Weather Service Storm reports (Gourley et al., 2013). The duration of large floods from 1985 to present are presented in the Global Active Archive of Large Flood Events Database of the Dartmouth Flood Observatory (Brakenridge, 2010). In FEMA (2015)'s Flood Risk Database (FRD) table of dam release scenarios (L_Dams_XS_MDL_Results), one attribute is TIME_DUR, the time of the duration of the flood wave measured in minutes. In this database, a raster dataset (the dam release flood inundation duration grid) shows the times at which a flood wave arrives at, passes through, and leaves a particular location.

2.7.3 Flood Duration as a Predictor Variable for Flood Damage

Flood duration is a key predictor variable for flood damage models. Based on the survey of floodplain residence in Ontario, McBean, Gorrie, Fortin, Ding, and Monlton (1988) concluded that the total damages should be increased by 6% for longer duration floods (taken as greater than 24 hours). The increment of damage is mainly due to the structures with basement (McBean et al., 1988). The tangible flood losses are illustrated by Thieken et al. (2008) as space-time diagrams, as shown in Figure 2-10.

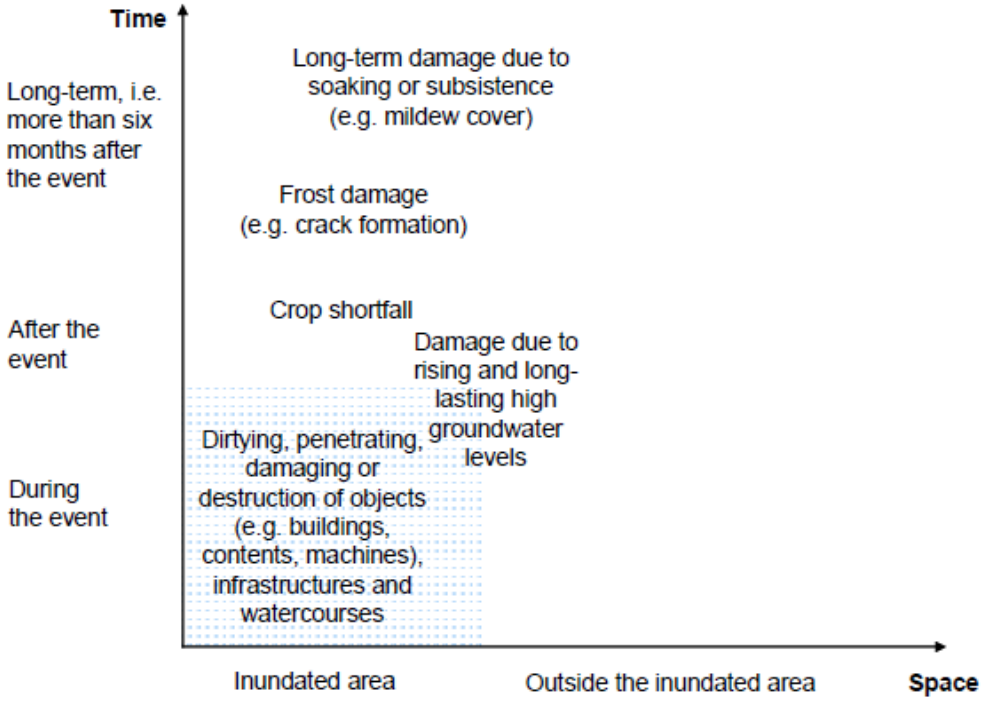

(a)

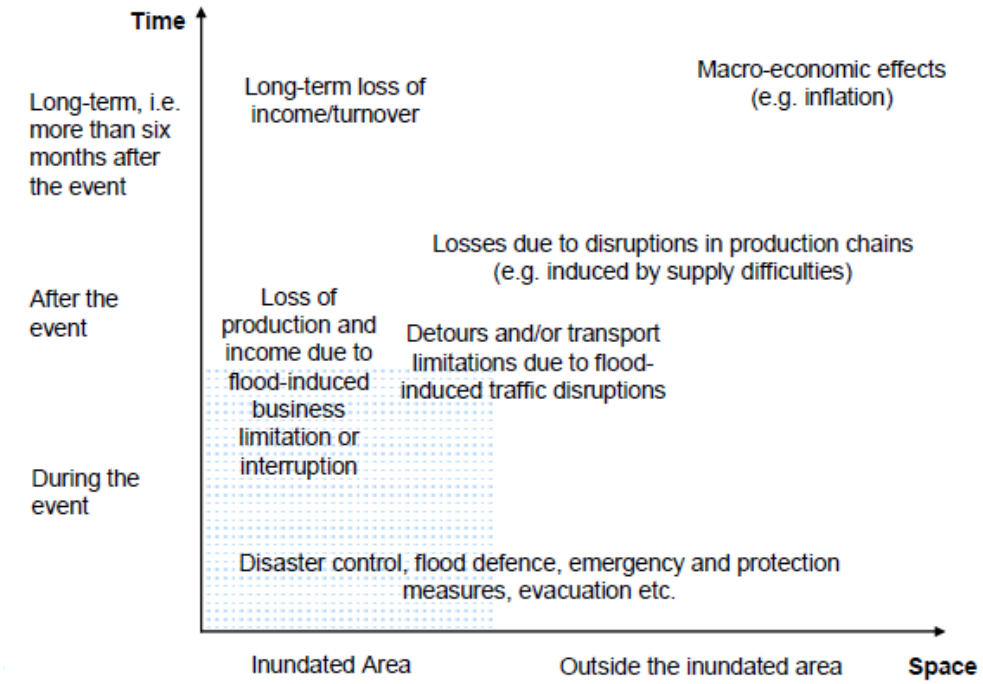

(b)

Figure 2-10. Spatial and temporal occurrence of tangible flood losses (a) direct (b) indirect (Thieken et al., 2008)

Flood duration is mostly treated as an interval or threshold in the current flood damage models and handled as a modifier. Penning-Rowsell and Chatterton are the pioneers to consider flood duration in the flood damage assessment (Penning-Rowsell & Chatterton, 1977). Two flood damage curves are plotted against flood depth, one for duration exceeding 12 hours and the other for duration below 12 hours (Penning-Rowsell & Chatterton, 1977; Penning-Rowsell & Wilson, 2003; Smith, 1994). In the FEMA Substantial Damage Estimator (SDE), the 12 hour flood duration threshold is a criterion for estimating percent interior and plumbing damage as functions of depth for non-residential structure (FEMA, 2013a). For the Methods for the Evaluation of Direct and Indirect Flood Losses (MEDIS) Project, inundation duration is classified into 4 categories (1-3 days, 4-7 days, 8-11 days, > 11 days) for the agricultural damage model. The flood inundation duration is coded into a damage impact factor, which is a multiplier of the overall damage function (Förster,

Kuhlmann, Lindenschmidt, & Bronstert, 2008; Pfurtscheller & Schwarze, 2008; Thieken et al., 2008). In Hazus, a duration modifier is used to estimate crop damage. It is developed for a set of duration factors for 0, 3, 7, and 14 days (FEMA, 2009):

$$Initial\ Loss = Yield\ in\ flooded\ area \times \$ \times \%\ damaged\ crop \tag{2-28}$$

$$Duration\ Loss = Initial\ Loss \times duration\ modifier \tag{2-29}$$

In the 1993 floods in Story County, Iowa, crop loss was attributed to potholes - the standing water from accumulated rainfall (FEMA, 2009). The flood loss is estimated by

$$L = A\left(pY_0 - H\right)\cdot D(t)\cdot R(t) \tag{2-30}$$

where L is loss ($), A is cultivated area (acres), P is price ($/bushel), Y_0 is normal annual yield (bushels/acre), H is harvest cost ($/acre), $D(t)$ is crop loss at day t of the year (% of maximum net revenue), and $R(t)$ is the crop loss modifier for flood duration (percent of maximum potential loss) (FEMA, 2009).

Nicholas, Holt, and Proverbs (2001) proposed a flood damage repair index for building properties. It is a function of flood characteristics and building characteristics. Along with the velocity and contaminant content of flood water, duration of flood is one of the three predictor variables to describe the flood characteristics.

Dutta et al. (2003) modeled traffic interruption loss due to flood by marginal cost (*MC*) and delay cost (*DC*). They are both functions of flood duration.

$$MC = \sum_{i=1}^{n}\left[\sum_{j=1}^{m}[E_l(i)\left\{a(j) + \frac{b(j)}{v(i,j)} + c(j)v(i,j)^2\right\}T_v(i,j)td]\right] \tag{2-31}$$

$$DC = \sum_{i=1}^{n}\left[\sum_{j=1}^{m}[E_l(i)v(i,j)Dc(i)T_v(i,j)td]\right] \tag{2-32}$$

where n is number of roads flooded; m is mode of transport in any road I; $E_l(i)$ is extra length to be covered due to floodwater in road i; $a(j)$, $b(j)$ and $c(j)$ are fuel consumption related constants for mode of transport j; $v(i,j)$ is average speed of model of transport j at road i; T_v is total volume

of traffic for mode of transport j in road i per hour; t is total duration of flood in hours; d is factor to consider the variation of traffic volume in weekdays and weekends; and D_c is delay cost per unit time for road i.

Emergency cost during flood event is related to flood duration. Based on a catastrophic flood event in the alpine province (Tyrol, Austria) in 2005, Pfurtscheller and Schwarze (2008) developed regression models for cleanup cost.

$$\begin{aligned} &\log\ (CLEAN\ UP) \\ &= 2.35\ +\ 0.06\ \log\ (INHAB)\ -\ 0.14\ \log\ (AREA) \\ &+ 0.37\ \log\ (INUND)\ *+\ 0.37\ (DAYS) +\ 0.43\ (ADD\ HAZ)\ \ +\ \varepsilon \end{aligned} \tag{2-33}$$

where $CLEAN\ UP$ is the cleanup cost; $INHAB$ is the number of inhabitants; $AREA$ is the settlement area; $INUND$ is the inundation area; $DAYS$ is the duration of flood in days and $ADD\ HAZ$ measures the occurrence of multiple extremes such as debris flows, rock falls, etc; and ε is the prediction error.

Socio-economic assessment of flood damage, such as mortality, can be expressed by dose response function, such as Probit function (*Prb*), which is also driven by duration (Jonkman, 2007).

$$Prb\ =\ a\ +\ b \times \ln(c^n t) \tag{2-34}$$

$$F_D(Prb) = \Phi_N\left(\frac{Prb - \mu_D}{\sigma_D}\right) \tag{2-35}$$

where a, b, and n are probit constants; c is concentration; t is the exposure duration. Φ_N is the cumulative normal distribution; and Prb is the probit value.

2.8 Flood Impact on WWTPs

The municipal wastewater treatment flooding can be trigged by (1) riverine flooding; (2) storm surge; (3) heavy precipitation and extreme influent sewer; and (4) internal flooding by accident.

These events are highly likely to occur simultaneously. According to Ten Veldhuis and Clemens (2010)'s study based on the municipal calls on urban drainage incidents, 3.4 % of the flood are wastewater related.

Floods may cause the following problems for a municipal wastewater treatment plant (Copeland, 2005; Sanders, 1997): shortage or loss of electric supply, functional loss of essential equipment, loss of communication and process control systems, restrictions to access, overload of the treatment system due to extreme storm water influx, backwater effects at plant outfalls, chemical and/or fuel leakages or overflows, disturbance of biological environment of the treatment processes. Any of these factors can cause a total or partial shutdown of WWTP processes and operation. The treatment capacity loss can result in significant environmental damage as well as public health problems (Table 2-13).

Table 2-13. Onsite wastewater treatment system related hazard and contributing factors

Item	Key hazard	Contributing factors
Wastewater treatment site	Release of contaminants due to failure of onsite wastewater treatment system	Soil; Planning (lot size); Environmental sensitivity; Flooding; Topography; Loading rates
Surrounding soil	Inability to renovate effluent and prevent contaminants from reaching groundwater and/or surface water	Soil type; Depth of soil horizons; Physical characteristics; Chemical characteristics; Water table depth
Public health	Contamination of water/surrounding environment such that a considerable health risk is evident due to the release of contaminants (namely pathogens) which have an impact on human health	Surface exposure; Water supply (ground surface); Aerosols; Pests (mosquitoes, etc.)
Environmental	Release of contaminants into the receiving environment (ground/surface waters) causing environmental degradation (such as eutrophication) and causing the environment to be unsuitable	Surface runoff; Groundwater discharge; Flooding; Water table

Source: Carroll et al. (2006)

During the 1993 Midwest U.S. flood, 109 wastewater treatment facilities in the state of Missouri experienced damage or service interruption, ranging from minor operational problems to complete inundation (Sanders, 1997). One month after the occurrence of Hurricane Katrina, Louisiana officials estimated that $35 billion was needed to restore the wastewater treatment infrastructure in the state, with an assumption that 50% of the wastewater treatment plants and 20% of the sewage collection systems would need to be rebuilt (Copeland, 2005).

Recently, the 2012 superstorm Sandy that impacted many populated parts of the East Coast highlighted the effects of extreme events on urban flooding and critical infrastructure in urban/suburban areas. For New York State, an estimated $1.1 billion was needed to repair the treatment plants damaged by Hurricane Sandy (Schwirtz, 2012). The underground tunnels and galleries of the Newark Bay Treatment Plant were inundated by over 200 million gallons of flood water (State of New Jersey Passaic Valley Sewerage Commission, 2013). Engines for the main pumping system in Bay Park sewage treatment plant were under 12 feet of water in less than 30 minutes. Nine feet of saltwater surged into the plant's basement and sub-basement (Figure 2-11). Wastewater overflowed into low-lying streets and homes, causing environmental and public health problems. Seventy-five million gallons of untreated wastewater flowed from Middlesex County Utility Authority Plant (Sayreville, N.J.) into Raritan Bay for nearly a week before power was restored (Schwirtz, 2012). More than 50,000 gallons overflow was estimated for three location in the Lexington Park sewerage system on October 29, 2012 (St. Mary's County Metropolitan Commission, 2012). Structural and functional damage of the municipal wastewater treatment plants in New Jersey and New York has brought attention to the urgent need for a systematic method of infrastructure vulnerability assessment and the development of response/recovery plans.

Figure 2-11. Underground tunnel inundation of Bay Park Sewage Treatment Plant (Hazen and Sawyer, 2012)

During Hurricane Sandy, eleven billion gallons of untreated and partially treated sewage polluted receiving waterbodies (Kenward et al., 2013). Table 2-14 summarizes the bypass flow, plant down time and flood impact on selected WWTPs (City of New York, 2016; Climate Central, 2014; Kenward et al., 2013; State of New Jersey Passaic Valley Sewerage Commission, 2014).

Table 2-14. Impact of Hurricane Sandy on municipal wastewater treatment plants

	Location	Receiving waterbody	Design capacity (MGD)	Consequences	Untreated sewage (MGD)	Partially treated sewage (MGD)	Duration of completely shutdown (day)	Duration of partially shutdown (day)
Bay Park Sewage Treatment Plant	Nassau County, Long Island, NY	Rockaway Bay	400	Underground tunnel inundated; equipment damaged	104	2200	1.83	44
Yonkers Treatment Plant	Westchester, NY	Hudson River		Basement chambers flooded and power cut; motor removed, disassembled, and dried; wires corroded by the salt water and completely replaced	49	1200	0.58	14
Passaic Valley Sewage Commission	Newark, NJ	Newark Bay	330	4-foot wall of water hit the plant, destroyed buildings, flooded underground substructure, washed away vehicles short-circuited automated systems, and damaged essential equipment.	840	3000	7.00	14
Yonkers Joint Wastewater Treatment Plant	Yonkers, NY	Hudson River		Power out	1100			14
Sayreville Pump Station (Middlesex County Sewage Authority)	Sayreville, NJ	Washington Canal		Two pumping stations damaged	1200			90
O Street Combined Sewer Overflow	Washington, D.C.	Anacostia River		Overflow in the city's combined sewer system	30, 475			
Bridgeport Sewage Treatment Plants	Bridgeport, CT	Pequonnock River			17	2.5		
Mystic Sewage Treatment Plant	Stonington, CT	Mystic River				2.3		
City of Lewes Wastewater Treatment Plant	Lewes, Delaware	Delaware Bay		Plant shutdown to prevent further losses		2.4		
Little Patuxent Water Reclamation Facility	Savage, MD	Little Patuxent River		Power loss; on-site emergency generator ran out of fuel within a few hours	19.5			
Town of Snow Hill Wastewater Treatment Plant	Worcester, MD	Pocomoke River		Plant flooded	2.4			

Continue Table 2-14

	Location	Receiving waterbody	Design capacity (MGD)	Consequences	Untreated sewage (MGD)	Partially treated sewage (MGD)	Duration of completely shutdown (day)	Duration of partially shutdown (day)
The Coney Island Wastewater Treatment Plant	Coney Island, NY	Sheepshead Bay	110	Inundated	213	284	0.08	1
The Oakwood Beach Wastewater Treatment Plant	Staten Island, NY	Lower New York Bay	39.9	Key electrical equipment damaged		237.5		4
Rockaway Wastewater Treatment Plant	Queens, NY	Jamaica Bay	45			201		
Hunts Point Wastewater Treatment Plant	Bronx, NY	Upper East River	200		153.8			
Newtown Creek Wastewater Treatment Plant	Brooklyn, NY	East River	310	Inundation; out of power--operated by backup generators and electrical turbines	143			
26th Ward Wastewater Treatment Plant	Brooklyn, NY	Jamaica Bay	26	Power cut to prevent further damage		89		
North River Wastewater Treatment Plant	New York, NY	Hudson River	170	First floor of plant inundated; pump out	83			
Owls Head Wastewater Treatment Plant	Brooklyn, NY	Upper New York Bay	120	Power loss		76.2		
Port Richmond Wastewater Treatment Plant	Staten Island, NY	Kill Van Kull	60	Equipment damaged		30		
Bucklin Wastewater Treatment Facility	East Providence, Rhode Island	Seekonk River		Power loss		17.5		
Middletown's Wave Avenue Pumping Station	Rhode Island					0.075		
Newport's Wellington Avenue CSO structure	Rhode Island				0.76			
Front Royal Wastewater Treatment Plant	Front Royal, VA	Shenandoah River	6		5.3			

Source: Climate Central (2014); Kenward et al. (2013); City of New York (2016); State of New Jersey Passaic Valley Sewerage Commission (2014)

3 UNIVARIATE FLOOD STAGE-FREQUENCY ANALYSIS INCORPORATING CLIMATE CHANGE[1]

3.1 Overview

Climate change and sea level rise are expected to alter the likelihood of extreme events, such as floods, within the design lifetime of infrastructure components. Critical civil infrastructure facilities, including wastewater treatment, transportation, and energy, need site-specific flood contingency plans that reflect the effects of changing climate. In this section, a sensitivity analysis method is developed to assess future flood risk by estimating flood frequency under conditions of higher sea level and stream flow response to increased precipitation intensity. The method was applied to an ungauged location on a tidal estuary in the Mid-Atlantic region as a case study.

One-dimensional steady and unsteady flow analyses were performed using the Hydrologic Engineering Center's River Analysis System (HEC-RAS) to predict discharge rates and water surface elevations along an estuary reach, subject to prescribed boundary conditions of upstream discharge and downstream water surface elevation. For the steady flow analysis, the discharges and water surface elevations associated with specific return period were applied as the upstream and downstream boundary conditions. For the unsteady flow analysis, a current-climate flood stage frequency curve was estimated for the study site based on simulations of high-flow events in the 18 years for which simultaneous upstream and downstream records were available.

To develop the future climate-based stage frequency curves, the simulations were repeated, applying additive Water Surface Elevation (WSEL) perturbations at the downstream

[1.] A version of this chapter has been published. This chapter is expanded from the published manuscript.

Feng and Brubaker (2016). "Sensitivity of Flood-Depth Frequency to Watershed-Runoff Change and Sea-Level Rise Using a One-Dimensional Hydraulic Model." J. Hydrol. Eng., 10.1061/(ASCE)HE.1943-5584.0001378, 05016015.

boundary (to represent anticipated sea level rise) and multiplicative event discharge perturbations at the upstream boundary (to represent anticipated change in watershed hydrology). The perturbations were applied separately and together. Revised flood stage frequency curves were calculated for each set of perturbations.

3.2 Study Site

The study site is a 370 MGD municipal wastewater treatment plant, the Blue Plains Advanced Wastewater Treatment Plant (BPAWWTP). It is located on the southern tip of the District of Columbia, and on the left bank of the Potomac River (Figure 3-1). The drainage area of the study site is 11,890 mi^2. The Anacostia River flows into the Potomac River above the BPAWWTP, with a minor contribution of 122 mi^2. During a flood event, the river water surface elevation (WSEL) at the study location can be affected by the upstream freshwater input from the Potomac and Anacostia Rivers, the downstream tidal surge from the Chesapeake Bay, or both (Figure 3-2). The tidal-riverine boundary is believed to be close to the Little Falls. The Potomac River at Little Falls has a drainage area of 11,560 mi^2. The WWTP's upstream processes are generally at higher ground elevation than the downstream processes (Figure 3-3). Thus, the downstream processes are more vulnerable to floods. In addition, the facility would be vulnerable to both surface and underground inundation in a major flood event. Surface flooding can disrupt WWTP processes and operator access/egress. In addition, water can enter underground tunnels and galleries (indicated by polygons in Figure 3-3) if the surface water level rises to the elevations of hatches, stairs, or head houses (indicated by red dots in Figure 3-3). Essential equipment that are underground may be damaged by inundation (Figure 3-4). Disruption to service can contribute to significant environmental damage by way of environmental overflows of untreated or partially treated wastewater.

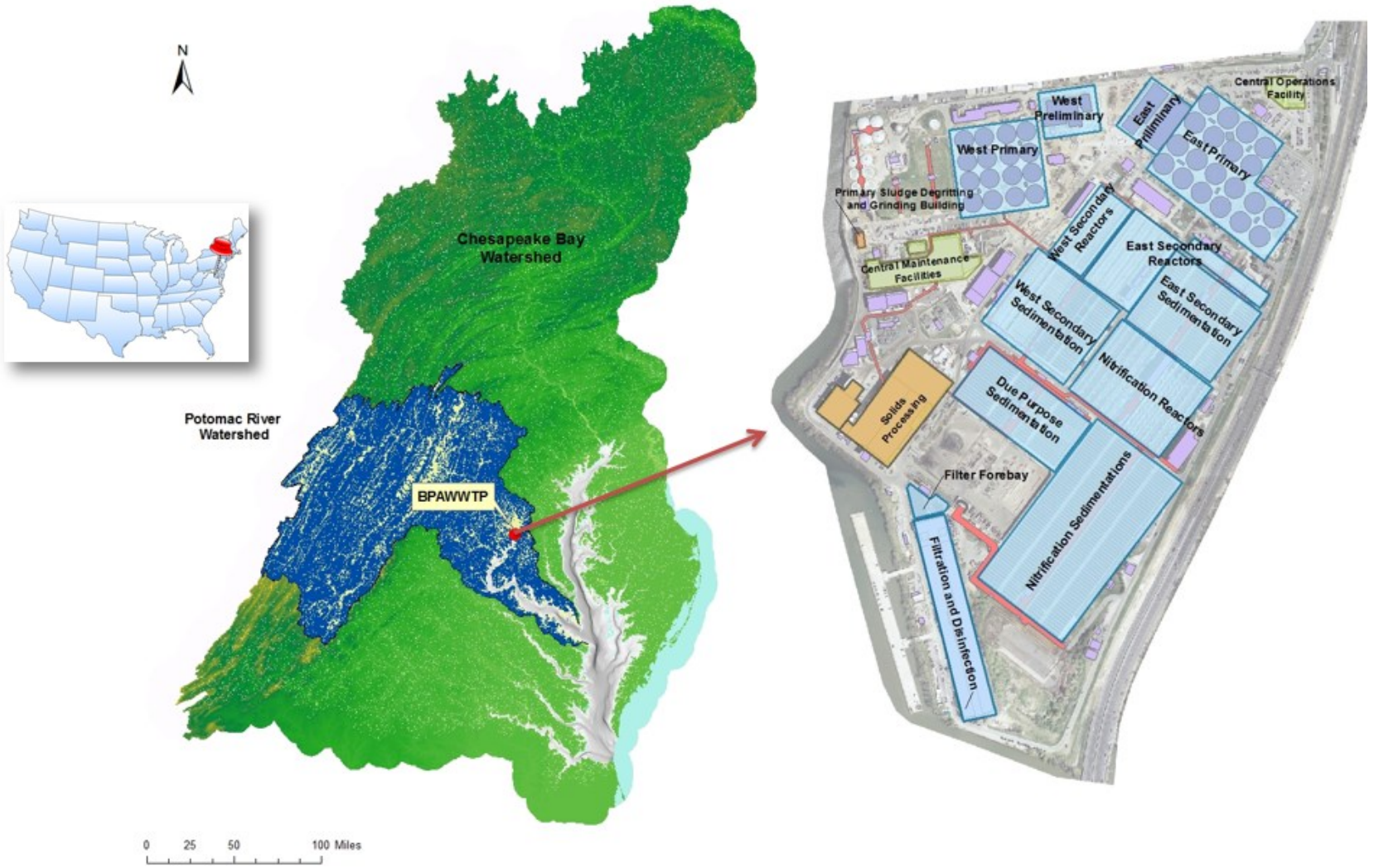

Figure 3-1. Location of the study site

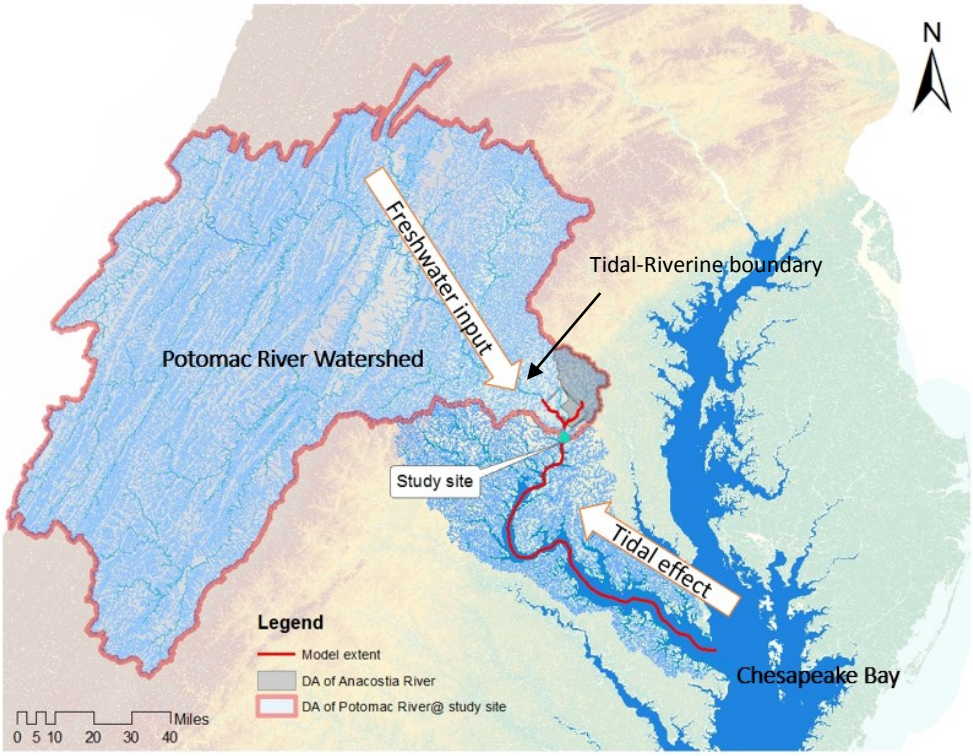

Figure 3-2. Freshwater and tidal effect of Potomac River at the study site

Figure 3-3. Vulnerable points of the study site (Elevation values are relative to North American Vertical Datum 1988)

Figure 3-4. Essential equipment inside the tunnel and gallery

3.3 Steady and Unsteady Flow Simulation

The Hydrologic Engineering Center's River Analysis System (HEC-RAS), version 4.1.0., developed by the US Army Corps of Engineers (USACE), was the modeling environment used for this study. HEC-RAS is a hydraulic analysis software currently supported and upgraded by USACE. It is widely used for analyses of open channel hydraulics, water surface profile computations, floodplain mapping, dam breach analysis, and sediment transport analysis [Cook & Merwade, 2009; Knebl, Yang, Hutchison, & Maidment, 2005; Pappenberger et al., 2006; Suriya & Mudgal, 2012; U.S. Army Corps of Engineers Hydrologic Engineering Center (USACE HEC), 2014; Yerramilli, 2012]. The software package and its GIS extension, HEC-GeoRas, are available to the public free of charge. The U.S. Army Corps of Engineers' Hydrologic Engineering Center Data Storage System (HEC-DSS) is a database system used to store the HEC-RAS input and output sequential data, such as the time series of unsteady flow boundary input. In this chapter, one-dimension steady and unsteady

flow analyses are performed to estimate the flood stage and frequency for the current and future climate.

For the steady flow analysis, the conveyance corresponds to the ability of a cross section to convey flow.

$$Q = KS_f^{1/2} \tag{3-1}$$

$$K = \frac{1.468}{n} AR^{2/3} \tag{3-2}$$

where K is conveyance; S_f is the friction slope; n is Manning's roughness coefficient; A is the flow area (ft^2); and R is hydraulic radius (ft). Each cross section is subdivided into three components, left overbank (LOB), right overbank (ROB) and the main channel (CH). The Manning's coefficients for the model extent of Potomac River and the Anacostia are listed in Table 3-1. K is calculated separately for the three subdivisions. The summation of the conveyance is then used for computing the flow (Brunner, 2010).

Table 3-1. Manning's coefficients for the Potomac River HEC-RAS model

River	Reach	Max Manning's coef			Min Manning's coef		
		LOB	CH	ROB	LOB	CH	ROB
Potomac River	Upper reach	0.070	0.049	0.070	0.049	0.028	0.049
Potomac River	Lower reach	0.025	0.021	0.025	0.0175	0.015	0.0175
Anacostia River	Lower reach	0.016	0.015	0.016	0.016	0.015	0.016

The standard step method is used to solve the energy equation iteratively to calculate the water surface elevation (WSEL) from one cross section to the next.

$$Z_2 + Y_2 + \frac{\alpha_2 V_2^2}{2g} = Z_1 + Y_1 + \frac{\alpha_1 V_1^2}{2g} + h_e \tag{3-3}$$

where Z_1 and Z_2 are the elevation of the main channel inverts; Y_1 and Y_2 are the depth of water at the cross sections; V_1 and V_2 are the average velocities; α_1 and α_2 are the velocity weighting coefficients; g is the gravity acceleration; and h_e is the energy head loss (Brunner, 2010).

The energy loss between the two cross sections comprises the friction loss, the first term in Eq. (3-4), and the contraction and expansion losses, the second term in Eq. (3-4).

$$h_e = L\overline{S_f} + C\left|\frac{\alpha_2 V_2^2}{2g} - \frac{\alpha_1 V_1^2}{2g}\right| \tag{3-4}$$

$$L = \frac{L_{lob}\,\overline{Q_{lob}} + L_{ch}\,\overline{Q_{ch}} + L_{rob}\,\overline{Q_{rob}}}{\overline{Q_{lob}} + \overline{Q_{ch}} + \overline{Q_{rob}}} \tag{3-5}$$

where L is the discharge weighted reach length; $\overline{S_f}$ is the representative slope between two cross sections; C is the expansion or contraction loss coefficient; L_{lob}, L_{ch}, L_{rob} are the cross section reach lengths specified for flow in the left overbank, main channel, and the right overbank, respectively; $\overline{Q_{lob}} + \overline{Q_{ch}} + \overline{Q_{rob}}$ is the arithmetic average of flows between sections for the left overbank, main channel, and the right overbank, respectively (Brunner, 2010).

The interactive procedure of the steady flow analysis starts by assuming a water surface elevation at the upstream cross section (if subcritical) and computing the total conveyance [Eq.(3-2)], velocity head, representative slope $\overline{S_f}$ [Eq.(3-1)], and then solving Eq. (3-3) for the energy loss, h_e [Eq.(3-4)]. The downstream water surface elevation, Z_2+Y_2, is then solved by Eq. (3-3). The value is compared with the assumed water surface elevation and the iterative procedure is repeated until a user-defined tolerance is satisfied. Note that the energy equation is only applicable to gradually varied flow. If the flow passes through critical depth, the momentum equation is applied (Brunner, 2010).

For the unsteady flow analysis, the principle of conservation of mass, represented by the continuity equation, and the principle of conservation of momentum, represented by the

momentum equation, are the governing physical laws (Brunner, 2010). The implicit finite difference scheme is used to solve the one-dimensional unsteady flow equations. The details are explained in Brunner (2010).

3.4 Model Input

The HEC-RAS 1D hydraulic model requires three types of input: geometry, boundary conditions, and parameters. A calibrated HEC-RAS model was provided by the NOAA NWS Middle Atlantic River Forecast Center (MARFC) (Mashriqui, Halgren, & Reed, 2014); this study used the MARFC's geometry upstream of the Potomac/Anacostia confluence, and generated new river cross sections for the tidal Potomac. The model extent is illustrated in Figure 3-5.

3.4.1 Model Geometry

A seamless bathymetric and topographic digital elevation model (DEM) was developed by combining 1/3 arc-second (about 10 meter) digital elevation raster data from the National Elevation Dataset (NED) with the National Ocean Service's (NOS) Estuarine Bathymetry product with a grid resolution of 30 meters (NOAA, 2012). The NOS bathymetry dataset is available for a section of the Potomac River that is downstream of the District of Columbia (Figure 3-5). The NED uses the North American Vertical Datum of 1988 (NAVD88), and the NOS Bathymetry uses a tidal datum, mean lower low water (MLLW). Transformation grids provided by VDatum (NOAA, 2013b) were resampled to match the cell size of the bathymetry dataset and then used for datum conversion between MLLW and NAVD88. The NOS bathymetry raster was then mosaicked to the NED land topography raster.

The geometry input, including the cross sections, reach lengths, and bank points, were prepared using HEC-GeoRas and ArcGIS (Figure 3-6). The cross sections were cut from the

mosaicked continuous surface described above. Bank points were defined by the intersection of the cross-section cutlines with the National Hydrography Dataset (NHD) Stream/River boundary (USGS, 2013). For the river reaches outside the extent of the bathymetry data, the MARFC cross-section geometry was preserved.

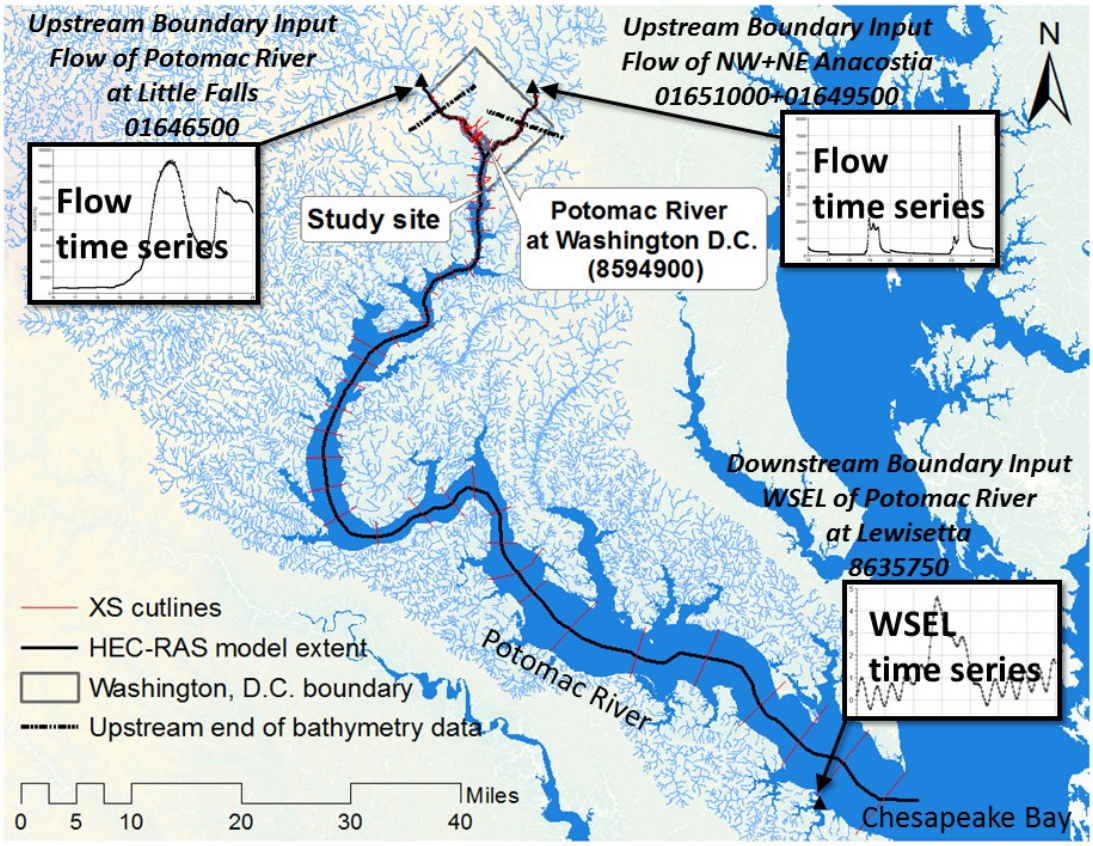

Figure 3-5. HEC-RAS model extent

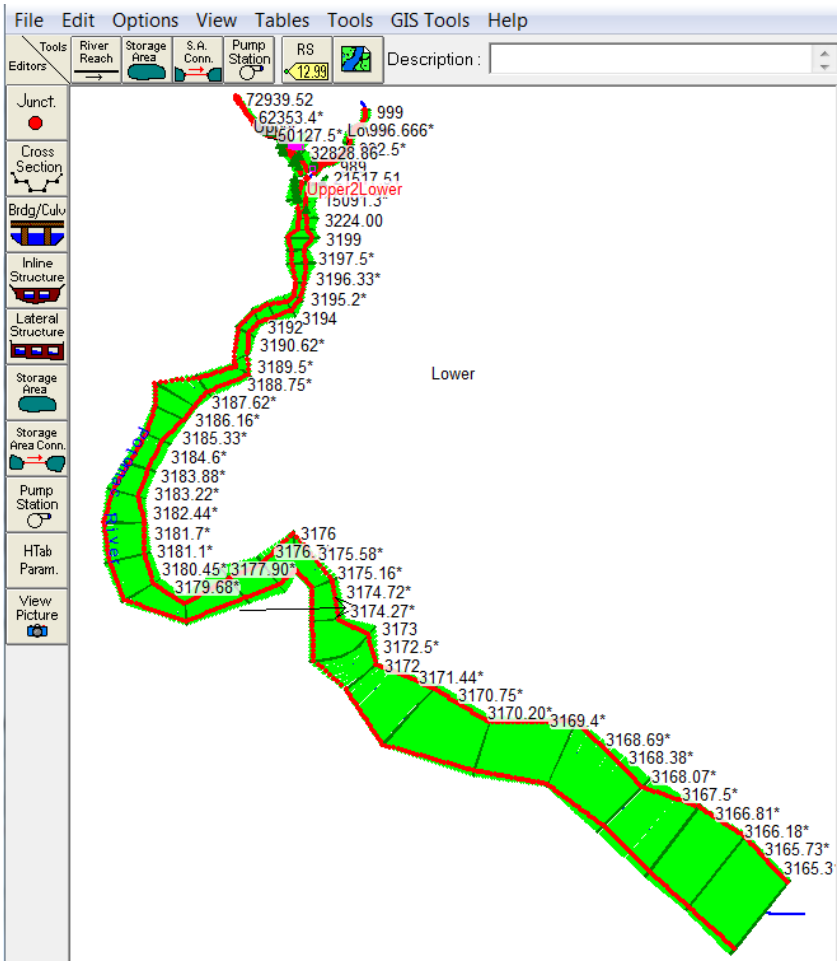

Figure 3-6. HEC-RAS model geometry input

3.4.2 Boundary Conditions

3.4.2.1 Gauge Selection

The hydraulic computations require boundary condition inputs of flows or water surface elevations at the open ends of the river system. Measured gauge data are the best available information for prescribing boundary conditions. The gauges to provide appropriate boundary conditions for hydraulic modeling need to be selected by the following criteria: long record length, time series resolution, location, and gauge continuity/calibration. These criteria are discussed below.

(1) Long record length

A longer annual peak time series provides a larger sample size, thus leading to greater confidence in the frequency analysis. Therefore, gauges with longer records are desirable for setting up the boundary conditions. According to FEMA (2002), annual maximum flood record with a record length equal to or longer than 10 years could be used to estimate probabilities on gaged streams. The gauge sites near the study site with data records longer than 10 years are listed in Table 3-2.

Table 3-2. Description of the riverine and tidal gauge sites near the study site

Site name	Station ID	Data type	Data available period	Gauge type	Drainage area (mi^2)
Potomac River near Washington, D.C. Little Falls Pump Station	1646500	Discharge (hourly)	1972 to present	Riverine	11,560
Potomac River at Wisconsin Ave, Washington D.C.	1647600	Stage (15 min)	1991 to present	Tidal	NA
Potomac River at SW waterfront / Washington D.C.	8594900	Stage (hourly)	1933 to present	Tidal	NA
Potomac River at Lewisetta, VA	8635750	Stage (hourly)	1996 to present	Tidal	NA
Anacostia River at Aquatic Garden	1651750	Stage (6 min)	2007 to present	Tidal	NA
Northeast Branch Anacostia River at Riverdale, MD	1649500	Discharge (hourly)	1990 to present	Riverine	72.8
Northwest Branch Anacostia River near Hyattsville, MD	1651000	Discharge (hourly)	1990 to present	Riverine	49.4

(2) Time series resolution

The temporal resolution determines the simulation accuracy, as well as the computational cost. The annual peak flows of the Potomac River at Little Falls obtained from the 15-min data are higher than those from the daily data (Figure 3-7). The following is a measure of the relative bias (Rb):

$$Rb = \frac{AM_{15min} - AM_{daily}}{AM_{15min}} \tag{3-6}$$

where AM_{15min} is the annual maximum stream flow based on the 15-min time series; AM_{daily} is the annual maximum stream flow based on the daily time series. The relative bias (Rb) of the annual peaks using 15-min data and daily data is 8.9% [Eq. (3-6)]. The 15-min time series is the best temporal resolution for the Potomac River at Little Falls. Suppose that the 15-min data are the most accurate data available, then an increase of 8.9% accuracy is gained by sacrificing 96 times of the data length or simulation cost compared to a daily time step. Whether it is worthwhile is a judgment call for the modelers. In this study, one-hour time series data was used for the upstream and downstream boundary conditions.

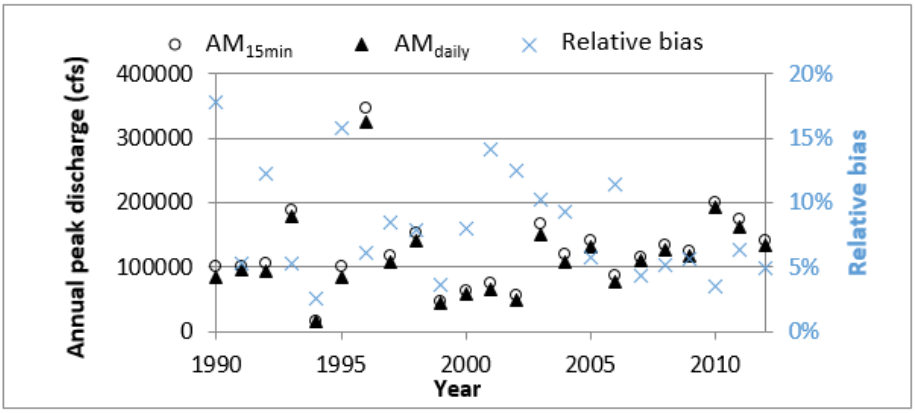

Figure 3-7. Annual peak discharge of Potomac River at Little Falls Pump Station (daily data v.s. 15-min data)

(3) Reasonable location with respect to the modeling purpose

The Potomac River HEC-RAS model simulates the upstream freshwater input and the downstream tidal influence and their combined effects on the study site. The ideal gauge sites to provide boundary conditions for the model should capture the characteristic of the upstream freshwater input and downstream tidal fluctuation. Figure 3-8 shows the location of the upstream gauge sites.

The tidal effect ends approximately at the Potomac River near Chain Bridge, which is downstream of the Potomac River at Little Falls and upstream of all the other sites in Figure 3-8. Therefore, the Potomac River at Little Falls is the best candidate for the upstream flow boundary, reflecting the riverine effect alone. The downstream gauge, Potomac River at Lewisetta, is located at the mouth of the Chesapeake Bay (Figure 3-5). It is the best representative of the tidal effects.

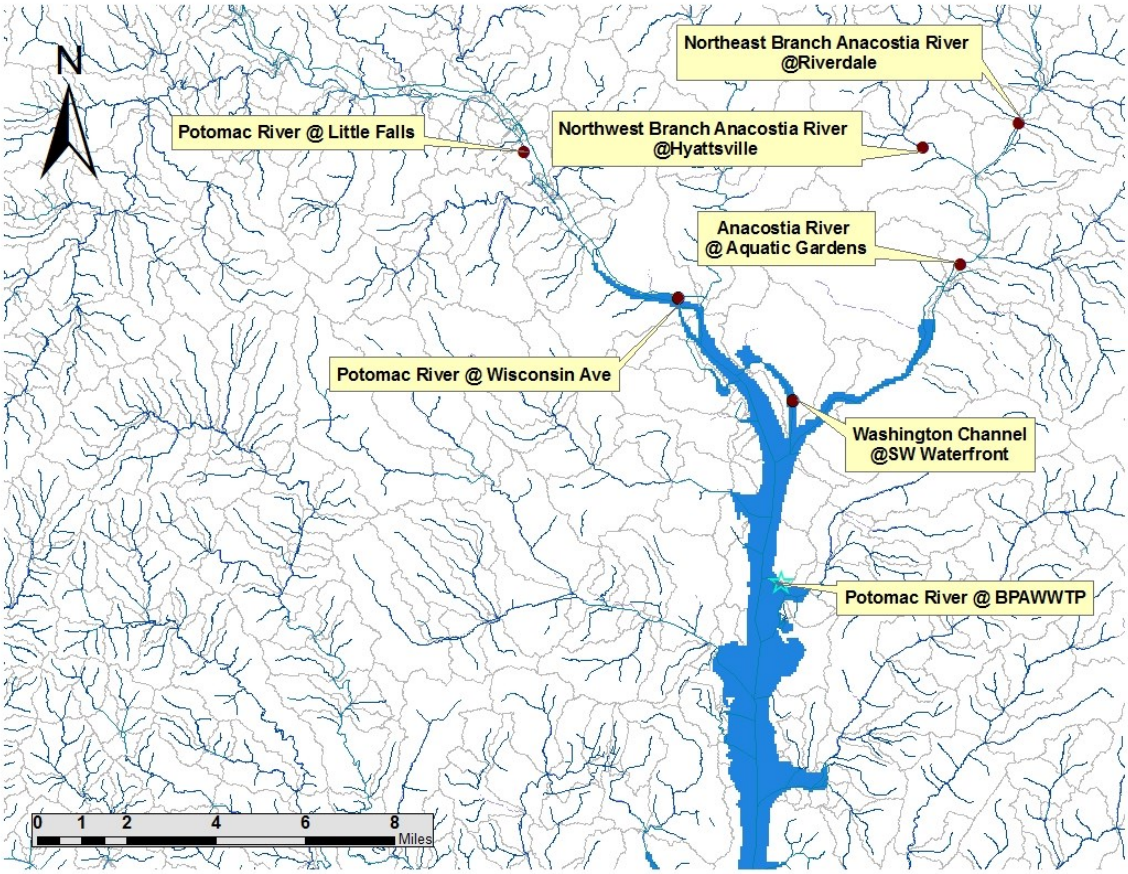

Figure 3-8. Gauge sites upstream of the study site

(4) Continuous operation and calibration

It is preferable to select a gauge site with continuous time series data that is well calibrated over the operation periods. Instantaneous flood peaks may be missing due to a discontinuity in the

time series data. Gaps in time series data also create difficulty in matching the other boundary condition time series. In this study, the Potomac River at Lewisetta constrained the simulation length since it had shorter records available compared to the other gauges.

Based on the selection criteria, the upstream boundary conditions for HEC-RAS model are the flow of the Potomac River at Little Falls (LF) (USGS 01646500) and the summation of Northeast Branch of the Anacostia River at Riverdale (USGS 01649500) and the Northwest Branch of the Anacostia River near Hyattsville (USGS 01651000) (Figure 3-5). The downstream boundary condition is the WSEL at LEW (NOAA 8635750). The Potomac River at Washington D.C. (DC) (NOAA 8594900) is the closest gauge to the study site with long record length. It serves as a model validation site.

The annual maximum time series are presented in Figure 3-9. The sample quantiles corresponding to the given probability of 0.5, 0.75 and 0.95 are plotted as the dashed lines. The values shown are computed by the Type 8 sample quantile definition recommended by Hyndman and Fan (1996). The correlation between the sites can be visualized in Figure 3-10. Each point represents a water year, in some cases the annual maximum at two locations was associated with the same event (black dots); in other cases, with different events (red dots).

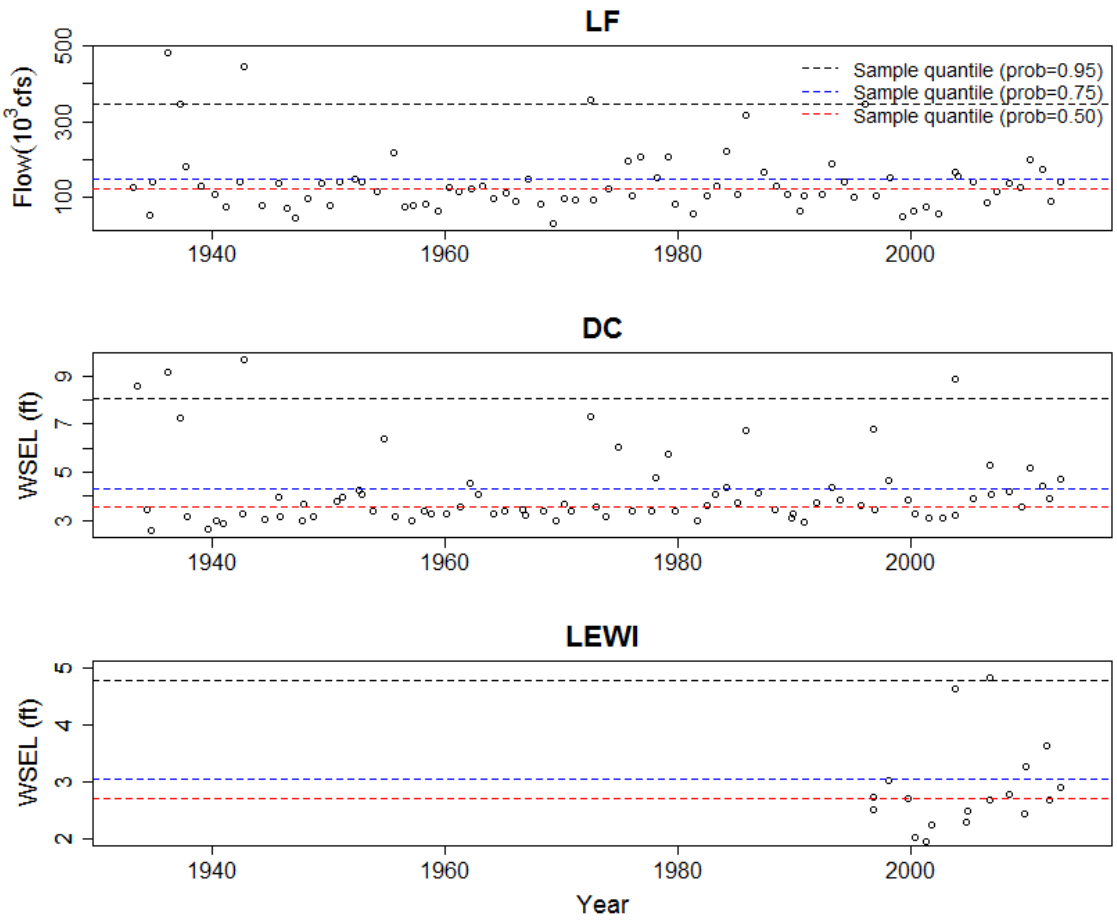

Figure 3-9. Annual maximum time series for Potomac River at Little Falls (LF), Washington, D.C. (DC) and Lewisetta (LEWI)

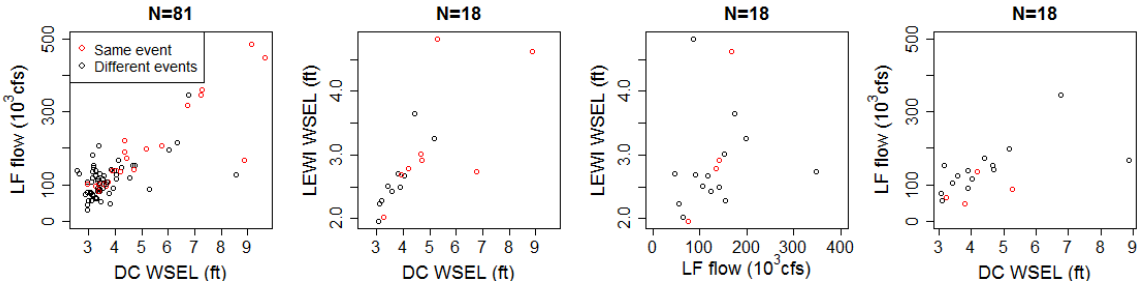

Figure 3-10. Annual maximum event correlation between Potomac River at LF, DC and LEWI

3.4.2.2 Steady Flow Boundaries

For steady flow analysis, it is assumed that the upstream and downstream boundary conditions with the same return period occur simultaneously. Based on this assumption, the HEC-RAS profiles are defined by the return period. The boundary conditions corresponding to 5-, 10-, 20-, 50-, 100-, and 500-year events are used as model input (Figure 3-11). This requires the frequency analysis of the upstream flow annual peak series and the downstream WSEL annual peak series.

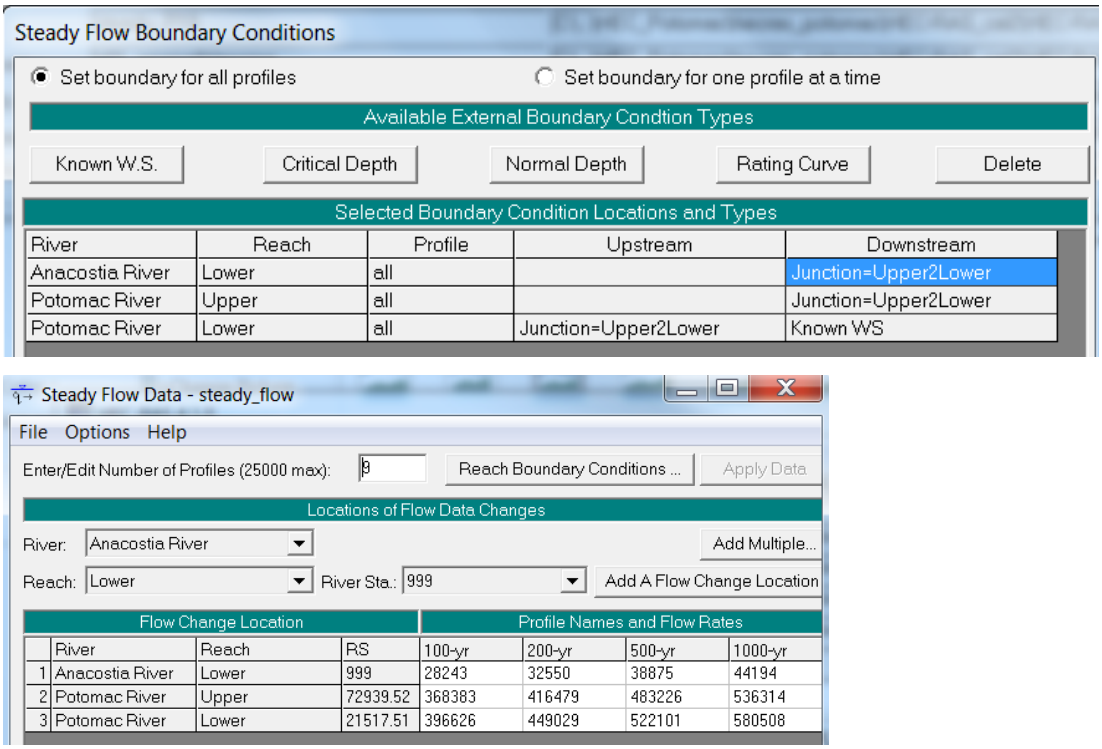

Figure 3-11. HEC-RAS model steady flow input

To select the best frequency distribution for the WSEL, annual peak series of WSEL of four gauged sites in the Mid-Atlantic region of the U.S. were selected. They represent independent WSEL samples of riverine and tidal sites. The two sites with semidiurnal tidal influence are the Potomac River at Washington, D.C. (8594900), and the Battery, NY (8518750). The two riverine

sites are the Susquehanna River at Harrisburg, PA(01570500), and Western Run at Western Run, MD(01583500) (Figure 3-12). The Battery, NY(8518750), is a station in the Upper New York Bay at the southern tip of Manhattan, NY, and is directly affected by the tides (NOAA, 2016a). The Potomac River at Washington, D.C. (8594900), is a tidal estuary. It is influenced by the upstream freshwater input from the Potomac River and the downstream tidal effect from the Chesapeake Bay (NOAA, 2016b). The Susquehanna River at Harrisburg, PA (01570500), with a drainage area of 24,100 square miles (USGS, 2016a), is representative of a large riverine site. The Western Run at Western Run, MD (01583500), is a smaller riverine site with a drainage area of 59.8 square miles (USGS, 2016b).

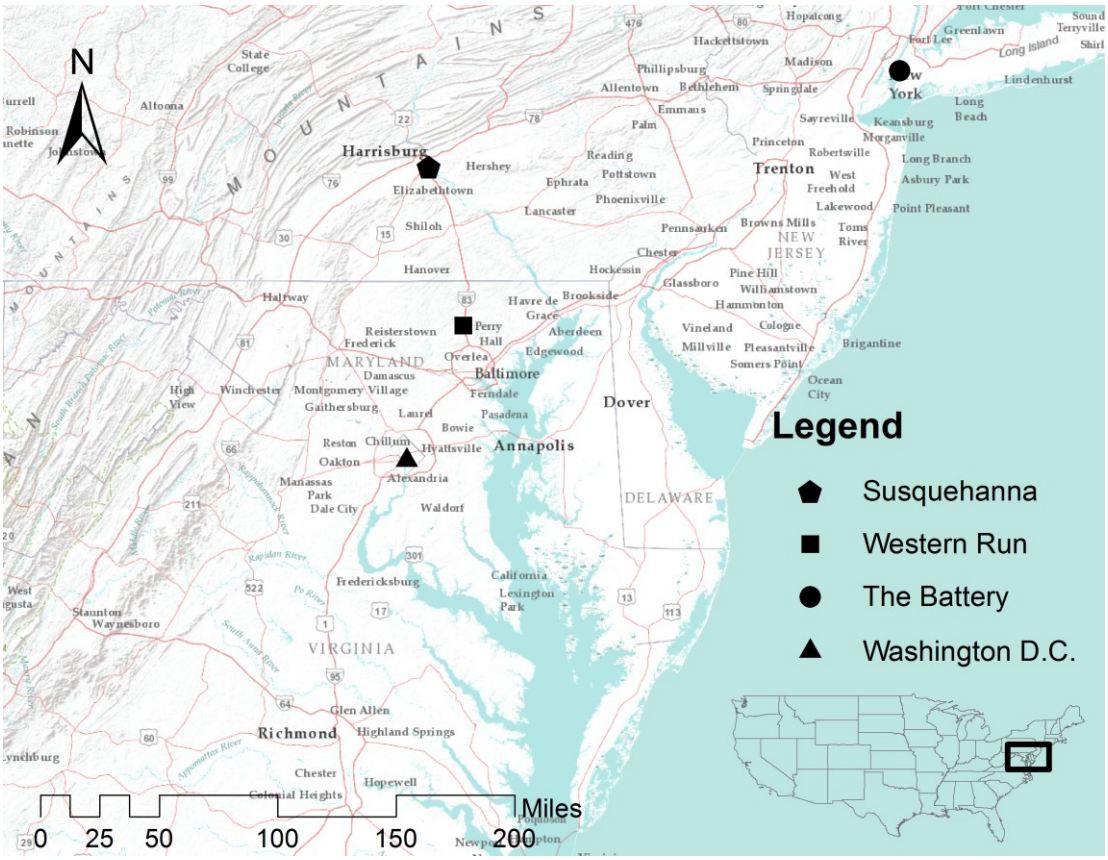

Figure 3-12. Location of one tidal, one estuary and two riverine study sites in the Mid-Atlantic region

Log Pearson Type III (LPIII), gamma, log normal and generalized extreme value (GEV) distribution were tested to fit the stage time series (Figure 3-13). The Kolmogorov-Smirnov (KS) one-sample test was applied for all four sites assuming the null hypothesis that the sample is drawn from the reference distribution. The p-values are reported in Table 3-3. The p-value represents the probability of observing a test statistic greater than or equal to the one calculated if the null hypothesis is true. It indicates whether the data population – as inferred from the sample – differs substantially from the theoretical expectations. A very small p-value implies rejection of the null hypothesis. It should be noted that the KS test is based on the largest difference detected between the sample distribution and the assumed population. A smaller p-value does not necessarily indicate a better model. It should be considered with the graphical analysis, as well as the range of interest for the analysis purpose, e.g., for the flood risk assessment, the upper tail is more critical.

Based on the graphical analysis in Figure 3-13 and KS test results, GEV is the overall best choice (Table 3-3). For DC, GEV and LPIII are both acceptable. However, LPIII provides slightly more conservative estimation of WSEL at the upper tail (Figure 3-13). It is selected as the choice for this Chapter. Bulletin 17B provides regional skew coefficients for river discharge, but not for river stage (IACWD, 1982). The relationship between stage and discharge is nonlinear; therefore, the regional (or generalized) discharge skew should not be applied to stage. However, a regional value is not required in this case. Following FEMA (2010), the Potomac River Basin is a large watershed and the sample skew can be used without weighting by the generalized skew.

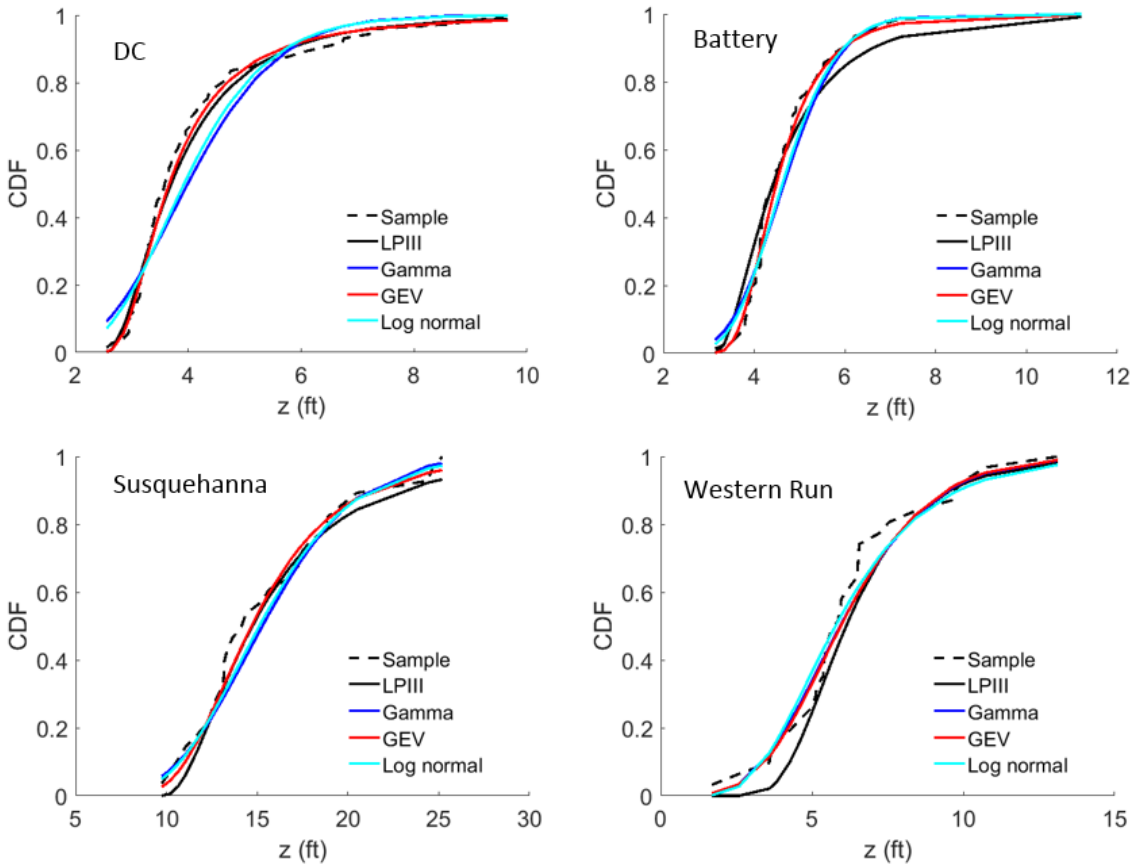

Figure 3-13. Sample distribution and inferred population distribution of WSEL for the four study sites

Table 3-3. P-value of the Kolmogorov-Smirnov one sample test on probabilistic distribution of WSEL for the four study sites

	LPIII	Gamma	Log Normal	GEV
DC	0.7904	0.0165	0.0528	0.9244
The Battery	0.0410	0.1447	0.2838	0.6717
Susquehanna	0.9734	0.6946	0.8104	0.9741
Western Run	0.3883	0.5369	0.5874	0.5345

For the study site, 18 years of annual peak event data (1996-2013) were used to estimate the Log-Pearson Type III (LPIII) distribution of the annual peak stage of Lewisetta, the annual peak discharge of LF, and the annual peak discharge of Anacostia (Figure 3-14, Figure 3-15, and Figure 3-16). For the steady flow simulations, the boundary conditions corresponding to specified probabilities were drawn from these inferred LPIII distributions.

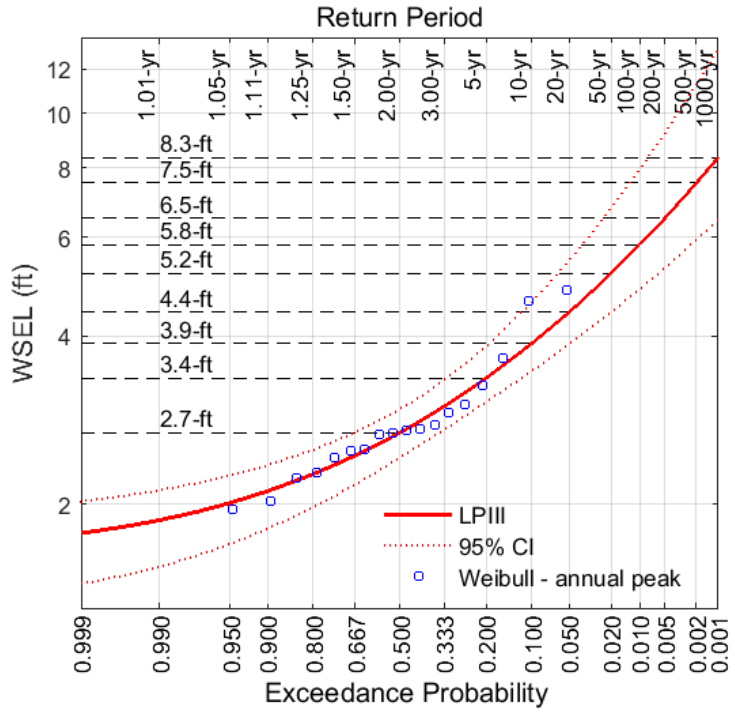

Figure 3-14. LPIII distribution of annual peak stage at LEWI

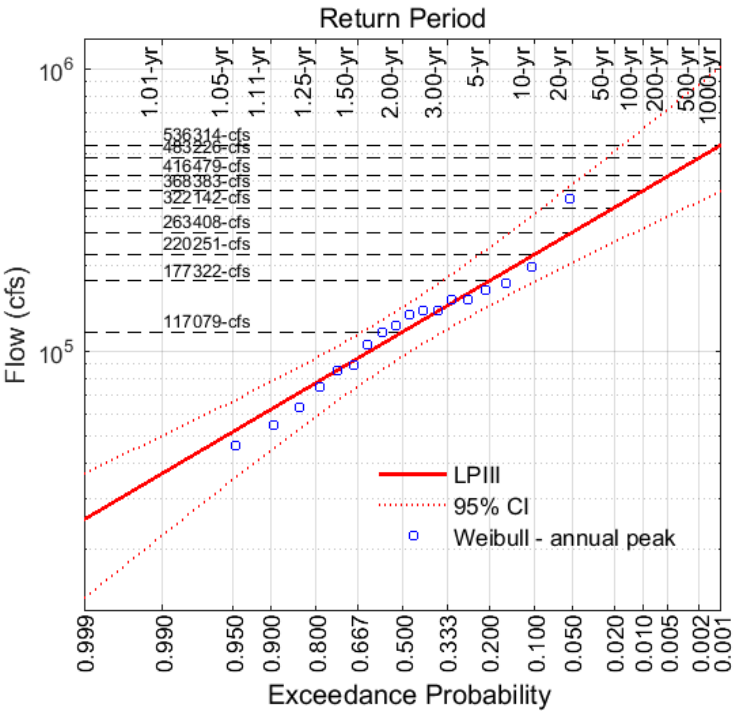

Figure 3-15. LPIII distribution of annual peak flow at LF

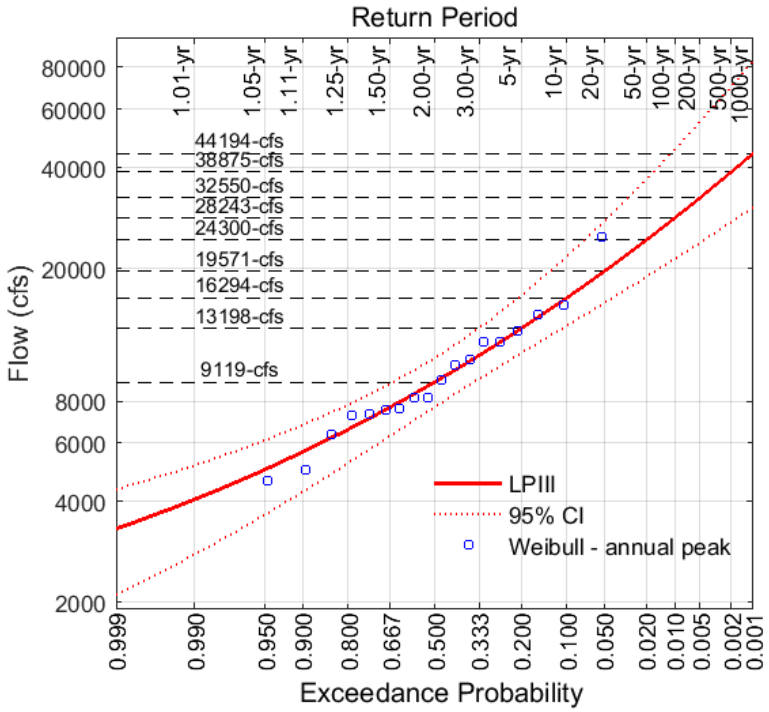

Figure 3-16. LPIII distribution of annual peak flow at NW+NE Anacostia

3.4.2.3 Unsteady Flow Boundaries

To avoid long-duration continuous simulation for the unsteady flow analysis, the following event-simulation procedure was followed. For each year, three events were simulated: (a) the event that produced the highest WSEL at the long-term gauge nearest to the study site, the Potomac River at Washington D.C. (DC) (NOAA 8594900); (b) the event associated with the maximum upstream inflow at LF; and (c) the event associated with the maximum downstream tidal WSEL at LEW. The Anacostia River contributes about 1/10 of the flow in the Potomac River on an annual basis; the Anacostia flow was not used to define the annual peak events. In a given water year, the maximum WSEL or flow at the three gauged sites (NOAA 8594900, USGS 01646500, and NOAA 8635750) are not always temporally coincident; furthermore, the time lags between the peak WSEL or flow at these measured points and peak WSEL at the study site are variable. Therefore,

the annual maximum event of this study was defined as 'maximum-of-the-maxima' (Figure 3-17). For each water year, a HEC-RAS simulation was run for each of the three annual peak event periods, as defined by the three gauges. For each run, simultaneous observed hourly upstream flow input and downstream WSEL input were used as the boundary conditions. A 1-minute simulation time step was used. The peak WSEL output at the study site was collected from each of the three runs. The maximum of the three simulated peak WSELs was used as the maximum WSEL at the study site for the water year.

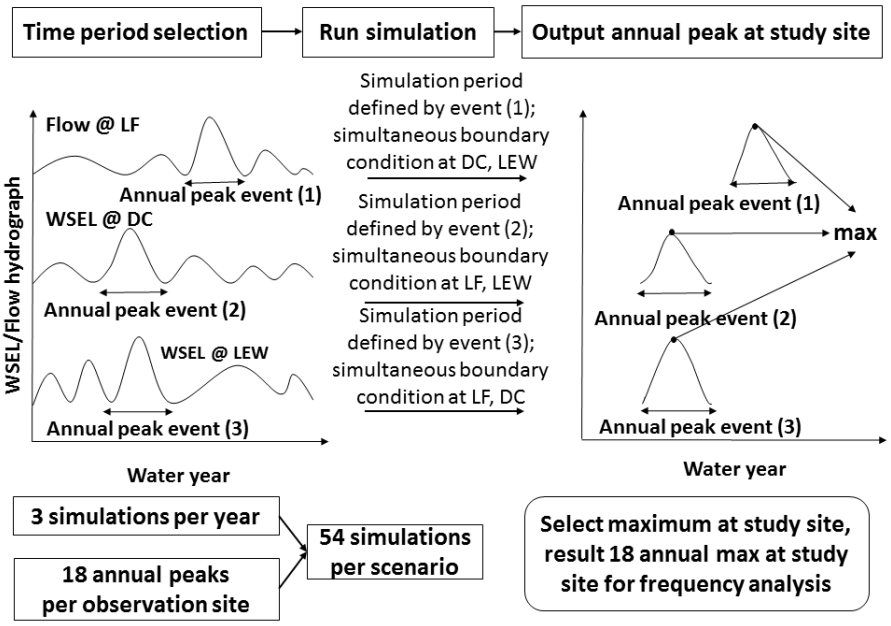

Figure 3-17. Maximum-of-the-maxima approach to determine the annual peak water surface elevation

It is conceivable that the highest water level at the study site in a given year might be associated with neither the peak downstream elevation nor the peak upstream inflow, but with simultaneous occurrence of high, but non-maximum, values at both boundaries. The maximum-of-the-maxima method described above would miss such events. The DC gauge (NOAA 8594900)

is about 5 miles upstream of the study site. A check of the time of 18 annual peaks for DC showed that for all flood events greater than a 5-year event magnitude, the annual peak of at least one of the other two sites, LF and LEW, occurred within 5 days of the DC annual peak. This means that the annual peak at DC is temporally associated with the annual maximum upstream freshwater input or downstream WSEL, or both. Taking the DC observed data as an indicator of the annual peaks at the study site, it is reasonable to conclude that the 'maximum-of-the-maxima' method covers all of the possible upstream and downstream events that cause the annual peak in the study site.

In a given water year, the maximum WSEL or flow at the three gauged sites (NOAA 8594900, USGS 01646500, and NOAA 8635750) are not always temporally coincident; furthermore, the time lags between the peak WSEL or flow at these measured points and peak WSEL at the study site are variable. Simulated events used in this study were defined to begin 4 days before the observed peak (at LF, LEW, or DC, respectively) and end 4 days after.

3.5 Scenario Development for Changed Hydroclimate and Sea-Level Rise

3.5.1 General Approach

Future climate scenarios were developed by perturbing the boundary conditions, both upstream freshwater and downstream tidal effects. The expected increase in the magnitude of large precipitation events in the region was incorporated as incremental multiplicative increases in freshwater event discharge at the upstream flow boundary. The predicted sea level rise was incorporated as incremental additive increases in the event WSEL at the downstream WSEL boundary. The geometry and hydraulic parameters of the HEC-RAS model were unchanged.

Boesch et al. (2013) recommend a projected 3.7 feet of RSLR for the Maryland coastal plain, for infrastructure with life that is not intended to extend beyond this century, and 5.7 feet for infrastructure with life that is intended to extend beyond this century. Assuming that the WWTP's planning horizon is not beyond this century, this study implemented downstream SLR by increasing river WSEL at Lewisetta from 0 ft to 4 ft in 0.5 ft increments. This perturbation was applied by adding the specified depth to the entire event hydrograph [Figure 3-18 (a)], which would reflect the constant increase in water surface elevation due to regional RLSR only, independent of any increased precipitation in the watershed.

In contrast to RSLR, neither the precipitation nor the stream gauge record gives a clear indication of a trend in the magnitude, frequency, or severity of runoff flood events in the region. However, GCMs indicate that in the mid-Atlantic region, while total annual precipitation may decrease, the intensity of individual storms may increase. In an intercomparison of nine different GCMs, Meehl, Arblaster, and Tebaldi (2005) found a consistent signal of up to 2 standard deviations increase in average precipitation intensity in the northeastern United States. The Interstate Commission on the Potomac River Basin (2013) predicted the impact of climate change on streamflow by the Chesapeake Bay Program's Phase 5 Watershed Model, using meteorological inputs based on 18 downscaled global climate model projections. For the Potomac River Basin above Little Falls, scenario B_B1 gives the highest increase (11%) in average annual stream flow in the year 2040. To study the impact of climate change on Mid-Atlantic region streamflow change, Neff et al. (2000) ran the Susquehanna River water balance model with the British Hadley Centre climate change scenarios. The simulation output indicated a 7% increase of annual stream flow for 2025-2034 period and a 24% increase for the 2090 to 2099 period. In addition to climate change, urbanization, decreasing evapotranspiration due to increased CO_2 emission can also cause future streamflow increase (Neff et al., 2000).

This study applied a flow multiplier to the upstream boundary input of high-flow event discharge (Potomac River at Little Falls), increasing the discharge by 0 to 30% in increments of 5% [Figure 3-18 (b)]. All possible combinations of the nine downstream and seven upstream boundary settings (including the no-change or 0 perturbation) generated 63 climate change scenarios (Figure 3-19).

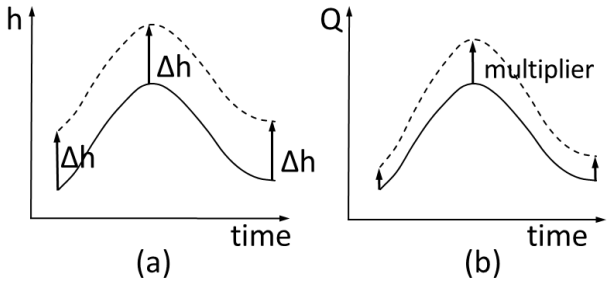

Figure 3-18. Boundary conditions represent climate change
(a) Downstream WSEL increment; (b) Upstream flow increment

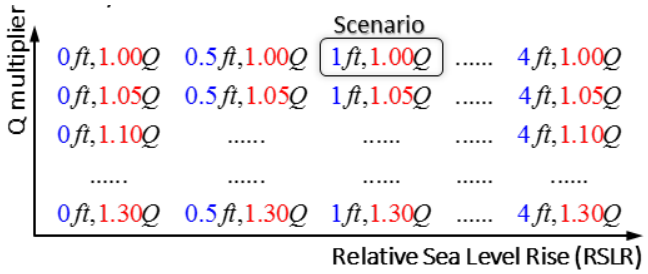

Figure 3-19. Climate change scenarios developed for the steady and unsteady flow analysis by prescribed flow multiplier and relative sea level rise

3.5.2 Steady Flow

For steady flow analysis, the current climate scenario boundary condition is set up based on the Log-Pearson Type III analysis for the upstream and downstream annual peaks, as explained in Section 3.4.2.2. The procedures of the steady flow analysis for 63 climate change scenarios are illustrated in Figure 3-20.

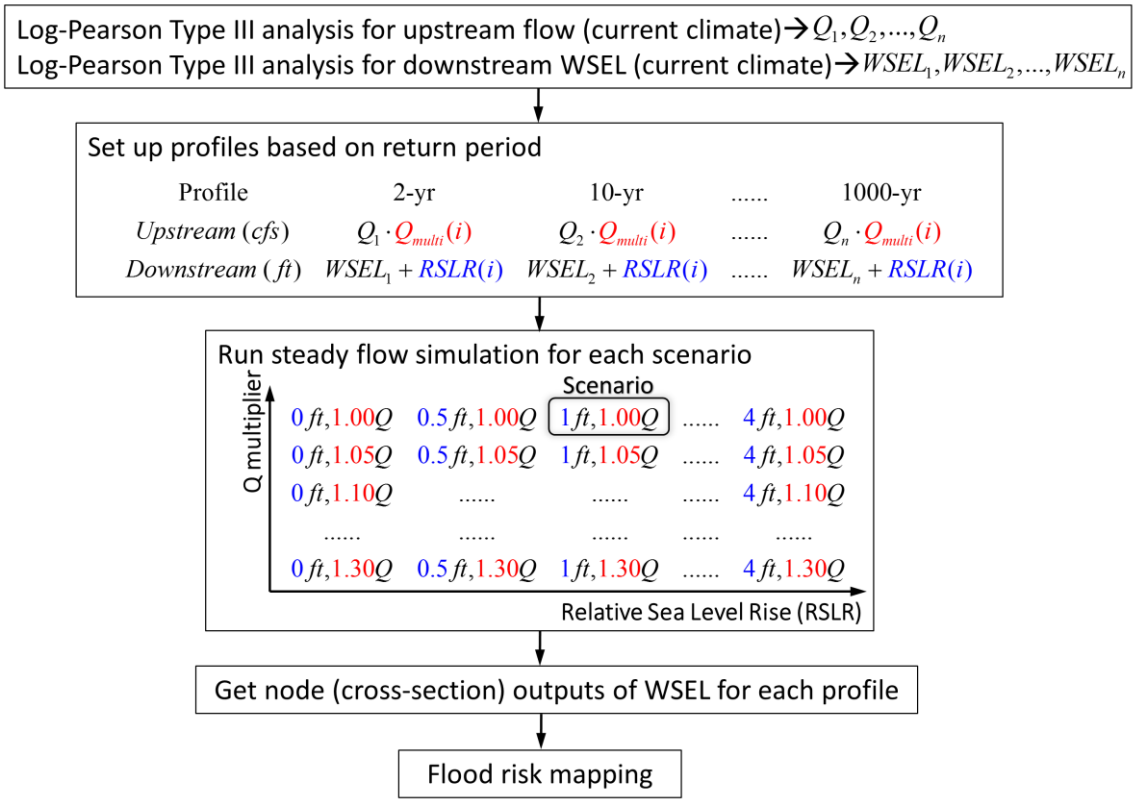

Figure 3-20. Summary of procedures (Steady flow analysis)

3.5.3 Unsteady Flow

For unsteady flow analysis, the appropriate upstream and downstream perturbations were applied to each of the three maximum events per year for each frequency estimation scenario. Three simulations per year and 18 years of data resulted in 54 HEC-RAS unsteady flow analyses per scenario, for a total of 3402 unsteady flow runs. A customized external C# code automatically generated the HEC-RAS unsteady flow (.u) and plan files (.p), ran the simulations, and stored the output. With a simulation time step of one minute, the run time using a desktop computer with average performance was 45 minutes per scenario.

For each scenario, the 18 annual maximum WSEL at the study site were identified using the maximum-of-the-maxima approach and fit with a Log Pearson III (LPIII) distribution (Figure 3-17). The procedures are summarized in.Figure 3-21.

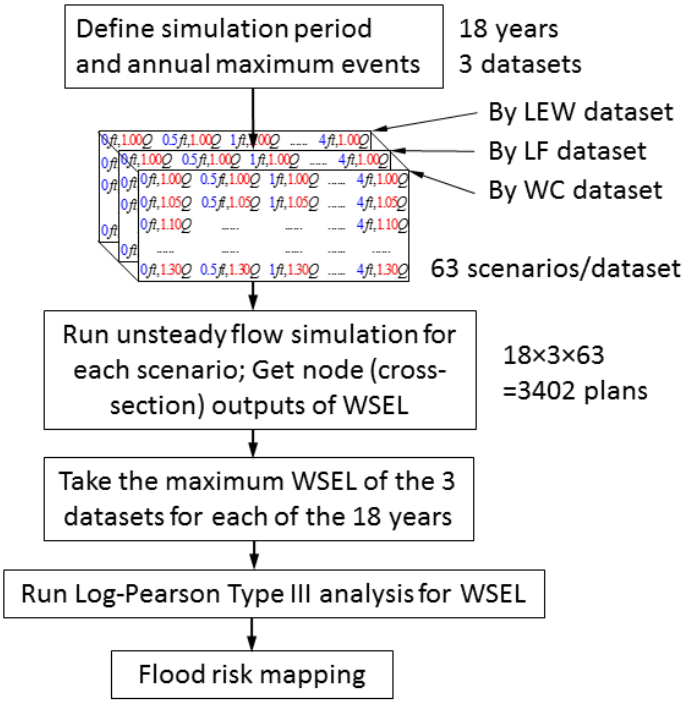

Figure 3-21. Summary of procedures (Unsteady flow analysis)

3.6 Automating HEC-RAS Simulation

The understanding of regional climate change and the associated water resources change are continuously being updated. Design standards and policies of adaptive management should be upgraded at an acceptable frequency. Annual peak event simulation with various combination of climate change scenarios is extremely time consuming if manually running HEC-RAS using its graphical user interface (GUI). This involves setting up unsteady flow file, plan file, running the simulation and collecting output data for each scenario. It is not practical to work with thousands

of climate change scenarios without an automation tool. It is necessary to develop an approach that is reproducible and cost-effective as climate change scenarios are updated.

HEC-RASContoller enables the possibility of probabilistic analysis using HEC-RAS. As part of the HEC-RAS application programming interface (API), HEC-RASController is a collection of programming classes. HEC-RAS specific functions and subroutines can be called during run time. HEC-RAS API is compiled as a component object model (COM) dynamic link library (DLL), which can be used by any programming language that calls a DLL. Automatic setting of input data, running HEC-RAS plans, and retrieving of output data can be achieved by programming (Goodell & Brunner, 2014). For RAS41, there are three programming classes (HECRASController, HECRASFlow, and HEC-RASGeometry) and 266 variables available.

In this study, an object-oriented programming language, C#, is the programming language for the HEC-RAS automation and Microsoft Visual Studio is the integrated development environment (IDE). By calling the procedures in the HECRASController class, variable outputs can be generated for probabilistic analysis. If any change is made, e.g., revised estimates of regional sea-level rise or future hydroclimate or updated hydraulic parameters, the analyst can reset the model and rerun it in a consistent and timely fashion.

3.7 Results of the Steady and Unsteady Flow Simulation

3.7.1 Flood Stage-Frequency for Current Climate

The model outputs for the study site based on the observed boundary input time series were considered a sample of the current climate. Figure 3-22 shows the LPIII stage-frequency curve of WSEL at the study site plotted on a normal probability paper. For the steady flow analysis, the blue cross on the curve shows the analysis points assuming simultaneous occurrence of the upstream and downstream boundary condition with specific return period or exceedance

probability. For example, the 10-year WSEL at the study site based on the steady flow analysis is 6.3 feet, which assumes that the 10-year upstream flow at LF and the 10-year downstream WSEL at LEWI occur at the same time. For unsteady flow analysis, the circles are the Weibull plotting position for the 18 annual peaks. The thick black dashed line is the inferred LPIII population model based on Bulletin 17B (IACWD, 1982). The light black dashed lines are the 95% confidence interval [LPIII plots in this study were inspired by Matlab code by Burkey (2009)]. The WSEL based on the steady and unsteady flow analysis are listed in Table 3-4.

For the low frequency events (T >5 yr), the predicted WSEL at the study site based on the steady flow analysis is higher than the unsteady flow analysis. The lower the frequency, the greater the difference. For the low frequency range, which is the region of interest of the flood risk study, the WSEL prediected by the steady flow analysis lies within the 95% CI of the unsteady flow analysis. However, for the high frequency events, the steady flow analysis output is outside the range of the 95% CI of the unsteady flow analysis.

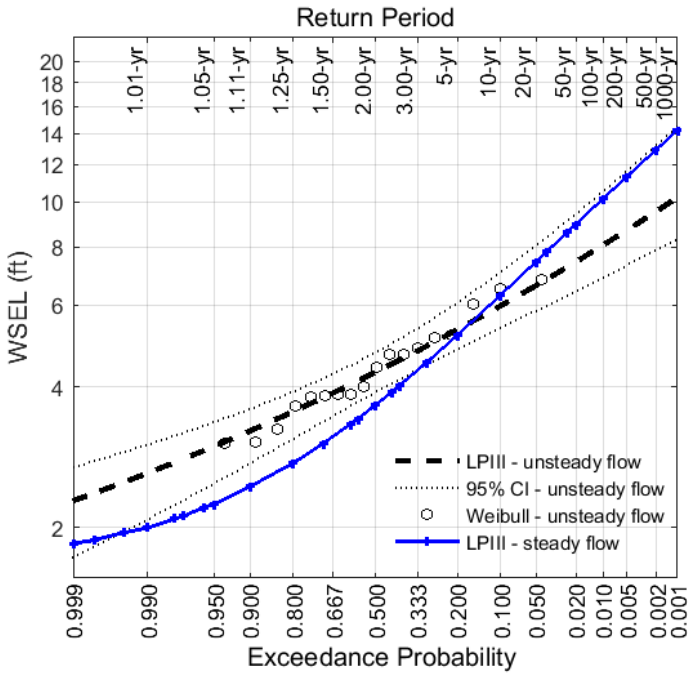

Figure 3-22. Stage frequency distribution (steady v.s. unsteady model output) (BPAWWTP)

Table 3-4. Comparison of steady and unsteady flow analysis outputs (BPAWWTP)

Return period (T-year)	Stage at BPAWWTP (ft, NAVD 88)	
	Steady flow analysis	Unsteady flow analysis
2	3.7	4.3
5	5.2	5.3
10	6.3	6
20	7.4	6.6
50	9.0	7.4
100	10.1	8.1
200	11.3	8.7
500	13.0	9.5
1000	14.2	10.2

3.7.2 Model Accuracy Assessment Based on Current Climate

To assess model accuracy, model-generated annual maximum WSEL at the location of the nearest tide gauge was determined using both the steady flow (coincident occurrence of events with the same return period) and unsteady flow (maximum-of-the-maxima) analysis methods described in the previous sections. The results were compared to the observations. The Washington, D.C. (DC) tide gauge (NOAA 8594900), the closest gauge to the WWTP study site, has 81 years of hourly WSEL (1933-2013). As explained above, the model analysis is restricted to 18 years of annual maximum WSEL prediction due to the availability of simultaneous upstream and downstream boundary time series. The model-derived annual maximum WSEL were compared to the corresponding observed values for DC.

For unsteady flow analysis, the modeled 18 annual peaks are compared with the corresponding observed annual peaks. The root-mean-square error (RMSE) of the model prediction is 0.88 ft and the mean bias is 0.32 ft with sample size 18. The model underpredicted the maximum WSEL for Water Year 2003, when the annual peak event was associated with Hurricane Isabel, probably because the equations of the 1D unsteady HEC-RAS do not include the wind and pressure effects acting on the river between its Chesapeake Bay mouth and the study

site (2.6 mile). The modeled annual peaks are a fair match to the observations. Since event simulation is not applied for the steady flow analysis, the RMSE is herein not a measurement for the simulation accuracy.

Without being an exact match to the observations, the modeled annual peak WSELs may still give a reasonable estimate of the frequency distribution. Two questions arise: (1) Because the study of the ungauged site is restricted to 18 years, how well do those 18 years capture the LPIII distribution inferred from the full 81-year record, and (2) Does the LPIII model inferred from the 18 simulated annual peaks match the one inferred from the same 18 years of observations?

The LPIII frequency analysis of the observed WSEL at Washington, D.C., for the 18 study years was compared with the analyses based on the full 81-year record at DC (see Figure 3-23). The frequency distribution derived from the 81-year observed peak WSEL represents the best available information (although it is still a sample of an unknown population). The difference between the 18-year observed LPIII and the 81-year observed LPIII indicates the bias due to the limitation of the length of the records. The 95% confidence intervals (CI) of 18-year observed LPIII and those of the 81-year observed LPIII overlap for the range of frequency estimates. This indicates that the 18 years available for the study period are reasonably representative of the full 81-year record (which is not available for the model boundary conditions), in the sense that the two samples give estimates of the population probabilities that do not disagree at a 5% level of significance.

The difference between the 18-year observed LPIII and the 18-year model-derived LPIII indicates the error introduced by the model (Figure 3-24). The distribution by the 18-year unsteady flow model is less skewed than the 18-year observed and the 18-year steady flow model. The unsteady flow model under estimates the 500-year, 200-year and 100-year WSELs compared to the observed WSELs, while the steady flow model slightly over estimates the WSELs for the

100-year and 200-year events, but converges to a good match for the 500-year events. For the events with return periods lower than 20 years, the unsteady flow simulation slightly over estimates the peak WSEL with respect to observed. The steady flow simulation does not predict the low frequency events as well as the steady flow simulation.

The conclusion of this accuracy assessment at a gauged site upstream from the study site is: The steady flow simulation is a better candidate to predict the WSEL for the low frequency events. In contrast, unsteady flow simulation provides better estimates of the high frequency events. Although the unsteady flow simulation seems to be an overall better method, given that the best estimate always lies within the 95% CI of the observed (Figure 3-24), the steady flow analysis is a more conservative choice for the flood risk assessment.

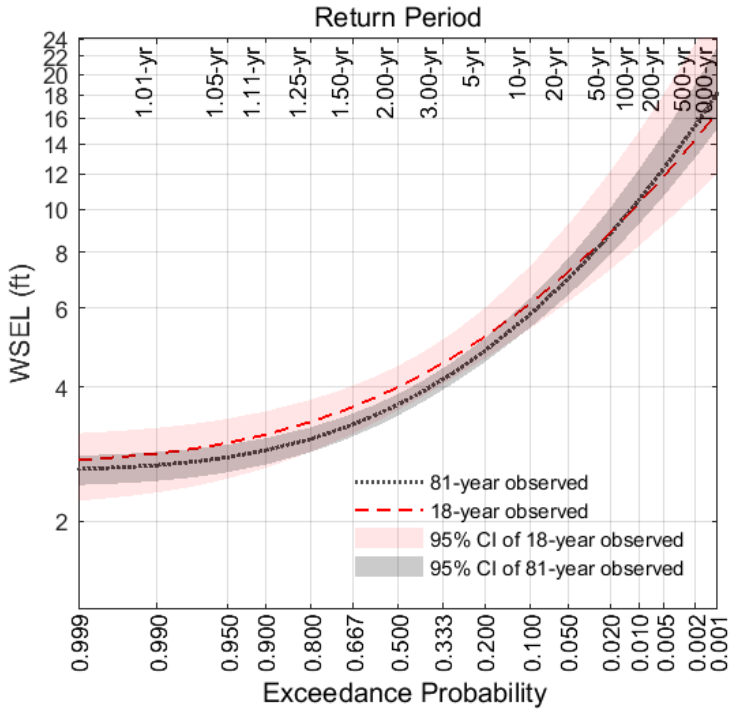

Figure 3-23. LPIII distribution of 18-year and 81-year observed WSEL (Potomac River at Washington, D.C.)

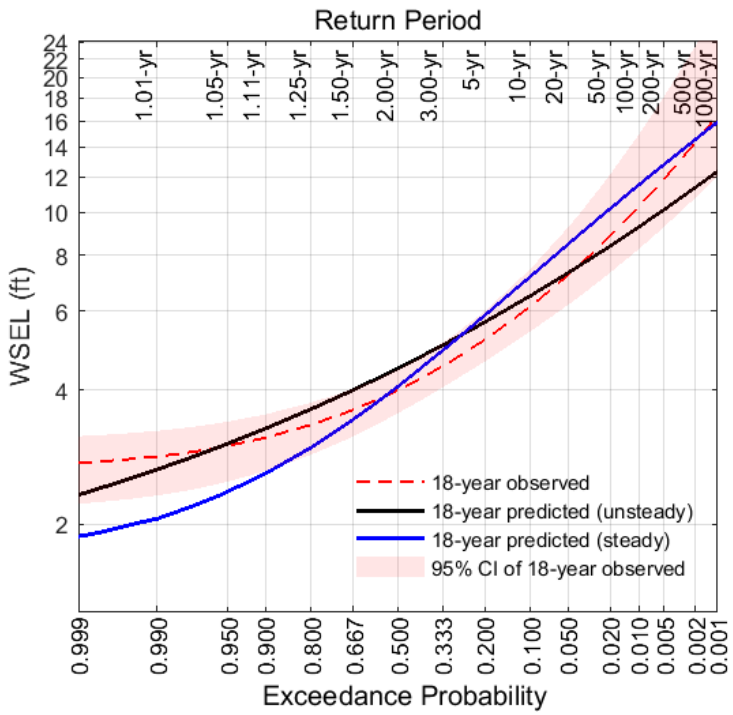

Figure 3-24. LPIII distribution of 18-year observed and predicted WSEL (Potomac River at Washington, D.C.)

The model derived current-climate WSEL frequency distribution for the ungauged study site is inaccurate due to both factors: non-representativeness of the 18-year sample, and inaccuracy of the hydraulic model. The second source of inaccuracy is greater. All model errors present in simulating the current climate are also present in the future climate scenarios; therefore, the comparisons between “current climate” and “future climate” scenarios can be interpreted as sensitivity study or planning guidance, not accurate predictions of future flood depth probabilities.

3.7.3 Flood Stage-Frequency for Changing Climate

The LPIII analysis of annual maximum WSEL at the study site with downstream sea level rise alone (0% increase in upstream discharge, first row of the table in Figure 3-19) appears in Figure 3-25. Each line denotes the LPIII probability of annual maximum WSEL with the specified rise in sea level at the Chesapeake Bay mouth of the Potomac River. The heavy line corresponds to the current-climate LPIII curve in Figure 3-22. For unsteady flow analysis, under current climate, the 1% annual exceedance elevation is 8 ft; with 1 ft of sea level rise, this elevation has a 2% probability of being exceeded in a given year, but with 4 ft of sea level rise, the probability rises to 67%. The effect of sea level rise on flood frequency assessment is less significant for the steady flow analysis, which is observed by the convergence of the set of curves at the low frequency end [Figure 3-25 (a)]. The probability associated with the steady flow 100-year elevation (10.1ft) changes to 1.5% and 5.5% for the 1 ft and 4 ft of sea level rise, respectively.

The LPIII analysis for changed-hydroclimate alone (upstream flow increment scenarios, RSLR = 0, first column of the table in Figure 3-19), are shown in Figure 3-26. The 1% annual exceedance WSEL based on unsteady flow analysis under current climate (8 ft) becomes increasingly likely, with return periods of about 60 yr, 40 yr, and 30 yr, respectively, for the 10%, 20% and 30% increases in event discharge. For the steady flow analysis under current climate, the 100-year flood elevation (10.1 ft) will be redefined as 66 yr, 50 yr and 36 yr, for the 10%, 20% and 30% increases in event discharge, respectively. The current-climate 0.2% annual exceedance (500-yr) WSEL has an average return period of 75 years and 144 years in the 1.3Q scenario, for unsteady and steady flow simulation, respectively.

For the unsteady flow analysis, the 100-year flood WSEL in the 30% flow increase scenario (0ft, 1.3Q) is 1.8 feet above the baseline scenario (0ft, 1Q) 100-year WSEL. The difference between scenarios for the less frequent floods is greater than for the more frequent floods; for example,

500-year WSEL rises from 9.5 ft to 12.6 ft, a difference of 3.1 ft. A similar trend is observed for the steady flow analysis.

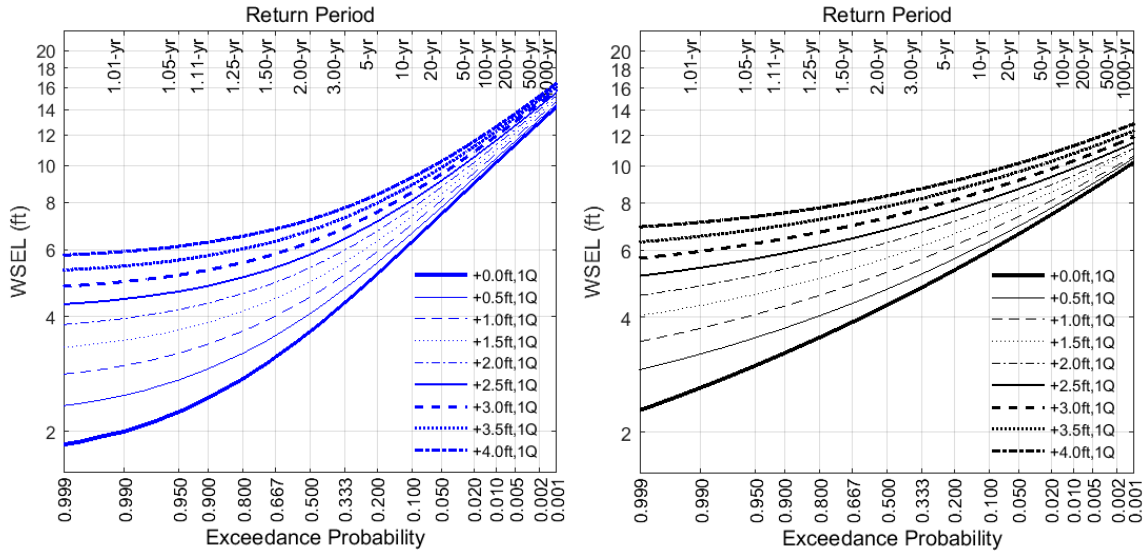

(a) Steady (b) Unsteady

Figure 3-25. LPIII analysis of the sea-level rise only scenarios (Potomac River at WWTP)

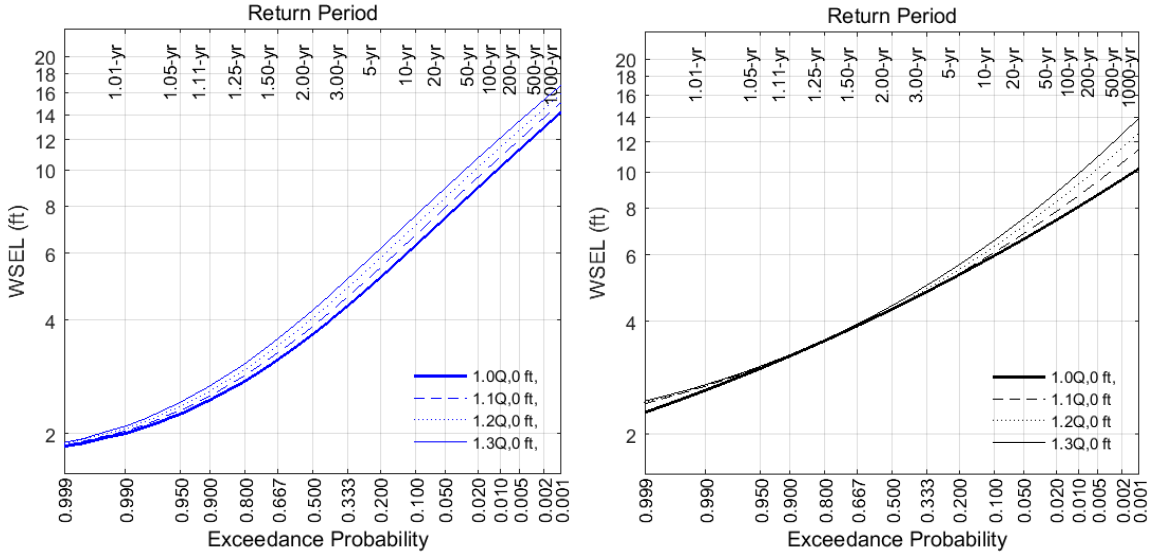

(a) Steady (b) Unsteady

Figure 3-26. LPIII analysis of the flow increment only scenarios (Potomac River at WWTP)

All 63 combinations of the SLR and hydroclimate increments were simulated, as shown in Figure 3-19. The worst case scenario [4 ft, 1.3Q] is illustrated in Figure 3-27, together with (a) current climate, (b) the highest flow increase alone scenario (0ft, 1.3Q), and (c) the highest sea level rise alone scenario [4ft, 0Q]. Taken alone, each perturbation (SLR or upstream flow increase) increases the likelihood of exceeding a specified depth and increases the depth associated with a specified exceedance probability. However, the effects are not additive (Table 3-5).

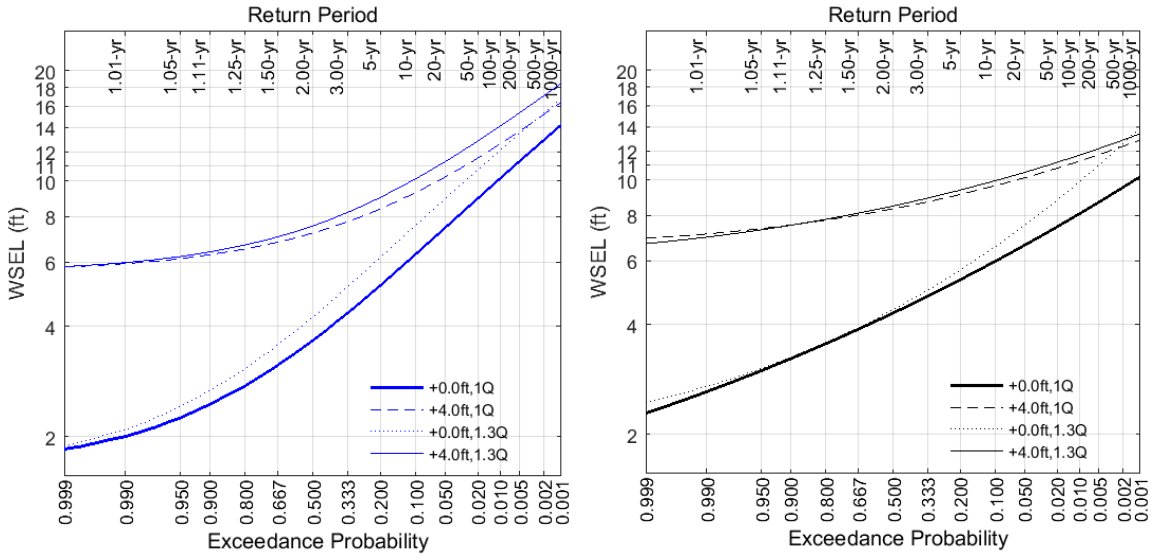

(a) Steady (b) Unsteady

Figure 3-27. Scenario comparison – modeled current climate, highest sea level rise alone scenario, highest flow increase alone scenario and worst case scenario (Potomac River at WWTP)

Table 3-5. Additive effects evaluation

	Unsteady flow	Steady flow
$\Delta Elev_{500\text{-yr, (4ft SLR, 1Q)}}$	12.4 ft – 9.5 ft = 2.9 ft	15.21 ft –12.96 ft = 2.25 ft
$\Delta Elev_{500\text{-yr, (0ft SLR, 1.3Q)}}$	12.6 ft– 9.5 ft= 3.1 ft	15.35 –12.96=2.39 ft
$\Delta Elev_{500\text{-yr, (4ft SLR, 1.3Q)}}$	12.9 ft– 9.5 ft = 3.4 ft	17.11 –12.96=4.15 ft
Conclusion	$\Delta Elev_{500\text{-yr, (4ft SLR, 1.3Q)}} < \Delta Elev_{500, (4ft SLR, 1Q)} + \Delta Elev_{500\text{-yr, (0ft SLR, 1.3Q)}}$	$\Delta Elev_{500\text{-yr, (4ft SLR, 1.3Q)}} < \Delta Elev_{500, (4ft SLR, 1Q)} + \Delta Elev_{500\text{-yr, (0ft SLR, 1.3Q)}}$

This result indicates that when planners consider multiple physical factors that may change the probability of flood depths, superposition does not apply. In fact, it appears that predicting the effects of the two factors separately, then adding them, would give an overly conservative estimate of their combined effects. Mathematically, the equations that describe flow in rivers are nonlinear. Physically, the propagation and attenuation of a flood signal depend on water depth. A dynamic model, such as the unsteady HEC-RAS used in this study, is needed to explore and understand the combined factors that affect rivers such as the tidal Potomac.

When dealing with future climate prediction, observed data are not available to assess the simulation accuracy. However, the difference among the models yielded useful information for model selection. As shown in Figure 3-28 to Figure 3-30, the steady flow analysis provide higher estimates of the WSEL for low frequency floods compared to the unsteady flow analysis. The opposite trend is observed for the high frequency floods. The transition point is indicated by the intersection of the solid red curve and the dashed diagonal reference line. For the sea level rise only scenarios, the transition points tend to move upward towards the rare floods when the effect of sea level rise is increased. In contrast, for the flow increment only scenarios, the transition points tends to move downward towards the frequent flood when the flow increments is increased.

The LPIII analysis of annual peak WSEL was repeated for each combination of relative sea level rise and event discharge increase. The 1% annual exceedance (100-year) depth for all 63 scenarios is summarized by the contour lines in Figure 3-31. The differences between the steady and unsteady flow analysis are shown by Figure 3-32. The contours present a difference surface by subtracting the unsteady flow outputs from the steady flow outputs. Smaller difference is observed at higher RSLR and lower flow increment for the 100-year flood.

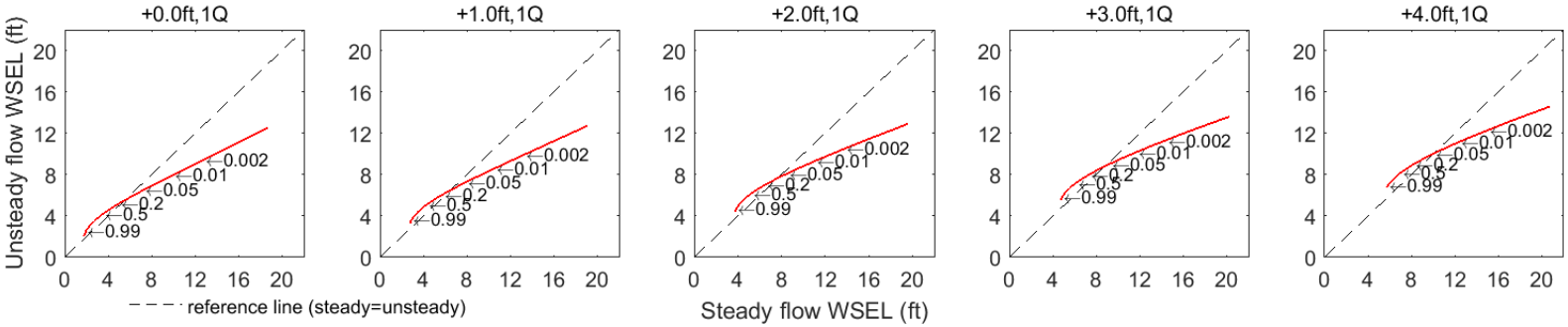

Figure 3-28. Comparison of steady and unsteady flow outputs – the sea-level rise only scenarios (Potomac River at WWTP)

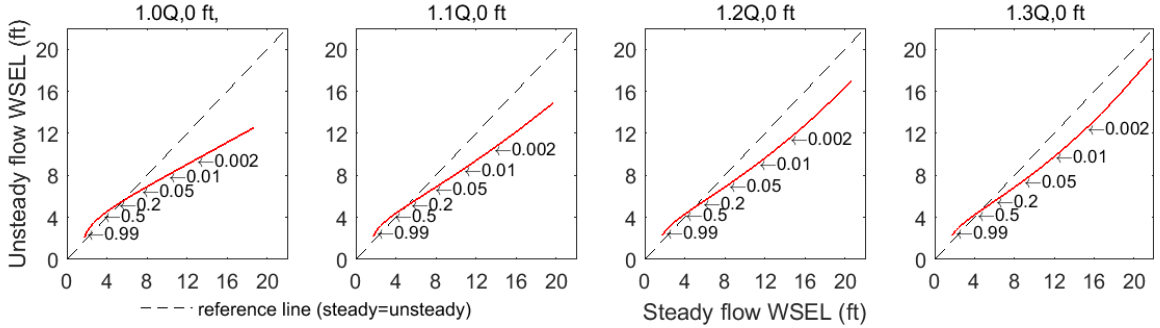

Figure 3-29. Comparison of steady and unsteady flow outputs – the flow increment only scenarios (Potomac River at WWTP)

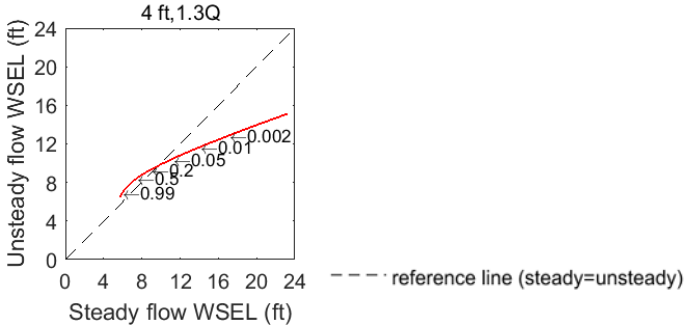

Figure 3-30. Comparison of steady and unsteady flow outputs – the worst case scenarios (Potomac River at WWTP)

Note: the numbers with an arrow point to the curve (Figure 3-28, Figure 3-29, Figure 3-30) are the corresponding exceedance probability.

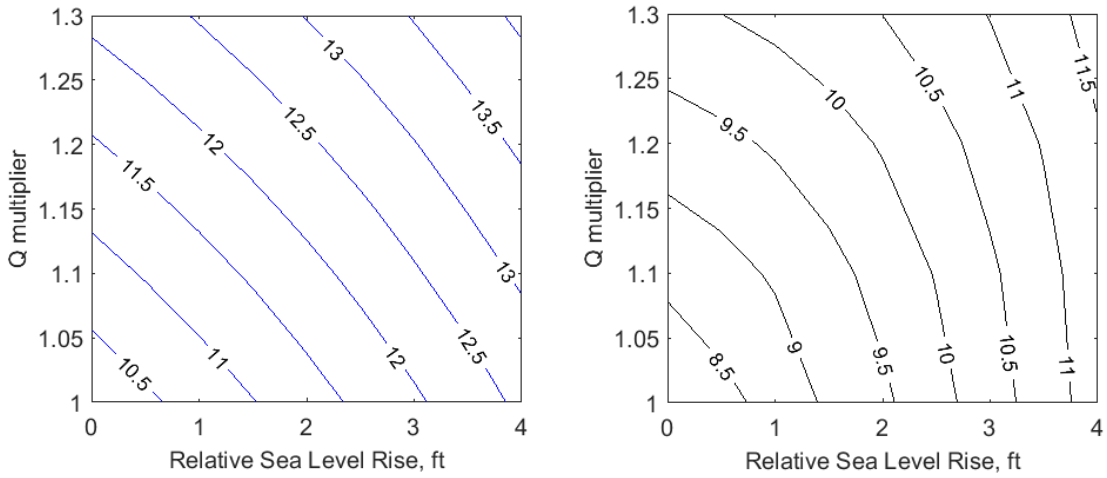

(a) Steady (b) Unsteady

Figure 3-31. Contour of 1% annual exceedance (100-year) flood WSEL (ft) for WWTP

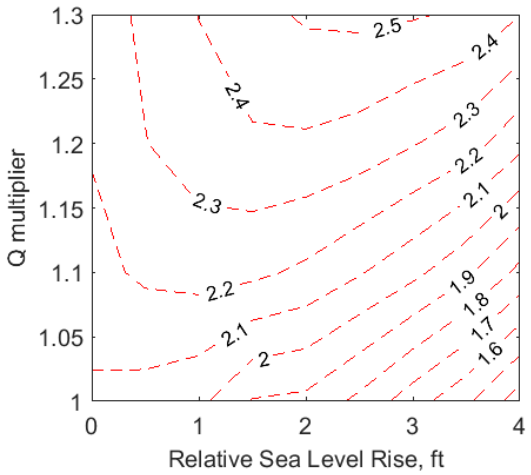

Figure 3-32. Difference contour of 1% annual exceedance (100-year) flood WSEL (ft) for WWTP

The results of this case study are intended to help decision makers to consider the increasing likelihood of inundation at the WWTP in future years. Supposing that the head houses, the entrances to the underground tunnels, are at elevation 11.5 ft (NAVD88), the contour plot of annual exceedance probability of this critical elevation provides information for underground safety assessment (see Figure 3-33). In the current climate, the underground equipment is safe based on the unsteady flow assessment (< 0.001 annual probability of exceedance), but unsafe

based on the steady flow analysis if a 500-year flood prevention regulation is applied. With a downstream sea level rise of 4 ft, the probability of flooding above that elevation increases to 0.0075 for the unsteady flow analysis, lying between the 1% annual exceedance (100-year) and the 0.5% annual exceedance (200-year) event. For the steady flow analysis, a 4 ft sea level rise increases the likelihood of overtopping from 0.005 to 0.02. Likelihood of exceedance becomes increasingly sensitive to both incremental sea level rise and event discharge at higher sea levels.

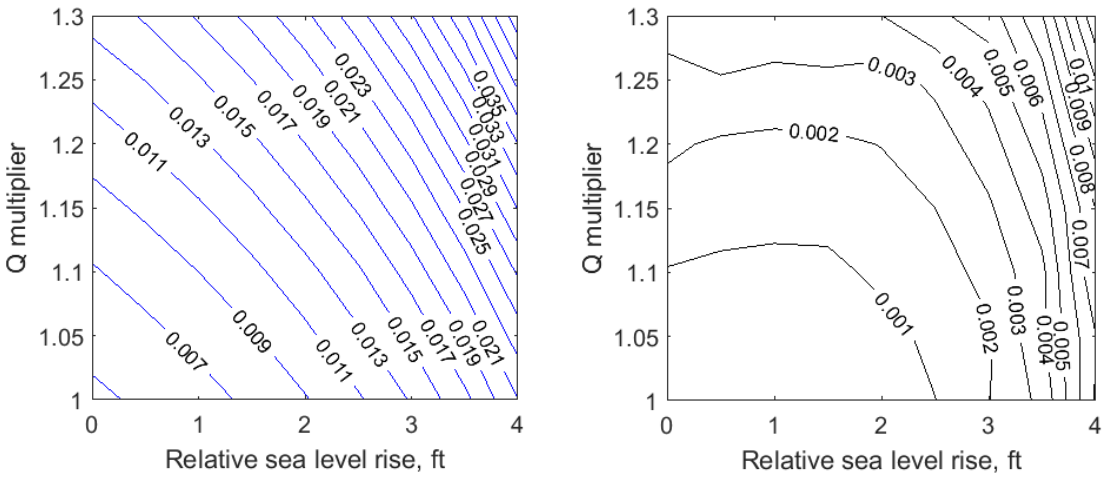

(a) Steady (b) Unsteady

Figure 3-33. Contour plot of annual exceedance probability of 11.5 ft (Potomac River at WWTP)

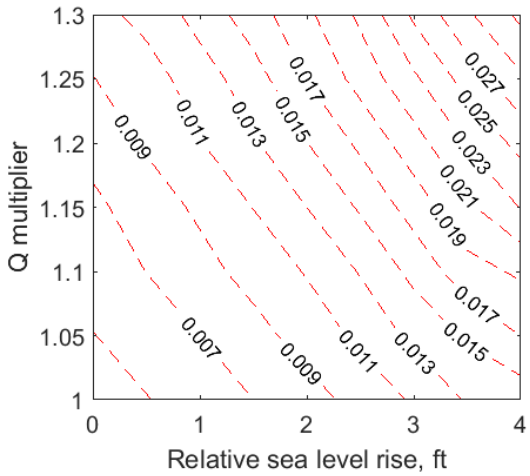

Figure 3-34. Difference contour of annual exceedance probability of 11.5 ft (Potomac River at WWTP)

3.8 Conclusions

This study analyzed the exceedance frequency of annual peak flood WSEL for a wastewater treatment plant located along a tidal estuary under conditions of environmental change that are expected in the next 50 – 100 years. The upstream freshwater input (river flow) and downstream sea level were increased numerically and annual maximum WSEL values were estimated for the ungauged study site under these conditions using HEC-RAS in steady and unsteady mode. The simulation input and output were automated by calling the HEC-RASController. Eighteen years of annual peak events were used for the one-dimensional flow simulation. The exceedance probabilities associated with flood WSEL were calculated for all combinations of sea level rise (9 increments) and increased flood flow (4 increments).

The key findings are:

(1) The steady flow analysis predicts higher WSEL for the study site for low frequency floods compared to the unsteady flow analysis. The opposite trend is observed for the high frequency floods.

(2) Based on the observations in Washington, D.C., the steady flow estimate of the WSEL is more accurate for the low frequency floods compared to the unsteady flow analysis. The opposite trend is observed for the high frequency floods.

(3) The effects of sea level rise and increased event discharge on probability of exceeding a given depth, or the depth associated with a given probability, are not additive, and combine differently for different elevations and probabilities.

Eighteen years of annual peak events were used to estimate future flood WSEL probabilities. Although this is the best available information for this analysis of the study site, and the 18-year period was shown to be reasonably representative of the 81-year period of record for

a gauged site on the estuary, it is a short time period for flood frequency analysis. Nonetheless, this 1-D analysis is an efficient method to examine infrastructure vulnerability through the sensitivity of water level to changing upstream and downstream boundary inputs, and can provide valuable knowledge to stakeholders. The analysis can and should be updated as more measurements become available.

4 BIVARIATE FLOOD STAGE-DURATION FREQUENCY ANALYSIS

4.1 Overview

Most flood risk studies quantify flood likelihood and damage as functions of flood depth. Traditional flood frequency studies provide estimates of exceedance probabilities of various stages or discharges (Davis et al., 2008). The length of time (duration) that a flood remains above a stage is also necessary to define the critical state of a flood and the vulnerability of low-lying infrastructure.

As an alternative to the conventional single-variable assessment, the 1% annual exceedance (100-year) flood can be redefined to reflect both flood stage and duration. The guidance curve provided by the traditional univariate model is two-dimensional, that is, probability is a function of a single variable [Figure 4-1 (a)]; the 1% probability corresponds to a single stage. With the additional dimension of time, the flood stage-duration-frequency curve developed from the bivariate model is three-dimensional, i.e., a function of two variables [Figure 4-1 (b)]; the 1% probability corresponds to a set of (stage, duration) pairs. The proposed method is applicable for gauged streams, estuaries, and tidal sites.

The implementation of this concept can be illustrated by Figure 4-2, which shows a hypothesized WWTP service interruption diagram superimposed on a flood stage hydrograph. The duration of plant inundation, service interruption and outage, and duration of repair is critical to a wastewater treatment flood risk assessment. In Section 2.8, large sample variation is observed for the time required for service interruption and repair. The data available is not sufficient to develop a site-specific service interruption model. However, for the duration of plant inundation, analyses of the joint distribution of flood stage and event duration associated with

stage can be used to quantify the likelihood that the critical infrastructure may be inundated for a certain period of time.

By developing a joint distribution of flood stage and duration, this approach adds a second dimension, time, into flood risk studies. The flood stage-duration-frequency curves serve as new guidance curve for the flood risk management community, as an alternative to the traditional flood stage-frequency curves. By developing the stage-duration-damage relationship, this joint distribution approach also leads to a new concept of expected annual damage to the critical infrastructure.

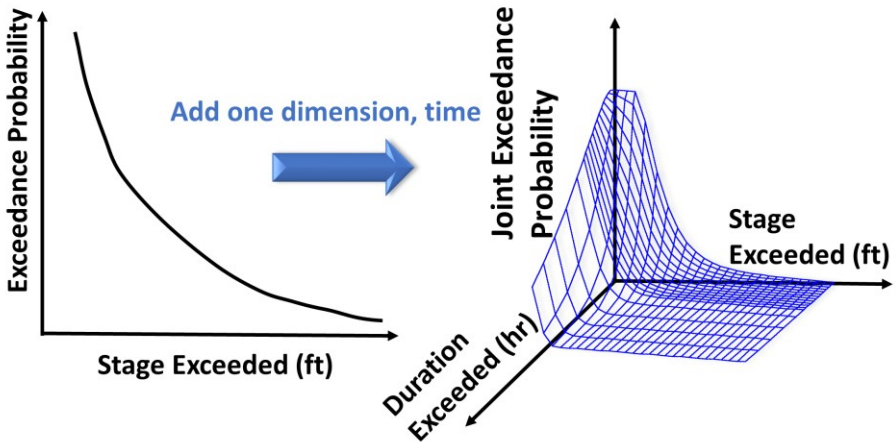

Figure 4-1. Information added to the traditional flood exceedance probability curve

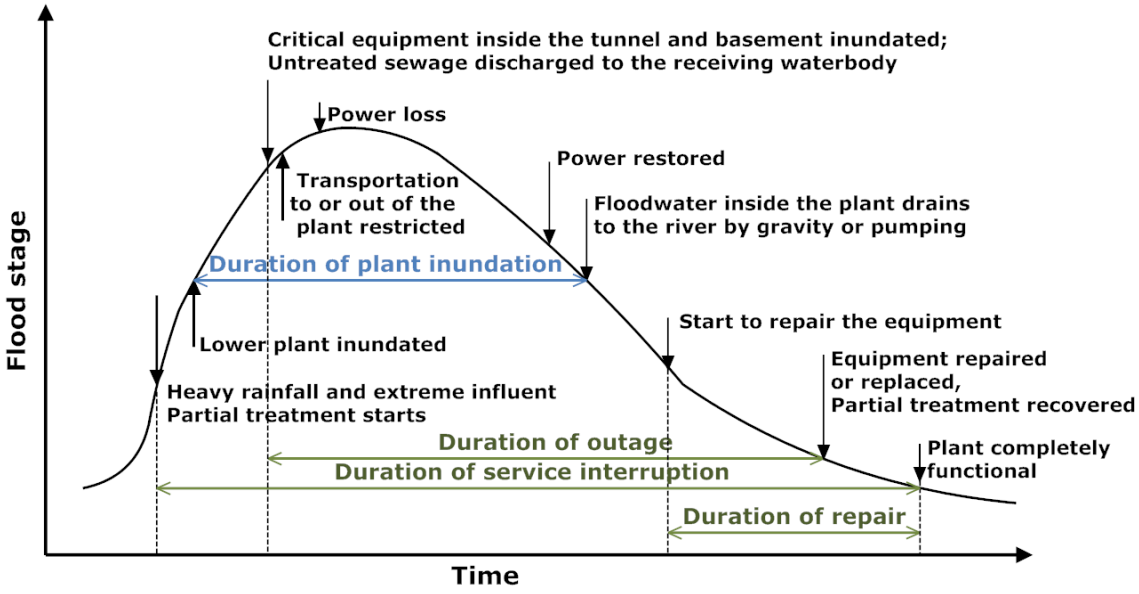

Figure 4-2. Hypothesized service interruption during a flood event

4.2 Methods

4.2.1 Bivariate Flood Model Governing Equation

This study proposes a new method of quantifying the probabilistic relation between flood event duration and the water surface stage. This requires a statistical model that simultaneously considers the two random variables, flood stage (z) and event duration (τ). Beyond the widely-accepted analysis of "What is the likelihood of exceeding a specified elevation (or depth) in a given year?" as expressed by the following equation,

$$\Pr(z \geq z_0) \; in \; a \; given \; year \tag{4-1}$$

the focus is to quantify the likelihood of exceeding a specified elevation for more than a specified time in a given year.

$$\Pr(z \geq z_0, \tau \geq \tau_0) \; in \; a \; given \; year \tag{4-2}$$

When calculated for all (z_0, τ_0), this probability gives a joint exceedance probability function. It describes the stage/event-duration/frequency relationship for a specified location. It is believed *a priori* that flood stage and duration are dependent variables, since lower stages are more likely to be exceeded for longer periods of time. The bivariate exceedance probability can be expressed in terms of a conditional and a univariate probability:

$$\begin{aligned}&\Pr(z \geq z_0, \tau \geq \tau_0 \ in\ a\ given\ year) \\ &= \Pr(\tau \geq \tau_0 \ in\ a\ given\ year \mid z \geq z_0 \ in\ that\ year) \cdot \Pr(z \geq z_0 \ in\ a\ given\ year)\end{aligned} \tag{4-3}$$

The joint exceedance probability is the product of the conditional probability that duration (τ) exceeds a certain time span (τ_0) given that the stage (z) exceeds a specified depth (z_0), and the probability that flood stage (z) exceeds z_0. The former portrays the relationship between flood duration and stage, while the latter equates to the traditional univariate practice.

4.2.2 Hydrological Event Separation and Time Series Extraction

To develop the bivariate flood model, individual events in either a measured database or a simulated sequence need to be identified before being subjected to a statistical analysis. In order to estimate exceedance probabilities and determine the distribution that adequately represents the variables of interest, the data sample needs to be developed from a continuous record of instantaneous stages. The flood duration time series associated with flood stage are prepared using the following steps.

Step 1. Identify a specified stage z_0. For an annual time series of stage, identify all of the upcrossing durations and all of the downcrossing durations associated with this stage. In Figure 4-3, t_1, t_3, t_5 are the upcrossing durations, which are the time periods when the ordinates lie above stage z_0; t_2 and t_4 are the downcrossing durations, which are the time periods when the ordinates lie below z_0.

Step 2. Specify the inter-event duration T_{int}. T_{int} is the prescribed minimum time interval between two different, consecutive events. The end of an event above z_0 is assured when the stage stays below z_0 for a period of T_{int} or longer. Thus, T_{int} defines the maximum allowed downcrossing duration within a single flood event; if the downcrossing duration is less than T_{int}, the upcrossing durations before and after it are considered as a single event. An example of this step is illustrated in Figure 4-3; if $t_2<T_{int}$ and $t_4>T_{int}$, the durations collected for this time series are $D_1= t_1+t_2+t_3$, $D_2= t_5$, where D is the duration after considering T_{int}. In this example, if T_{int} is set to 0, then $D_1=t_1$, $D_2=t_3$ and $D_3 = t_4$.

Step 3. Identify the annual maximum exceedance duration ($\tau|z>z_0$). The value of annual maximum duration for any one year is the longest period of time over which the stage does not drop below z_0. It can also be viewed as the maximum length of time that the hydrograph stays above stage z_0 in a given year. For a gauged site, τ is a function of z_0 and T_{int}. For example, suppose that Figure 4-3 shows the stage time series for a water year (WY), if $T_{int}<t_2<t_4$, the annual maximum exceedance duration above stage z_0 is τ_1. In this case, t_2 and t_4 are large enough compared to T_{int} to separate the stage time series into three separate events (t_1, t_3, and t_5) and the event with the longest duration in this water year is $\tau_1=t_1$. For $t_2<T_{int}<t_4$ and $t_2<t_4<T_{int}$, the annual maximum duration exceeds stage z_0 are τ_2 and τ_3, respectively. For simplicity, the annual maximum exceedance duration is referred to as the annual maximum duration.

Step 4. Assemble the record of annual maximum durations. The record is developed by repeating step 1 to 3 for all stages in the observed range, which provides the conditional annual maximum duration $\tau|z>z_0$ for all available water years. This record consists of at most one duration per year of record and depends on z_0 and T_{int}.

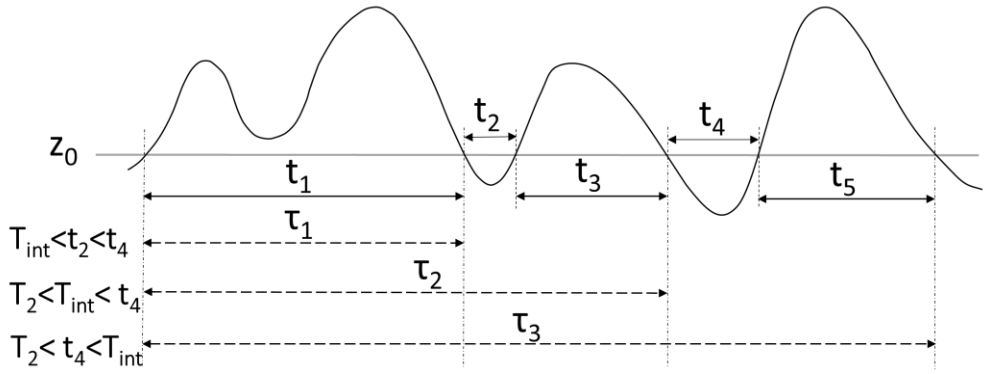

Figure 4-3. Effect of inter-event time T_{int} on extracting event duration from stage time series

The hourly stage time series from WY 1933 to 2013 of a tidal gauge, Potomac River at Washington, D.C., (NOAA 8594900), is analyzed as an example. Figure 4-4 shows the hourly data for WY 1996. The river stage exceeded 6.5 ft during three events, with exceedance durations of 6, 3, and 4 hours; therefore, the annual maximum duration (τ) of 6.5 ft is 6 hours. The raw instantaneous data can be viewed as an equivalent to setting T_{int} as zero.

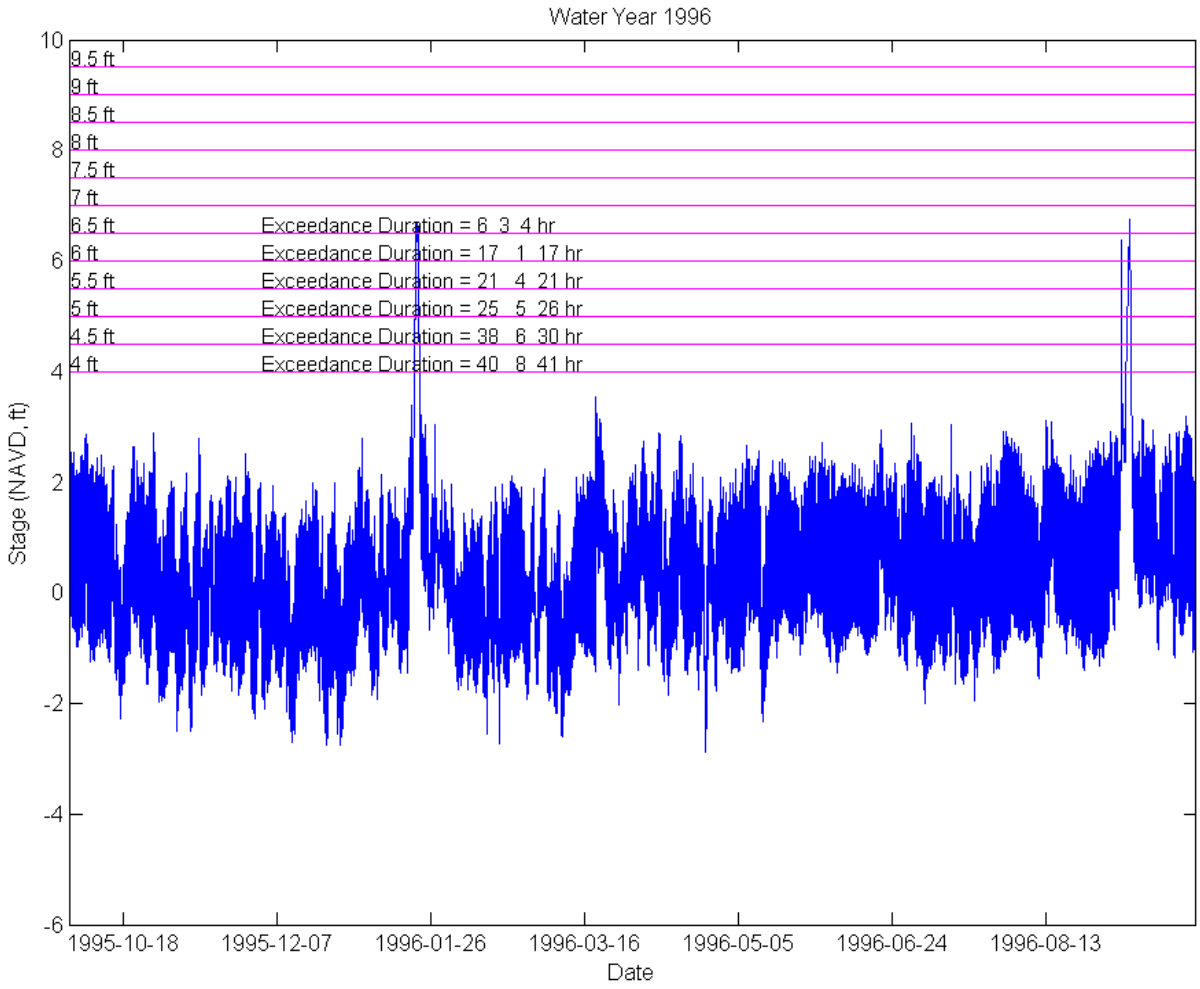

Figure 4-4. Hourly stage time series for Potomac River at Washington, D.C. (NOAA 8594900)

4.2.3 Development of the Joint Probability Distribution of Stage and Duration

As formulated in the previous section, the joint probability distribution of stage and duration is a product of the marginal distribution of stage and the conditional distribution of duration. As discussed in Section 3.4.2.2, the GEV distribution is the overall best fit for WSEL. To ensure consistency of marginal distribution model for the four study sites, GEV is selected for the bivariate model in this Chapter.

The conditional probability distribution, $\Pr(\tau>\tau_0$ in a given year$|z>z_0$ in that year), is modeled by the exponential distribution function.

$$f\ (\tau \mid z > z_0) = \begin{cases} \lambda \exp(-\lambda \tau) & t \geq 0 \\ 0 & t < 0 \end{cases} \quad \text{(4-4a)}$$

$$\lambda = \frac{1}{\mu} \quad \text{(4-4b)}$$

where λ is the scale parameter ($\lambda > 0$) and μ is the mean of the annual maximum durations. The corresponding conditional exceedance probability (conditional complementary cumulative distribution) is given by

$$P(\tau > \tau_0 \mid z > z_0) \ = \ \exp(-\lambda \tau_0) \quad \text{(4-5)}$$

For each stage, z_0, and T_{int}, the sample distribution of τ can be fitted with the exponential distribution. Exponential distributions are commonly used to characterize time related climatological variables. For example, the probability density functions of storm duration and time between storms have been modeled by the exponential distribution [Eagleson (1972), Leclerc and Schaake (1972)].

$$\textit{Storm duration for point rainfall} \qquad f(t_r) = \lambda \cdot \exp(-\lambda \cdot t_r) \quad \text{(4-6)}$$

$$\textit{Time between storms} \qquad f(\tau) = \lambda \cdot \exp(-\lambda \cdot \tau) \quad \text{(4-7)}$$

$$\textit{Storm total depth} \qquad f(d \mid t_r) = \beta \exp(-\beta d / t_r) \quad \text{(4-8)}$$

where t_r is duration in hours and $t_r>0$; λ is the parameter for the distribution; d is depth in inch; τ is time between storms (Leclerc & Schaake, 1972).

In this study, the mean, μ, of the conditional distribution of τ is expected to be a decreasing function of z_0, consistent with the prior reasoning that time series upcrossings above lower z_0 are by necessity longer than those above the higher z_0. By physical reasoning, this function should asymptotically approach zero as z_0 becomes very large. This is rational because there should exist some stage high enough that the flood water will never have exceeded the

value for the duration of the flood record (mean conditional duration equals zero). At the minimum value of z_0 (lowest possible stage of the river or estuary), μ must equal 1 year, because that depth is exceeded in every year. Additionally, the slope of the function should be zero at the low end. This is rational because any stage lower than the physical minimum is exceeded for the entire year (8760 hours) in every year. How the function varies between these two endpoints must be determined from analysis of the data. An inflection point must exist between these two boundary conditions. Conceptual examples are shown in Figure 4-5.

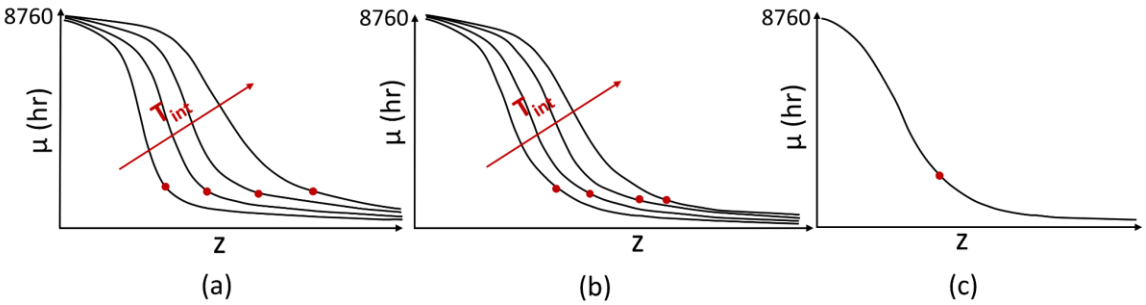

Figure 4-5. Trends of mean annual maximum duration above stage z for (a) tidal, (b) estuary, and (c) riverine sites

Note: dot =breakpoint of the composite model; T_{int} increases in the direction indicated by the arrow

To further establish the link with T_{int}, three assumptions are made for the mean annual maximum duration (μ) as a function of stage (z).

- Assumption 1: For the tidal and estuary sites, the mean annual maximum duration is a function of inter-event time T_{int}. For each stage (z), the mean annual maximum duration is expected to increase in the direction indicated by the arrow in Figure 4-5. For the riverine sites, the effect of T_{int} is negligible. The rationality of this assumption is that the variation of the water surface elevation is less significant for the river than for a tidal estuary. If the

hydrographs for the riverine sites and tidal sites are graphed based on the same time interval, e.g., one day, the rising and falling limbs of the riverine hydrograph are less sloped than the semi-diurnal tidal hydrograph. For the same time interval, more peaks are observed for the tidal hydrograph. Therefore, a small T_{int} is more likely to separate the tidal fluctuations into multiple events above the specified stage.

- Assumption 2: When the mean duration above stage is plotted as a function of stage, there is one value of stage, termed the stage breakpoint, below which the function can be modeled by an exponential decay. The curve above the breakpoint can be modeled by a logistic function. For the tidal and estuary sites, the breakpoint is expected to vary with T_{int}. For the riverine sites, the breakpoint is the same for all T_{int}. The exponential decay section allows the mean annual maximum duration (μ) to asymptotically approach zero at higher stages. The logistic function approaches a constant value as stage approaches negative infinity. These analytical conditions are physical and rational, as discussed above.
- Assumption 3: When the tidal effect is significant, the logistic section dominates the curves; that is, the stage breakpoint is higher than for a riverine site with a similar range of stage. As riverine effects dominate, a greater proportion of the stage range will fall in the exponential decay section; that is, the stage breakpoint is lower than for a tidal site with a similar range. This relation is due to the physical nature of tidal sites, which are usually characterized by greater open water and less peaked flood stage hydrographs.

Based on these assumptions, a model was developed to estimate the mean annual maximum duration (μ) using stage (z) and T_{int} as the predictor variables. For the riverine sites, a value of 0 is used for T_{int} because μ is not sensitive to T_{int}=0.

$$\mu = \begin{cases} \dfrac{a \cdot exp(b \cdot z)}{\left(\dfrac{T_{int}}{12}+1\right)^{d}+c} & if\ z \geq breakpoint \quad (4\text{-}9a) \\ min\left[8760,\ \dfrac{f_i}{g_i + exp(e_i \cdot z)} + h_i\right] & if\ z < breakpoint \quad (4\text{-}9b) \end{cases}$$

where z is water surface elevation or stage, the subscript i indicates that the parameters e, f, g, h and *breakpoint* vary with T_{int}; 8760 is the total hours in a year, which is also the longest possible duration that a stage (z) can be exceeded in a year; a, b, c, d, e, f, g, h are parameters estimated using least-square regression.

It should be noted that in order to ensure the independence of hydrological events, only the floods that produced the annual maximum values of each variable are considered in the analysis. Annual maximum stages are selected to compute the marginal distribution, $\Pr(z>z_0)$. An annual maximum exceedance duration is only meaningful when it is mentioned with the flood stage that is exceeded, $\Pr(\tau>\tau_0 \mid z>z_0)$. Based on the rationality of the annual maximum series, the stages below the minimum value of the annual maximum stage are not applicable in the calculation of the joint exceedance probability. Nevertheless, the dependence of mean annual maximum duration (μ) on the stage exceeded is developed for all stages less than the minimum annual maximum stage; including the lower stages that provide the information required to estimate the shape of the $\mu(z)$ curve, in particular, its value and slope at the minimum annual maximum. Only the part that is above the minimum annual maximum stage is used in the joint distribution computation in this study. Therefore, the regression analysis for the mean annual maximum duration (μ) should be performed for the full range of stages and then the applicable section should be selected for calculating the conditional and joint distributions.

With the marginal complementary cumulative distribution (exceedance probability) of annual maximum stage calculated by Eq.(4-1), and the conditional complementary cumulative

distribution (conditional exceedance probability) of ($\tau_0|z>z_0$) calculated by Eq.(4-4) using the conditional mean [Eq.(4-9)], the joint exceedance probability function, Eq.(4-3), can be calculated. This value provides an estimate of the probability of exceeding a specified stage for longer than a specified duration in a given year. The procedure is illustrated with examples in the following section.

4.3 Testing of the Model

Hourly stage time series for four gauged sites in the Mid-Atlantic region of the U.S. were selected to test the model on a variety of tidal and riverine locations (Figure 3-12). The four study sites are introduced in Section 3.4.2.2. An annual maximum stage analysis was conducted for each site; the inferred GEV population distributions are shown in Figure 4-6. The Kolmogorov-Smirnov test suggests that the null hypothesis that the population and the sample are from the same distribution cannot be rejected at the 5% significance level for all four sites, with p value of 0.92, 0.67, 0.97, 0.53 for DC, the Battery, Susquehanna, and Western Run, respectively (Table 3-3).

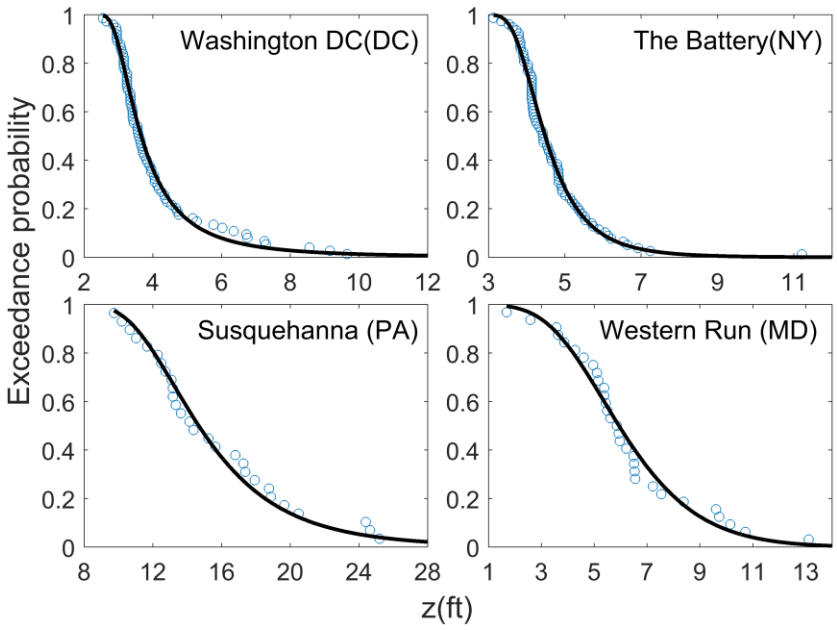

Figure 4-6. Marginal distribution (GEV) of flood stage

Exploratory analysis of annual maximum duration above stage, τ, confirmed that the inter-event time T_{int} plays a more important role in a tidal environment than in a riverine site. The sample distribution of the conditional annual maximum duration for a tidal estuary [Potomac River at Washington, D.C. (DC)] is compared in the trellis plot of (Figure 4-7). For the same stage, the distribution shifts to the right when T_{int} is higher, consistent with including longer time periods in the definition of an upcrossing duration. Beyond 12 hours, the frequency distribution does not change noticeably with increase in T_{int}, implying that the tidal cycle is filtered out when T_{int} is greater than or equal to 12 hours. For the same T_{int}, the distribution is positively skewed when the stage is high and negatively skewed when the stage is low. It is verified that the exponential distribution of $\tau|z>z_0$ is applicable for a wide range of stages and T_{int}. The fitted exponential distribution for the four study sites are plotted against the sample Weibull plotting position (see Figure 4-8). Although the fit to observations is not perfect, the exponential distribution is confirmed as an appropriate model for purposes of this study. Further analysis could improve on the model of μ, particularly at the DC location [Fig. 4-8 (a)].

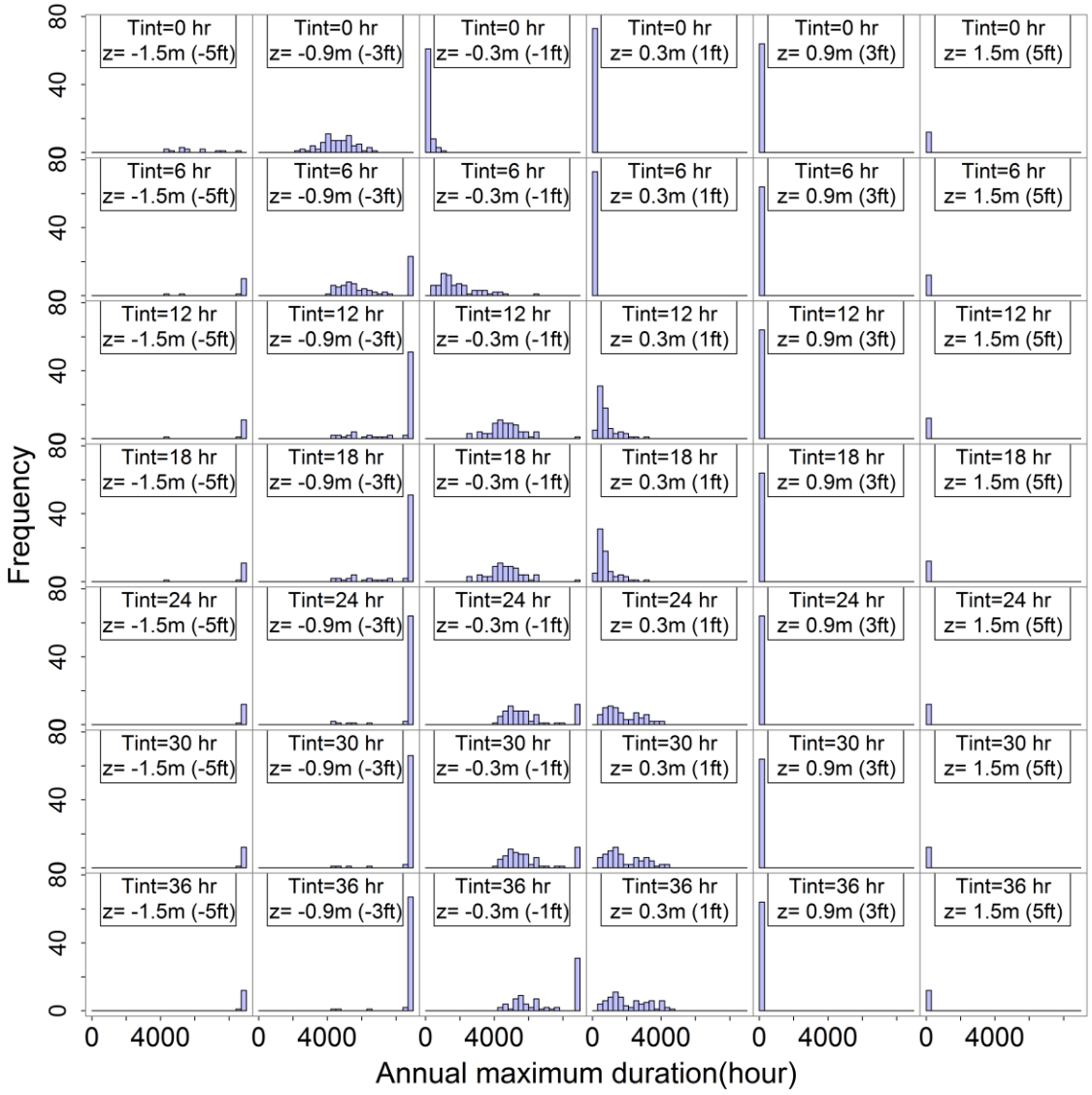

Figure 4-7. Sample frequency distribution of annual maximum duration (Potomac River at Washington, D.C.)

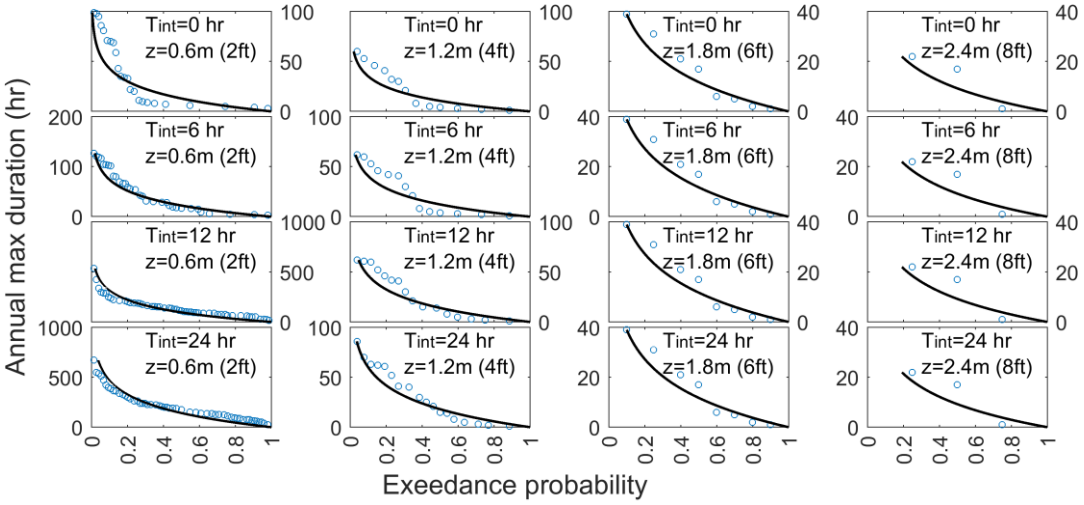

(a) Washington, D.C.

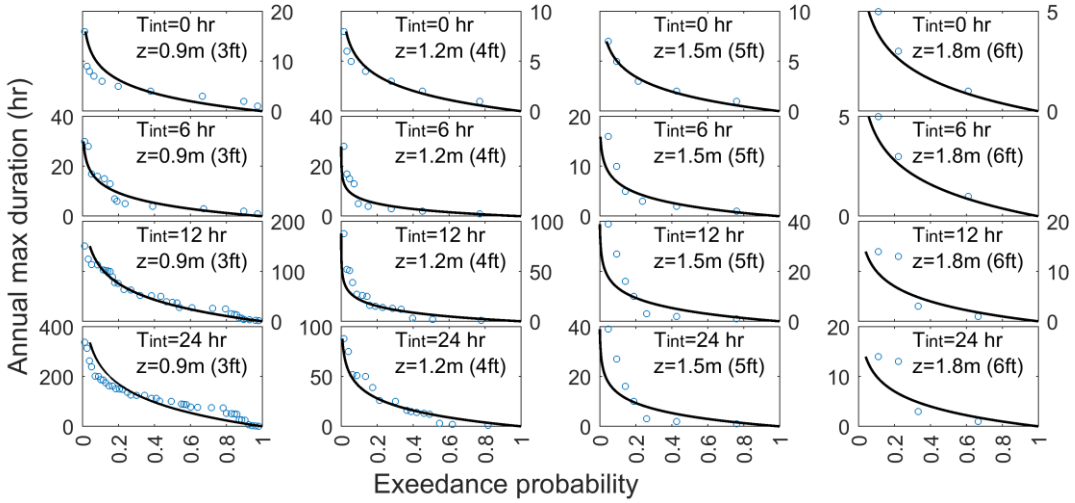

(b) The Battery

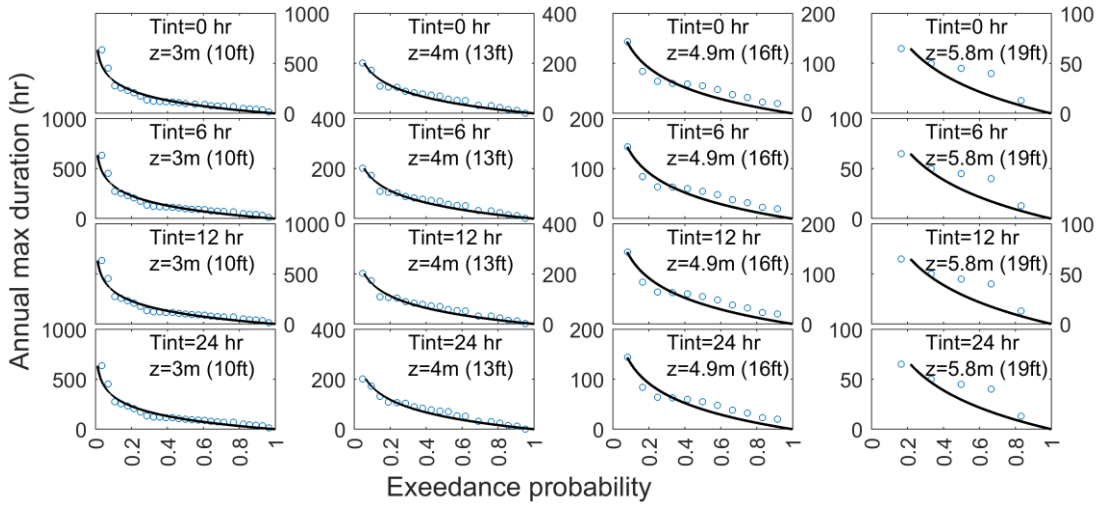

(c) Susquehanna

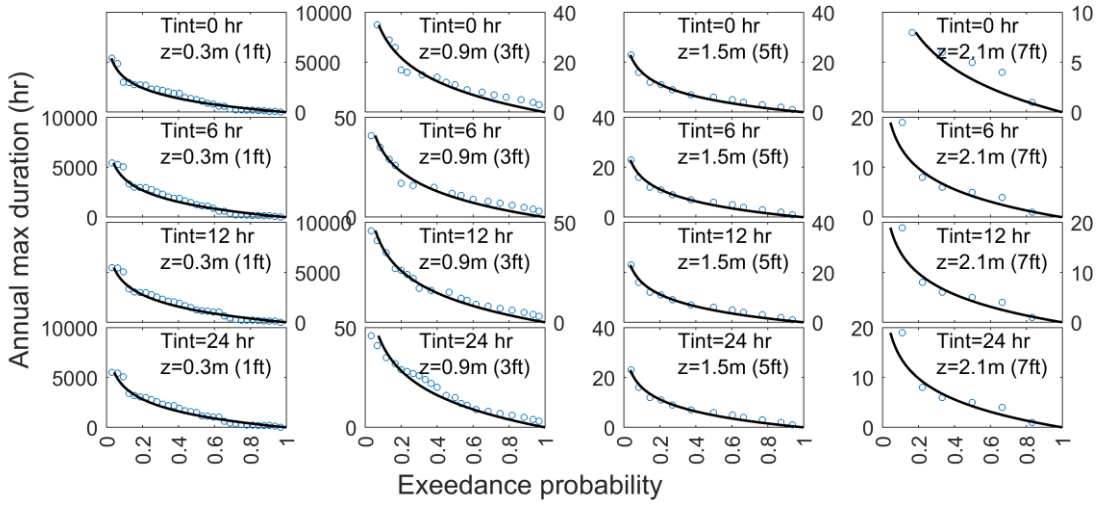

(d) Western Run

Figure 4-8. Exponential distribution of annual maximum duration

In further parameterizing the exponential distribution of annual maximum duration and verifying the three assumptions for the mean, the sample mean annual maximum durations for the four study sites are graphed in Figure 4-9. The riverine sites were much less sensitive to T_{int} than were the tidal sites. For the tidal sites, a longer T_{int} corresponds to higher value of the annual maximum duration, which resulted in a larger mean annual maximum duration. As the stage

increases, the sample size of annual maximum duration decreases, as fewer event hydrographs above that stage occur.

It is also observed that T_{int} is less influential for the higher stage range than for the lower stage range. Data analyses suggest that the few extreme high stage events observed in a water year are more likely to be further apart temporally than the many low stage events. Therefore, T_{int} is less likely to play a significant role in separating the events and alter the shape of the sample distribution of duration.

Results of the regression analyses of the annual mean duration for the study sites are illustrated in Figure 4-10. The parameters in Eq.(4-9) are solved based on continuity of magnitude and slope. Based on continuity of magnitude, the μ computed by logistic function and exponential function are equal at the stage of break.

$$\frac{a \cdot \exp\ (b \cdot break_i)}{\left(\frac{T_{\text{int}}}{12}+1\right)^d + c} = \frac{f_i}{g_i + \exp\ (e_i \cdot break_i)} + h_i \tag{4-10}$$

This leads to

$$h_i = - \frac{a \cdot \exp(b \cdot break_i)}{\left[\left(\frac{T_{\text{int}}}{12}+1\right)^d + c\right]} - \frac{f_i}{g_i + \exp(e_i \cdot break_i)} \tag{4-11}$$

The slope of the curve evaluated at '*break*' is

$$\left.\frac{d\ \mu}{d\ z}\right|_{z=break} = \begin{cases} \dfrac{a \cdot b \cdot \exp\left(b \cdot break_i\right)}{\left(\frac{T_{\text{int}}}{12}+1\right)^d + c} & if\ z \geq break_i \\ \dfrac{-f_i \cdot e_i \cdot \exp\left(e_i \cdot break_i\right)}{\left[g_i + \exp\left(e_i \cdot break_i\right)\right]^2} & if\ z < break_i \end{cases} \tag{4-12}$$

Based on continuity of slope, the slope of the exponential and the logistic section of Eq. (4-9) are equal, which leads to

$$f_i = - \frac{a \cdot b \cdot \exp(b \cdot break_i)[g_i + \exp(e_i \cdot break_i)]^2}{\left[\left(\frac{T_{\text{int}}}{12}+1\right)^d + c\right] \cdot e_i \cdot \exp(e_i \cdot break_i)} \tag{4-13}$$

$$h_i = - \frac{a \cdot \exp(b \cdot break_i)}{\left[\left(\frac{T_{\text{int}}}{12}+1\right)^d + c\right]} - \frac{f_i}{g_i + \exp(e_i \cdot break_i)} \tag{4-14}$$

Finally, the parameters are estimated by minimizing the least-squares objective function F.

$$F = \sum_{i=1}^{n} (\mu_i - \mu_i)^2 \tag{4-15}$$

where n is the number of observations, $\hat{}$ is the ith predicted mean of the annual maximum exceedance duration and μ_i is the ith observed mean of annual maximum exceedance duration. The parameters in Eq. (4-9) are summarized in Table 4-1.

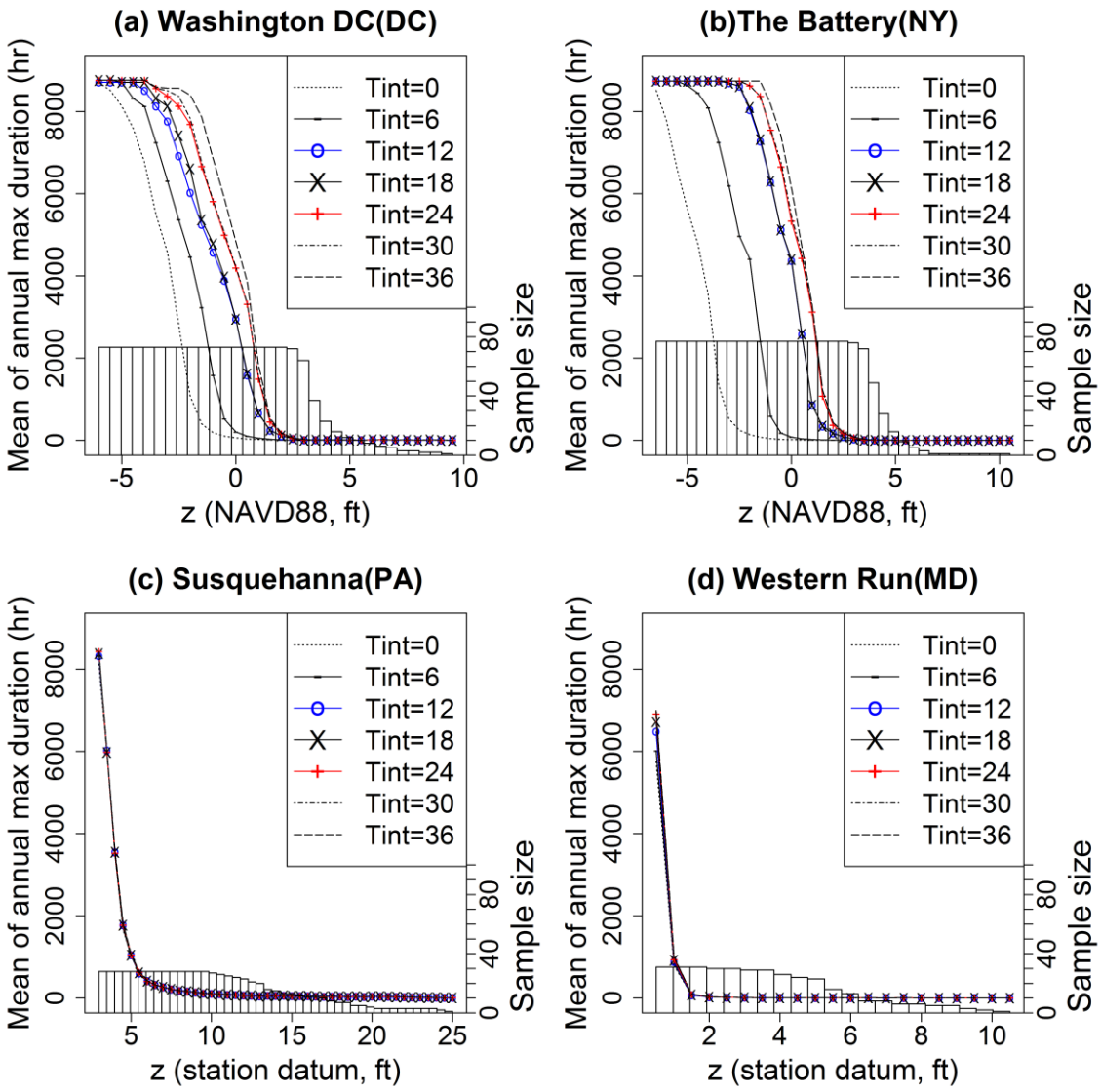

Figure 4-9. Mean annual maximum duration conditional on stage, with sample size

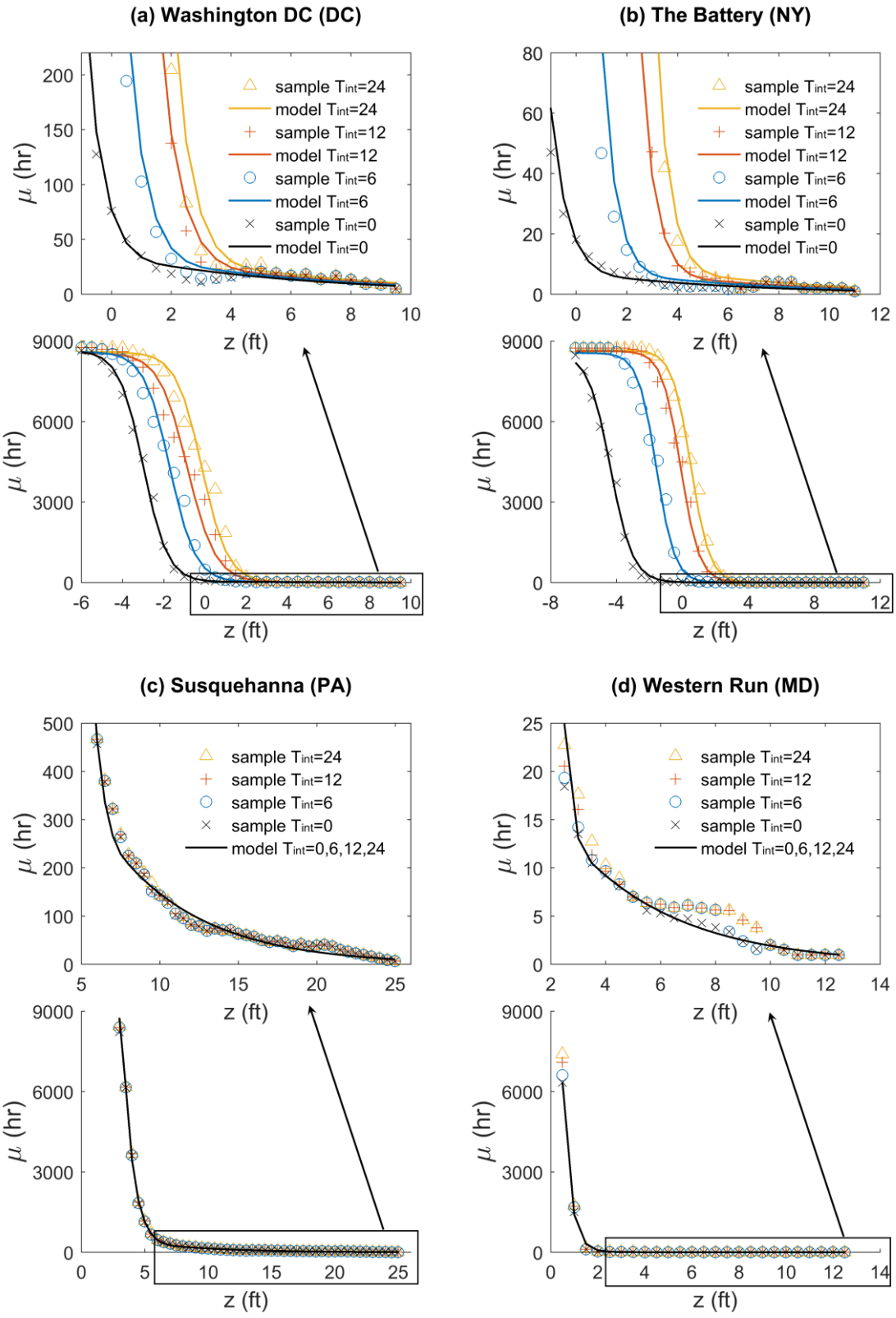

Figure 4-10. Regression analysis of conditional mean annual maximum duration (μ)

Table 4-1. Parameters for least squares curve fitting of mean annual maximum exceedance duration (μ)

	Parameter	Washington, D.C.	The Battery	Susquehanna	Western Run
T_{int}=0,6,12,24	a	4.9342	6.6855	45.3201	43.7085
	b	-0.1600	-0.1627	-0.1737	-0.2596
	c	-0.8600	-0.0880	-0.9457	0.6801
	d	-0.0340	-0.5325	-0.5325	-0.5325
T_{int}=0	e	1.6954	1.4835	1.2265	3.0201
	f	53.9698	13.0266	440404.9712	28731.1899
	g	0.0063	0.0015	0.0015	0.0015
	h	23.8745	4.6314	184.5716	9.7667
	break	1.8146	2.1088	7.8100	3.4272
T_{int}=6	e	1.6096	1.8037	NA	NA
	f	547.9136	495.1177	NA	NA
	g	0.0638	0.0578	NA	NA
	h	20.3734	4.5025	NA	NA
	break	3.4141	3.8873	NA	NA
T_{int}=12	e	1.4632	1.7667	NA	NA
	f	2445.9042	7109.4504	NA	NA
	g	0.2862	0.8237	NA	NA
	h	17.4365	4.1009	NA	NA
	break	4.8117	5.5166	NA	NA
T_{int}=24	e	1.6060	1.7622	NA	NA
	f	6736.9924	21453.2117	NA	NA
	g	0.7859	2.4764	NA	NA
	h	19.2626	4.8241	NA	NA
	break	5.0176	6.0639	NA	NA

For the stages of interest, the composite model [Eq.(4-9)] adequately captures the sample distribution of conditional mean annual maximum duration (μ). The conditional distribution of duration given stage exceeded is then computed by Eq. (4-4) according to the regression analyses of the mean annual maximum duration (see Figure 4-11).

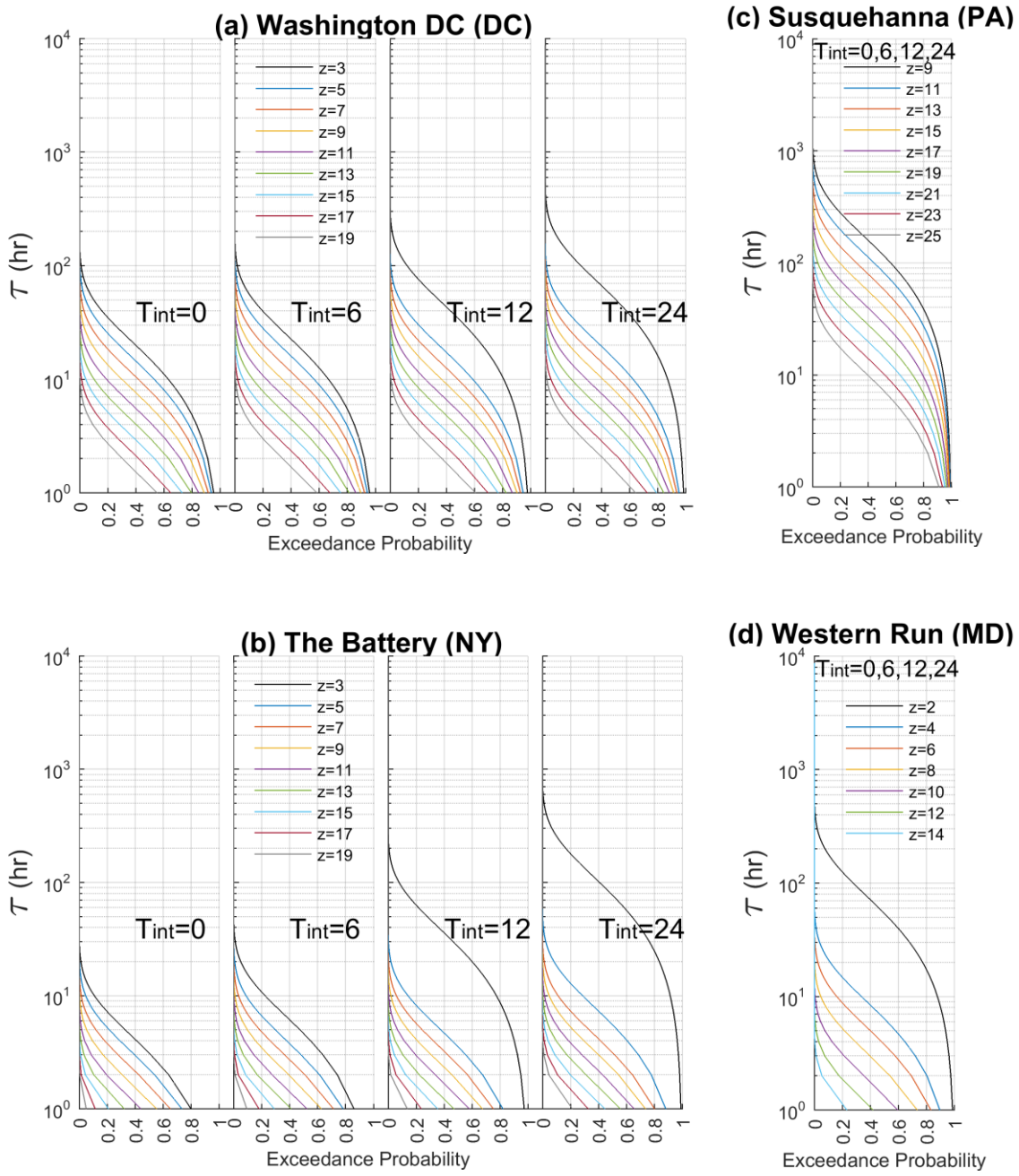

Figure 4-11. Conditional exceedance probability of annual maximum duration (μ)

To measure the dispersion of the annual maximum exceedance duration, the standard error of the mean is estimated by

$$SE_{\bar{\tau}} = \frac{S}{\sqrt{n}} = \frac{\sqrt{\sum_{i=1}^{n}(\tau_i - \bar{\tau})^2}}{\sqrt{n(n-1)}} \quad (4\text{-}16)$$

where S is the sample standard deviation; n is the sample size, and τ is the annual maximum exceedance duration (Ayyub & McCuen, 2011). The mean of annual maximum exceedance duration is presented in Figure 4-12 , with $\pm$1.96*SE plotted as error bars. Assuming that the sample size of annual maximum exceedance duration is large enough that the Central Limit Theorem is valid, the sample mean can be assumed to be normally distributed. Suppose that when the sample size is large enough, the difference of student t distribution and the normal distribution is negligible, the error bars in Figure 4-12 can also be a rough estimate of the 95% confidence interval (CI) of the mean, which implies 95% confidence that the true value of mean (μ) lies within the upper and lower bounds. The annual maximum exceedance duration is not normally distributed for all stages. This approximation of 95% CI is only valid for stages within the middle range, e.g., stages between -2.5 to 1.5 ft for T_{int}=6 hours (Washington, D.C.). It is not valid for high and low stages.

With the marginal exceedance (complementary cumulative) distribution function of stage and the conditional exceedance (complementary cumulative) distribution function of event duration determined, the joint exceedance probability function can be calculated following Eq.(4-3). The result is a bounded function of two variables, shown as a three-dimensional surface and the corresponding contour graph in Figure 4-13. When a higher T_{int} is assumed, the shorter annual maximum duration may be captured for each year, so that the likelihood of certain stage and duration being exceeded are smaller.

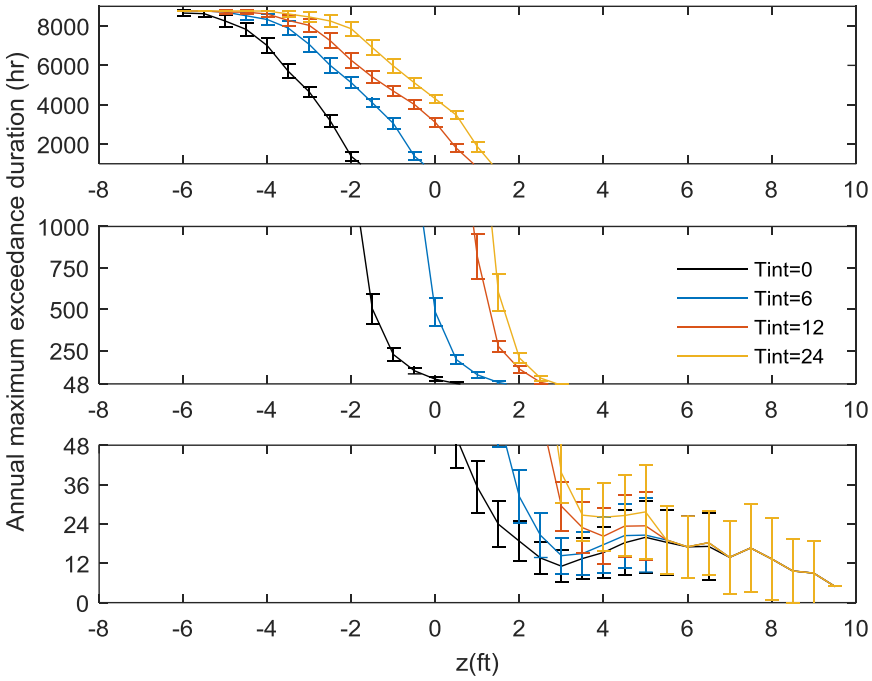

(a) Washington, D.C.

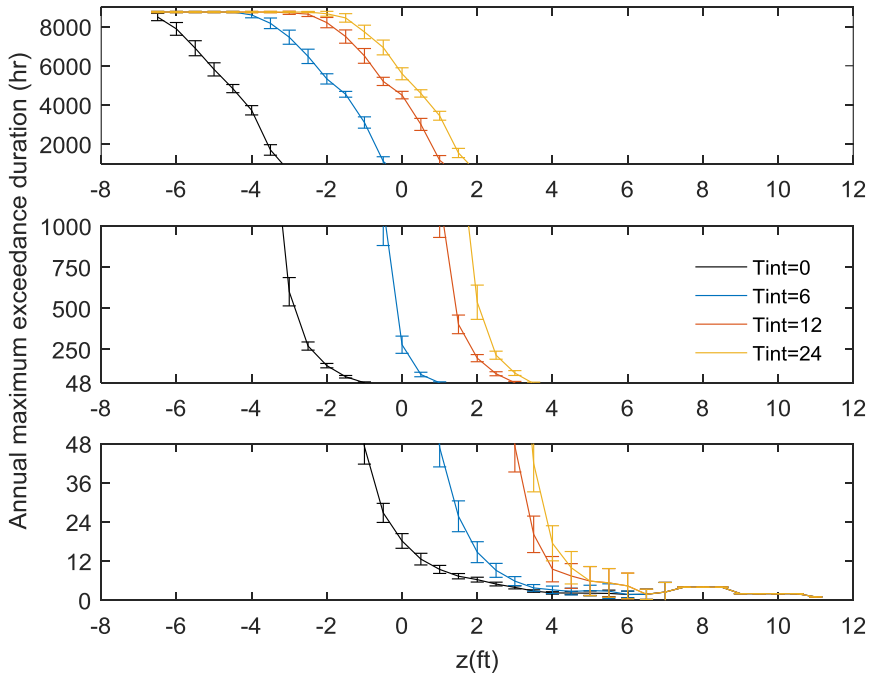

(b) The Battery

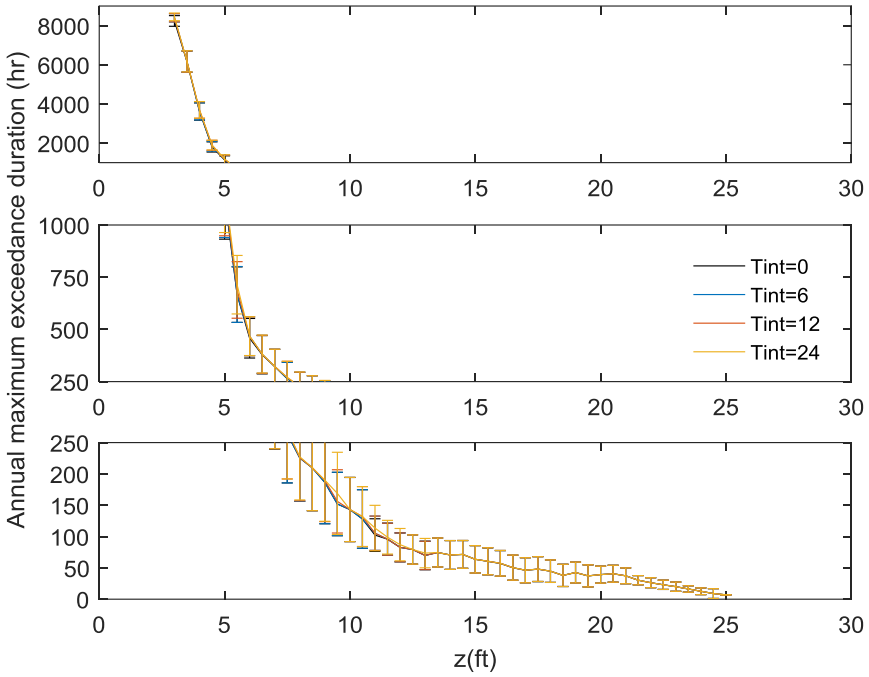

(c) Susquehanna

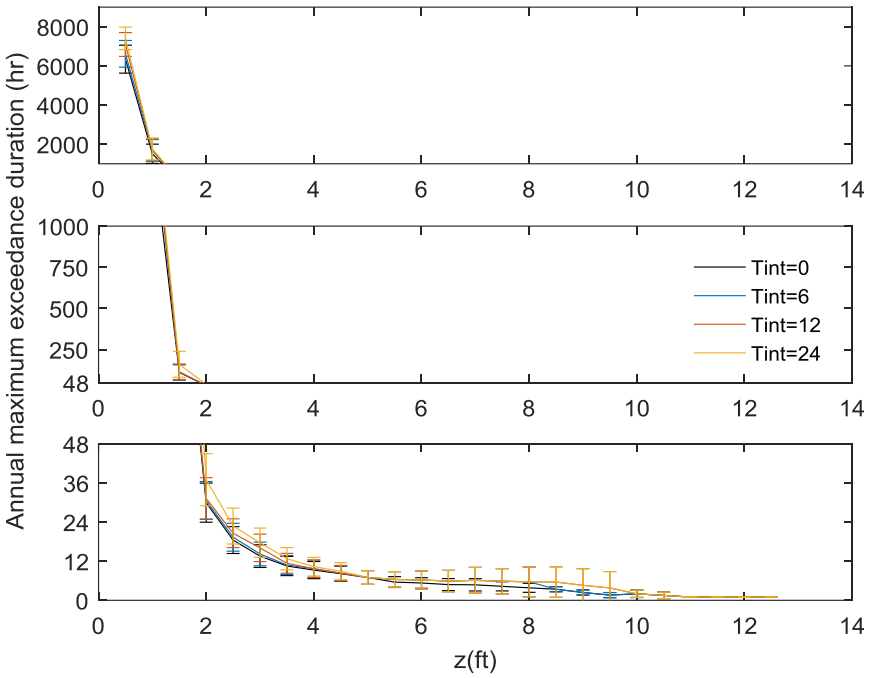

(d) Western Run

Figure 4-12. Mean and error bar of annual maximum exceedance duration (τ)
Note: Error bar shows $\bar{\tau} \pm 1.96 * SE$

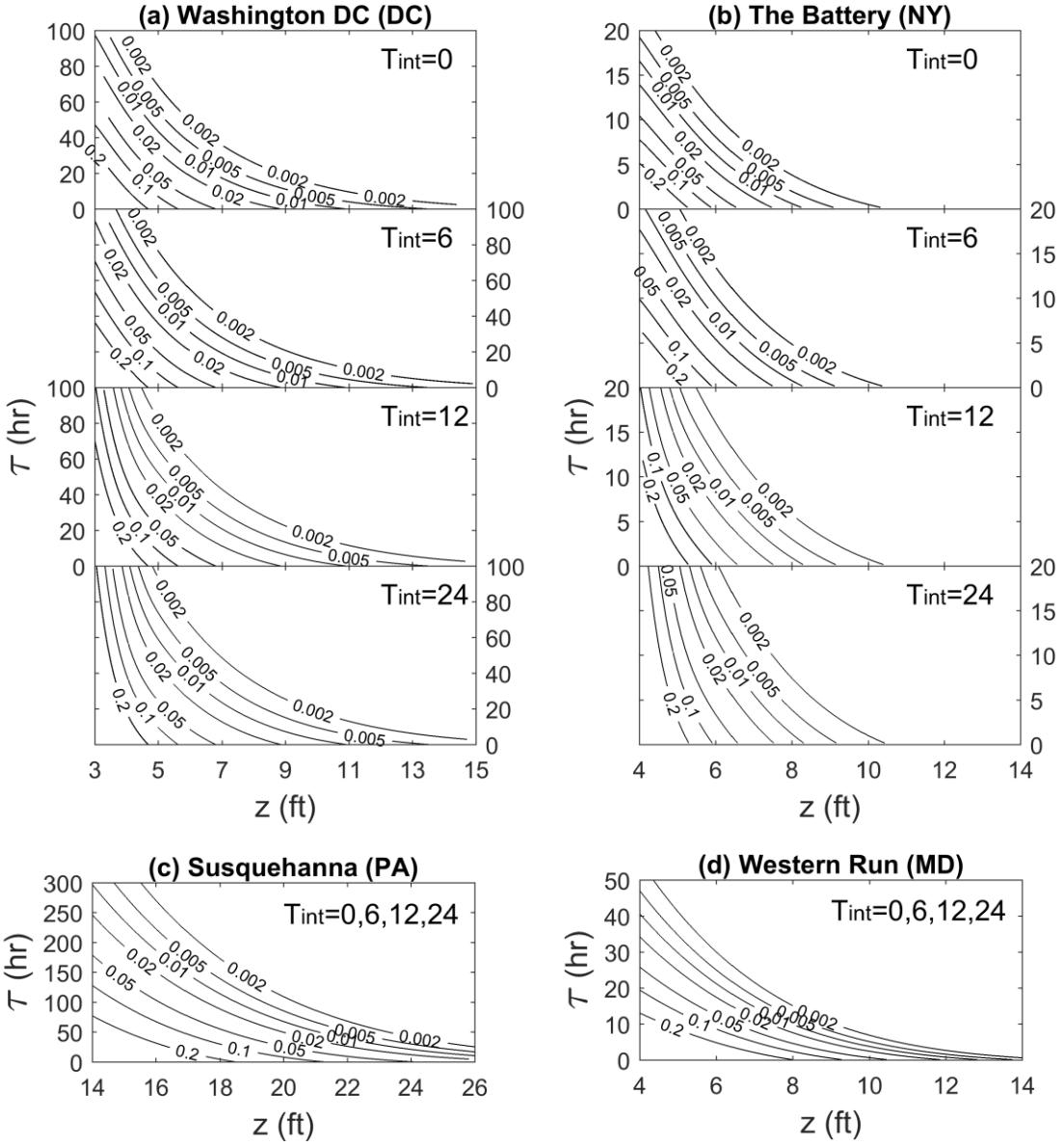

Figure 4-13. Joint Exceedance Probability Function of stage and duration

4.4 Implications

In the traditional flood risk study, the one percent annual probability (100-year) flood is described by a single flood stage magnitude. However, the bivariate model in this study produces a set of flood stage and duration combinations that have one percent probability of being exceeded, as

indicated by the 1% (100-year) contour line. For a specified stage, longer durations are less likely, as shown by the lower probabilities (corresponding to longer return periods) moving up on the graph (see Figure 4-13); for a given duration, higher stages are less likely, as shown by lower probabilities moving right on the graph. The duration $\tau = 0$ corresponds to exceeding stage z_0 for any length of time; therefore, the z-axis intercept of each Probability/Return Period curve represents the T-year instantaneous peak flood stage for a given return period T. The τ-axis intercept gives the duration of excursion above any stage that is exceeded with that probability in a given year; very short durations are very likely to be exceeded, and the exceedance probability goes to zero as τ goes to infinity.

In the traditional univariate flood stage-frequency study, the one percent (100-year) flood is considered a severer flood than the two percent (50-year flood), since the 100-year flood stage is higher than the 50-year flood stage. However, in the bivariate flood stage-duration-frequency study, a one percent (100-year) flood may correspond to a lower stage than a two percent (50-year) flood if the duration above lower stage is much longer. This result is reasonable from a risk perspective, because a facility may be offline for a longer duration with a greater loss of production; the less severe flood stage is compensated by the longer duration. Professional judgment is required to define the severity of flood according to appropriate criteria. When the duration of flooding has economic, societal, or environmental implications, it may be negligent to ignore the out-of-service time due to a relatively shallow, but long-lasting, inundation. Additionally, when considering structural damage, the building inundation time span may be a critical criterion, although the inundation depths that differ one foot may not change the damage significantly. In this case, the portion of the joint exceedance distribution curve that reflects the sensitivity of duration to frequency is essential.

4.5 Conclusions

In this Chapter, flood event duration is considered, in addition to flood stage or depth as a critical variable for flood frequency assessment. Although the traditional univariate flood model is widely accepted and applied in flood risk assessment, the bivariate flood frequency model (stage and event duration) can serve as an alternative due to its advantage in simultaneous consideration of two important variables. Knowledge of this additional dimension, flood duration, is essential for the design of sustainable and resilient infrastructure systems. The joint distribution provides information about the duration that an infrastructure element is likely to be submerged or out of service. The stage-duration-frequency curves provide guidance for civil infrastructure design and flood mitigation planning.

The application on four study sites demonstrated that the model is feasible for both tidal and riverine environments. The method for preparing the duration dataset is robust, which indicates the potential of implementation on any gauged location. The inter-event interval (T_{int}) is a user defined value depending on the purpose of the flood risk analysis. If the analysis is prepared for a critical infrastructure, a T_{int} equal to or longer than the best estimate of the recovery and restoration time is recommended. If the river stage draws down below a critical level for a time period shorter than the recovery and restoration time, the flood event should be taken as a continuous event. To illustrate the potential real world application, Figure 4-3 can be viewed as an instantaneous stage time series at the location of a critical infrastructure element, e.g., a wastewater treatment plant, and the elevation z_0 can be assumed to be a critical inundation elevation above which the infrastructure is rendered inoperable. When preparing the sample data for the bivariate model, if the recovery time of the infrastructure is longer than t_2 and t_4, the duration of the flood event should be treated as τ_3, since corrective action could not be taken during the short periods t_2 and t_4, even though the river stage drops below the critical elevation.

To estimate the volume of water that intrudes into underground tunnels, only the amount of time that the stage is above the elevation required to flood the tunnel is vital to the computation; in this case, T_{int} should be set to zero. Further physical modeling would be required to estimate the likelihood of damage or out-of-service time for underground facilities.

5 FLOOD IMPACT MODEL

5.1 Overview

In this chapter, the flood risk assessment methods and results illustrated in the previous chapters are implemented on the primary study site. The flood impact model has two major modules: ground level and subsurface. The univariate flood stage-frequency curve developed in Chapter 3 provides information for the ground level flood impact assessment, while the bivariate flood stage-duration-frequency relationship derived in Chapter 4 serves as the statistical foundation for the subsurface flood risk assessment.

A flood event at the WWTP is characterized by the change of river level, plant influent flow rate, and bypass flow rate. Figure 5-3 illustrates the Potomac River level during Hurricane Sandy. Although the datum of the river gauge is unknown, the time series shows the general response of the river to an extreme hydrological event. It is also observed that more than double the average plant influent flow occurred during the event.

Due to the limitation of the historical plant operation data, the Flood Impact Model is developed using synthetic data. The ground level inundation module comprises (1) Inundation Mapping, (2) Building Damage Model, and (3) GIS-Assisted Risk Register for Safe Evacuation. The subsurface inundation module consists of (1) Subsurface Flow intrusion Model, (2) Equipment Damage Model, and (3) Expected Annual Damage Calculator.

The methods developed for the ground level and subsurface modules are introduced in sections 5.2.1 and 5.2.2, respectively. All of the case study results are shown in Section 5.3. Figure 5-2 illustrates the data inputs and outputs of the flood impact model. The hydrological inputs are in the red boxes. The yellow ovals indicates the model outputs (products).

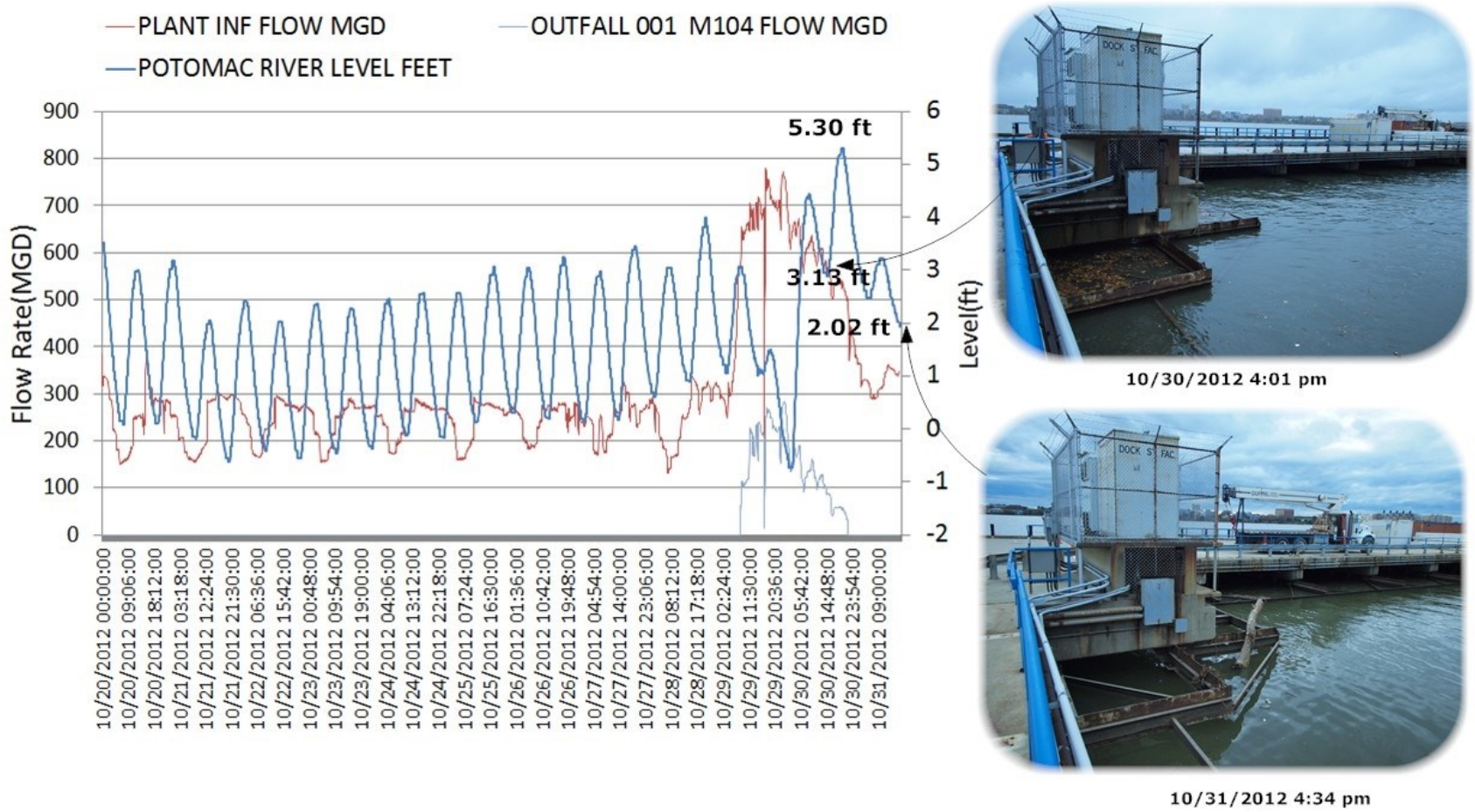

Figure 5-1. Hydrological response of the study site during Hurricane Sandy

Note: the PLANT INF FLOW is the total plant influent flow; OUTFALL 001 measures the partially treated wastewater flow. The photographs at right are taken by the author at the Potomac River at the BPAWWTP

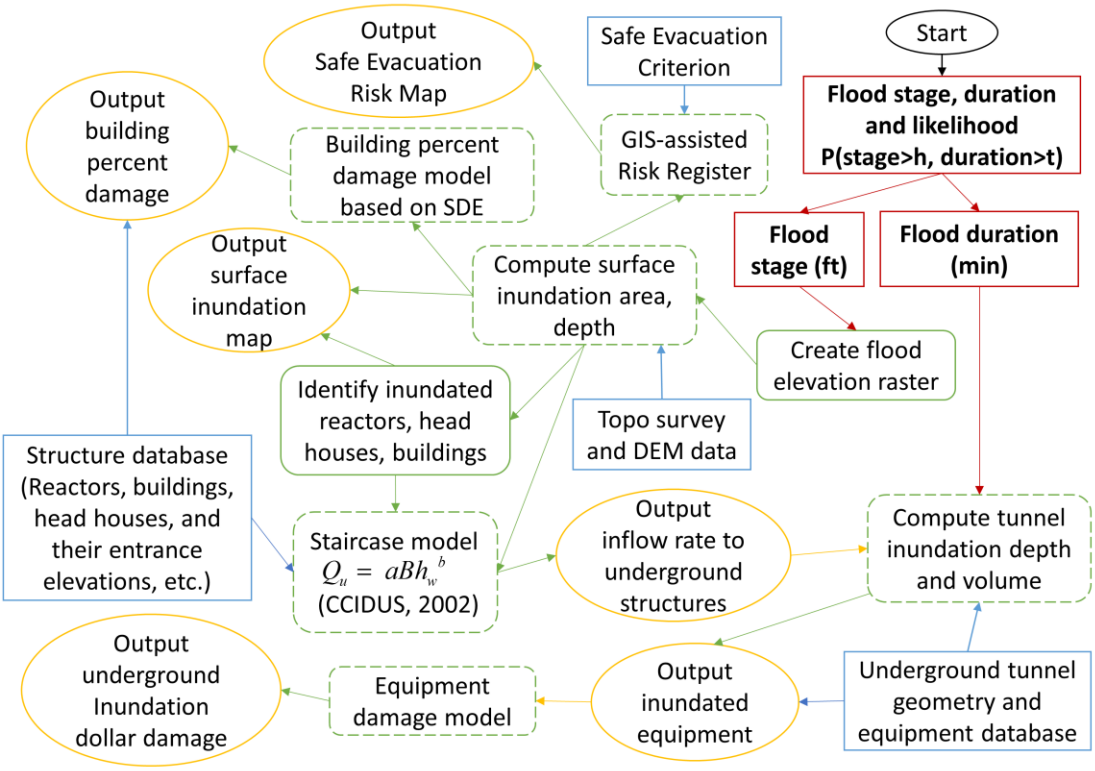

Figure 5-2. Underground tunnel inundation model flow chart

5.2 Model Components

5.2.1 Ground Level Modules

5.2.1.1 Inundation Mapping

The surface inundation map is the first component of the ground level module. It was created for (1) visualizing the inundated area inside the plant; (2) computing the inundation depth to assist evacuation planning; and (3) identifying the inundated entrance to the underground tunnels and galleries, including stairs, head houses, etc. The model inputs include the Digital Elevation Model (DEM) created by the 2009 topographic survey, structure database, and river stage of various flood scenarios for current and future climate.

A customized Python script was created to automate the following eight steps in ArcGIS.

Step 1. Create triangulated irregular network (TIN) to represent the ground surface of the study site. The TIN is created from elevation points (irregularly spaced) surveyed in 2009 and the reactor polygons by using the top wall elevation of the reactor. The TIN is then converted to a raster.

Step 2. For each flood scenario, create a constant WSEL raster based on the river stage.

Step 3. Calculate the volumetric difference between the two surfaces (Step 1 and 2) using the Surface Difference_3D tool.

Step 4. Select the largest polygon from the output of Step 3, which is the inundated zone inside the plant. The small polygons that are adjacent to the river are the 'sinks' that need to be removed. The flood water may not be able to enter these areas before the surrounding area is inundated.

Step 5. Compute the inundated area. Compute the area of the inundated zone polygon in Step 4.

Step 6. Compute inundation depth [Raster math, WSEL (step 2) – topographic raster (step 1)].

Step 7. Output the inundated building, reactors, and underground tunnel/gallery entrances by the Identity tool and the spatial join tool. The tool computes the geometric intersection of the headhouses/stairs and the inundation zone polygon in step 3.

Step 8. Sum the total inundation area of the building and reactors.

Surface inundation maps are generated based on the inundation depth raster. In this study, the depth values are grouped into classes that relate to the safe evacuation criteria, which will be introduced in Section 5.2.1.3. For visual comparison, the same classified symbology is applied to all the 18 scenarios.

5.2.1.2 Building Damage Model

The flood actions on buildings can be categorized into hydrostatic (including lateral pressure and capillary rise), hydrodynamic (related to velocity and waves), erosion, buoyancy, debris, and non-

physical flood actions (including chemical, nuclear, and biological) (Kelman & Spence, 2004). In this study, the building damage is quantified by percent damage, based on the recommendation for non-residential structure by FEMA Substantial Damage Estimator (SDE) (see Section 2.4.5 for the details of the percent damage by SDE).

The percent damage to foundation is a function of flood depth outside the building. It is computed by a customized Python Script for ArcGIS analysis. The spatial join analysis identifies the inundated buildings. The building polygons are converted to point features. The flood depth values are extracted to the points to represent the flood depth outside the building. The results for the building foundation percent damage are presented in Section 5.3.2.

The floor elevations of the affected buildings are essential for estimating shallow flooding effects (Penning-Rowsell & Fordham, 1994). For the rest of the percent damage modules, including superstructure, interiors, plumbing, electrical system and HVAC systems, a survey of the first floor and lowest floor elevation is needed for each building structure. The percent damage analysis of these sections can only be performed when the survey information is available.

5.2.1.3 GIS-Assisted Risk Register (GARR) for Safe Evacuation

Safe evacuation is critical to prevent injuries and fatalities during a flood event. It is especially important to critical infrastructure, such as a WWTP, since chemical spills, moving debris, and other flood related damage can cause severe injury or health impacts to personnel. Flood depth directly determines whether the road inside the critical infrastructure is safe for evacuation. The safe evacuation flood depth for an adult is 1.6-2.3ft [Kamei (1984), Takayama et al. (2007)]. The limit of water depth for safe evacuation from the door of a vehicle is 2.3-2.6 ft (Baba, Ishigaki, Toda, & Nakagawa, 2011).

Risk register is a commonly used technique to assess risk. Cox (2008) defined risk matrices as tables that relate "frequency" and "severity" ratings to corresponding risk priority levels. In this study, the likelihood of occurrence was characterized by the return period, as shown in Table 5-1. For example, the likelihood was defined as UNLIKELY for the 500-year steady flow output. The consequences of occurrence were grouped into four categories: negligible, marginal, significant and critical (Table 5-2). They were based on the lower value of the flood depth threshold for safe evacuation. Risk level was defined as a function of likelihood and consequences (Table 5-3).

Table 5-1. Likelihood of occurrence

Likelihood	Return interval
LIKELY	100-year
UNLIKELY	500-year
VERY UNLIKELY	1000-year

Table 5-2. Consequences of occurrence

Impact of consequences of occurrence	Inundation depth range (ft)	Area inundated	Safe for evacuation by foot	Safe for evacuation from vehicle door
NEGLIGIBLE	h=0	NO	YES	YES
MARGINAL	0<h≤1.6	YES	YES	YES
SIGNIFICANT	1.6<h≤2.3	YES	NO	YES
CRITICAL	2.3≤h	YES	NO	NO

*h is flood inundation depth above ground

Table 5-3. Risk characterization by likelihood and consequences

Risk level

Likelihood of occurrence				
Likely	LOW	MODERATE	HIGH	HIGH
Unlikely	LOW	MODERATE	MODERATE	HIGH
Very Unlikely	LOW	LOW	MODERATE	MODERATE
	NEGLIGIBLE	MARGINAL	SIGNIFICANT	CRITICAL

Consequences of occurrence

Inspired by the method of the tabulated risk register, this study created a GIS-Assisted Risk Register (GARR) to define the safe evacuation risk in this study. The evacuation risk was analyzed for 3 cases: (C1) current climate, (C2) future climate within this century, and (C3) future climate beyond this century. Each case was subjected to 3 river stages, each of which is the mean stage of the steady and unsteady state outputs (Table 5-4). Combining Table 5-1, Table 5-2, Table 5-3, and Table 5-4, evacuation risk registers for the three cases with 100-year, 500-year and 1000-year return periods were developed (see Table 5-5). They were also assigned risk scores. Low, moderate and high risks were assigned 1, 2, and 3 points, respectively (Table 5-5).

Table 5-4. Flood depth of three cases for evacuation risk analysis

	Current climate	Future climate	
	Case 1 (C1)	Case 2 (C2)	Case 3 (C3)
Return period		Within this century	Beyond this century
100-year	9.1 ft	12.0 ft	13.7 ft
500-year	11.3 ft	13.9 ft	15.6 ft
1000-year	12.2 ft	14.8 ft	16.5 ft

Table 5-5. Evacuation risk register and risk scores for 12 Scenarios

	h=0	0<h≤1.6	1.6<h≤2.3	2.3<h
C1/C2/C3: 100-year	LOW(1)	MODERATE(2)	HIGH(3)	HIGH(3)
C1/C2/C3: 500-year	LOW(1)	MODERATE(2)	MODERATE(2)	HIGH(3)
C1/C2/C3: 1000-year	LOW(1)	LOW(1)	MODERATE(2)	MODERATE(2)

Note: h is flood inundation depth above ground. The number next to the risk level is the assigned risk score.

The risk level was spatially evaluated for each grid cell of the raster data. For each river stage in each case, risk scores were assigned to each location on the map (grid cell in the depth

raster). For each location on the map, three 'votes' for the scores were based on 100-year, 500-year, and 1000-year river stages. The final risk score for each location (cell in the depth raster) were estimated by rounding the mean of the three scores to the nearest integer.

The GARR is applicable for any depth related flood risk assessment. The details of the application is illustrated in Section 5.3.3. It demonstrated a new method of visualizing the traditionally tabulated risk register.

5.2.2 Subsurface Module

Typical surface-depth-dependent risk calculations are insufficient for WWTP infrastructure because many of the critical operations, connectivity, and access paths are underground (Section 3.2). Damage and disruption to these areas is not simply a function of flood depth, but of the volume of flood water that intrudes into these spaces.

5.2.2.1 Flow Intrusion Model

The first component of the subsurface module is the flow intrusion model, which simulates the inflow to the underground tunnels. The underground tunnel inundation depth depends on the total volume of inflow, which is in turn a function of the flood depth above ground, the duration that flood depth remains above ground, and the properties of connection to the underground (Figure 5-3).

Flood stage and duration are the hydrological inputs for the model. The river stage is used to calculate the depth at the underground tunnel entrances. The duration represents the length of time that the river stays above any level sufficient to inundate the underground tunnel entrances.

Head houses, as shown in Figure 3-3, are the major entrances to the underground tunnel. The door of a head house opens to the ground and its stairs lead to the underground space. The mechanisms of door and window failure due to flooding have been studied, and the physical vulnerability was modeled for residential properties in coastal, eastern England (Kelman, 2002). If the door is not watertight, water may enter the head houses and flow downstairs through the staircases.

Each flood stage-duration pair is viewed as one scenario. The WSEL inside the underground tunnel can be computed. The empirical weir formula proposed by National Institute for Land and Infrastructure Management of Japan in Guidelines for Measures against Inundation of Underground Spaces (CCIDUS, 2002) was used to simulate water intrusion to the underground space [Eq. (5-1)]. Shao (2010) also used this formula for underground inundation modeling.

$$Q_u = aBh_e^{\,b} \tag{5-1}$$

where Q_u is discharge intruding into the underground space through staircases (m^3/s), h_e is overflow depth (m) at the ground level entrance of the staircase, B is sum of the entrance widths of flooding staircases (m), a and b are constants (a=1.590 and b=1.650 for CCIDUS (2002), or a=1.705 and b=1.500 by assuming the critical water depth has been reached at the ground level entrance).

The geometry input consists of the topographic elevation (Z_{ground}) and the underground tunnel geometry, as well as the width (B) and elevation of the entrances. Figure 5-4 shows the simplified geometry of head houses and underground tunnels. The tunnel inundation elevation ($WSEL_{tunnel}$) is computed by Eqs. (5-2) to (5-4).

$$WSEL_{tunnel}(t+1) = WSEL_{tunnel}(t) + dQ(t) / A(t) \quad (5\text{-}2)$$

$$A(t) = \sum_{i}^{n} EA(i)_t \quad (5\text{-}3)$$

$$dQ(t) = \sum_{i}^{n} Q_u(i)_t \quad (5\text{-}4)$$

where n is the total number of tunnel entrances; EA is the effective area in each tunnel. For each time step, effective area is defined as the top surface area at the inundation water level, $WSEL_{tunnel}$. A is the total effective area, considering multiple tunnels. dQ is the total inflow to the tunnel, considering inflow through multiple entrances. Since the underground tunnels are all connected, they are treated as a single volumetric space. This model makes the following simplifying assumptions: (1) the water reaches the lowest point of the tunnel immediately after it enters the tunnel, and (2) the tunnel only connects to the outside environment by the entrances of the head houses. Volume is not reduced through leakage or recharge to groundwater.

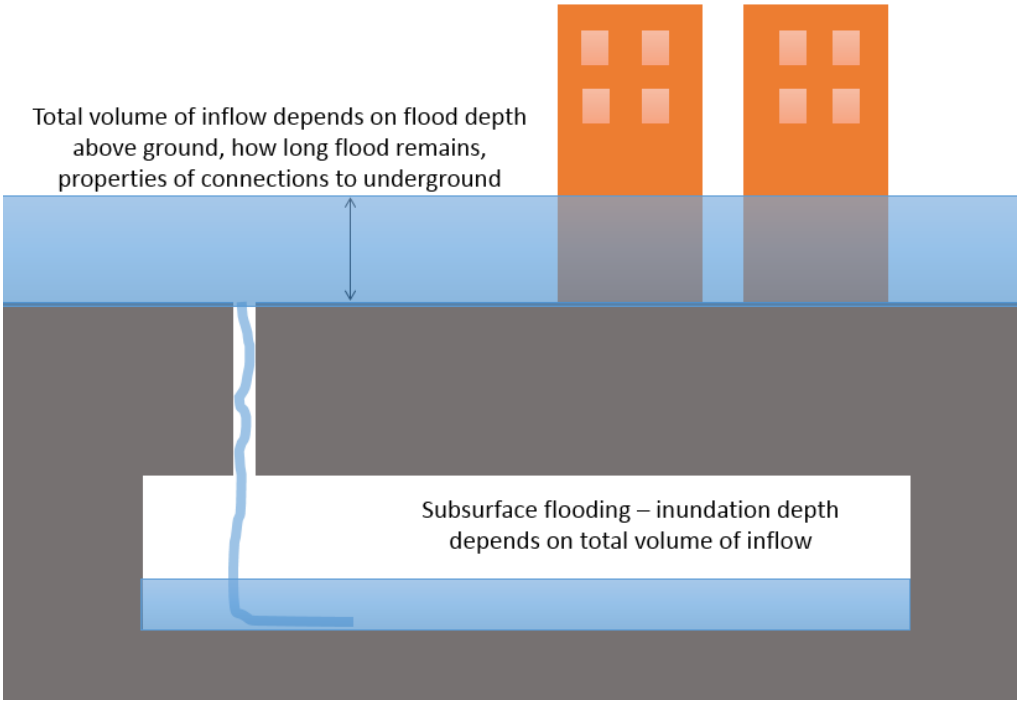

Figure 5-3. Underground tunnel inundation mechanism

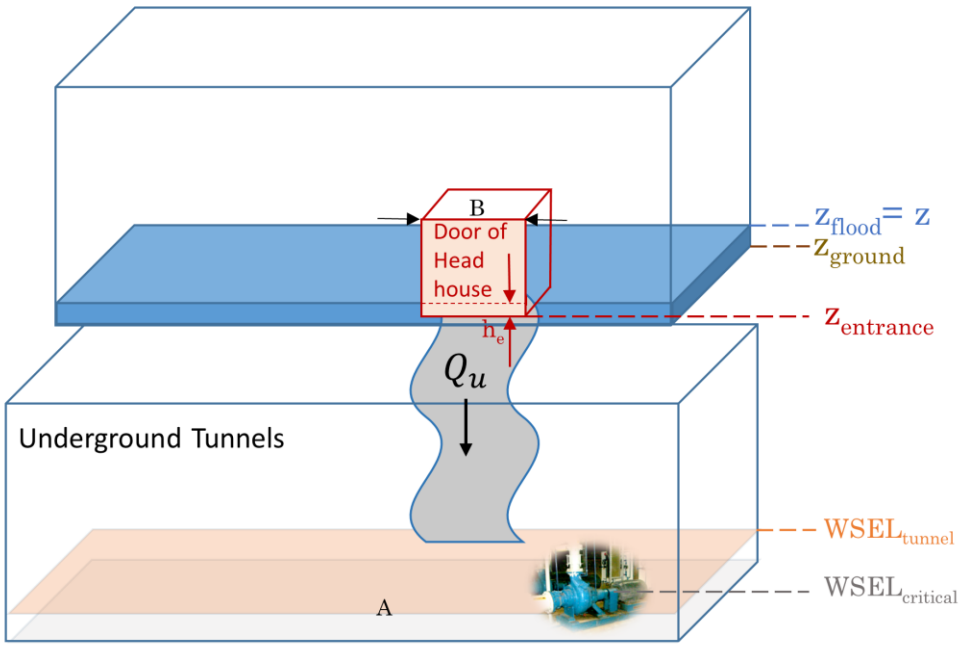

Figure 5-4. Simplified underground inundation model

The tunnels are grouped into three types by geometry. Each tunnel section can be represented by the following parameters: length (L), width (W), minimum floor elevation (h_{fmin}), maximum floor elevation (h_{fmax}), minimum ceiling elevation (h_{cmin}), and maximum ceiling elevation (h_{cmax}). The geometric database containing these fields for each tunnel provides flexibility in characterizing existing or new underground spaces. When construction projects modify the tunnel geometries in one or more locations, the user can update the tunnel geometry database and rerun the model without a global revision of the geometry.

Type 1. Flat tunnel, no slope (h_{fmin}=h_{fmax}; h_{cmin}=h_{cmax}). This is the most common type of underground structure. It has a flat floor and ceiling. The horizontal cross section area is the same for any elevation within the tunnel (Figure 5-5).

Type 1A
$$EA = L * W \tag{5-5}$$

Type 2. Short tunnel, mild slope (h_{fmin}<h_{fmax}; h_{cmin}≥h_{fmax}). The floor surface has a mild slope. One end of the tunnel has a lower floor elevation than the other end (Figure 5-6); but all points on the ceiling are higher than the highest point on the floor. Due to this slope, the inundated surface area changes with elevation, and may intersect the ceiling at the downslope end.

Type 2A
$$EA = L_A * W = \frac{\left(WSEL_A - h_{f\min}\right) * W}{tg\alpha} = \frac{\left(WSEL_A - h_{f\min}\right) w}{h_{f\max} - h_{f\min}} * L * W \tag{5-6}$$

Type 2B
$$EA = L_B * W = L * W \tag{5-7}$$

Type 2C
$$EA = L_C * W = \frac{\left(WSEL_C - h_{f\min}\right) * W}{tg\alpha} = \frac{\left(WSEL_C - h_{f\min}\right) * W}{h_{f\max} - h_{f\min}} * L * W \tag{5-8}$$

Type 3. Long tunnel, steep slope (h_{cmin}<h_{fmax}). In this type of tunnel, the length and floor slope are such that the minimum elevation of the tunnel ceiling in one end is lower than the maximum

elevation of the tunnel floor at the other end (Figure 5-7). As water depth rises in the tunnel, the inundated surface area is likely to intersect the ceiling at the downslope end.

Type 3A $$EA = L_A * W = \frac{\left(WSEL_A - h_{f\min}\right) * W}{tg\alpha} = \frac{\left(WSEL_A - h_{f\min}\right) w}{h_{f\max} - h_{f\min}} * L * W \quad (5\text{-}9)$$

Type 3B $$EA = L_B * W = L * W \quad (5\text{-}10)$$

Type 3C $$EA = L_A * W = \frac{\left(WSEL_A - h_{f\min}\right) * W}{tg\alpha} = \frac{\left(WSEL_A - h_{f\min}\right) w}{h_{f\max} - h_{f\min}} * L * W \quad (5\text{-}11)$$

The tunnel geometry is used to calculate $WSEL$ in the tunnel as flood water intrudes, following Eq. 5-2.

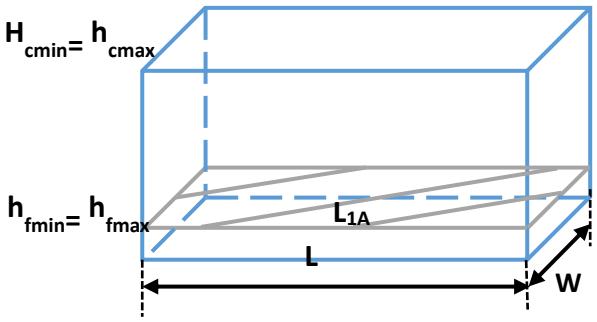

Figure 5-5. Flat tunnel (no slope)

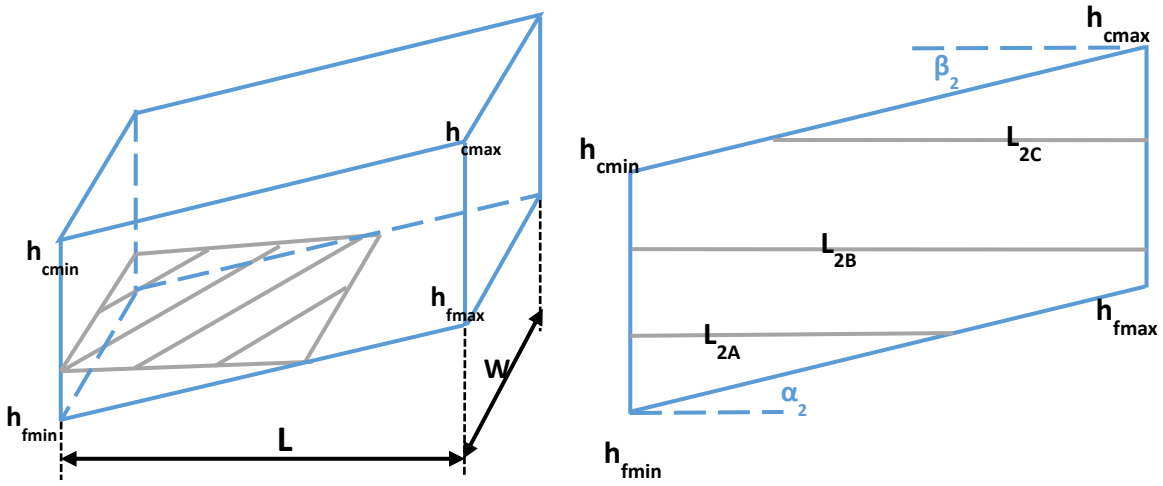

Figure 5-6. Short tunnel (mild slope)

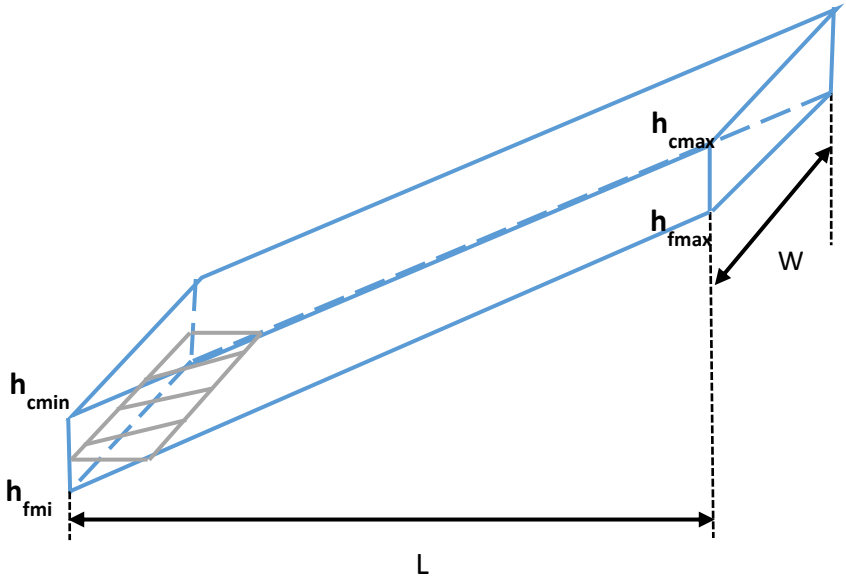

(a)

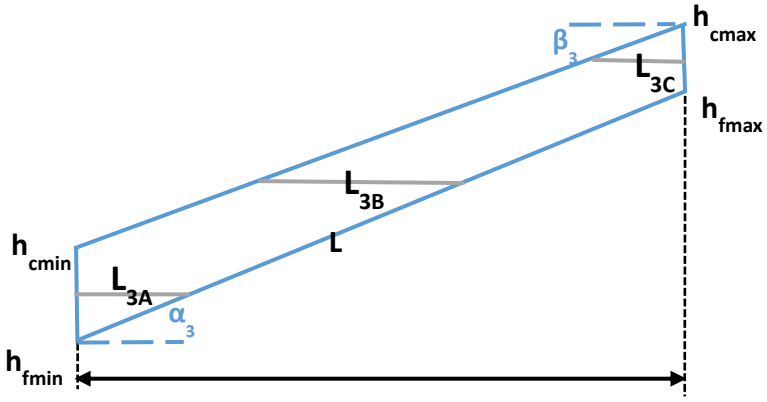

(b)

Figure 5-7. Long tunnel (steep slope)

5.2.2.2 Equipment Damage Model

DEFRA (2001) considered three main factors for asset valuation: (1) the location of assets that lie within the areas at risk from flooding or erosion; (2) the economic value attached to the loss or damage of those assets; and (3) the probability that those assets may be lost or damaged. Damage (D) is the monetary loss [dollars] due to equipment inundation, which is a function of z and τ. An underground inundation damage model is needed to quantify $D\ (z, \tau)$. An inventory-based model is developed herein to generate the bivariate damage curves.

In the equipment database, each equipment is assigned a critical elevation ($WSEL_{critical}$) as an attribute. The critical elevation is defined as the best estimate of the water inundation level that is likely to cause major damage to that equipment. The majority of the essential equipment inside the tunnels are pumps and their appurtenances. For example, the critical level of the electrical pump could be the elevation of the horizontal shaft of the motor; the critical elevation of the local control panel could be the bottom elevation of the control box (Figure 5-8).

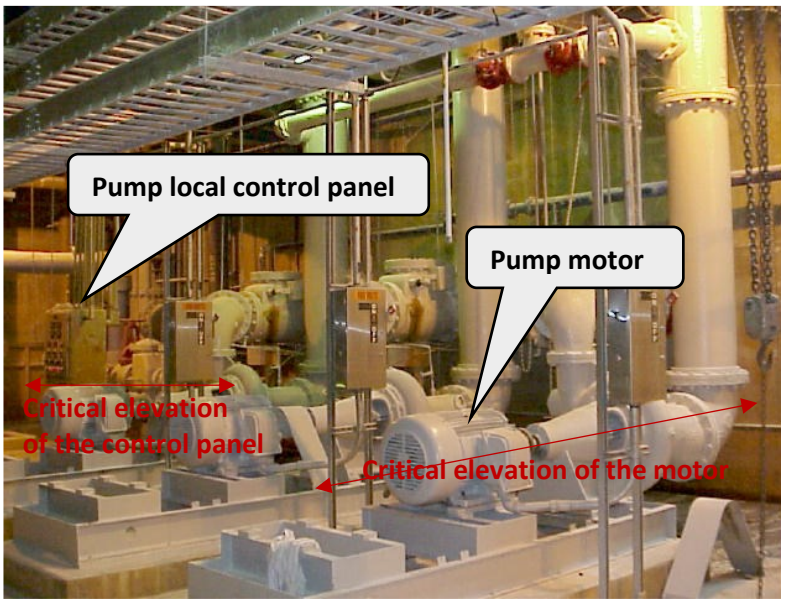

Figure 5-8. Critical elevation of East Secondary Waste Sludge Pump (DCWASA, n.d.-e)

Experimental data were not available to determine the magnitude of equipment failure due to inundation. Two deterministic models were used in this study.

(1) Linear inundation failure model

For each equipment, the model estimates the loss ($\hat{\$}_i$) due to inundation by a linear function [Figure 5-9(a)]. The dollar loss linearly increases until the WSEL in tunnel reaches the critical elevation of the equipment. When the WSEL reaches the critical elevation, the equipment is considered completely damaged.

(2) Step inundation failure model

The loss ($\hat{\$}_i$) is estimated by a step function [Figure 5-9 (b)]. The loss estimate for each equipment is boolean. If the WSEL reaches the critical elevation, the equipment is considered completely damaged. If the WSEL is lower than the critical elevation, no damage is considered. The damage of the two model are identical when the $WSEL_{tunnel}$ exceeds the $WSEL_{critical}$. Before the $WSEL_{tunnel}$ reaches the critical elevation of the equipment, the loss estimated from the linear model is greater than that of the step model.

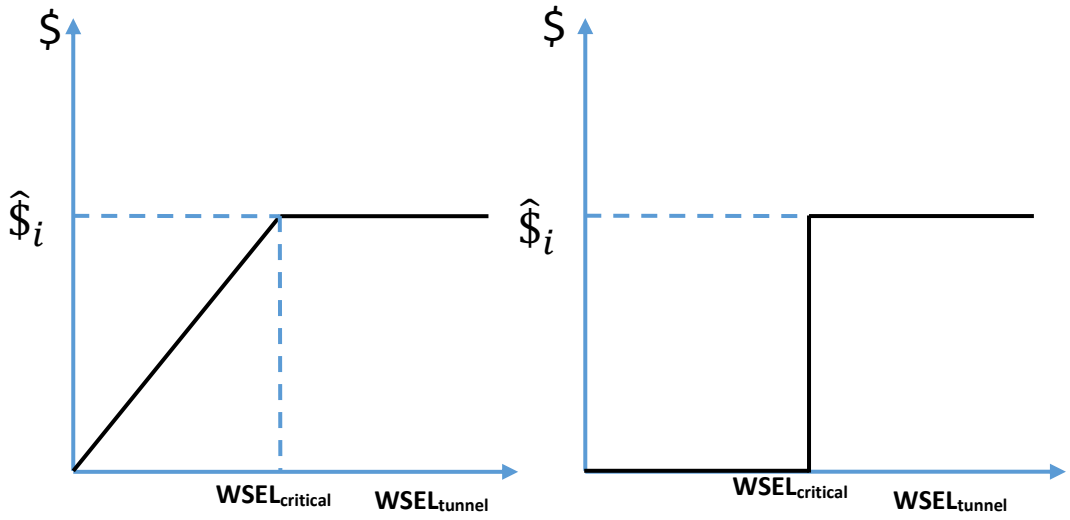

(a) (b)

Figure 5-9. Equipment inundation damage function

The total equipment inundation damage, D, is estimated by Eq. (5-12).

$$D = \sum_{i=1}^{n} \hat{\$}_i \tag{5-12}$$

where $\hat{\$}_i$ is the estimated dollar loss of equipment i due to tunnel inundation; and n is the number of inundated equipment. Table A-1 shows an example of the data collection sheet of the essential equipment inside the underground tunnel.

Given the combination of flood stage and duration above ground, the tunnel inundation depth is determined by the underground flow intrusion model (see Section 5.2.2.1). For each subsurface inundation depth ($WSEL_{tunnel}$), the step or linear inundation damage model can be applied to each equipment underground. If damage is measured as a monetary value, the summation of the estimated dollar loss of all of the equipment reflects the total inundation damage (D), a function of flood stage and duration as propagated through the underground water intrusion and tunnel-filling model.

5.2.2.3 Expected Annual Damage

To link the damage to an associated probability, the deterministic damage function is combined with the bivariate joint distribution developed in Chapter 4. The expected annual damage due to equipment inundation is computed based on this bivariate model, analogous to the univariate case, as indicated by Eq. (2-9) and Eq. (2-11).

$$E(D) = \int_0^\infty \int_{z_{\min AM}}^\infty D(z,\tau) f(z,\tau) dz d\tau \tag{5-13}$$

$$f(z,\tau) = \frac{dF(z,\tau)}{dz d\tau} \tag{5-14}$$

$$\begin{aligned} F(z,\tau) &= \Pr(z \le z_0, \tau \le \tau_0) \\ &= 1 - \Pr(\tau \ge \tau_0) - \Pr(z \ge z_0) + \Pr(z \ge z_0, \tau \ge \tau_0) \end{aligned} \tag{5-15}$$

where $E(D)$ is the expected value (annual mean) damage. D is the monetary loss [dollars] due to equipment inundation damage, which is a function of z and τ, z_{minAM} is the lower limit of the annual maximum flood stage, defined by the GEV distribution. $\Pr(z \ge z_0, \tau \ge \tau_0)$ and $\Pr(z \ge z_0)$ are computed by Eq. (4-3) and (4-1) in Chapter 4, respectively. $\Pr(\tau \ge \tau_0)$ is the exceedance probability of duration, which is the likelihood that a flood exceeds τ_0 hour. In this analysis, a flood is a period during which the river stage equals or exceeds the lower limit of the marginal distribution defined by the GEV distribution (that is, the minimum of the annual maximum river stage marginal distribution):

$$\Pr(\tau \ge \tau_0) = \Pr(\tau \ge \tau_0 \mid z \ge z_{\min AM}) \tag{5-16}$$

This conditional expression of the $\Pr(\tau \ge \tau_0)$ can be further calculated by Eqs. (4-4), (4-5) and (4-9). The joint probability density function of flood stage and duration $f(z, \tau)$ is needed. It is computed by numerically differentiating the joint cumulative distribution function, $F(z, \tau)$, using a centered difference approximation. $F(z, \tau)$ is computed by Eq.(5-14). By integrating over the feasible range of stage and duration, the expected annual damage, $E(D)$, can be computed by equation (5-13).

5.3 Case Study

5.3.1 Inundation Mapping

Steady and unsteady flow analyses (HEC-RAS model) based on historical event frequency represents the current climate. The future climate scenarios are a combination of expected relative sea level rise and the maximum projected freshwater increases for the Potomac River Basin above Little Falls (Chapter 3). Boesch et al. (2013) recommended 3.7 feet of relative sea level rise for an infrastructure planning horizon within this century and 5.7 feet of relative sea level rise for a planning horizon beyond this century. The maximum projected freshwater increase for the Potomac River Basin above Little Falls is 11% based on scenario B_B1 (Interstate Commission on the Potomac River Basin, 2013). Those predictions were adopted for the Blue Plain Advanced Wastewater Treatment Plant (BPAWWTP) for future-climate based simulations. Compared to the unsteady flow analysis outputs, the steady flow analysis outputs are higher for low frequency events and lower for high frequency events (Table 5-6).

In this section, surface inundation maps of 18 scenarios were generated for the study site. The events of interest are shaded in Table 5-6. The 18 events include 6 scenarios for the current climate and 12 scenarios for the future climate conditions. The plant inundation area, total area of inundated reactors, total area of inundated buildings, and the river stages that correspond to each scenario are plotted in Figure 5-10. The surface inundation depth for each of the 18 scenarios are shown in Figure 5-11 to Figure 5-28. For the same expected flood frequency, larger inundation area of buildings and reactors are observed for the future climate, which indicates more severe damage potential.

Table 5-6. Flood stage at BPAWWTP (NAVD 88, ft) for current and future climate

	Current climate		Future climate			
			Within this century (11% flow increase & 3.7 feet RSLR)		Beyond this century (11% flow increase & 5.7 feet RSLR	
Return period	Steady flow	Unsteady flow	Steady flow	Unsteady flow	Steady flow	Unsteady flow
2	3.7	4.3	7	8.1	8.9	10.1
5	5.2	5.3	8.4	8.9	10.1	10.9
10	6.3	6	9.3	9.4	11	11.4
20	7.4	6.6	10.3	9.9	11.9	11.9
50	9	7.4	11.8	10.6	13.2	12.6
100	10.1	8.1	12.9	11	14.2	13.1
200	11.3	8.7	14.1	11.5	15.4	13.6
500	13	9.5	15.7	12.1	16.9	14.2
1000	14.2	10.2	16.9	12.6	18.1	14.8

Table 5-7. Current and future climate scenarios for BPAWWTP

	Current climate		Future climate			
			Within this century (11% flow increase & 3.7 feet RSLR)		Beyond this century (11% flow increase & 5.7 feet RSLR)	
Return period	Steady flow	Unsteady flow	Steady flow	Unsteady flow	Steady flow	Unsteady flow
100-year	Scenario 1 (10.1 ft)	Scenario 4 (8.1 ft)	Scenario 7 (12.9 ft)	Scenario 10 (11.0 ft)	Scenario 13 (14.2 ft)	Scenario 16 (13.1 ft)
500-year	Scenario 2 (13.0 ft)	Scenario 5 (9.6 ft)	Scenario 8 (15.7 ft)	Scenario 11 (12.1 ft)	Scenario 14 (16.9 ft)	Scenario 17 (14.2 ft)
1000-year	Scenario 3 (14.2 ft)	Scenario 6 (10.2 ft)	Scenario 9 (16.9 ft)	Scenario 12 (12.6 ft)	Scenario 15 (18.1 ft)	Scenario 18 (14.7 ft)

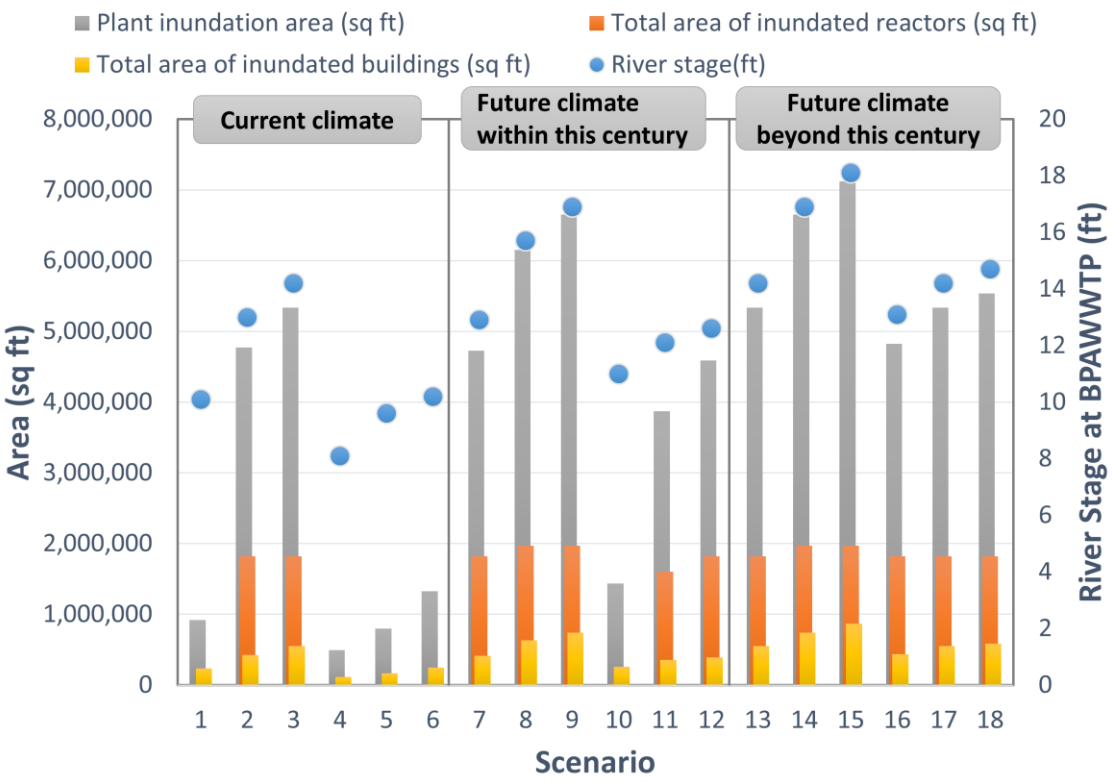

Figure 5-10. River stage and inundation area of 18 Scenarios

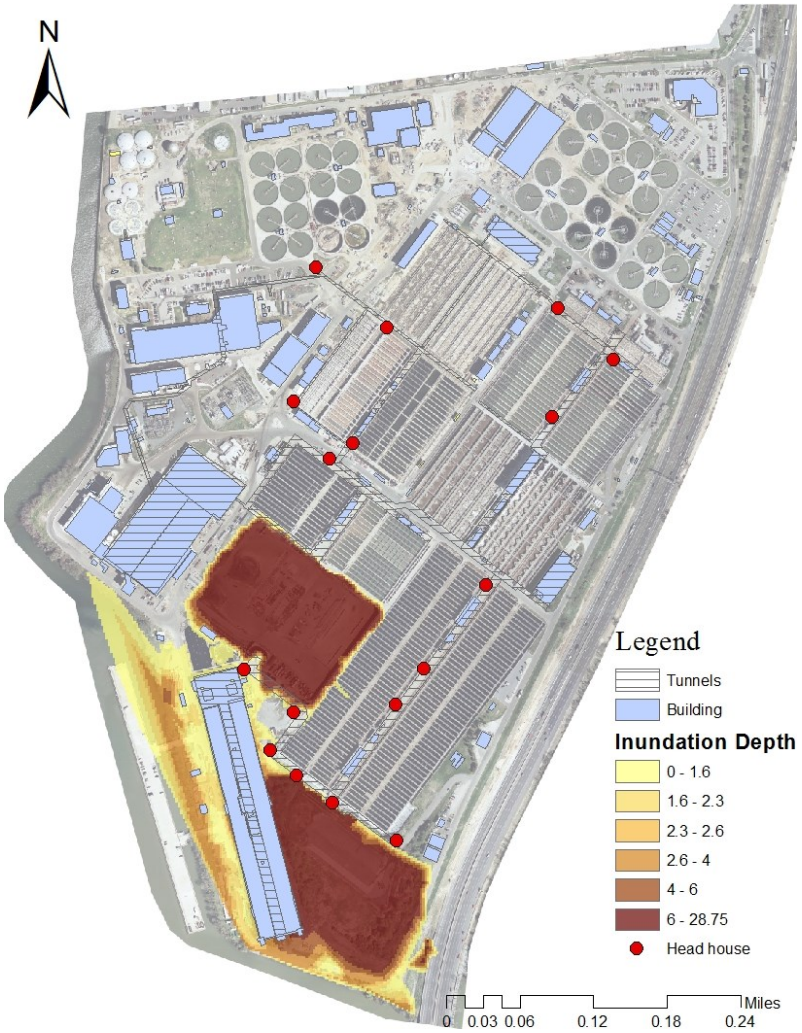

Figure 5-11. Surface inundation map (S1)
*100-year flood, HEC-RAS steady flow, current climate

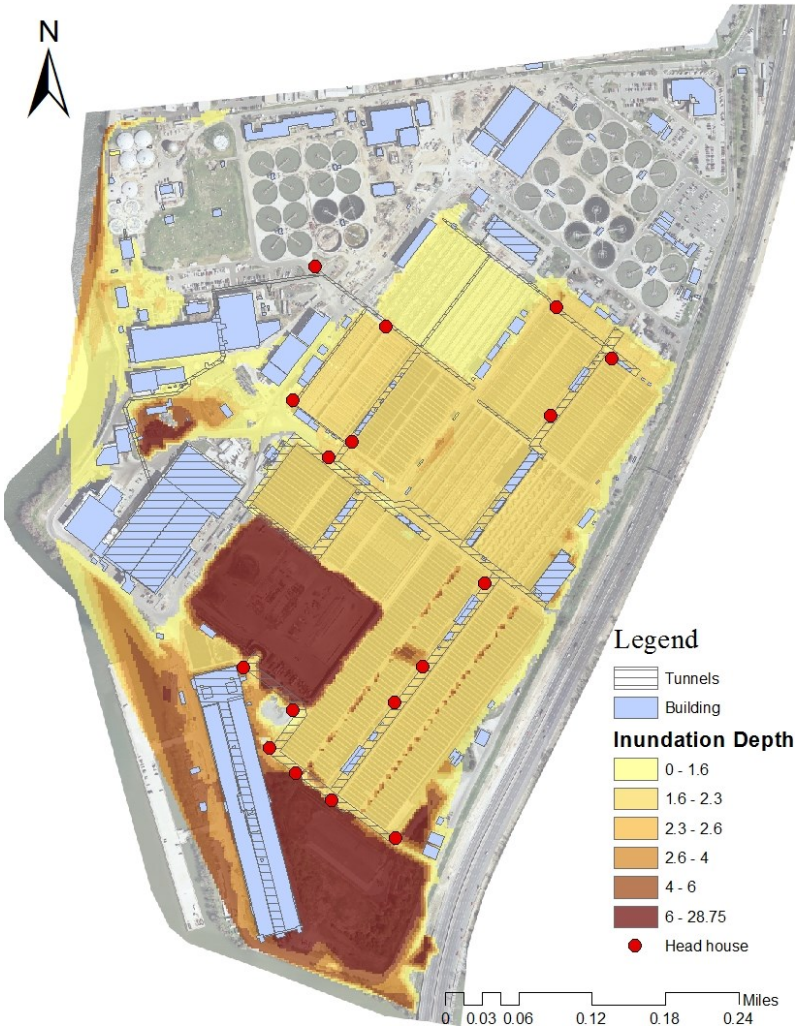

Figure 5-12. Surface inundation map (S2)
*500-year flood, HEC-RAS steady flow, current climate

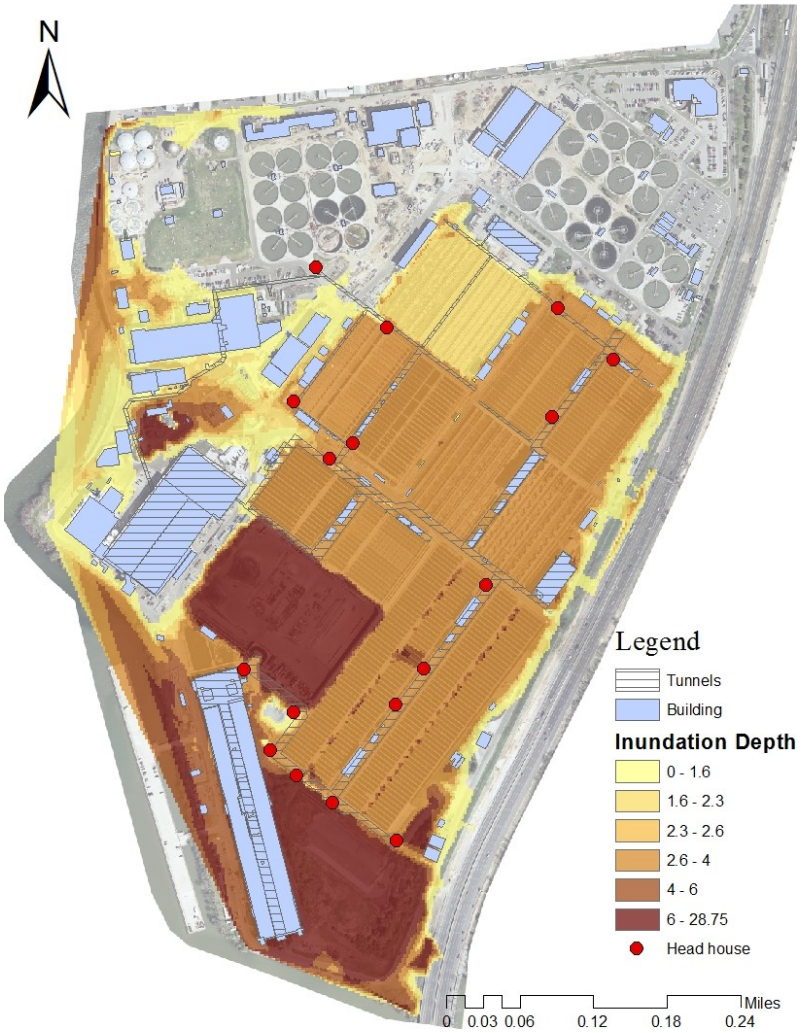

Figure 5-13. Surface inundation map (S3)
*1000-year flood, HEC-RAS steady flow, current climate

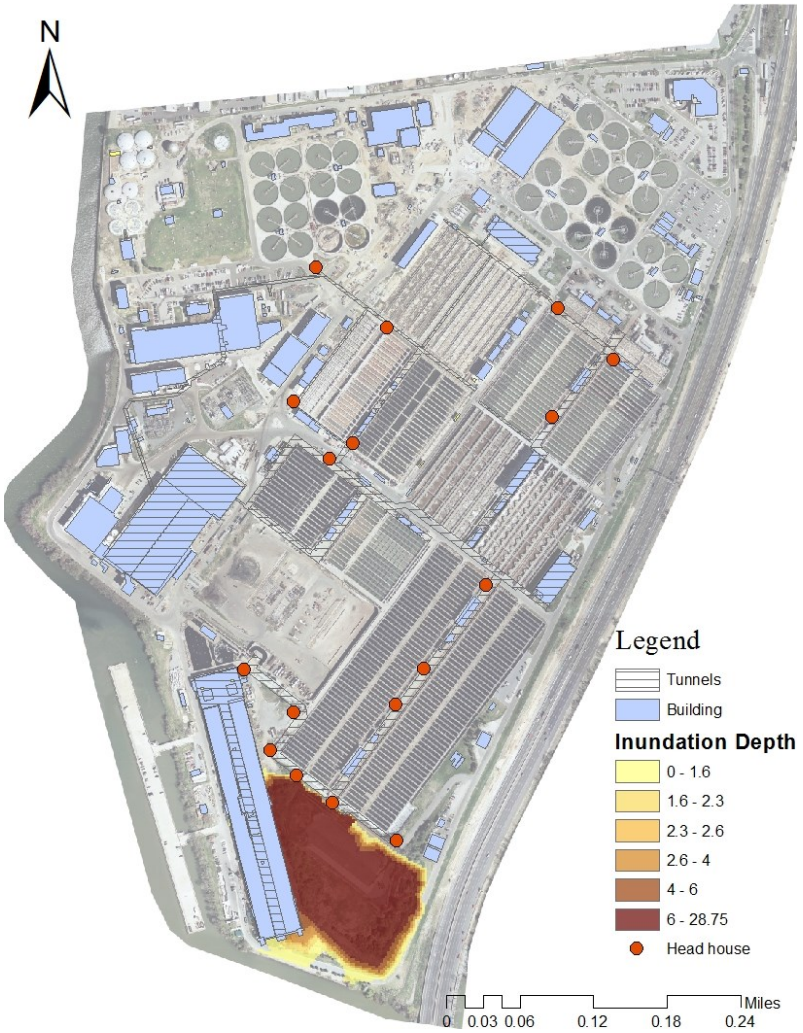

Figure 5-14. Surface inundation map (S4)
*100-year flood, HEC-RAS unsteady flow, current climate

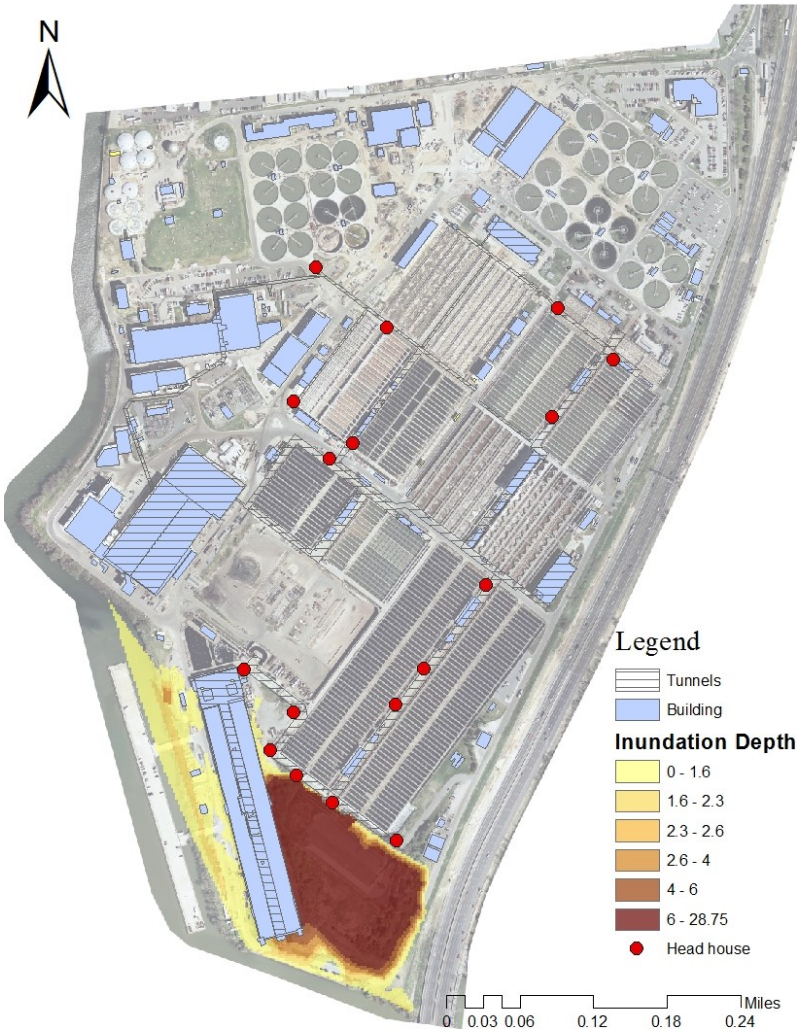

Figure 5-15. Surface inundation map (S5)
*500-year flood, HEC-RAS unsteady flow, current climate

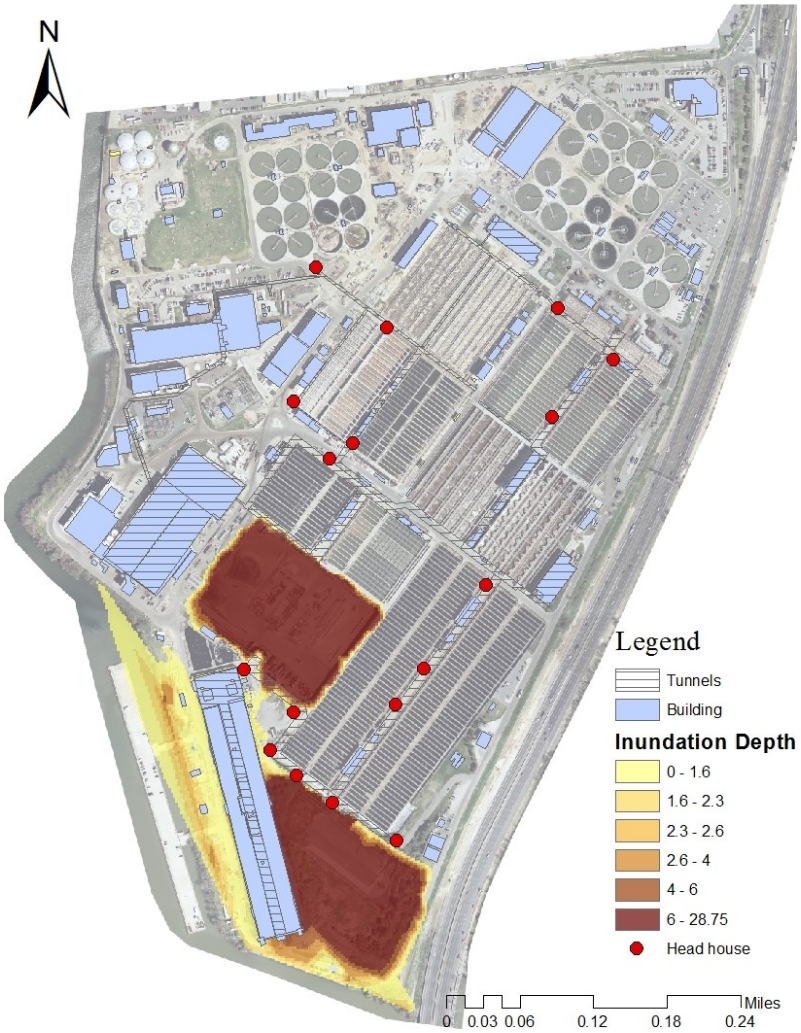

Figure 5-16. Surface inundation map (S6)
*1000-year flood, HEC-RAS unsteady flow, current climate

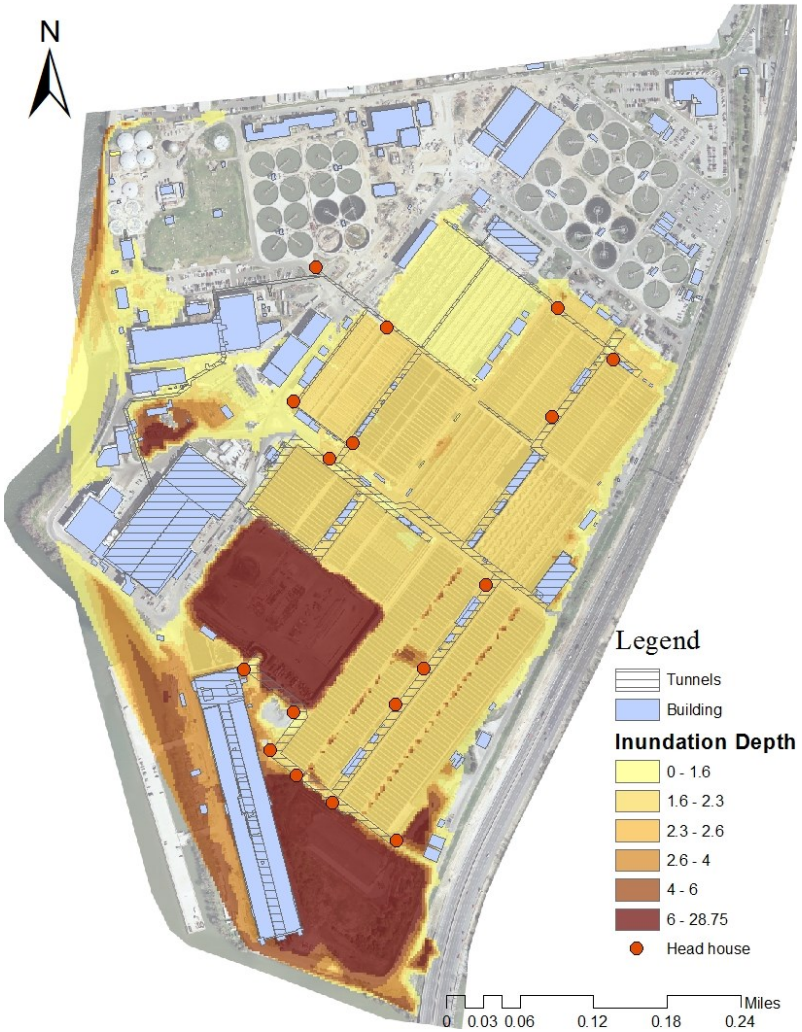

Figure 5-17. Surface inundation map (S7)
*100-year flood, HEC-RAS steady flow, future climate within this century

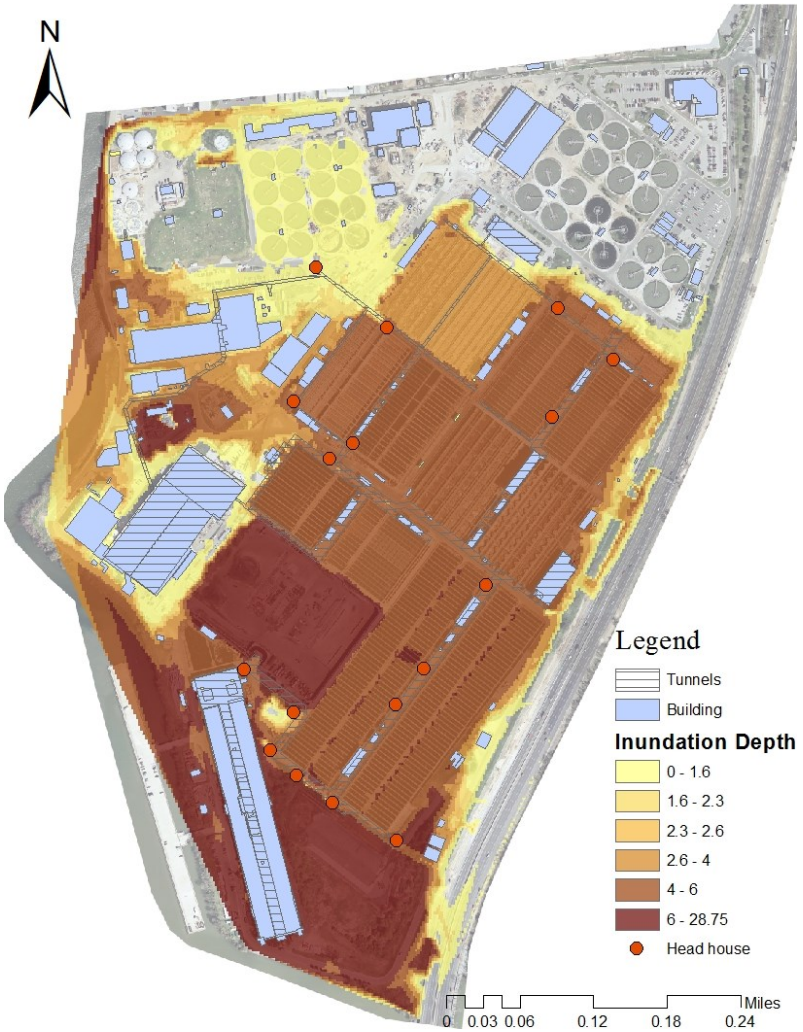

Figure 5-18. Surface inundation map (S8)
*500-year flood, HEC-RAS steady flow, future climate within this century

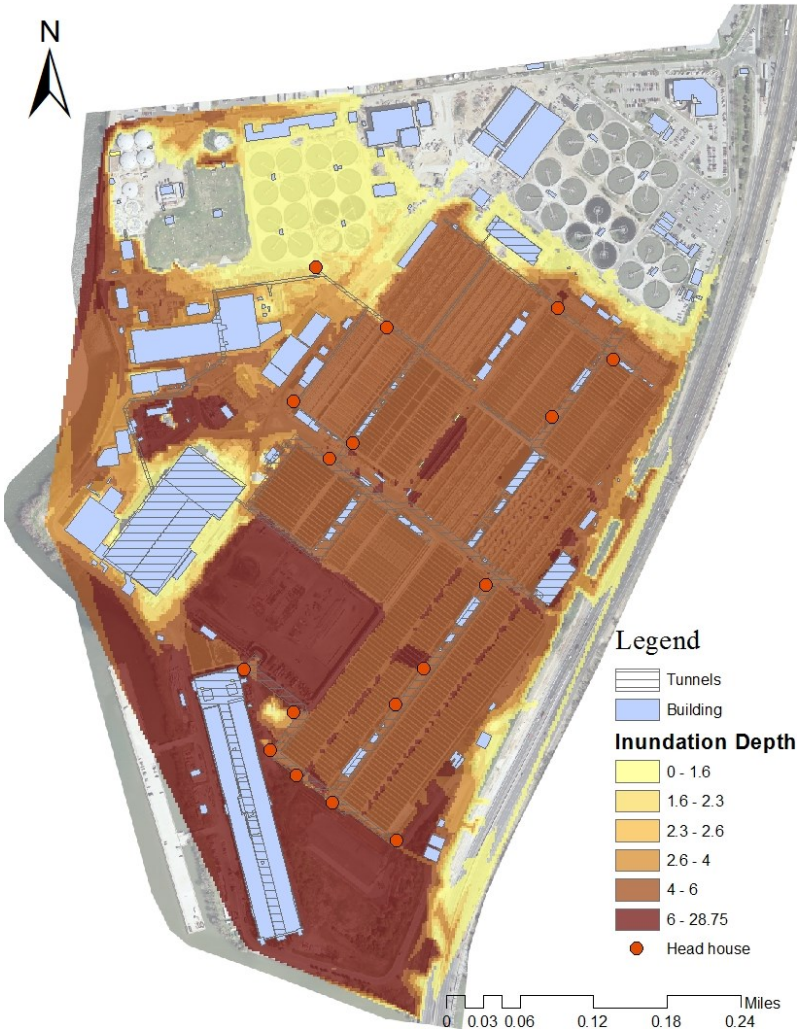

Figure 5-19. Surface inundation map (S9)
*1000-year flood, HEC-RAS steady flow, future climate within this century

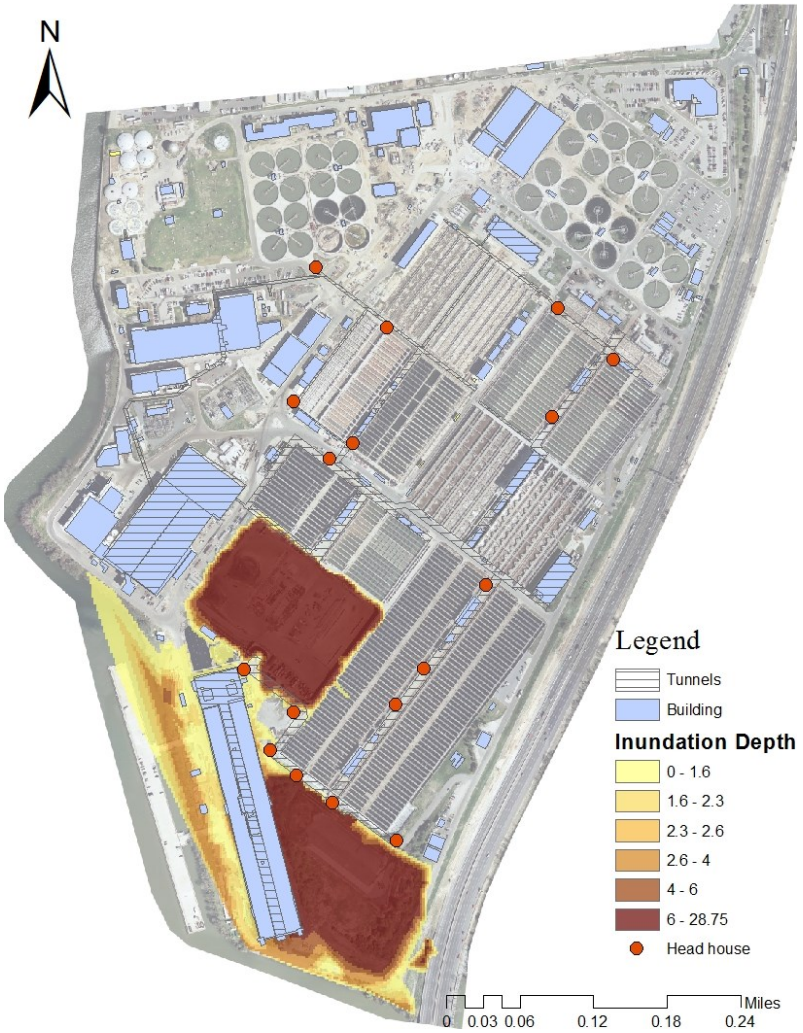

Figure 5-20. Surface inundation map (S10)
*100-year flood, HEC-RAS unsteady flow, future climate within this century

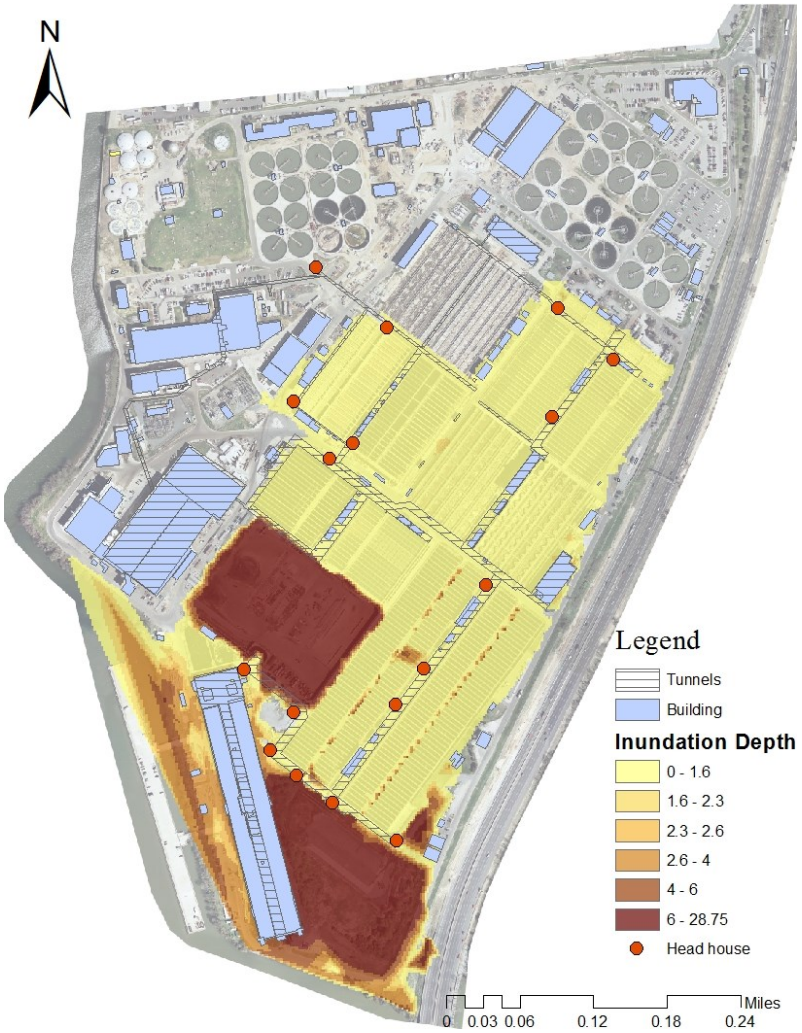

Figure 5-21. Surface inundation map (S11)
*500-year flood, HEC-RAS unsteady flow, future climate within this century

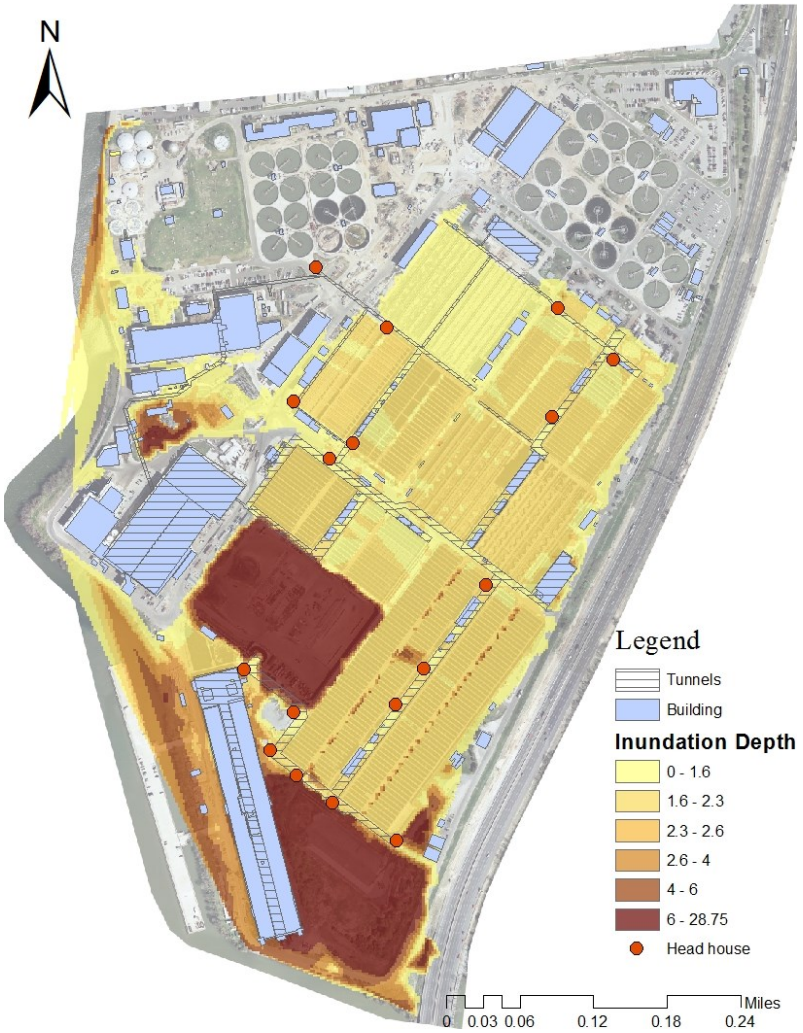

Figure 5-22. Surface inundation map (S12)
*1000-year flood, HEC-RAS unsteady flow, future climate within this century

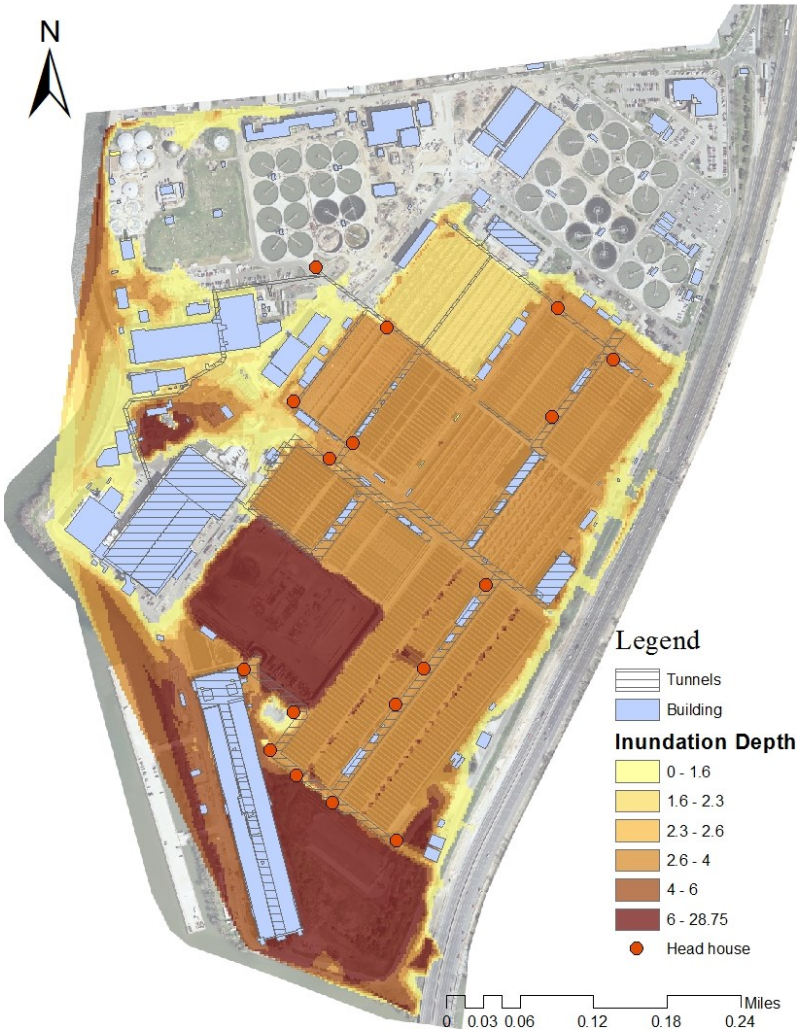

Figure 5-23. Surface inundation map (S13)
*100-year flood, HEC-RAS steady flow, future climate beyond this century

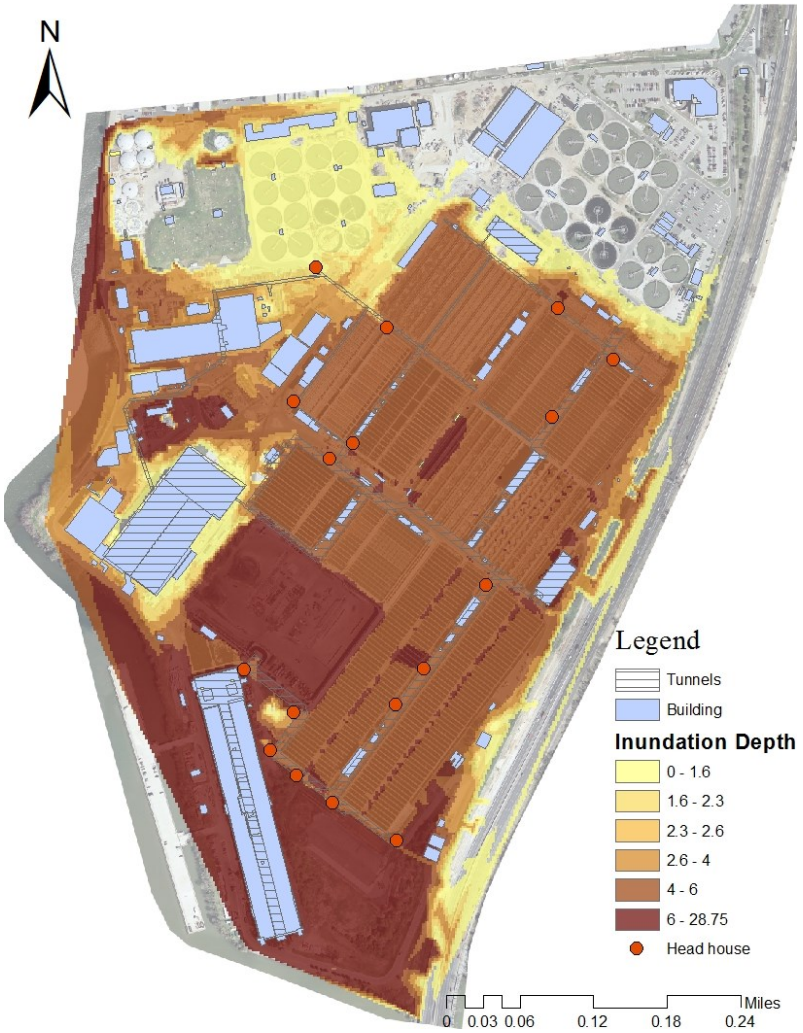

Figure 5-24. Surface inundation map (S14)
*500-year flood, HEC-RAS steady flow, future climate beyond this century

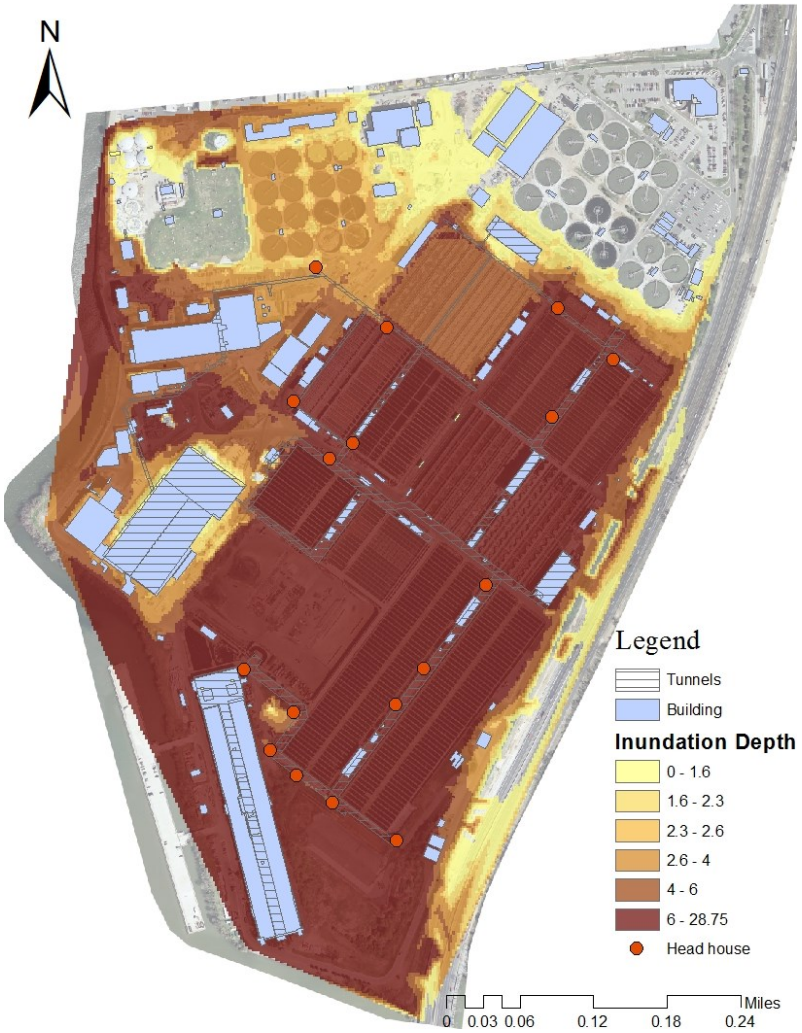

Figure 5-25. Surface inundation map (S15)
*1000-year flood, HEC-RAS steady flow, future climate beyond this century

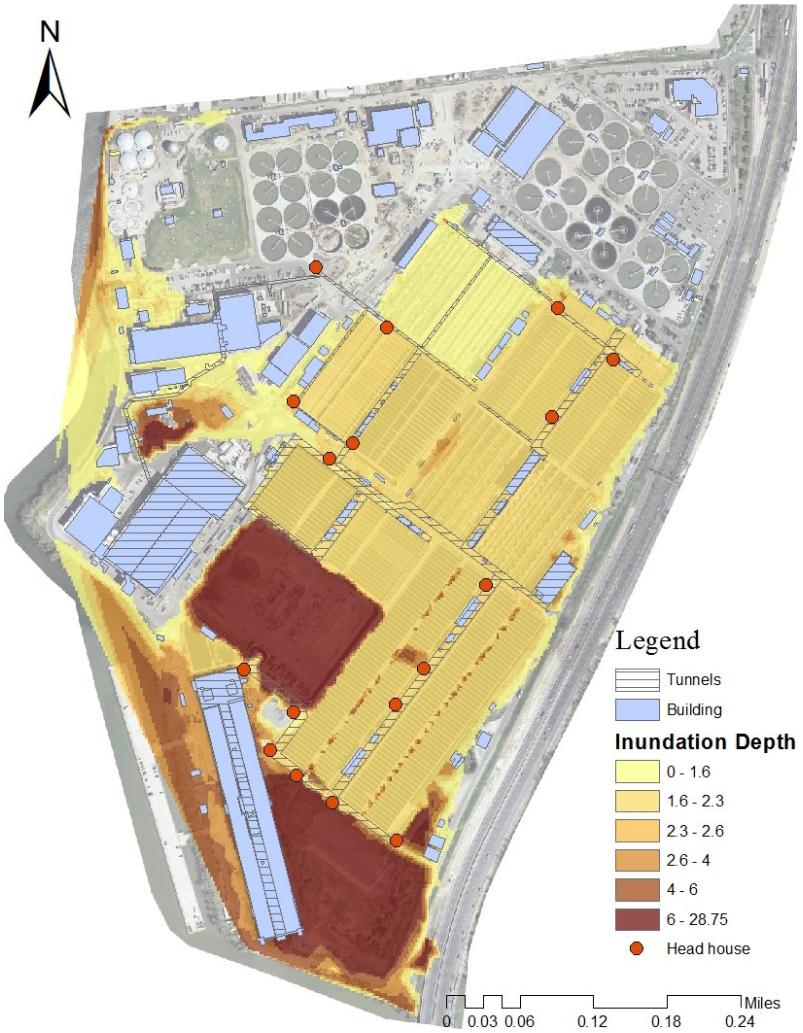

Figure 5-26. Surface inundation map (S16)
*100-year flood, HEC-RAS unsteady flow, future climate beyond this century

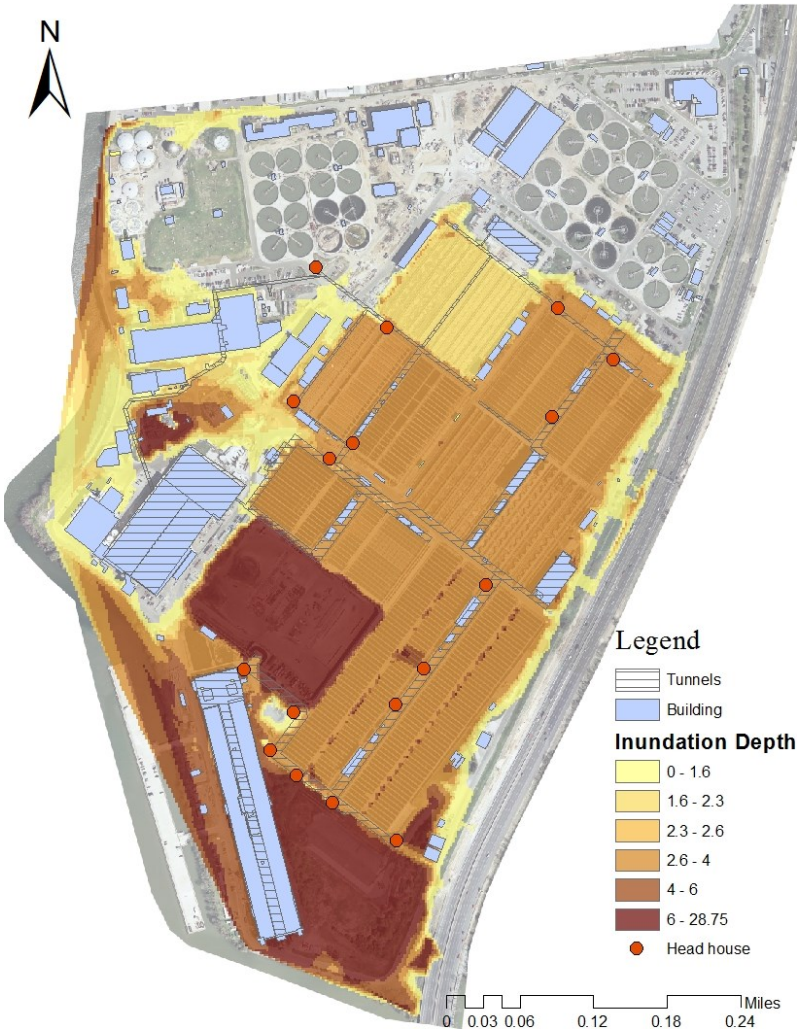

Figure 5-27. Surface inundation map (S17)
*500-year flood, HEC-RAS unsteady flow, future climate beyond this century

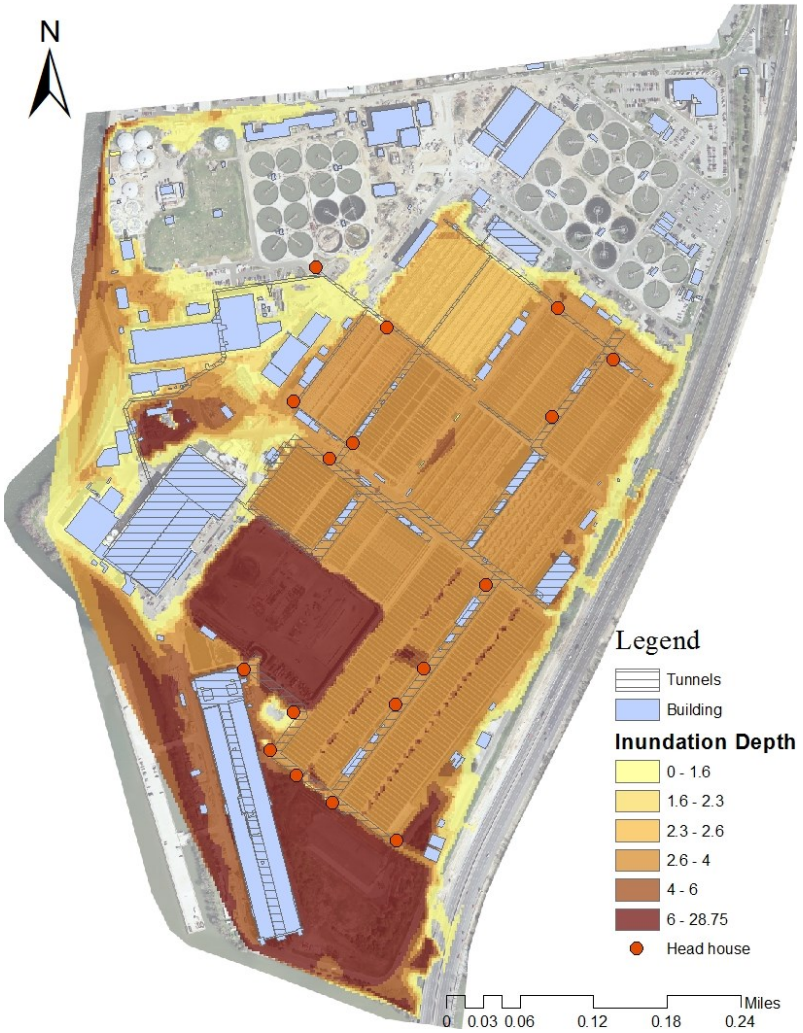

Figure 5-28. Surface inundation map (S18)
*1000-year flood, HEC-RAS unsteady flow, future climate beyond this century

5.3.2 Building Percent Damage

As introduced in Section 5.2.1.2, the building foundation percent damage criteria for non-residential structures based on FEMA Substantial Damage Estimator (SDE) was used herein to estimate the percent damage for the buildings inside the BPAWWTP for the 18 scenarios (FEMA, 2013a). All of the 18 scenarios are subject to the 1 percent or greater chance of flooding in any given year, which verifies the rationality of this application. The 18 scenarios satisfy the Special Flood Hazard Area (SFHA) definition (FEMA, 2014). They can be viewed as the SFHA modeled by the current and future climate scenarios. The outputs for the 18 scenarios (Table 5-7) are color coded in Table 5-8, with green for the percent damage between 0-25%, yellow for 25-50% damage, and red for damage above 50%.

Table 5-8. Building foundation percent damage (BPAWWTP)

Scenarios	1	2	3	4	5	6	7	8	9	10	11	12	13	14	15	16	17	18
River stage (ft)	10.1	13	14.2	8.1	9.6	10.2	12.9	15.7	16.9	11	12.1	12.6	14.2	16.9	18.1	13.1	14.2	14.7
Area Sub-Station 2	0	0	0	0	0	0	0	0-25%	0-25%	0	0	0	0	0-25%	0-25%	0	0	0
Bypass Building	0	0	0	0	0	0	0	0	0-25%	0	0	0	0	0-25%	0-25%	0	0	0
Cart Shop 2	0	0-25%	0-25%	0	0	0	0-25%	0-25%	25-50%	0	0	0-25%	0-25%	25-50%	25-50%	0-25%	0-25%	0-25%
Central Maintenance Facility	0	0	0-25%	0	0	0	0	0-25%	0-25%	0	0	0	0-25%	0-25%	25-50%	0-25%	0-25%	0-25%
Central Operations Building	0	0	0	0	0	0	0	0	0	0	0	0	0	0	0	0	0	0
Chemical Batching Building	0	0-25%	0-25%	0	0	0	0-25%	0-25%	25-50%	0	0	0-25%	0-25%	25-50%	25-50%	0-25%	0-25%	0-25%
Chemical Building	0	0	0	0	0	0	0	0-25%	0-25%	0	0	0	0	0-25%	0-25%	0	0	0
Chlorination Building	0	0	0-25%	0	0	0	0	0-25%	0-25%	0	0	0	0-25%	0-25%	0-25%	0	0-25%	0-25%
Chlorine Building	0	0	0	0	0	0	0	0	0-25%	0	0	0	0	0-25%	0-25%	0	0	0
CM-3A (CDG) Trailer	0	0-25%	0-25%	0	0	0	0-25%	25-50%	25-50%	0	0-25%	0-25%	0-25%	25-50%	25-50%	0-25%	0-25%	0-25%
Construction Management Trailers	0	0-25%	0-25%	0	0	0	0-25%	25-50%	25-50%	0	0-25%	0-25%	0-25%	25-50%	25-50%	0-25%	0-25%	0-25%
Dechlorination Building (Sodium Bisulfite)	0	0-25%	0-25%	0	0	0	0-25%	25-50%	25-50%	0	0-25%	0-25%	0-25%	25-50%	25-50%	0-25%	0-25%	0-25%
Denitrification Control Building	0	0-25%	0-25%	0	0	0	0-25%	25-50%	25-50%	0	0-25%	0-25%	0-25%	25-50%	50-75%	0-25%	0-25%	0-25%
Department of Information Technology	0	0	0	0	0	0	0	0	0	0	0	0	0	0	0	0	0	0
Department of Information Technology Trailer	0	0	0	0	0	0	0	0	0	0	0	0	0	0	0	0	0	0
Dewatered Sludge Loading Facility	0	0	0	0	0	0	0	0-25%	0-25%	0	0	0	0	0-25%	0-25%	0	0	0

Continue Table 5-8

Scenarios	1	2	3	4	5	6	7	8	9	10	11	12	13	14	15	16	17	18
River stage (ft)	**10.1**	**13**	**14.2**	**8.1**	**9.6**	**10.2**	**12.9**	**15.7**	**16.9**	**11**	**12.1**	**12.6**	**14.2**	**16.9**	**18.1**	**13.1**	**14.2**	**14.7**
DMSS-3 (CDG) Trailer	0	0-25%	0-25%	0	0	0	0-25%	0-25%	25-50%	0	0-25%	0-25%	0-25%	25-50%	25-50%	0-25%	0-25%	0-25%
Dry Polymer Receiving Building	0	0	0	0	0	0	0	0	0-25%	0	0	0	0	0-25%	0-25%	0	0	0
Dual Purpose Sedimentation	0	0-25%	0-25%	0	0	0	0-25%	25-50%	25-50%	0	0-25%	0-25%	0-25%	25-50%	50-75%	0-25%	0-25%	0-25%
Dual Purpose Sedimentation Control Building	0	0-25%	0-25%	0	0	0	0-25%	25-50%	25-50%	0	0-25%	0-25%	0-25%	25-50%	25-50%	0-25%	0-25%	0-25%
East Secondary Sedimentation	0	0-25%	0-25%	0	0	0	0-25%	25-50%	25-50%	0	0-25%	0-25%	0-25%	25-50%	50-75%	0-25%	0-25%	0-25%
EGMCH	0	0	0	0	0	0	0	0	0	0	0	0	0	0	0	0	0	0
EMA Trailer	0	0	0	0	0	0	0	0	0	0	0	0	0	0	0	0	0	0
EPMC-1 (Metcalf & Eddy) Trailer	0	0	0	0	0	0	0	0	0	0	0	0	0	0	0	0	0	0
EPMC-2 (O'Brien & Gere) Trailer	0	0	0	0	0	0	0	0	0	0	0	0	0	0	0	0	0	0
EPMC-3A (G&H) Trailer	0	0-25%	25-50%	0	0	0	0-25%	25-50%	25-50%	0	0-25%	0-25%	25-50%	25-50%	50-75%	0-25%	25-50%	25-50%
EPMC-4 (CH2MHill) Trailer	0	0	0	0	0	0	0	0	0	0	0	0	0	0	0	0	0	0
Flowmeter M8 Access House	0	0	0	0	0	0	0	0	0	0	0	0	0	0	0	0	0	0
Fueling Station	0	0	0	0	0	0	0	0-25%	0-25%	0	0	0	0	0-25%	0-25%	0	0	0
Garage	0	0	0	0	0	0	0	0	0-25%	0	0	0	0	0-25%	0-25%	0	0	0
Gate A Security Shed	0	0	0	0	0	0	0	0	0	0	0	0	0	0	0	0	0	0
Gate B Security Building	0	0	0	0	0	0	0	0	0-25%	0	0	0	0	0-25%	0-25%	0	0	0
GHCH	0	0	0	0	0	0	0	0-25%	0-25%	0	0	0	0	0-25%	0-25%	0	0	0
Gravity Thickener Control Building	0	0-25%	0-25%	0	0	0	0-25%	0-25%	25-50%	0	0	0	0-25%	25-50%	25-50%	0-25%	0-25%	0-25%

Continue Table 5-8

Scenarios	1	2	3	4	5	6	7	8	9	10	11	12	13	14	15	16	17	18
River stage (ft)	**10.1**	**13**	**14.2**	**8.1**	**9.6**	**10.2**	**12.9**	**15.7**	**16.9**	**11**	**12.1**	**12.6**	**14.2**	**16.9**	**18.1**	**13.1**	**14.2**	**14.7**
Grit and Screenings Loading Station 1	0	0	0	0	0	0	0	0	0	0	0	0	0	0	0	0	0	0
Grit and Screenings Loading Station 2	0	0	0	0	0	0	0	0	0	0	0	0	0	0	0-25%	0	0	0
Grit Chamber Building 2	0	0	0	0	0	0	0	0	0	0	0	0	0	0	0-25%	0	0	0
Grit Chamber Building 1	0	0	0	0	0	0	0	0	0	0	0	0	0	0	0	0	0	0
Headhouse Stair 15	0	0-25%	0-25%	0	0	0	0-25%	25-50%	25-50%	0	0-25%	0-25%	0-25%	25-50%	50-75%	0-25%	0-25%	0-25%
Headhouse Stair 16	0	0-25%	0-25%	0	0	0	0-25%	25-50%	25-50%	0	0-25%	0-25%	0-25%	25-50%	25-50%	0-25%	0-25%	0-25%
Headhouse Stair 17	0	0-25%	0-25%	0	0	0	0-25%	25-50%	25-50%	0	0-25%	0-25%	0-25%	25-50%	50-75%	0-25%	0-25%	0-25%
Headhouse Stair 20	0	0-25%	0-25%	0	0	0	0-25%	25-50%	25-50%	0	0-25%	0-25%	0-25%	25-50%	50-75%	0-25%	0-25%	0-25%
Headhouse Stair 21	0	0-25%	0-25%	0	0	0	0-25%	25-50%	25-50%	0	0-25%	0-25%	0-25%	25-50%	50-75%	0-25%	0-25%	0-25%
Headhouse Stair 22	0	0-25%	0-25%	0	0	0	0-25%	25-50%	25-50%	0	0-25%	0-25%	0-25%	25-50%	25-50%	0-25%	0-25%	0-25%
Headhouse Stair 23	0	0-25%	0-25%	0	0	0	0-25%	25-50%	25-50%	0	0-25%	0-25%	0-25%	25-50%	50-75%	0-25%	0-25%	0-25%
Headhouse Stair 24	0	0-25%	0-25%	0	0	0	0-25%	25-50%	25-50%	0	0-25%	0-25%	0-25%	25-50%	25-50%	0-25%	0-25%	0-25%
Headhouse Stair 25	0	0	0	0	0	0	0	0-25%	0-25%	0	0	0	0	0-25%	0-25%	0	0	0
Headhouse Stair 26	0	0-25%	0-25%	0	0	0	0-25%	25-50%	25-50%	0	0-25%	0-25%	0-25%	25-50%	50-75%	0-25%	0-25%	0-25%

Continue Table 5-8

Scenarios	1	2	3	4	5	6	7	8	9	10	11	12	13	14	15	16	17	18
River stage (ft)	10.1	13	14.2	8.1	9.6	10.2	12.9	15.7	16.9	11	12.1	12.6	14.2	16.9	18.1	13.1	14.2	14.7
Headhouse Stair 28	0	0-25%	0-25%	0	0	0	0-25%	25-50%	25-50%	0	0-25%	0-25%	0-25%	25-50%	50-75%	0-25%	0-25%	0-25%
Headhouse Stair 29	0	0-25%	0-25%	0	0	0	0-25%	25-50%	25-50%	0	0-25%	0-25%	0-25%	25-50%	50-75%	0-25%	0-25%	0-25%
Headhouse Stair 31	0	0-25%	0-25%	0	0	0	0-25%	0-25%	25-50%	0	0	0-25%	0-25%	25-50%	25-50%	0-25%	0-25%	0-25%
Headhouse Stair 32	0	0-25%	0-25%	0	0	0	0-25%	25-50%	25-50%	0	0-25%	0-25%	0-25%	25-50%	50-75%	0-25%	0-25%	0-25%
Headhouse Stair 36	0-25%	25-50%	25-50%	0	0-25%	0-25%	0-25%	25-50%	50-75%	0-25%	0-25%	0-25%	25-50%	50-75%	50-75%	25-50%	25-50%	25-50%
Headhouse Stair 37	0	0-25%	0-25%	0	0	0	0-25%	25-50%	25-50%	0-25%	0-25%	0-25%	0-25%	25-50%	50-75%	0-25%	0-25%	0-25%
Headhouse Stair 38	0	0	0-25%	0	0	0	0	0-25%	0-25%	0	0	0	0-25%	0-25%	25-50%	0-25%	0-25%	0-25%
Headhouse Stair 39	0	0-25%	0-25%	0	0	0	0-25%	25-50%	25-50%	0-25%	0-25%	0-25%	0-25%	25-50%	50-75%	0-25%	0-25%	25-50%
Headhouse Stair 45	0	0-25%	0-25%	0	0	0	0-25%	25-50%	25-50%	0-25%	0-25%	0-25%	0-25%	25-50%	50-75%	0-25%	0-25%	25-50%
Headhouse Stair 46	0-25%	0-25%	25-50%	0	0	0-25%	0-25%	25-50%	50-75%	0-25%	0-25%	0-25%	25-50%	50-75%	50-75%	0-25%	25-50%	25-50%
Headhouse Stair 6	0	0-25%	0-25%	0	0	0	0-25%	25-50%	25-50%	0	0-25%	0-25%	0-25%	25-50%	25-50%	0-25%	0-25%	0-25%
Headhouse Stair 60	0	0	0	0	0	0	0	0	0	0	0	0	0	0	0-25%	0	0	0
Headhouse Stair 61	0	0	0	0	0	0	0	0	0	0	0	0	0	0	0-25%	0	0	0
Headhouse Stair 7	0	0-25%	0-25%	0	0	0	0-25%	25-50%	25-50%	0	0-25%	0-25%	0-25%	25-50%	25-50%	0-25%	0-25%	0-25%

Continue Table 5-8

Scenarios	1	2	3	4	5	6	7	8	9	10	11	12	13	14	15	16	17	18
River stage (ft)	**10.1**	**13**	**14.2**	**8.1**	**9.6**	**10.2**	**12.9**	**15.7**	**16.9**	**11**	**12.1**	**12.6**	**14.2**	**16.9**	**18.1**	**13.1**	**14.2**	**14.7**
Headhouse Stair 9	0	0-25%	0-25%	0	0	0	0-25%	25-50%	25-50%	0	0-25%	0-25%	0-25%	25-50%	50-75%	0-25%	0-25%	0-25%
Heating Plant	0	0-25%	0-25%	0	0	0	0-25%	0-25%	25-50%	0	0	0	0-25%	25-50%	25-50%	0-25%	0-25%	0-25%
HVAC Shop	0	0-25%	0-25%	0	0	0	0-25%	25-50%	25-50%	0	0-25%	0-25%	0-25%	25-50%	25-50%	0-25%	0-25%	0-25%
Interim Hypochlorite Facility	0	0	0	0	0	0	0	0	0-25%	0	0	0	0	0-25%	0-25%	0	0	0
Lab	0	0	0-25%	0	0	0	0	0-25%	0-25%	0	0	0	0-25%	0-25%	25-50%	0	0-25%	0-25%
Lime Storage and Feed Building	0	0-25%	0-25%	0	0	0	0-25%	25-50%	25-50%	0	0-25%	0-25%	0-25%	25-50%	50-75%	0-25%	0-25%	0-25%
Metal Salts Chemical Recycling Station	0	0-25%	0-25%	0	0	0	0-25%	25-50%	25-50%	0	0	0-25%	0-25%	25-50%	25-50%	0-25%	0-25%	0-25%
Methanol Storage and Pump Facility	0	0-25%	0-25%	0	0	0	0-25%	25-50%	25-50%	0	0-25%	0-25%	0-25%	25-50%	25-50%	0-25%	0-25%	0-25%
NaOH Building 2	0	0-25%	0-25%	0	0	0	0-25%	25-50%	25-50%	0	0-25%	0-25%	0-25%	25-50%	25-50%	0-25%	0-25%	0-25%
Nitrification Blower Building	0	0-25%	0-25%	0	0	0	0-25%	25-50%	25-50%	0	0-25%	0-25%	0-25%	25-50%	50-75%	0-25%	0-25%	0-25%
Nitrification Control Building	0	0-25%	0-25%	0	0	0	0-25%	25-50%	25-50%	0	0-25%	0-25%	0-25%	25-50%	50-75%	0-25%	0-25%	0-25%
Nitrification Reactors	0	0-25%	0-25%	0	0	0	0-25%	25-50%	25-50%	0	0-25%	0-25%	0-25%	25-50%	50-75%	0-25%	0-25%	0-25%
Nitrification Reactors Electrical Building 1	0	0-25%	0-25%	0	0	0	0-25%	25-50%	25-50%	0	0-25%	0-25%	0-25%	25-50%	25-50%	0-25%	0-25%	0-25%

Continue Table 5-8

Scenarios	1	2	3	4	5	6	7	8	9	10	11	12	13	14	15	16	17	18
River stage (ft)	**10.1**	**13**	**14.2**	**8.1**	**9.6**	**10.2**	**12.9**	**15.7**	**16.9**	**11**	**12.1**	**12.6**	**14.2**	**16.9**	**18.1**	**13.1**	**14.2**	**14.7**
Nitrification Reactors Electrical Building 2	0	0-25%	0-25%	0	0	0	0-25%	25-50%	25-50%	0	0-25%	0-25%	0-25%	25-50%	25-50%	0-25%	0-25%	0-25%
Nitrification Sedimentation	0	0-25%	0-25%	0	0	0	0-25%	25-50%	25-50%	0	0-25%	0-25%	0-25%	25-50%	50-75%	0-25%	0-25%	0-25%
OMAP (Peer) Trailer	0	0-25%	0-25%	0	0	0	0-25%	25-50%	25-50%	0	0-25%	0-25%	0-25%	25-50%	50-75%	0-25%	0-25%	0-25%
Pepco Switching Station	0	0-25%	0-25%	0	0	0	0-25%	25-50%	25-50%	0	0	0-25%	0-25%	25-50%	50-75%	0-25%	0-25%	25-50%
pH Adjustment (NaOH) Building	0	0-25%	0-25%	0	0	0	0-25%	25-50%	25-50%	0	0-25%	0-25%	0-25%	25-50%	25-50%	0-25%	0-25%	0-25%
Plumber's Shop	0	0	0-25%	0	0	0	0	0-25%	0-25%	0	0	0	0-25%	0-25%	25-50%	0-25%	0-25%	0-25%
Primary Sludge Degritting and Grinding Building	0	0-25%	0-25%	0	0	0	0-25%	25-50%	25-50%	0	0	0-25%	0-25%	25-50%	25-50%	0-25%	0-25%	0-25%
PSCH A	0	0	0	0	0	0	0	0-25%	0-25%	0	0	0	0	0-25%	0-25%	0	0	0
PSCH B	0	0	0	0	0	0	0	0-25%	0-25%	0	0	0	0	0-25%	0-25%	0	0	0
PSCH C	0	0	0	0	0	0	0	0-25%	0-25%	0	0	0	0	0-25%	0-25%	0	0	0
PSCH D	0	0	0	0	0	0	0	0-25%	0-25%	0	0	0	0	0-25%	0-25%	0	0	0
PSCH E	0	0	0	0	0	0	0	0	0	0	0	0	0	0	0	0	0	0
PSCH F	0	0	0	0	0	0	0	0	0	0	0	0	0	0	0	0	0	0
PSCH G	0	0	0	0	0	0	0	0	0	0	0	0	0	0	0	0	0	0
PSCH H	0	0	0	0	0	0	0	0	0	0	0	0	0	0	0	0	0	0
PSCH I	0	0	0	0	0	0	0	0	0	0	0	0	0	0	0	0	0	0
Raw Wastewater Pump Station 1	0	0	0	0	0	0	0	0	0	0	0	0	0	0	0-25%	0	0	0
Raw Wastewater Pump Station 2	0	0	0	0	0	0	0	0	0	0	0	0	0	0	0-25%	0	0	0

Continue Table 5-8

Scenarios	1	2	3	4	5		7	8	9	10	11	12	13	14	15	16	17	18
River stage (ft)	**10.1**	**13**	**14.2**	**8.1**	**9.6**	**10.2**	**12.9**	**15.7**	**16.9**	**11**	**12.1**	**12.6**	**14.2**	**16.9**	**18.1**	**13.1**	**14.2**	**14.7**
Sample Building 001	0	0-25%	0-25%	0	0	0	0-25%	0-25%	25-50%	0	0	0-25%	0-25%	25-50%	25-50%	0-25%	0-25%	0-25%
Sample Building 002	0	0-25%	0-25%	0	0	0	0-25%	0-25%	25-50%	0	0-25%	0-25%	0-25%	25-50%	25-50%	0-25%	0-25%	0-25%
Secondary Blower Building	0	0	0	0	0	0	0	0	0-25%	0	0	0	0	0-25%	0-25%	0	0	0
Secondary Control Building	0	0-25%	0-25%	0	0	0	0-25%	25-50%	25-50%	0	0-25%	0-25%	0-25%	25-50%	50-75%	0-25%	0-25%	0-25%
Secondary Effluent Pump Station	0	0	0	0	0	0	0	0-25%	0-25%	0	0	0	0	0-25%	0-25%	0	0	0
Secondary Electrical Building	0	0-25%	0-25%	0	0	0	0-25%	25-50%	25-50%	0	0-25%	0-25%	0-25%	25-50%	50-75%	0-25%	0-25%	0-25%
Security Building	0	0	0	0	0	0	0	0	0	0	0	0	0	0	0	0	0	0
Security Bus Shed	0	0	0	0	0	0	0	0	0	0	0	0	0	0	0	0	0	0
Security Main Gate Shed	0	0	0	0	0	0	0	0	0	0	0	0	0	0	0	0	0	0
Solids Processing Building	0	0	0	0	0	0	0	0	0-25%	0	0	0	0	0-25%	0-25%	0	0	0
Standby Chlorination/ Dechlorination Building	0-25%	0-25%	25-50%	0	0	0-25%	0-25%	25-50%	50-75%	0-25%	0-25%	0-25%	25-50%	50-75%	50-75%	0-25%	25-50%	25-50%
Supply Building 1	0	0	0	0	0	0	0	0-25%	0-25%	0	0	0	0	0-25%	0-25%	0	0	0-25%
Supply Building 2	0	0	0	0	0	0	0	0-25%	0-25%	0	0	0	0	0-25%	0-25%	0	0	0
Truck Wash Station	0	0-25%	0-25%	0	0	0	0-25%	25-50%	25-50%	0	0-25%	0-25%	0-25%	25-50%	25-50%	0-25%	0-25%	0-25%
TSRS	0	0	0-25%	0	0	0	0	0-25%	0-25%	0	0	0	0-25%	0-25%	25-50%	0	0-25%	0-25%
Used Oil & Special Waste Storage Building	0	0-25%	0-25%	0	0	0	0-25%	0-25%	25-50%	0	0-25%	0-25%	0-25%	25-50%	25-50%	0-25%	0-25%	0-25%
Weighing Station	0	0	0	0	0	0	0	0-25%	0-25%	0	0	0	0	0-25%	0-25%	0	0	0-25%
West Secondary Electrical Building	0	0-25%	0-25%	0	0	0	0-25%	25-50%	25-50%	0	0-25%	0-25%	0-25%	25-50%	50-75%	0-25%	0-25%	0-25%
WGMCH	0	0	0	0	0	0	0	0	0	0	0	0	0	0	0	0	0	0

5.3.3 Safe Evacuation

According to the risk level defined in Section 5.2.1.3, the outputs of the GIS-Assisted Risk Register (GARR) are presented as safe evacuation risk maps (Figure 5-29 to Figure 5-31). The red zones indicate high evacuation risk; the yellow zones indicate moderate risk; and the green zones indicate relatively low risk. If limited flood remediation resources are available, the red zones are recommended as priority.

Based on the safe evacuation criteria introduced in section 5.2.1.3, Figure 5-11 to Figure 5-28 can also be used to identify the areas that are safe for evacuation by foot and from a vehicle. The yellow area (0-1.6 ft) and the light orange zone (1.6-2.3 ft) are safe for evacuation by foot. The dark orange zone (2.3-2.6 ft) is the inundation depth threshold for safe evacuation from a vehicle door.

For the future climate scenarios, the risk levels for the studied critical infrastructure are more severe than the current climate scenarios. For example, processes such as secondary sedimentation, nitrification reactors, nitrification sedimentation, and dual purpose sedimentation are at low risk under current climate, but at moderate risk under future climate within this century. If planning horizon is beyond this century, these processes are at high risk. Climate change may alter the flood risk level of a critical infrastructure component. GIS-Assisted Risk Register (GARR) assists the visualization of this change.

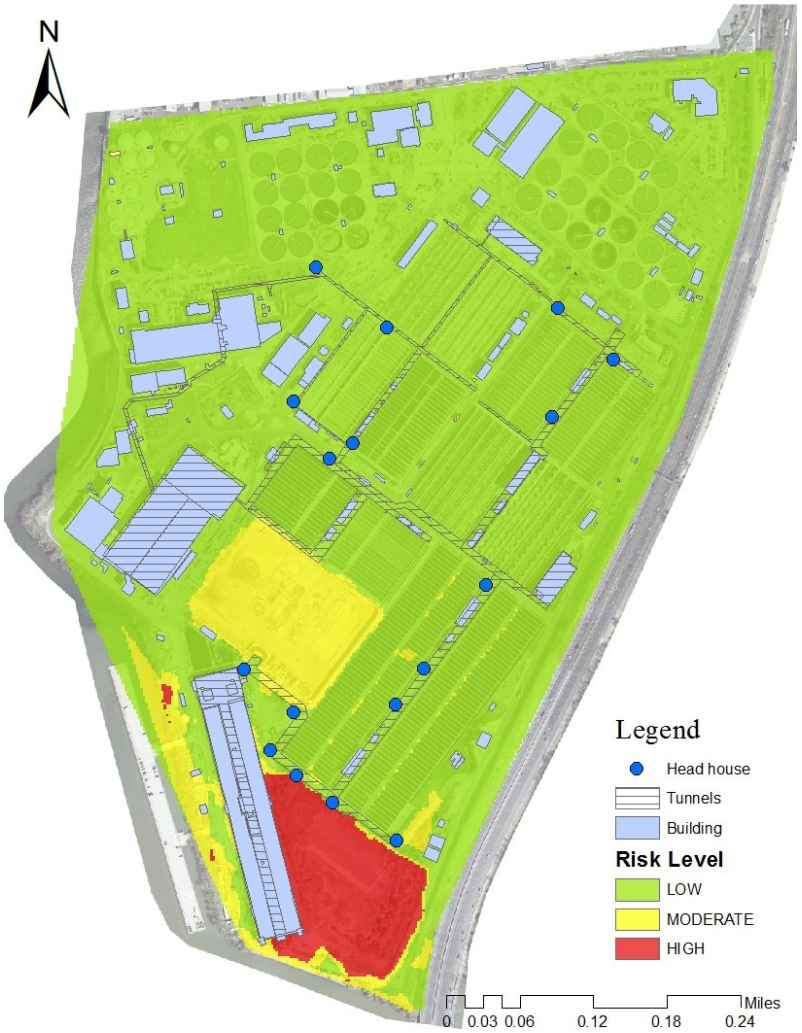

Figure 5-29. Evacuation risk map by GARR (Case 1)
*Current climate

Figure 5-30. Evacuation risk map by GARR (Case 2)
*Future climate within this century

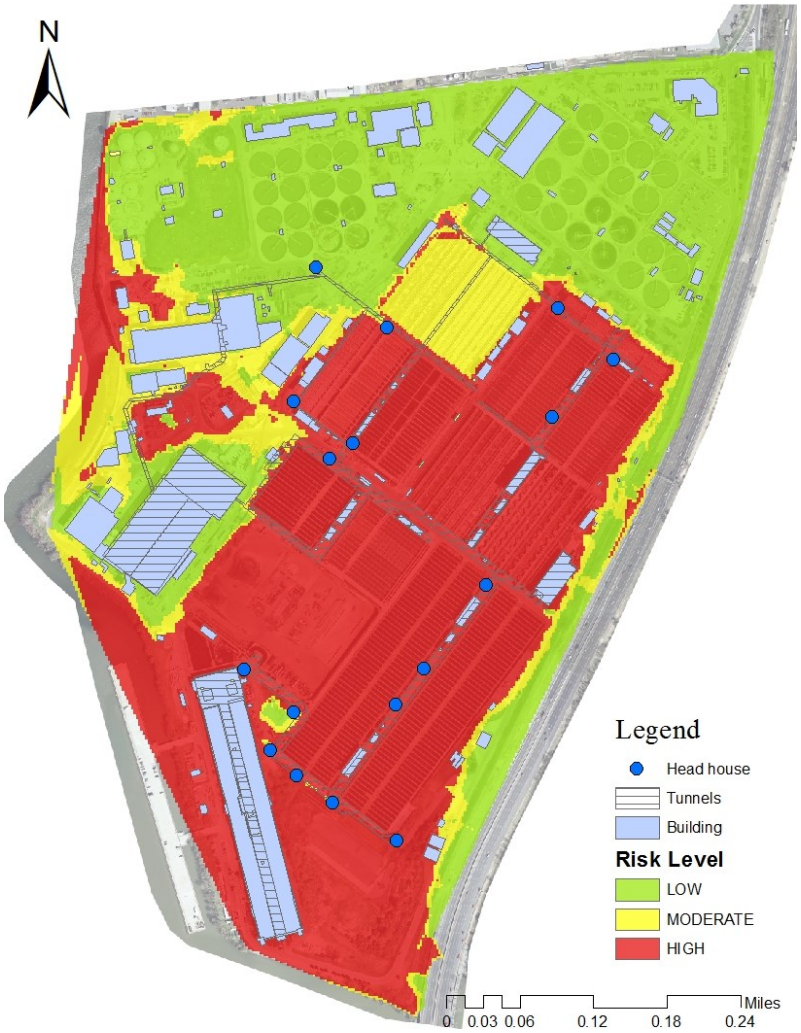

Figure 5-31. Evacuation risk map by GARR (Case 3)
* Future climate beyond this century

5.3.4 Underground Inundation and Equipment Damage

The underground inundation damage estimate was based on the methods introduced in Sections 5.2.2.1 to 5.2.2.3. Due to the lack of continuous long-term river stage monitoring at the study site, a simplified assumption was made for demonstration purposes: the joint distribution of stage and duration developed for the nearest gauge site, Potomac River at Washington, D.C. (8594900), is applied directly to the study site.

The approximate locations of the essential equipment inside the Denitrification Return Sludge Gallery, Nitrification Sedimentation Gallery, Waste Sludge Gallery, Nitrification Reactor Gallery, East and West Secondary Sedimentation Gallery, Air Main Gallery, Air Main Tunnel, Secondary Reactor Gallery, Secondary Reactor Tunnel, Return Sludge Tunnel, Dual Purpose Sedimentation Gallery 1, 2 and 3, etc., were surveyed and mapped in ArcGIS (see Appendix A). The critical elevation of each piece of equipment (defined in Figure 5-8) was measured from the tunnel floor by a laser tape measure. The floor and surface elevations of the underground tunnels were based on the best estimate from available as-built drawings, as well as laser-tape measurements from the ground level where visibility permitted.

The hydraulic profiles of each process provided helpful information. For example, Figure 5-32 shows the hydraulic profile of primary to secondary processes; it provides the floor and ceiling elevations of the return sludge tunnel, chemical feed gallery, and west secondary sedimentation gallery. This approximate, preliminary data provided by the tunnel survey and data search are sufficient for a research and demonstration study, but are not recommended for any construction management purpose. A complete survey is needed to further develop an accurate underground tunnel geometry.

Figure 5-33 shows the joint probability density function (JPDF) of stage and duration at DC, computed by Eq.(5-14). The damage function is shown in Figure 5-34, assuming that the repair and

replacement cost of each pump and its appurtenances is $10,000. Based on the flow intrusion model in Section 5.2.2.1, the relationship among underground inundation depth ($WSEL_{tunnel}$), flood duration (τ), and flood stage (z) are shown as the contour lines in Figure 5-34(a). Based on the equipment damage model in Section 5.2.2.2, the damage (D) is shown as a function of underground inundation depth ($WSEL_{tunnel}$) in Figure 5-34(b) for both the step damage and the linear damage models. The step model predicts lower damages than the linear model, consistent with Figure 5-9. Figure 5-34(c) and Figure 5-34(d) are the three-dimensional damage functions, derived from Figure 5-34(a) and Figure 5-34(b), respectively.

By numerically integrating the element-wise product of Figure 5-34(c) and Figure 5-33, the expected annual damages $E(D)$ due to underground inundation damage is $\$4.60\times10^{6}C$ based on the step damage model. Similarly, by integrating the element-wise product of Figure 5-34(d) and Figure 5-33, the expected annual damage $E(D)$ due to underground inundation damage is $\$6.95\times10^{6}C$ based on the linear damage model. C is a correction factor used to adjust the best estimate of the current replacement cost. If the inundated equipment could be repaired for less than the replacement cost, then C is less than 1. If the equipment is aged and deteriorated, the current worth of damaged equipment is less than the replacement cost and the C is greater than 1.

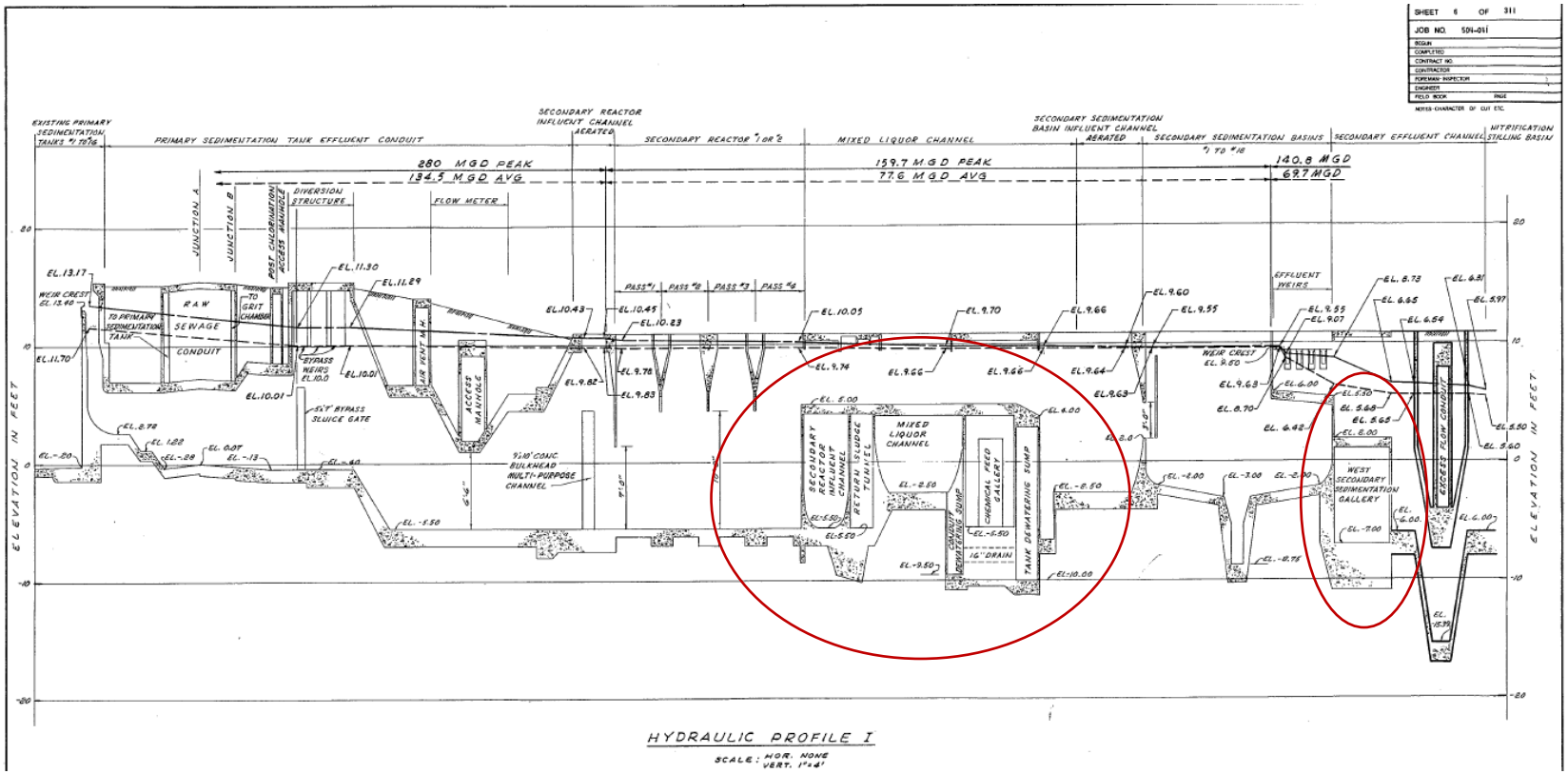

Figure 5-32. Hydraulic profile of primary to secondary processes (DCWASA, n.d.-a)

Note: the underground tunnels/galleries are circled.

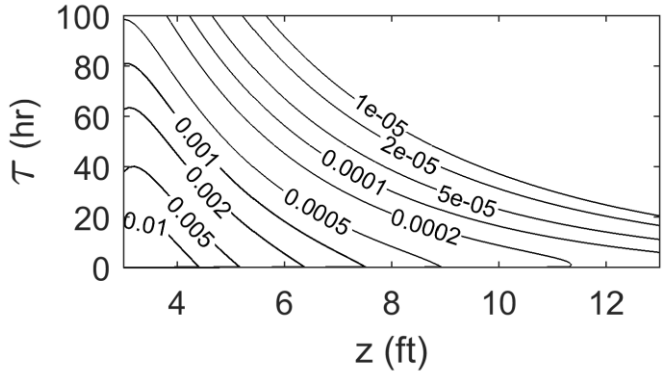

Figure 5-33. Joint Probability Density Function (JPDF) of flood stage and duration (Washington, D.C.)

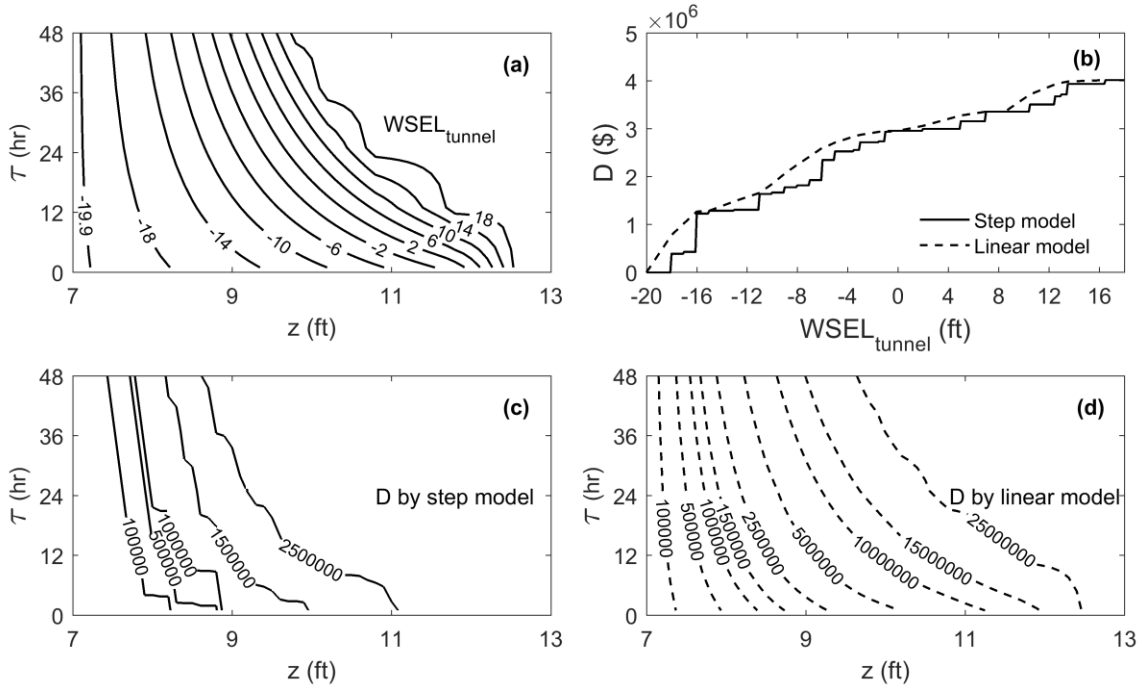

Figure 5-34. Underground equipment damage function

5.4 Conclusions

In this chapter, customized programs were developed with assistance of ArcGIS for the ground level module and the subsurface module. The ground level module evaluated the risk associated

with flood inundation depth. The subsurface module computed risks related to flood volume, requiring the quantification of both flood depth and duration.

For the ground level module, inundation depth was visualized by maps for 18 scenarios, including current climate, future climate within this century, and future climate beyond this century. The building percent damage was estimated by the foundation damage guidelines proposed by FEMA Substantial Damage Estimator (SDE). A GIS-Assisted Risk Register was created to communicate the evacuation risk, which can be applied to depth related risk severity assessment.

Risk register is a subjective risk assessment method. Cox (2008) states that poor resolution, errors, suboptimal resource allocation, and ambiguous input and outputs are the limitations of this method. The user should be aware that the GIS-Assisted Risk Register (GARR) also has these limitations. If the risk scores are assigned based on a different criterion, or the risk level are assigned differently to the combinations of probability and consequences of occurrence, the final output and conclusion may change. Cox (2008) recommends checking weak consistency, betweenness and consistent coloring in the use of the risk matrix tool.

The subsurface module quantified essential equipment damage. Linear and step damage functions were developed for each equipment inside the underground tunnels. An overall subsurface WSEL-damage function was generated. Combining the joint density function of stage and duration, the expected annual damage was estimated for the study site, for both the step damage model and the linear damage model.

6 CONCLUSIONS AND RECOMMENDATIONS

6.1 Unique Aspects of Critical Civil Infrastructure

Each critical infrastructure sector has unique aspects related to flooding. A wastewater treatment plant (WWTP) is one critical infrastructure element that is particularly vulnerable to floods. The WWTP's resiliency to flood significantly influences the residents, industry and business inside and outside its service area. This research develops and demonstrates methods to assess infrastructure flood risk with emphasis on municipal wastewater treatment plants. These methods can assist the appropriate allocation of efforts to risk mitigation.

The following unique characteristics of the WWTP subject to flooding are identified during this research.

- A WWTP is typically located close to a river bank. In the U.S. Mid-Atlantic region, many cities and their associated WWTPs lie along tidally-influenced water bodies. These facilities will be among the first infrastructure elements affected by sea level rise.
- Flood effects on a treatment plant extend beyond damage to the facilities and equipment themselves. Discharge of untreated wastewater into waterways is a widespread threat to human health and the natural environment. Disruption of service hampers the municipality's economic and domestic function.
- Essential equipment is mostly located inside underground spaces, such as tunnels and galleries. Their vulnerability to flooding is not a simple function of flood depth. Flood duration is also a critical variable.

6.2 Contribution of This Research

The contribution of this research includes

1. The vulnerability of a facility lying along an estuary to flooding under climate change is quantified. Under expected ranges of sea level rise and watershed runoff increase, an increased likelihood of potentially damaging flooding is predicted. The effects of downstream and upstream change are found to be non-additive, which is an important consideration for planning.
2. A bivariate flood probability model is developed, accounting for flood duration as well as depth. The use of conditional probability (duration exceeded conditional on depth exceeded) allows data-driven construction of a joint probability distribution without reliance on a theoretical construct such as a copula.
3. The use of the bivariate model in estimating expected annual damages (EAD) is demonstrated for an example location where vulnerability is not a simple function of flood depth. As in current practice with univariate tools, the EAD can be used as a summary measure to evaluate mitigation alternatives.
4. A new spatial tool, the GIS-Assisted Risk Register (GARR) is developed. Its use in mapping the unique flood vulnerability aspects of a large treatment plant is demonstrated.

These methods were developed in the context of a municipal wastewater treatment plant. They are applicable to any infrastructure system or component that shares the fundamental properties of such a plant: location close to a water body simultaneously subject to downstream and upstream change; vulnerability that is not a simple function of depth; and widespread non-local disruptive effects of flood damage. For example, the methods would be applicable to underground transportation facilities.

The following sections discuss each of these topics and contributions in more detail, identifying some limitations of the study and proposing ideas for future follow-in research.

6.3 Climate Change

Flooding is part of nature. Floods have always existed and will continue to exist (Penning-Rowsell & Wilson, 2003; United Nations, 2000). Changes to the earth's climate system are generally expected to alter the regional climate factors that control the magnitude and likelihood of floods. Because the statistics of floods are changing (statistical non-stationarity), planners, managers, and designers cannot rely on past records to guide their decisions.

A Potomac River HEC-RAS model was developed to estimate flood frequencies for current and future climate conditions. A sensitivity analysis method was created for unsteady flow simulation to examine the impact of changes in upstream freshwater and downstream sea levels on the flood stage at the study site. Data capture and post-processing of model results were automated by C#+HECRASController. The results were compared with the steady flow analysis. Inundation depth was visualized for both current and future planning horizons. It is concluded that the steady flow analysis provides higher estimate of current and future floods.

Accurate upstream flow predictions and downstream sea-level rise predictions are critical for this approach, since they are the upstream and downstream boundaries for the 1D unsteady hydraulic model. For upstream freshwater input prediction, a more detailed and accurate assessment of hydro-climate change in the watershed is needed. For downstream water level predictions, a rising mean sea level is already apparent in the observational record, although projections of additional rise due to global ocean effects are less certain. This analysis did not account for the possible future intensification of marine storm surges. Storm surge is "an abnormal rise of water generated by a storm, over and above the predicted astronomical tides"

(NOAA, 2013a); the 18-year record used in this study included some storm surge events in the Lewisetta record; however, the sea level perturbations were applied equally to the entire record. Storm surge changes need to be incorporated in combination with the two change factors investigated here (i.e., regional sea level rise and intensified watershed flooding).

The changing probabilities associated with sea level rise will not be sudden, but will follow the time rate of SLR; predicting when the probability associated with a certain depth becomes intolerable may be useful in deciding when to initiate actions such as constructing sea walls. By updating the model as more data and better forecasts become available, the method can be used in adaptive management. This method is applicable to any location where the data (geometry and flow time series) and estimates of future conditions are available.

As indicated in Chapter 3, only a limited body of literature dealt with the upstream freshwater change due to climate change for the Potomac River. For future study, a watershed model that uses the downscaled projection of future precipitation as input is recommended to better characterize the upstream freshwater change during extreme events.

The HEC-RAS model for the Potomac River is a 1D hydraulic model. Two- and three-dimensional hydraulic model can be applied to the study reach to compare the inundation depth prediction of the study site under various scenarios. The additional information provided by the higher dimensional hydraulic model, such as the velocity vector that is not parallel to the river center line, can be used to quantify the momentum associated with building damage.

6.4 Flood Depth-Duration and Damage Quantification

Given the unique aspect of WWTPs, a bivariate flood risk model that incorporates both flood duration and depth was the motivation for this study. One more dimension, duration, is added to the traditional flood risk analysis to quantify flood likelihood. A bivariate flood stage-duration-

frequency relationship is fully characterized by a parametric model, applicable for tidal, estuary, and riverine sites.

The bivariate joint distribution model can also be applied to any continuous time series with measurements at an appropriate time interval, especially when the event duration is critical. For example, if the historical records are sufficient, it can be applied to the hourly time series of wastewater influent flow rate, to quantify how long the plant influent stays above certain magnitude (MGD) and the likelihood associated with it. This information may assist planning and process design for wet weather operation. The general concept is applicable to other parametric models and characterizations.

The accuracy of the bivariate probabilistic model is subject to the limit of sample data; sample size is always a major constraint for flood risk analyses. Future studies on investigating the tail distributions of the marginal, conditional, and joint distribution functions may yield useful information that could improve the bivariate flood risk model.

GIS integrated with hydrologic and hydraulic modeling software serves as a useful tool to communicate risk and assist emergency preparedness and response planning. In this research, by constructing a GIS database for the underground tunnels/gallery/basement and the essential equipment inside for the study site, the dollar damage of essential pumping equipment is estimated based on step and linear equipment inundation damage model. By integrating the joint probabilistic model of stage and duration, and the equipment damage model, a depth-duration-damage relationship is established and expected annual damage is quantified.

In highly urbanized areas, service interruptions of civil infrastructure are functions not only of stage, but also of the length of time that flood waters remain high. This study can be extended to quantify the probability associated with flood related out-of-service time for critical infrastructure, such as emergency access, traffic interruption, and supply chain disruption. When

the damage function is developed, the likelihood of flood damage and consequences can be quantified based on the method demonstrated in this study.

6.5 Flood Vulnerability Modeling

In general, flood vulnerability modeling of critical infrastructure can be grouped into two categories: (1) damage to the structure and equipment, (2) interdependency of the infrastructure in a system. The first category involves the database development of the essential equipment. The second category requires knowledge of system boundaries, functionality, and interdependency.

For the microscale analyses, the first category model is more critical since the infrastructure itself defines the risk modeling scale. In this research, customized programs with assistance of ArcGIS were developed for quantifying ground level and subsurface vulnerability at a treatment plant. The current and future scenarios developed in Chapter 3 were applied to the ground level module to quantify and visualize depth related risk, including building percent damage and safe evacuation risk. The bivariate joint distribution model developed in Chapter 4 was applied to estimate expected annual damage to essential equipment inside the underground tunnels.

Site-specific flood damage modeling is an inventory data-driven process. However, with the reality of data scarcity, assumptions are generally required. In this study, the Digital Elevation Model (DEM) was created from the topographic data points surveyed in 2009. The surface of the reactors were assumed to be at the top elevation of the reactor walls. Elevation values obtained from the construction documents were assumed to be referenced to the plant datum (known as the D.C. Engineering Datum), if a reference datum was not specified in the drawings or documents.

The quality of the model input strongly affects the accuracy of the model output and predictions. Cross-checking may be critical to ensure data accuracy. For example, NED DEM datasets such as 1/9 arcsecond and 1/3 arcsecond can be compared to the ground surface generated by the survey mass points or by LiDAR surveys of the site. The NED DEM cannot capture the finely-detailed, constructed ground surface of a municipal wastewater treatment plant, especially in the reactor/tank area. Sensitivity analyses of the flood mapping accuracy to DEM dataset resolution is recommended. For building percent damage estimate, a survey of the first floor and lowest floor elevation is needed for each building structure. The percent damage analysis of superstructure, interiors, plumbing, electrical system, and HVAC systems can only be performed when such information is available.

6.5.1 Capacity Loss Model

During a severe flood event, the municipal wastewater treatment plant may lose its treatment capacity, completely or partially. The overflow of untreated or partially treated wastewater is discharged to the river by bypass conduits. If combined sewers are dominant in the city, the wastewater treatment plant influent is highly correlated with extreme rainfall, overland flow, river discharge, and stage. In Table 2-14, the untreated and partially treated sewage discharges are included as measures of environmental damage associated with WWTPs during Hurricane Sandy. The capacity loss model is proposed to quantify the split among complete treatment (CT), partial treatment (PT), and untreated (UT) wastewater flow rate, as an indicator of the environmental damage of WWTP due to flooding.

The capacity loss model should be developed based on the treatment capacity of the WWTP. For example, the maximum influent flow rate permitted to the study site is 1076 MGD for the first 4 hours during wet weather and 847 MGD after the first 4 hours during normal conditions.

The complete treatment capacity of the study site is 740 MGD for the first 4 hours and 511 MGD after the first 4 hours. The excess flows go through primary treatment only, and are chlorinated and dechlorinated before being discharged to the river. The maximum flow through partial treatment is 336 MGD (Locke et al., 2006). During a major flood event, the treatment capacity may be further reduced due to surface and underground inundation. A preliminary example is presented in this section. The flow split can be demonstrated by a capacity loss diagram based on the wet-weather operational rule (Figure 6-1).

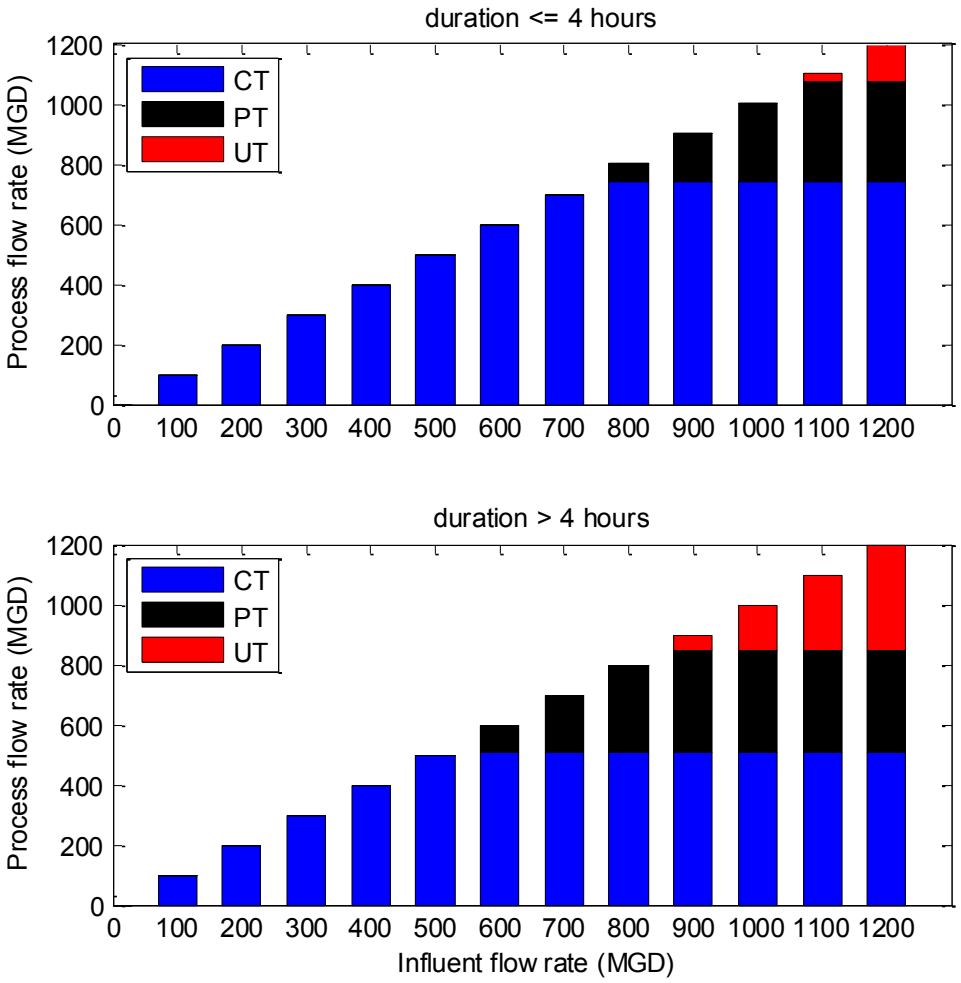

Figure 6-1. Treatment capacity loss diagram

For demonstration purposes, hourly time series of plant influent flow rate from the process control system (PCS) at BPAWWTP were analyzed. Annual peak plant influent flow rates were extracted from the hourly time series for eight water years (2006-2013). The sample frequency distribution of the annual peak influent flow rate is shown in Figure 6-2. The annual peak influent flow rate is modeled assuming a normal distribution (mean=815.5; standard deviation=53.9). The goodness of fit of the normal distribution is visualized in Figure 6-3. The P-P plot compares the empirical cumulative distribution function (CDF) with the modeled CDF, while the Q-Q plot compares the sample and modeled quantiles. For both plots, a 45 degree reference line indicates reasonable population model. The Kolmogorov–Smirnov (KS) test provides further confirmation with a p-value of 0.97.

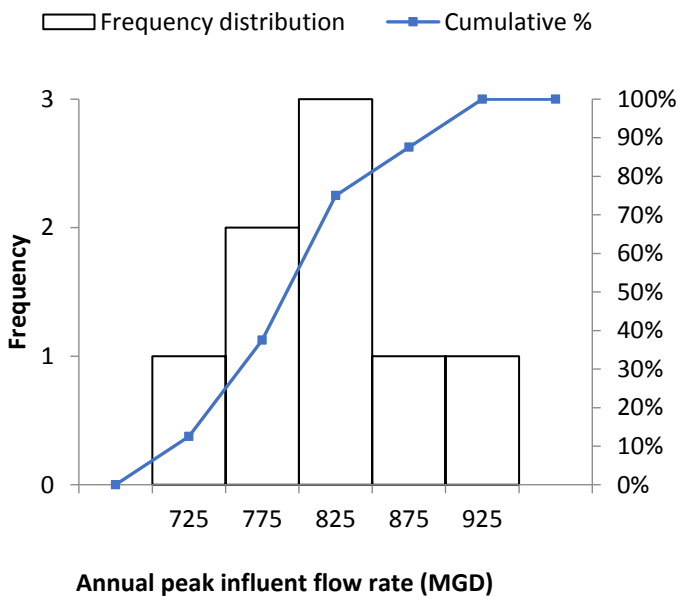

Figure 6-2. Sample frequency distribution of annual peak hourly influent flow rate of BPAWWTP

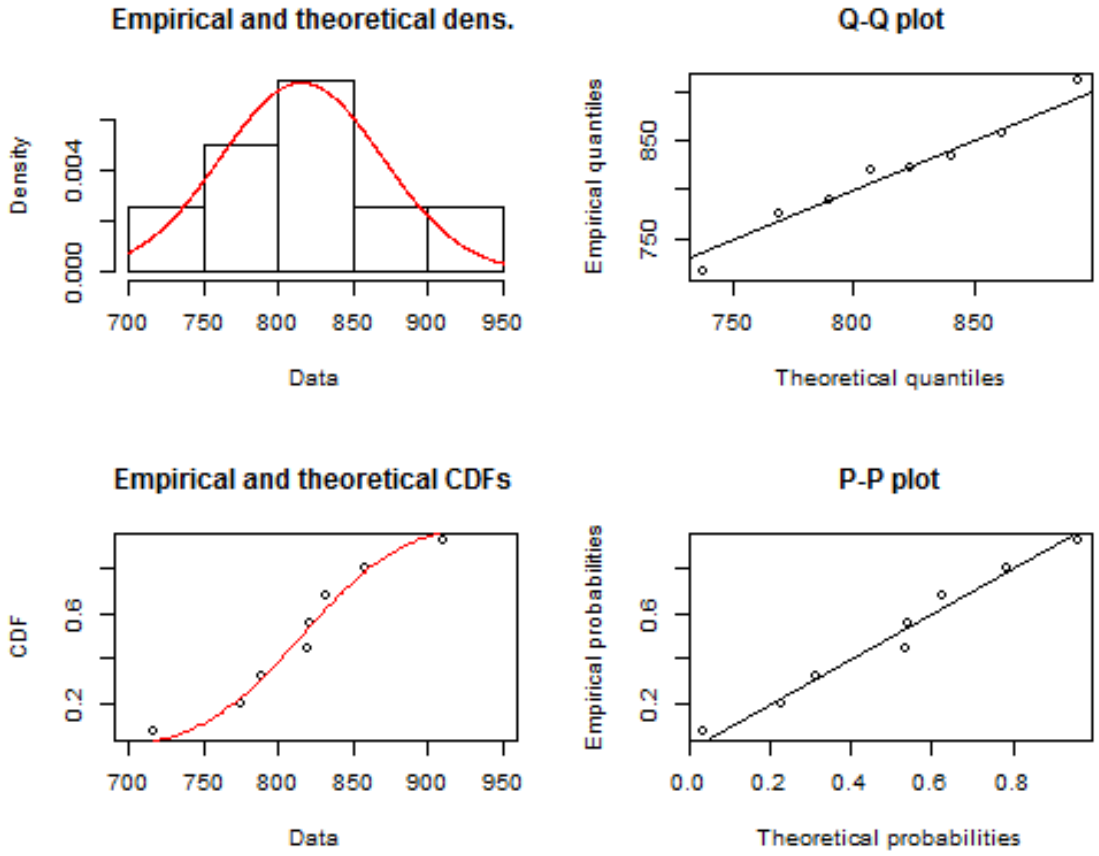

Figure 6-3. Annual peak influent flow rate fitted by normal distribution

When the exceedance probability, or return period associated with the influent flow rate is available, the modeler can estimate the likelihood of capacity loss, which reflects the risk associated with process flooding. For example, in Figure 6-4, the annual exceedance probability of 900 MGD wastewater influent is 0.06 (a 17-year event). The operator can refer to the bar that corresponds to 900 MGD in Figure 6-1, for the split of the effluent flow. The blue indicates good treatment quality; the black represents partial treatment, and the red shows that untreated wastewater will be discharged to the receiving water body. During the first four hours, no risk of untreated wastewater is identified for the 17-year peak wastewater influent. After the first four hours, the amounts of untreated and partially treated wastewater increase. The risk of

discharging partially treated and untreated wastewater into the Potomac River increases even though the influent rate remains constant. Combining the probability density function and the risk consequences illustrated by flow split, the expected annual environmental damage, presented by expected annual untreated wastewater (EAUT) and expected annual partially treated wastewater (EAPT), can be estimated.

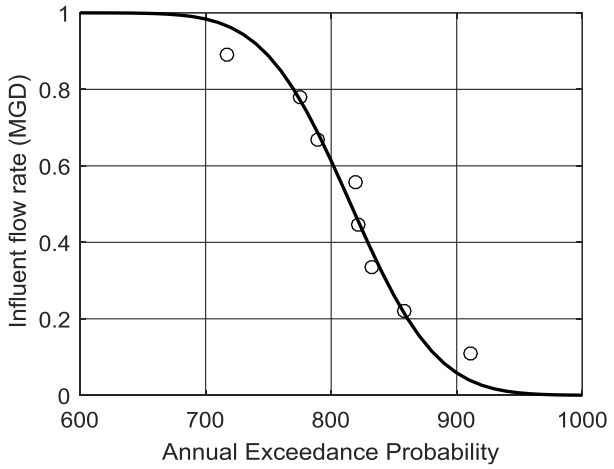

Figure 6-4. Annual exceedance probability of influent flow rate

In this preliminary example, only the wet-weather operational rules are considered. The potential partial or complete process disruption due to plant inundation (ground level or subsurface) are not considered in this example. A future study could explore the joint probability distribution of the wastewater influent, extreme precipitation and river discharge/stage, which are likely to coincide in time.

The probability distribution of wastewater flow rate based on the current operational rule and historical data does not reflect the potential risk due to changing climate. If a climate-change based wastewater influent assessment is available, this analysis can be further extended to quantify projected EAUT and EAPT for the future planning horizon.

To assign monetary value to the WWTP capacity loss or service interruption, the following equation is recommend based on willingness to pay (*WTP*) to the service, inspired by equation (2-27).

$$Estimated\ \cos t\ of\ disruption\ (\$)\ =\ N \times U \times WTP \times D \tag{6-1}$$

where N is the number of household affected by the WWTP service, U is the daily household water usage, since the daily household water usage is assumed to be close to the daily household wastewater discharge; WTP is the willingness to pay value per day to avoid the service outage, D is the estimated length of disruption. This is an 'inferential' method and a survey is needed to define the value of WTP. This indicates the potential of further quantifying the environmental damage and provide information for project appraisal.

6.5.2 Evacuation Risk

In this study, the underground evacuation risk has not been quantified. The literature suggests the potential of developing a subsurface evacuation model. People can be evacuated from the underground tunnels if (1) the basement door can open, and (2) the underground tunnels are walkable. Based on a real-size experiment, an average person can open a door blocked by water of up to 1.3 ft depth. The limiting water depth at the ground level of the staircases is 1 to 1.3 ft for safe evacuation (Ishigaki, Onishi, Asai, Toda, & Shimada, 2008). The momentum per unit width [Eq.(6-2)] is a safe evacuation criterion for stairs. Specific force per unit width [Eq.(6-3)] is a proposed criterion for save evacuation based on the real size model tests of 47 females and 257 males (Ishigaki et al., 2008):

$$u^2 h = 1.2 \tag{6-2}$$

$$u^2 h / g + h^2 / 2 = 0.125 \tag{6-3}$$

where u is the flow velocity, h is the water depth, g is the gravity acceleration. Oertal and Schlenkhoff (2008) states that the fall number SN (m^2/s) between 1.26 and 1.64 is safe for humans:

$$SN = vh \tag{6-4}$$

The risk of drowning increases if the water level rises above a critical water depth of 4.9 ft (Oertel & Schlenkhoff, 2008). Analyzing and mapping these conditions requires a higher dimensional hydraulic model to quantify flow velocity and momentum. The GIS-Assisted Risk Register (GARR) can also be applied to the underground tunnel risk severity scoring and underground safe evacuation risk mapping.

6.5.3 Need for Consistent Site Information Database

From a practical perspective, it became apparent in the course of this study that, even at a state-of-the-art advanced treatment plant, data related to elevation are not systematically recorded. Inverts of the piping system, and floor levels of the basement, tunnel and galleries were difficult to obtain. When the elevations were available, they were recorded relative to inconsistent vertical datums.

For an aging critical infrastructure, up-to-date data are critical for risk assessment. Effectively preserving and communicating the information are major challenges for both operational staff and the risk analyst. In order to better manage the assets and their location information, it is recommended that data can be organized systematically, e.g., Geodatabase, BIM system, with attributes of elevation referenced to a standard datum, e.g., NAVD 88. Also, the naming scheme of the equipment can be updated to avoid duplicates and to reflect the most recent state of the processes. Joint efforts of the risk analyst and site management personnel are needed.

Appendix A. Processes of the Study WWTP

The objective of this section is to develop a GIS database for the underground tunnel/gallery/basement and the essential equipment inside these underground spaces. It should be noted that the tunnel geometry, essential equipment and their critical elevations are based on the best available as-built drawings and the best information observed during the inspection. They are developed for demonstration purposes. They are not survey grade data. It is believed that the equipment above ground are mostly designed to sustain the wet condition. Only the essential equipment underground are presented in this section.

A.1 Primary Sedimentation

The liquid treatment process is generally divided into two process trains. The west process train treats 40% of the wastewater and the east process train treats 60% of the wastewater. After the preliminary treatment (screen and grit removal), the suspended solids settle in the 36 circular Primary Sedimentation Tanks (PSTs) and scum is partially removed. Polymer and ferric chloride are fed to the process as coagulant to improve the removal of suspended solids and organic matters (DCWASA, n.d.-d).

The essential equipment underground are the return sludge pumps and their appurtenances (Figure A-1) in the control houses. The primary sludge is pumped to the Gravity Thickener Control Building and Primary Sludge Screening and Degritting Building (DCWASA, n.d.-d). Table A-1 lists the underground essential equipment for the primary sedimentation process.

Figure A-1. Primary Sludge Pump – essential equipment in Primary Sedimentation

Table A-1. Essential equipment underground and their critical elevations – Primary Sedimentation

Equipment type	Equipment name	Location	No.	Critical depth from floor (ft)	Critical elev. (ft)
Primary Sludge Pump	PSP-1 to PSP -16	Primary Control House Basement_West	16	6	-3
Primary Sludge Pump Control Panel_West and Variable Frequency Drive (VFD)	Primary Sludge Pump Control Panel and VFD	Primary Control House operation floor	16	5	5
Primary Sludge Pump	PSP-17 to PSP -36	Primary Control House Basement_East	20	6	-1
Primary Sludge Pump Control Panel_East and VFD	Primary Sludge Pump Control Panel and VFD	Primary Control House operation floor	20	5	7

A.1.1 West Primary Sedimentation

Four control houses (CH A, CH B, CH C, CH D) are located in the West Primary Sedimentation Process. Each control house serves four primary sedimentation tanks (Figure A-2). The essential equipment in the control houses are the primary sludge pumps (PSP) and their appurtenances, including Primary Sludge Pump Variable Frequency Drive (PSP VFD), Primary Sludge Pump Control Panel, Primary Sludge Motor Operated Valves (MOV), Sludge Pump Magnetic Flow Transmitter,

etc. The locations of the pumps are show in the Figure A-2, Figure A-3 and Figure A-4 by the green dots.

The floor elevation of the control houses is around -9.25 ft. The critical elevation of the PSP is 6 ft from the floor of the control house basement. In Figure A-3 and Figure A-4, they are presented by the dots in their critical elevations. If they are inundated, the primary sludge pumping system will no longer remove the settled solids from the bottom of the primary sedimentation tanks and discharge to the Primary Sludge Screening / Degritting Building (PSSDB) for further treatment.

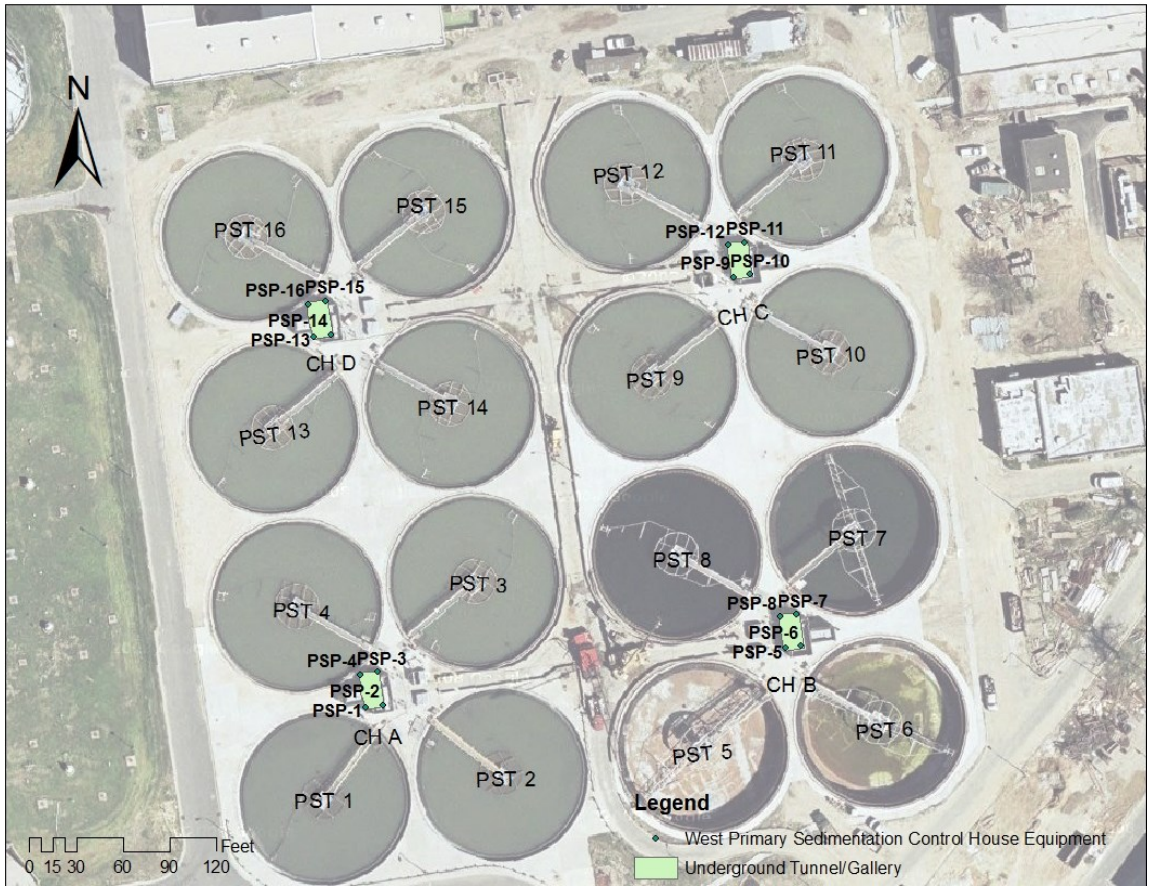

Figure A-2. West Primary Sedimentation View 1 (ArcMap plan view)

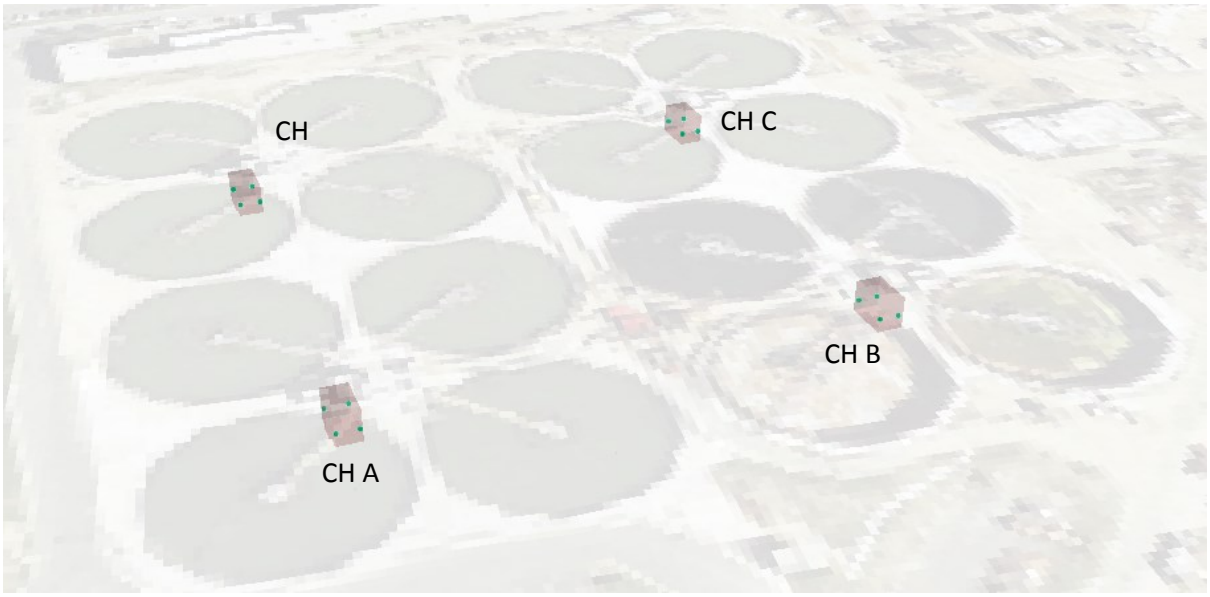

Figure A-3. West Primary Sedimentation View 2 (ArcScene)

Figure A-4. West Primary Sedimentation View 3 (ArcScene side view)

A.1.2 East Primary Sedimentation

There are five control houses (CH E, CH F, CH G, CH H) for the East Primary Sedimentation Process. Each control house serves four primary sedimentation tanks (Figure A-5). Similar to the west side process, the essential equipment in the control houses are the primary sludge pumps (PSP) and their appurtenances, including Primary Sludge Pump Variable Frequency Drive (PSP VFD), Primary Sludge Pump Control Panel, Primary Sludge Motor Operated Valves (MOV), Sludge Pump Magnetic Flow Transmitter, etc. The locations of the pumps are show in the Figure A-5, Figure A-6, and Figure A-7 by the green dots, placed at their critical elevations.

Figure A-5. East Primary Sedimentation View 1 (ArcMap plan view)

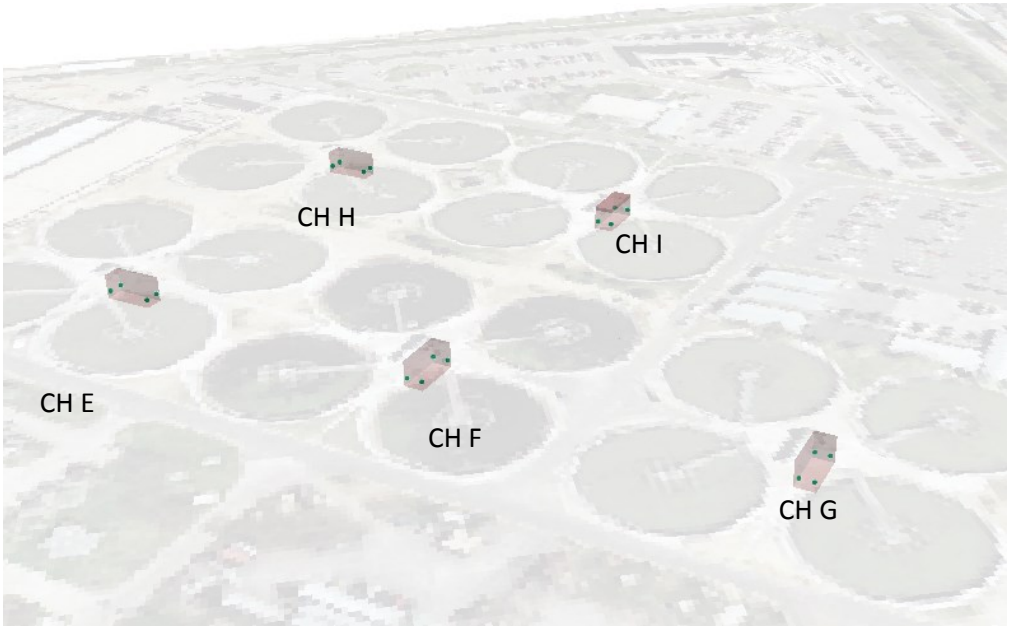

Figure A-6. East Primary Sedimentation View 2 (ArcScene)

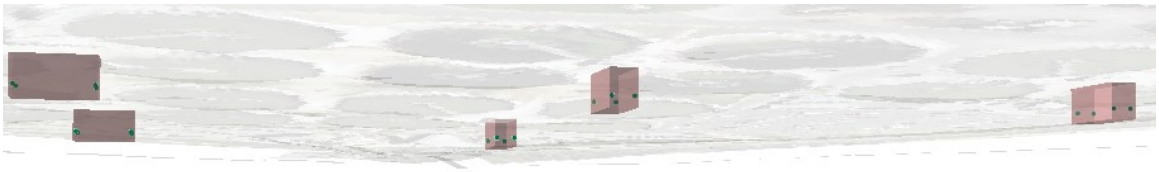

Figure A-7. East Primary Sedimentation View 3 (ArcScene side view)

A.2 Secondary Treatment

The secondary treatment facility is designed to reduce TSS and BOD in the primary effluent. It is part of the two stage biological nutrient removal system to provide the flow to the downstream biological nitrification system. There are two process trains for the secondary treatment, west secondary (40% of flow) and east secondary (60% of flow). Process air is supplied by 6 centrifugal blower located in the Secondary Blower Building. Metal salts, including ferric chloride, and waste pickle liquor are added to enhance phosphorus removal. Polymer is added as coagulant to the influent to improve settlement in the sedimentation basins.

The essential equipment in the secondary sedimentation galleries, secondary reactor gallery and return sludge tunnels are scum pumps, returns sludge pumps, waste sludge pumps, dewatering pumps, sump pumps and their appurtenances. The sump pumps are used to dewater the tunnel/gallery. The scum is pumped by the scum pumps to waste sludge lines, and to the Dissolved Air Flotation (DAF) thickeners in the Solids Processing Building. The active return sludge is pumped back to the reactors by the return sludge pumps. The waste sludge is pumped by the waste sludge pumps to the DAF thickeners in the Solids Processing Building. The secondary reactors and sedimentation basins can be dewatered by the dewatering pumps (DCWASA, n.d.-e).

(a) Return Sludge Pump

(b) Scum Pump

(c) West Waste Sludge Pump

(d) East Waste Sludge Pumps

(e) Dewatering Pump A1

(f) Dewatering Pump A7

Figure A-8. Essential equipment underground – Secondary Treatment (DCWASA, n.d.-e)

Table A-2. Essential equipment underground and their critical elevations – Secondary Treatment

Equipment type	Equipment name	Location	No.	Critical depth from floor (ft)	Critical elev. (ft)
Return Sludge Pump	RSP-1 to RSP-12, RSP-3S,7S,11S,2S,6S,10S	West Secondary Sedimentation Gallery	18	4	-6
Return Sludge Pump Control Panel	Return Sludge Pump Control Panel	West Secondary Sedimentation Gallery	18	5	-5
Scum Pump (control panel above ground)	SCP-1A,B to SCP-6A,B	West Secondary Sedimentation Gallery	12	4	-6
Waste Sludge Pump	WSP- 1,2,3	West Secondary Sedimentation Gallery	3	4	-11
Waste Sludge Pump Control Panel	Waste Sludge Pump Control Panel	West Secondary Sedimentation Gallery	3	5	-10
Sump Pump	SP-A24, A27,	West Secondary Sedimentation Gallery		2	-10
Return Sludge Pump	RSP-13 to RSP-24, RSP-13S,14S,17S,18S,21S,22S	East Secondary Sedimentation Gallery	18	5	-6
Return Sludge Pump Control Panel	Return Sludge Pump Control Panel	East Secondary Sedimentation Gallery	18	5	-6
Scum Pump	SCP-7A,B to SCP-9A,B	East Secondary Sedimentation Gallery	6	4	-7
Dewatering Pump	DWP-A3,A4,A5,A6	East Secondary Sedimentation Gallery	4	3	-8
Dewatering Pump Control Panel	Dewatering Pump Control Panel	East Secondary Sedimentation Gallery	4	5	-6
Waste Sludge Pump	WSP-4,5,6	East Secondary Sedimentation Gallery	3	4	-7
Sump Pump	SP-A9, A10A, A10B,A11A,A11B,A12A, A12B, A13	East Secondary Sedimentation Gallery	8	2	-9
Dewatering Pump	DWP-A7,A8	Return Sludge Tunnel_West Secondary Sedimentation Gallery	2	4	-1.5
Dewatering Pump Control Panel	Dewatering Pump Control Panel	Return Sludge Tunnel_West Secondary Sedimentation Gallery	2	5	-0.5
Dewatering Pump	DWP-A1,A2	Secondary Reactor Gallery	2	4	-7
Dewatering Pump Control Panel	Dewatering Pump Control Panel	Secondary Reactor Gallery	2	5	-6
Sump Pump	SP-A8	Secondary Reactor Gallery	1	2	-9
Sump Pump	SP-A5, A6	Air Main Gallery and Storage Area	2	2	-9
Sump Pump	SP-A3, A4	Air Main Tunnel West to East	2	2	-3.5
Sump Pump	SP-A23	Air Main Tunnel west	1	2	-3.5
Sump Pump	SP-A1, A2, A21, A22	Secondary Blower Building	4	2	2
Sump Pump	A17A, A17B	Secondary Tunnel	2	2	-13

A.2.1 West Secondary

The essential equipment in the West Secondary Sedimentation Gallery are 18 Return Sludge pumps (RSP-1 to RSP-12, RSP-3S,7S,11S,2S,6S,10S), 3 Waste Sludge Pumps (WSP-1, 2, 3), 12 Scum Pumps(SCP-1A,B to SCP-6A,B) and their appurtenances. The 2 Dewatering Pumps (DWP-A7, A8) are located in the Return Sludge Tunnel (Figure A-9). The critical elevations of these pumps are about 4 ft from the floor of the gallery. They are presented at their critical elevation by the dots in Figure A-10 and Figure A-11.

Figure A-9. West Secondary Sedimentation View 1 (ArcMap plan view)

Figure A-10. West Secondary Sedimentation View 2 (ArcScene)

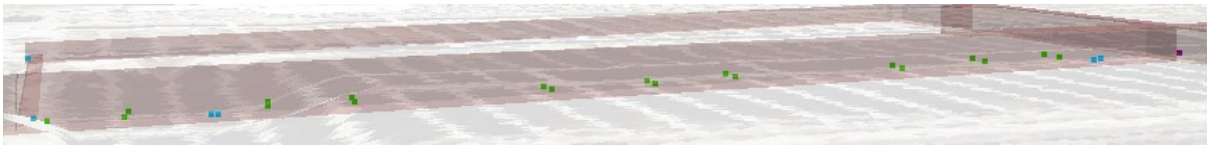

Figure A-11. West Secondary Sedimentation View 3 (ArcScene side view)

A.2.2 East Secondary

The essential equipment in the East Secondary Sedimentation Gallery are 18 Return Sludge pumps (RSP-13 to RSP-24, RSP-13S,14S,17S,18S,21S,22S), 3 Waste Sludge Pumps (WSP-4, 5, 6), 6 Scum Pumps(SCP-7A,B to SCP-9A,B) and their appurtenances. The 4 Dewatering Pumps (DWP-A3, A4, A5, A6) are located in the Return Sludge Tunnel (Figure A-12). The critical elevations of these pumps are about 4 ft from the floor of the gallery. They are presented at their critical elevations by the dots in (Figure A-13 and Figure A-14).

Figure A-12. East Secondary Sedimentation View 1 (ArcMap plan view)

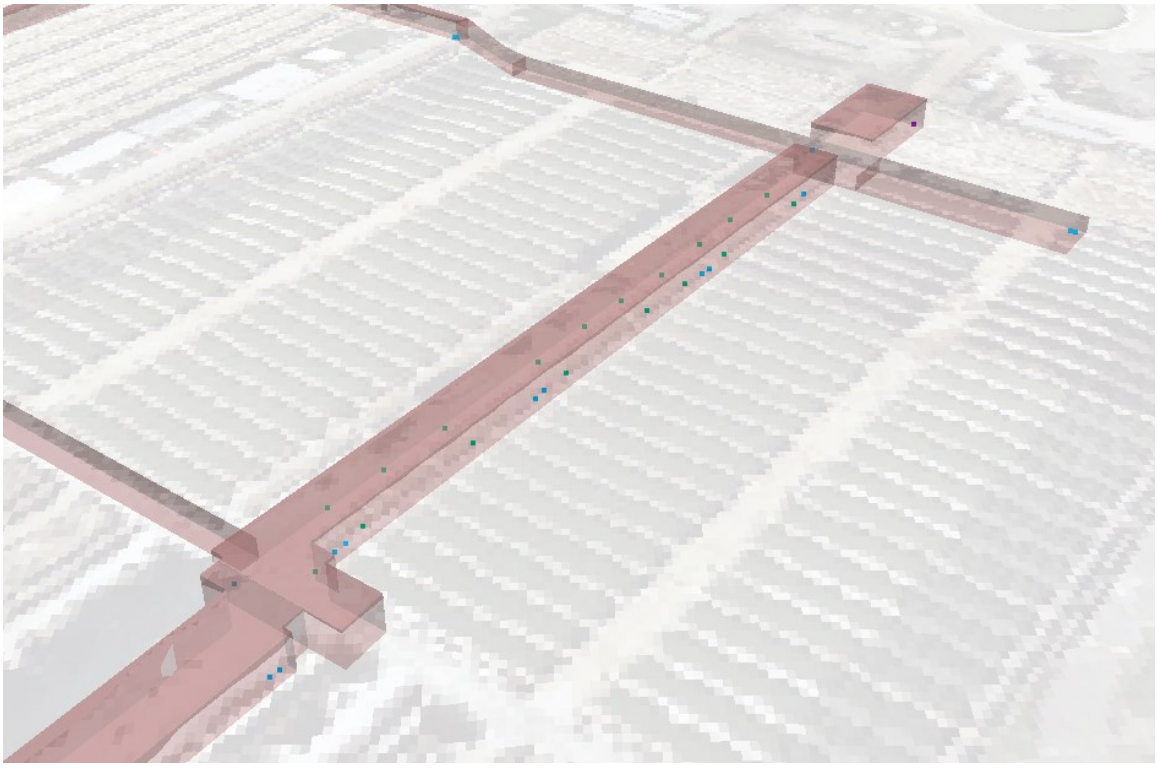

Figure A-13. East Secondary Sedimentation View 2 (ArcScene)

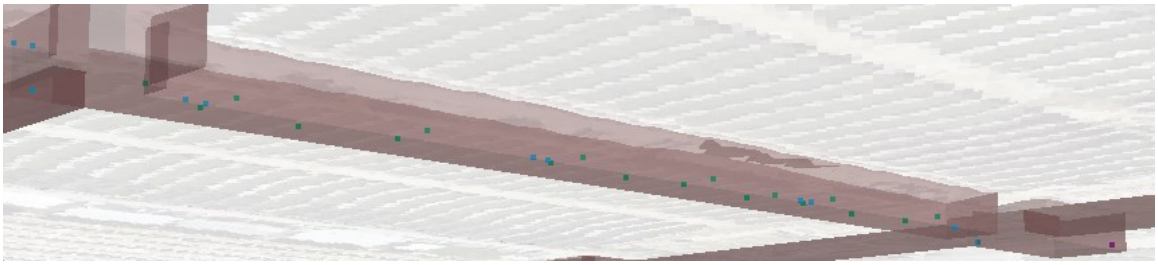

Figure A-14. East Secondary Sedimentation View 3 (ArcScene side view)

A.3 Nitrification and Denitrification

Nitrification and denitrification is a biological processes to remove ammonia and nitrogen. The nitrification and denitrification process in Blue Plains are divided into odd and even side process trains. There are 12 nitrification and denitrification reactors and 28 nitrification sedimentation basins. Five three-stage horizontally split centrifugal blowers in the Nitrification Blower Building supply process air to the diffusers in the nitrification reactors. Polymer is added to the influent as

coagulant to improve settling. Sodium hydroxide solution is fed to the system to add alkalinity and control pH. Methanol is added to the reactors as an external carbon source for the denitrification process.

The essential equipment in the nitrification reactor gallery, nitrification sedimentation gallery, waste sludge gallery, dual purpose sedimentation galleries, and waste sludge gallery are foam pumps, returns sludge pumps, waste active sludge pumps, scum pumps, dewatering pumps, sump pumps and their appurtenances (Figure A-15). The foam pump removes surface foam from the nitrification reactor mix liquor channels. Waste sludge is pumped by the waste sludge pumps to flotation thickeners in the solids processing building or to the secondary reactors. Active sludge is returned to the nitrification reactor by the return sludge pump. The details of the equipment, their locations and critical depths are listed in Table A-3.

(a) Foam Pump

(b) Dewatering Pump


(c) Return Sludge Pump (d) Waste Active Sludge Pump (e) Scum Pump

Figure A-15. Essential equipment underground – Nitrification and Denitrification (DCWASA, n.d.-c)

Table A-3. Essential equipment underground and their critical elevations – Nitrification and Denitrification

Equipment type	Equipment name	Location	No.	Critical depth from floor (ft)	Critical elev. (ft)
Return Sludge Pump	RSP25-52 and Stand-bys	Nitrification Sedimentation Gallery	42	4	-16
Scum Pump	SCP 10A,B-16A,B	Nitrification Sedimentation Gallery	14	2	-18
Waste Activated Sludge Pump	WSP 7,8,9,10	Nitrification Sedimentation Gallery	4	4	-16
Sump Pump	SPB6, SPC 3,4,5,6,7,8,10	Nitrification Sedimentation Gallery	8	2	-18
Sump Pump	DRSGP-31,32,36,37,38A,38B,39	Denitrification Return Sludge Gallery		2	-18
Dewatering Pump	DWP-B1 to B4	Nitrification Reactor Gallery_NS	4	4	-16
Sump Pump	SP-B1, B2, 7B, 2 SPs	Nitrification Reactor Gallery_NS	5	2	-18
Sump Pump	SP-10B, 11B, 12B	Nitrification Reactor Gallery_EW	3	2	-18
Sump Pump	SP-8B, 9B	Waste Sludge Gallery	2	2	-18
Foam Pump	FMP-1E,2E,FMP-1W,2W	Waste Sludge Gallery	4	3	-17
Return Sludge Pump	RSP 1A,B-8A,B	Dual Purpose Sedimentation Gallery 3	16	4	-16
Scum Pump	SCUM.P 1A,B - 2A, B	Dual Purpose Sedimentation Gallery 3	4	4	-16
Sump Pump	P1,P2	Dual Purpose Sedimentation Gallery 1	2	2	-16
Sump Pump	P6, P7, P8	Dual Purpose Sedimentation Gallery 2	3	2	-16
Sump Pump	P9, P10, P11, P12, P14	Dual Purpose Sedimentation Gallery 3	5	2	-16

A.3.1 Nitrification Reactor

There are 12 plug flow five-stage nitrification and denitrification reactors in Blue Plains. The odd and even side of the reactors are separated by the Nitrification Reactor Gallery. The Nitrification Reactor Gallery houses the four dewatering pumps, DWP-B1 to B4. They are used to dewater the reactors. Adjacent to reactor 11 and 12, the waste sludge tunnel houses the foam pumps (Figure A-16, Figure A-17 and Figure A-18).

Figure A-16. Nitrification Reactor Gallery View 1 (ArcMap plan view)

Figure A-17. Nitrification Reactor Gallery View 2 (ArcScene)

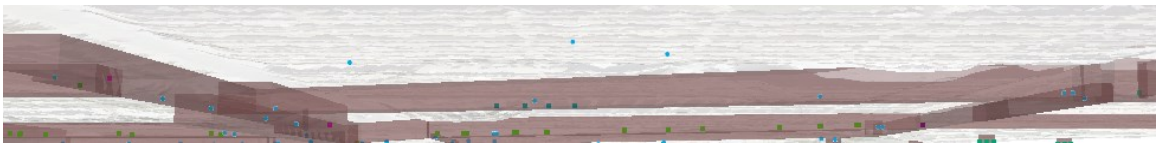

Figure A-18. Nitrification Reactor Gallery View 3 (ArcScene side view)

A.3.2 Nitrification Sedimentation

Nitrification Sedimentation Gallery houses the 42 return sludge pumps, 14 scum pumps, 4 waste active sludge pumps and sump pumps (Figure A-19, Figure A-20 and Figure A-21).

Figure A-19. Nitrification Sedimentation Gallery View 1 (ArcMap plan view)

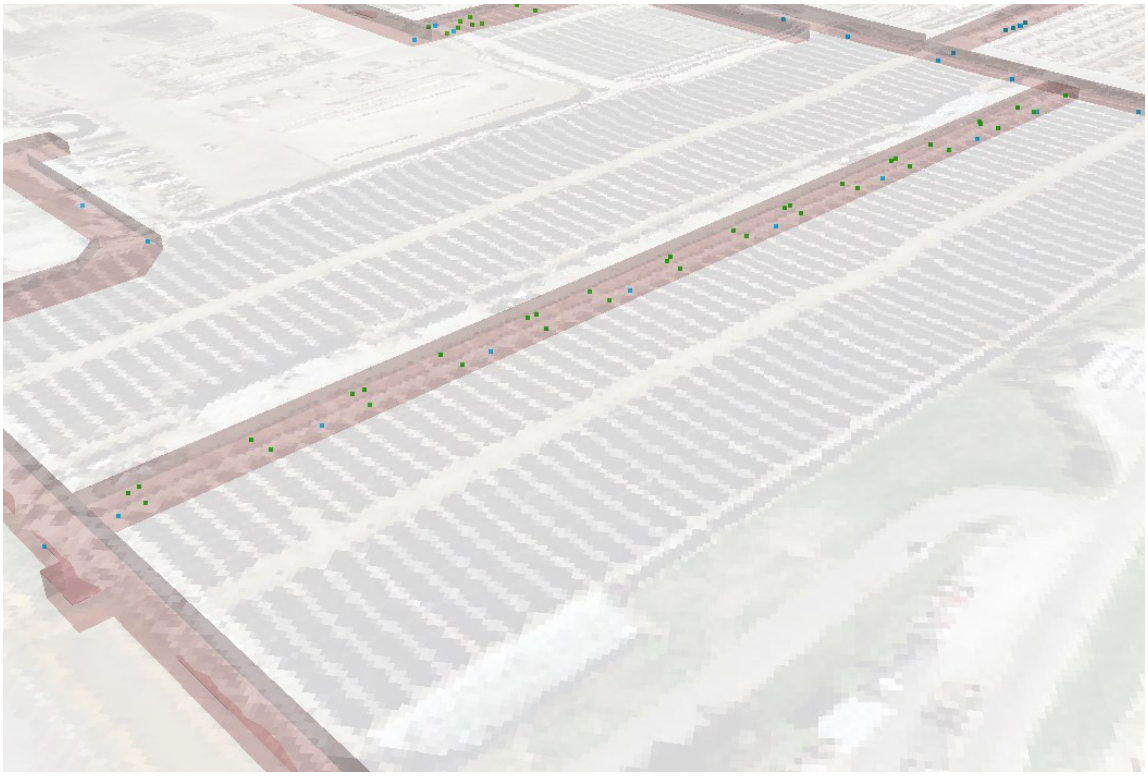

Figure A-20. Nitrification Sedimentation Gallery View 2 (ArcScene)

Figure A-21. Nitrification Sedimentation Gallery View 3 (ArcScene side view)

A.3.3 Dual Purpose Sedimentation

Most essential equipment in the dual purpose sedimentation process are in the Dual Purpose Sedimentation Gallery 3. There are 16 return sludge pumps and 4 scum pumps (Figure A-22, Figure A-23 and Figure A-24).

Figure A-22. Dual Purpose Sedimentation Gallery View 1 (ArcMap plan view)

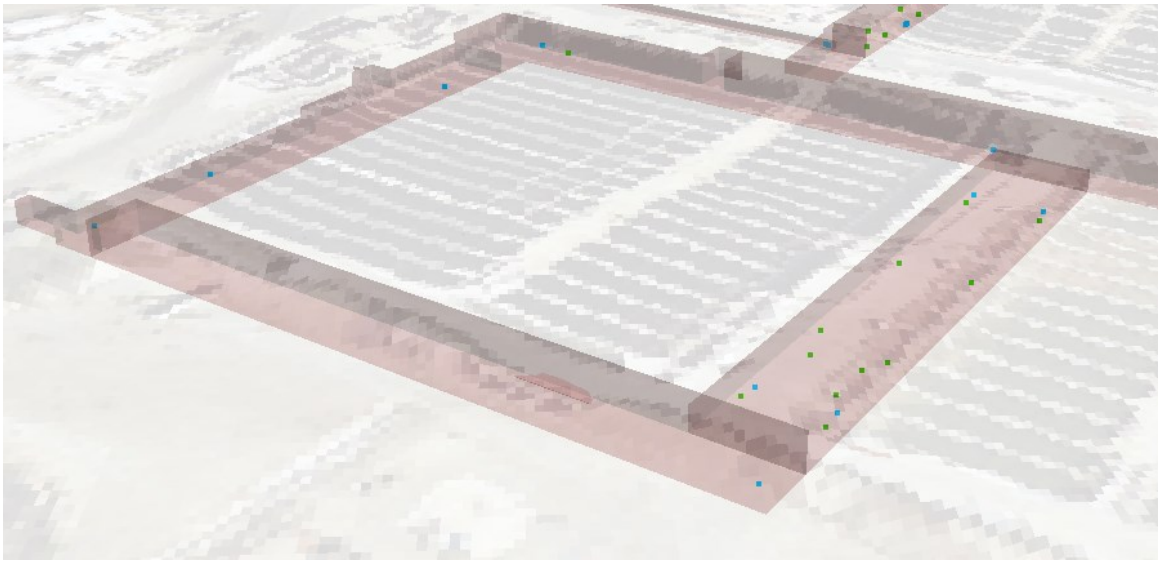

Figure A-23. Dual Purpose Sedimentation Gallery View 2 (ArcScene)

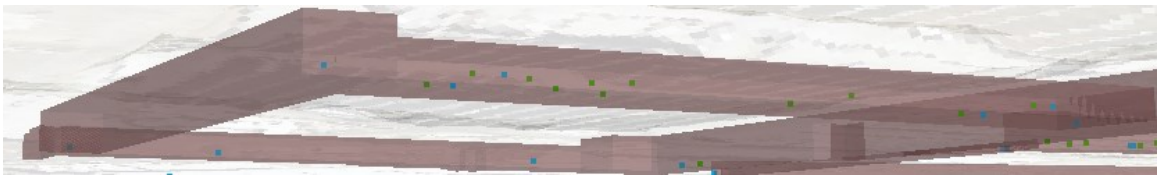

Figure A-24. Dual Purpose Sedimentation Gallery View 3 (ArcScene side view)

A.4 Multimedia Filtration

Multimedia filtration facility, including filter influent pumping, disinfection filtration, dechlorination, is the most downstream treatment process before the treated wastewater is discharged to the Potomac.

The essential equipment located in the filter pump room and filter gallery are 4 dewatering pumps, 4 chlorination injector water pumps, 3 variable speed high pressure reclaimed final effluent pumps (HPRFEP), 3 low pressure reclaimed final effluent pumps (LPRFEP), 5 vertical mixed-flow spent washwater pumps, 5 make-up water pumps (previous surface water Pump), 8 washwater pumps, and sump pumps (Figure A-25). The details of the equipment are listed in Table A-4. The essential underground equipment are presented at their critical elevations by the dots in Figure A-26, Figure A-27 and Figure A-28.

The chlorination injector water pumps are used to deliver sodium hypochlorite disinfection and minimize biological growth in the filter media. The spent washwater pumps pump the spent washwater, which is the water released from filter media during backwash, to the upstream treatment process. The make-up water pumps and air relief valves are used to prevent air accumulation in the washwater piping. The filtered water is pumped to the filter underdrains for backwashing by washwater pumps. High pressure reclaimed final effluent pumps transport the filtered effluent to the plant in a loop system to provide process service water. The low

pressure reclaimed final effluent pumps deliver the reclaim final effluent to the Solids Processing Building. The dewatering pumps are used to dewater the disinfection tanks (DCWASA, n.d.-b).

(a) Chlorination Injector Water Pump

(b) Washwater Pump

(c) Make-up Water Pump

(d) HPRFEP

(e) LPRFEP

(f) Spent Washwater Pump

(g) Dewatering Pumps

Figure A-25. Essential equipment underground – Multimedia Filtration (DCWASA, n.d.-b)

Table A-4. Essential equipment underground and their critical elevations – Multimedia Filtration

Equipment type	Equipment name	Location	No.	Critical depth from floor (ft)	Critical elev. (ft)
Dewatering Pump	DWP-F1,F2,F3,F4	Multimedia Filter Pump Room	4	4	12.5
Dewatering Pump Control Panel	Dewatering Pump Control Panel	Multimedia Filter Pump Room	4	5	13.5
Chlorination Injector Water Pump	CIWP-1 to CIWP-4	Multimedia Filter Pump Room	4	4.5	13
Chlorination Injector Water Pump Control Station	Chlorination Injector Water Pump Control Station	Multimedia Filter Pump Room	4	5	13.5
High Pressure Reclaimed Final Effluent Pump	HPRFEP -1 to HPRFEP-3	Multimedia Filter Pump Room	3	5	13.5
High Pressure Reclaimed Final Effluent Pump Control Station	High Pressure Reclaimed Final Effluent Pump Control Station	Multimedia Filter Pump Room	3	5	13.5
Low Pressure Reclaimed Final Effluent Pump	Low Pressure Reclaimed Final Effluent Pump	Multimedia Filter Pump Room	3	8	16.5
Low Pressure Reclaimed Final Effluent Pump Control Station	Low Pressure Reclaimed Final Effluent Pump Control Station	Multimedia Filter Pump Room	3	5	13.5
Spent Washwater Pump	SPWP-1 to SPWP 5	Multimedia Filter Pump Room	5	8	16.5
Spent Washwater Pump Control Panel	Spent Washwater Pump Control Panel	Multimedia Filter Pump Room	5	5	13.5
Make-up Water Pump (Previous Surface Water Pump)	SWP1, 2, 3, 4, 7	Multimedia Filter Gallery	5	4	12.5
Washwater Pump	WWP-1 to WWP-8	Multimedia Filter Gallery	8	4	12.5
Sump Pump	F1-4,	Multimedia Filter Pump Room	4	2	10.5
Sump Pump	S5-15	Multimedia Filter Gallery	11	2	10.5

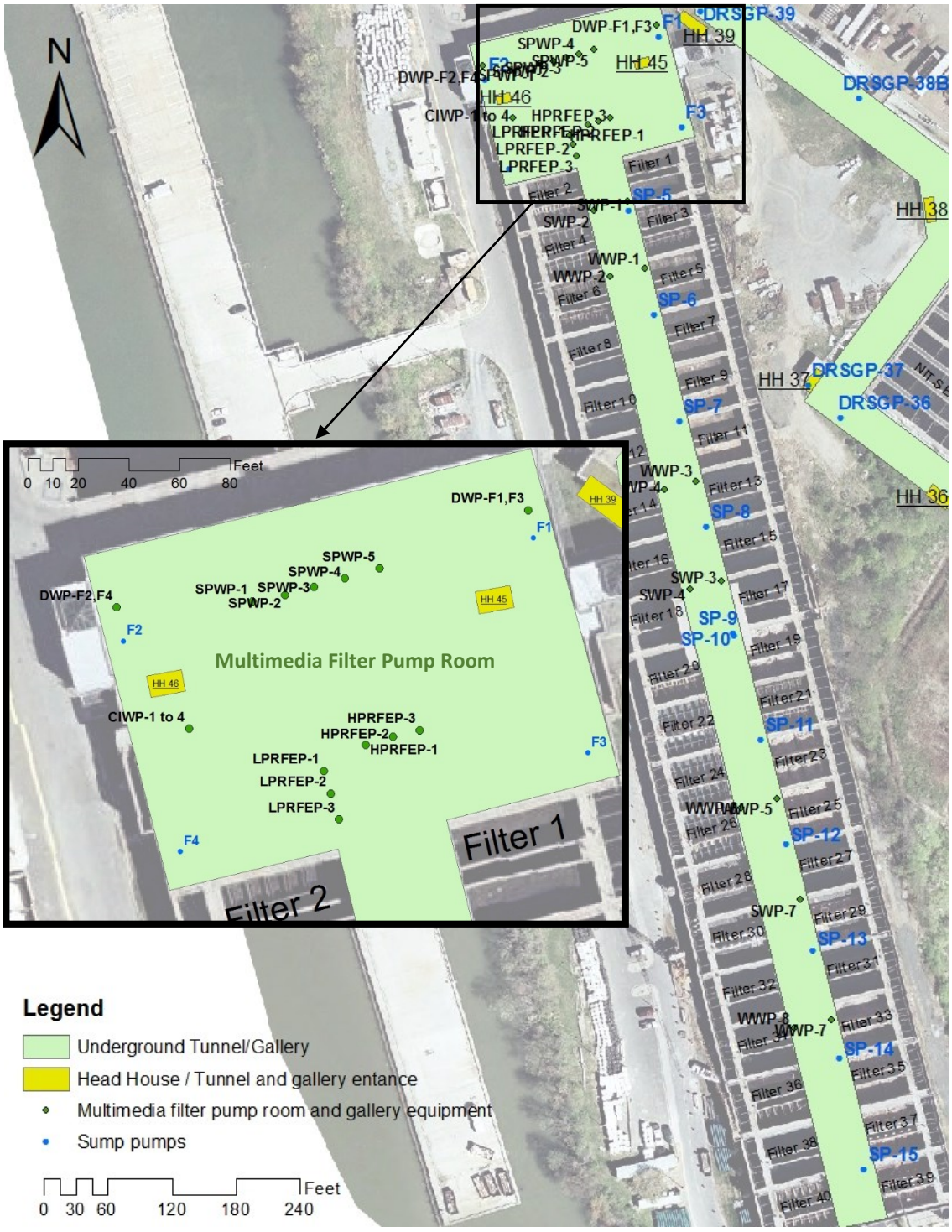

Figure A-26. Multimedia Filter Pump Room and Gallery View 1 (ArcMap plan view)

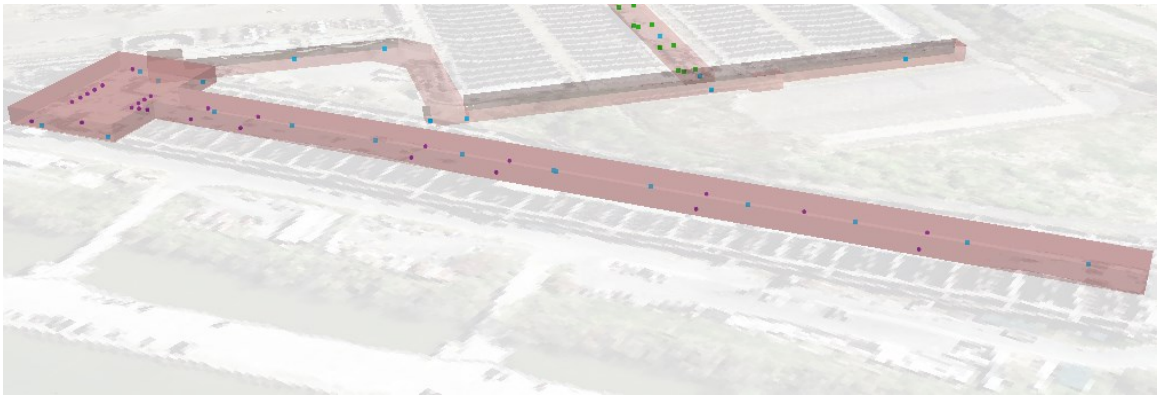

Figure A-27. Multimedia Filter Pump Room and Gallery View 2 (ArcScene)

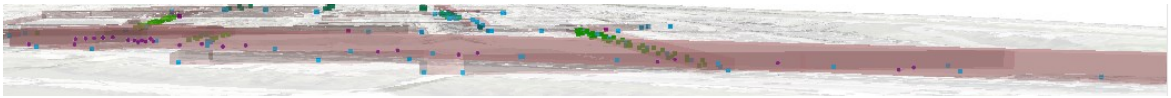

Figure A-28. Multimedia Filter Pump Room and Gallery View 3 (ArcScene side view)

REFERENCES

Allsop, W., Kortenhaus, A., Morris, M., Buijs, F., Hassan, R., Young, M., . . . ter Horst, W. (2007). *Failure Mechanisms for Flood Defence Structures*. FLOODsite Report. T04_06_01. Retrieved from http://hikm.ihe.nl/floodsite/data/Task4/pdf/failmechs.pdf

AMS. (2015). *American Meteorological Society Glossary of Meteorology-Flash Flood*. Retrieved from http://glossary.ametsoc.org/wiki/Flash_flood

Armstrong, W. H., Collins, M. J., & Snyder, N. P. (2014). Hydroclimatic Flood Trends in the Northeastern United States and Linkages with Large-Scale Atmospheric Circulation Patterns. *Hydrological Sciences Journal*, 59(9), 1636-1655.

Arnell, N. W. (1986). Average Annual Damage by Flood Frequency Zone. *Journal of Water Resources Planning and Management*, 112(1), 104-113.

Arnell, N. W., & Gosling, S. N. (2014). The Impacts of Climate Change on River Flood Risk at the Global Scale. *Climatic Change*, 134(3), 387–401.

Arora, K., & Singh, V. P. (1989). A Comparative Evaluation of the Estimators of the Log Pearson Type (LP) 3 Distribution. *Journal of Hydrology*, 105(1), 19-37.

Arrow, K., & Solow, R. (1993). *Report of the NOAA Panel on Contingent Valuation*. Washington, D.C.: National Oceanic and Atmospheric Administration. Retrieved from http://www.economia.unimib.it/DATA/moduli/7_6067/materiale/noaa%20report.pdf

Ashkar, F. (2008). Some Results and Recommendations on Bivariate Frequency Modeling in Hydrology. In *Proceedings of the World Environmental and Water Resources Congress*, Honolulu, HI.

Ayyub, B. M., & McCuen, R. H. (2011). *Probability, Statistics, and Reliability for Engineers and Scientists*. Boca Raton, FL: CRC press.

Ayyub, B. M., McGill, W. L., & Kaminskiy, M. (2007). Critical Asset and Portfolio Risk Analysis: An All-Hazards Framework. *Risk Analysis*, 27(4), 789-801.

Baba, Y., Ishigaki, T., Toda, K., & Nakagawa, H. (2011). Experimental Studies on Difficulty of Evacuation from Undergound Spaces under Inundated Situations Using Real Scale Models. *Journal of Japan Society of Civil Engineers*, 67, 12-27.

Bačová Mitková, V., & Halmová, D. (2014). Joint Modeling of Flood Peak Discharges, Volume and Duration: A Case Study of the Danube River in Bratislava. *Journal of Hydrology and Hydromechanics*, 62(3), 186-196.

Banks, J. C., Camp, J. V., & Abkowitz, M. D. (2014). Scale and Resolution Considerations in the Application of Hazus-MH 2.1 to Flood Risk Assessments. *Natural Hazards Review*, 16(3), 04014025.

Bao, Y., Tung, Y. K., & Hasfurther, V. R. (1987). Evaluation of Uncertainty in Flood Magnitude Estimator on Annual Expected Damage Costs of Hydraulic Structures. *Water Resources Research*, 23(11), 2023-2029.

Barker, K., & Haimes, Y. Y. (2009). Assessing Uncertainty in Extreme Events: Applications to Risk-Based Decision Making in Interdependent Infrastructure Sectors. *Reliability Engineering & System Safety*, 94(4), 819-829.

Barros, A. P., Duan, Y., Brun, J., & Medina Jr, M. A. (2013). Flood Nonstationarity in the Southeast and Mid-Atlantic Regions of the United States. *Journal of Hydrologic Engineering*, 19(10), 05014014.

Beard, L. R. (1960). Probability Estimates Based on Small Normal-Distribution Samples. *Journal of Geophysical Research*, 65(7), 2143-2148.

Beard, L. R. (1990). Discussion of "Expected Annual Damages and Uncertainties in Flood Frequency Estimation" by Nigel W. Arnell (January, 1989, Vol. 115, No. 1). *Journal of Water Resources Planning and Management*, 116(6), 847-850.

Beard, L. R. (1997). Estimating Flood Frequency and Average Annual Damage. *Journal of Water Resources Planning and Management*, 123(2), 84-88.

Bier, V. M., Haimes, Y. Y., Lambert, J. H., Matalas, N. C., & Zimmerman, R. (1999). A Survey of Approaches for Assessing and Managing the Risk of Extremes. *Risk analysis*, 19(1), 83-94.

Boes, D. C., Heo, J. H., & Salas, J. D. (1989). Regional Flood Quantile Estimation for a Weibull Model. *Water Resources Research*, 25(5), 979-990.

Boesch, D. F., Atkinson, L. P., Boicourt, W. C., Boon, J. D., Cahoon, D. R., Dalrymple, R. A., . . . Kopp, R. E. (2013). *Updating Maryland's Sea-Level Rise Projections*. Retrieved from http://www.umces.edu/sites/default/files/pdfs/SeaLevelRiseProjections.pdf

Boettle, M., Rybski, D., & Kropp, J. (2013). How Changing Sea Level Extremes and Protection Measures Alter Coastal Flood Damages. *Water Resources Research*, 49(3), 1199-1210.

Brakenridge, G. R. (2010). *Global Active Archive of Large Flood Events*. Dartmouth Flood Observatory, University of Colorado. Retrieved from http://floodobservatory.colorado.edu/Archives/index.html

Brunner, G. W. (2010). *HEC-RAS River Analysis System. Hydraulic Reference Manual*. Version 4.1. Retrieved from http://www.hec.usace.army.mil/software/hec-ras/documentation/HEC-RAS_4.1_Reference_Manual.pdf

Burkey, J. (2009). *Log-Pearson Flood Flow Frequency Using USGS 17B*. Retrieved from http://www.mathworks.com/matlabcentral/fileexchange/22628-log-pearson-flood-flow-frequency-using-usgs-17b

Carroll, S., Goonetilleke, A., Thomas, E., Hargreaves, M., Frost, R., & Dawes, L. (2006). Integrated Risk Framework for Onsite Wastewater Treatment Systems. *Environmental Management*, 38(2), 286-303.

Carson, R. T., Mitchell, R. C., Hanemann, W. M., Kopp, R. J., Presser, S., & Ruud, P. A. (1992). *A Contingent Valuation Study of Lost Passive Use Values Resulting from the Exxon Valdez Oil Spill*. Retrieved from http://www.evostc.state.ak.us/universal/documents/publications/economic/econ_passive.pdf

Committee of Countermeasures against Inundation Disasters in Underground Spaces (CCIDUS). (2002). *Guideline for Measures against Inundation of Underground Spaces*. Ministry of Land, Infrastructure, Transport and Tourism, Japan.

Chang, T. J. (1990). Effects of Drought on Streamflow Characteristics. *Journal of Irrigation and Drainage Engineering*, 116(3), 332-341.

Chen, Y., Liu, R., Barrett, D., Gao, L., Zhou, M., Renzullo, L., & Emelyanova, I. (2015). A Spatial Assessment Framework for Evaluating Flood Risk under Extreme Climates. *Science of The Total Environment*, 538, 512-523.

Choi, O., & Fisher, A. (2003). The Impacts of Socioeconomic Development and Climate Change on Severe Weather Catastrophe Losses: Mid-Atlantic Region (MAR) and the US. *Climatic Change*, 58(1-2), 149-170.

Chow, V. (1956). Hydrologic Studies of Floods in the United States. *International Association of Scientific Hydrology*, 42, 134-170.

Christian, J. T., & Baecher, G. B. (1999). Point-Estimate Method as Numerical Quadrature. *Journal of Geotechnical and Geoenvironmental Engineering*, 125(9), 779-786.

City of New York. (2016). *New York City's Wastewater Treatment System*. Retrieved from http://www.nyc.gov/html/dep/html/wastewater/wwsystem-plants.shtml

Clawson, M. (1959). *Method of Measuring the Demand for and Value of Outdoor Recreation*. Washington, D.C.: Resources for the future.

Climate Central. (2014). *11 Billion Gallons of Sandy Sewage Overflow*. Retrieved from http://www.climatecentral.org/news/11-billion-gallons-of-sewage-overflow-from-hurricane-sandy-15924

Coles, S., Bawa, J., Trenner, L., & Dorazio, P. (2001). *An Introduction to Statistical Modeling of Extreme Values*. London, UK: Springer.

Cook, A., & Merwade, V. (2009). Effect of Topographic Data, Geometric Configuration and Modeling Approach on Flood Inundation Mapping. *Journal of Hydrology*, 377(1), 131-142.

Copeland, C. (2005). *Hurricane-Damaged Drinking Water and Wastewater Facilities: Impacts, Needs, and Response*. (CRS: RS22285). Washington, D.C. : UNT Digital Library, Library of Congress, Congressional Research Service. Retrieved from http://digital.library.unt.edu/ark:/67531/metadc824633

Cox, L. A. (2008). What's Wrong with Risk Matrices? *Risk analysis*, 28(2), 497-512.

Crowther, K. G., Haimes, Y. Y., & Taub, G. (2007). Systemic Valuation of Strategic Preparedness through Application of the Inoperability Input-Output Model with Lessons Learned from Hurricane Katrina. *Risk Analysis*, 27(5), 1345-1364.

Cummings, C. A., Todhunter, P. E., & Rundquist, B. C. (2012). Using the Hazus-MH Flood Model to Evaluate Community Relocation as a Flood Mitigation Response to Terminal Lake Flooding: The Case of Minnewaukan, North Dakota, USA. *Applied Geography*, 32(2), 889-895.

Cunderlik, J. M., & Ouarda, T. B. M. J. (2006). Regional Flood-Duration–Frequency Modeling in the Changing Environment. *Journal of Hydrology*, 318(1–4), 276-291.

Davis, D., Faber, B. A., & Stedinger, J. R. (2008). USACE Experience in Implementing Risk Analysis for Flood Damage Reduction Projects. *Journal of Contemporary Water Research & Education*, 140(1), 3-14.

District of Columbia Water & Sewer Authority (DCWASA). (n.d.-a). *Hydraulic Profile*. Washington, D.C.: DCWASA.

DCWASA. (n.d.-b). *Multimedia Filtration Facilities Description, Operation and Controls.* Washington, D.C.: DCWASA.

DCWASA. (n.d.-c). *Nitrification-Denitrification Facilities Description, Operation and Controls.* Washington, D.C.: DCWASA.

DCWASA. (n.d.-d). *Primary Sedimentation Facilities Description, Operation and Controls*. Washington, D.C.: DCWASA.

DCWASA. (n.d.-e). *Secondary Treatment Facilities Description, Operation and Controls*. Washington, D.C.: DCWASA.

Department for Environment, Food & Rural Affairs (DEFRA). (2001). *National Appraisal of Assets at Risk from Flooding and Coastal Erosion, Including the Potential Impact of Climate Cange (Final Report)*. London, UK: DEFRA. Retrieved from http://randd.defra.gov.uk/Document.aspx?Document=FD2004_1033_TRP.pdf

DEFRA. (2005). *The Appraisal of Human-Related Intangible Impacts of Flooding*. (R&D Technical Report FD2005/TR). London, UK: Joint Defra / EA Flood and Coastal Erosion Risk Management R&D Programme. Retrieved from http://randd.defra.gov.uk/Document.aspx?Document=FD2005_1856_TSM.pdf

DEFRA. (2006). *Flood and Coastal Defence Appraisal Guidance. Economic Appraisal Supplementary Note to Operating Authorities - Climate Change Impacts*. London, UK: DEFRA. Retrieved from http://www.sdcg.org.uk/Climate-change-update.pdf

DEFRA. (2009). *Appraisal of Flood and Coastal Erosion Risk Management: A DEFRA Policy Statement*. London, UK: DEFRA. Retrieved from https://www.gov.uk/government/uploads/system/uploads/attachment_data/file/69419/pb13278-erosion-manage-090619.pdf

Dupuis, D. J. (2007). Using Copulas in Hydrology: Benefits, Cautions, and Issues. *Journal of Hydrologic Engineering*, 12(4), 381-393.

Dutta, D., Herath, S., & Musiake, K. (2003). A Mathematical Model for Flood Loss Estimation. *Journal of Hydrology*, 277(1–2), 24-49.

Eagleson, P. S. (1972). Dynamics of Flood Frequency. *Water Resources Research*, 8(4), 878-898.

Federal Emergency Management Agency (FEMA). (2002). *Guidelines and Specifications for Flood Hazard Mapping Partners*. Retrieved from http://www.fema.gov/media-library/assets/documents/13948

FEMA. (2009). *Multi-Hazard Loss Estimation Methodology Flood Model, Hazus-MH MR4 Technical Manual*. Washington, D.C.: Department of Homeland Security Emergency Preparedness and Response Directorate, FEMA Mitigation Division. Retrieved from https://www.fema.gov/media-library-data/20130726-1820-25045-8292/hzmh2_1_fl_tm.pdf

FEMA. (2010). *Flood Insurance Study-District of Columbia, Washington, D.C.* (Flood Insurance Study No. 110001V000A). Washington, D.C.: FEMA. Retrieved from https://www.ncpc.gov/DocumentDepot/Planning/flooding/DC_Flood_Insurance_Study_Pre-17th_Street_Levee.pdf

FEMA. (2013a). *Guidance for Estimating Percent Damage for Non-Residential Structures*. Retrieved from http://www.fema.gov/media-library-data/20130726-1735-25045-4710/sde_app_f_guidance_for_esimating_percent_damage_for_non_residential_structures.pdf

FEMA. (2013b). *Numerical Models Meeting the Minimum Requirements for the National Flood Insurance Program*. Retrieved from http://www.fema.gov/numerical-models-meeting-minimum-requirements-national-flood-insurance-program

FEMA. (2014). *Substantial Damage Estimator (SDE) User Manual and Workbook*. (FEMA P-784). Retrieved from http://www.fema.gov/media-library/assets/documents/18692

FEMA. (2015). *Flood Risk Database (FRD) Technical Reference*. Retrieved from http://www.fema.gov/media-library-data/1450470985498-1317835bcca5cd65a1595e2a3b465fa8/Flood_Risk_Database_Technical_Reference_Nov_2015.pdf

Feng, Y., & Brubaker, K. L. (2016). Sensitivity of Flood-Depth Frequency to Watershed-Runoff Change and Sea-Level Rise Using a One-Dimensional Hydraulic Model. *Journal of Hydrologic Engineering*, 21(8), 05016015.

Ferreira, L. V., & Stohlgren, T. J. (1999). Effects of River Level Fluctuation on Plant Species Richness, Diversity, and Distribution in a Floodplain Forest in Central Amazonia. *Oecologia*, 120(4), 582-587.

Fontanazza, C., Freni, G., & Notaro, V. (2012). Bayesian Inference Analysis of the Uncertainty Linked to the Evaluation of Potential Flood Damage in Urban Areas. *Water Science & Technology*, 66(8), 1669-1677.

Förster, S., Kuhlmann, B., Lindenschmidt, K. E., & Bronstert, A. (2008). Assessing Flood Risk for a Rural Detention Area. *Natural Hazards and Earth System Science*, 8(2), 311-322.

Fowler, H., Blenkinsop, S., & Tebaldi, C. (2007). Linking Climate Change Modelling to Impacts Studies: Recent Advances in Downscaling Techniques for Hydrological Modelling. *International Journal of Climatology*, 27(12), 1547-1578.

Genius, M., Manioudaki, M., Mokas, E., Pantagakis, E., Tampakakis, D., & Tsagarakis, K. (2005). Estimation of Willingness to Pay for Wastewater Treatment. *Water Science and Technology: Water Supply*, 5(6), 105-113.

Gilroy, K. L., & McCuen, R. H. (2012). A Nonstationary Flood Frequency Analysis Method to Adjust for Future Climate Change and Urbanization. *Journal of Hydrology*, 414, 40-48.

Goodell, C., & Brunner, G. (2014). *Breaking the HEC-RAS Code: A User's Guide to Automating HED-RAS*. Portland, Oregon: h2ls.

Goodwin, P., & Wright, G. (2007). *Decision Analysis for Management Judgment (3rd. Ed.)*. Chichester, UK: John Wiley & Sons.

Gormley, A., Pollard, S., Rocks, S., & Black, E. (2011). *Guidelines for Environmental Risk Assessment and Management. Green Leaves III*. Defra and the Collaborative Centre of Excellence in Understanding and Managing Natural and Environmental Risks, Cranfield University, Granfield, UK.

Gourley, J. J., Hong, Y., Flamig, Z. L., Arthur, A., Clark, R., Calianno, M., . . . Kirstetter, P. E. (2013). A Unified Flash Flood Database across the United States. *Bulletin of the American Meteorological Society*, 94(6), 799-805.

Green, P. E., & Srinivasan, V. (1978). Conjoint Analysis in Consumer Research: Issues and Outlook. *Journal of Consumer Research*, 5(2), 103-123.

Griffin, J. L., & Saxton, A. M. (1988). Response of Solid-Seeded Soybean to Flood Irrigation. II. Flood Duration. *Agronomy Journal*, 80(6), 885-888.

Guerrero-Salazar, P., & Yevjevich, V. (1975). *Analysis of Drought Characteristics by the Theory of Runs*. Hydrology Papers no. 80. Fort Collins, CO: Colorado State University.

Gumbel, E. J. (1941). The Return Period of Flood Flows. *The Annals of Mathematical Statistics*, 12(2), 163-190.

Gumbel, E. J. (1943). On the Plotting of Flood-Discharges. *Transactions American Geophysical Union*, 24(2), 699-719.

Gumbel, E. J., & Lieblein, J. (1954). *Statistical Theory of Extreme Values and Some Practical Applications: A Series of Lectures (Vol. 33)*. Washington, D.C.: US Government Printing Office.

Hall, J., & Solomatine, D. (2008). A Framework for Uncertainty Analysis in Flood Risk Management Decisions. *International Journal of River Basin Management*, 6(2), 85-98.

Hall, J. W., Lempert, R. J., Keller, K., Hackbarth, A., Mijere, C., & McInerney, D. J. (2012). Robust Climate Policies under Uncertainty: A Comparison of Robust Decision Making and Info-Gap Methods. *Risk Analysis*, 32(10), 1657-1672.

Hall, J. W., Meadowcroft, I. C., Sayers, P. B., & Bramley, M. E. (2003). Integrated Flood Risk Management in England and Wales. *Natural Hazards Review*, 4(3), 126-135.

Hansson, K., Larsson, A., Danielson, M., & Ekenberg, L. (2011). Coping with Complex Environmental and Societal Flood Risk Management Decisions: An Integrated Multi-Criteria Framework. *Sustainability*, 3(9), 1357-1380.

Hauptmanns, U. (2010). A Decision-Making Framework for Protecting Process Plants from Flooding Based on Fault Tree Analysis. *Reliability Engineering & System Safety*, 95(9), 970-980.

Hazen and Sawyer. (2012). *Emergency Response at Bay Park WWTP*. Retrieved from http://www.hazenandsawyer.com/news/emergency-response-at-bay-park-wwtp

Hensher, D., Shore, N., & Train, K. (2005). Households' Willingness to Pay for Water Service Attributes. *Environmental and Resource Economics*, 32(4), 509-531.

Hermanson, R. E., & Johnson, H. P. (1966). Generalized Flood-Frequency Relationships. *Iowa State College Journal of Science*, 41(3), 247-268.

Hewlett, J. D. (1982). *Principles of Forest Hydrology*. Athens, Georgia: University of Georgia Press.

Higgins, R. J., & Robinson, D. J. (1981). *An Economic Comparison of Different Flood Mitigation Strategies in Australia: A Case Study*. Canberra, Australia: Australian Water Resources Council, Australian Government Publishing Service.

Her Majesty's Treasury (HM Treasury). (2003). *The Green Book: Appraisal and Evaluation in Central Government*. London, UK: HM Treasury.

Hyndman, R. J., & Fan, Y. (1996). Sample Quantiles in Statistical Packages. *The American Statistician*, 50(4), 361-365.

Interagency Advisory Committee on Water Data [IACWD]. (1982). *Guidelines for Determining Flood Flow Frequency*. US Water Resources Council Bulletin (17B). Reston, VA: U.S. Department of Interior, Geological Survey, Office of Water Data Coordination. Retrieved from http://water.usgs.gov/osw/bulletin17b/dl_flow.pdf

Interstate Commission on the Potomac River Basin. (2013). *2010 Washington Metropolitan Area Water Supply Reliability Study. Part 2: Potential Impact of Climate Change*. Retrieved from http://www.potomacriver.org/publicationspdf/ICPRB13-07.pdf

Ishigaki, T., Onishi, Y., Asai, Y., Toda, K., & Shimada, H. (2008). Evacuation Criteria During Urban Flooding in Underground Space. In *Proceedings of 11th International Conference on Urban Drainage*, Edinburgh, Scotland, UK.

Jaffe, D. A., & Sanders, B. F. (2001). Engineered Levee Breaches for Flood Mitigation. *Journal of Hydraulic Engineering*, 127(6), 471-479.

Jam, D., & Singh, V. P. (1987). Estimating Parameters of EV1 Distribution for Flood Freqency Analysis. *Journal of the American Water Resources Association*, 23(1), 59-71.

Javelle, P., Ouarda, T. B., & Bobée, B. (2003). Spring Flood Analysis Using the Flood-Duration–Frequency Approach: Application to the Provinces of Quebec and Ontario, Canada. *Hydrological Processes*, 17(18), 3717-3736.

Javelle, P., Ouarda, T. B., Lang, M., Bobée, B., Galéa, G., & Grésillon, J. M. (2002). Development of Regional Flood-Duration–Frequency Curves Based on the Index-Flood Method. *Journal of Hydrology*, 258(1), 249-259.

Jiang, J., Wang, P., Lung, W. S., Guo, L., & Li, M. (2012). A GIS-Based Generic Real-Time Risk Assessment Framework and Decision Tools for Chemical Spills in the River Basin. *Journal of Hazardous Materials*, 227, 280-291.

Jonkman, S., Van Gelder, P., & Vrijling, J. (2003). An Overview of Quantitative Risk Measures for Loss of Life and Economic Damage. *Journal of Hazardous Materials*, 99(1), 1-30.

Jonkman, S. N. (2007). *Loss of Life Estimation in Flood Risk Assessment-Theory and Applications*. (Doctoral dissertation), Delft University of Technology, Delft, the Netherlands .

Jonkman, S. N., Bočkarjova, M., Kok, M., & Bernardini, P. (2008). Integrated Hydrodynamic and Economic Modelling of Flood Damage in the Netherlands. *Ecological Economics*, 66(1), 77-90.

Kamei, I. (1984). *Taifu Ni Tsuite, Tennsai Jinnsai Sumai No Bunnkashi*. Misawa, Japan: Misawa Homes Institute of Research and Development.

Karl, T. R., & Knight, R. W. (1998). Secular Trends of Precipitation Amount, Frequency, and Intensity in the United States. *Bulletin of the American Meteorological Society*, 79(2), 231-241.

Kelman, I. (2002). *Physical Flood Vulnerability of Residential Properties in Coastal, Eastern England*. (Doctoral dissertation), University of Cambridge, U.K. .

Kelman, I., & Spence, R. (2004). An Overview of Flood Actions on Buildings. *Engineering Geology*, 73(3), 297-309.

Kent, R., & Johnson, D. (2001). Influence of Flood Depth and Duration on Growth of Lowland Rice Weeds, Cote D'ivoire. *Crop Protection*, 20(8), 691-694.

Kent, S. (1964). Words of Estimative Probability. *Studies in Intelligence*, 8(4), 49-65.

Kenward, A., Yawitz, D., & Raja, U. (2013). *Sewage Overflows from Hurricane Sandy*. Princeton, NJ: Climate Central. Retrieved from http://www.climatecentral.org/pdfs/Sewage.pdf

Kharin, V. V., & Zwiers, F. W. (2005). Estimating Extremes in Transient Climate Change Simulations. *Journal of Climate*, 18(8), 1156-1173.

Knebl, M., Yang, Z. L., Hutchison, K., & Maidment, D. (2005). Regional Scale Flood Modeling Using NEXRAD Rainfall, GIS, and HEC-HMS/RAS: A Case Study for the San Antonio River Basin Summer 2002 Storm Event. *Journal of Environmental Management*, 75(4), 325-336.

Kortenhaus, A. (2007). *Breaching of Flood Defences and Resulting Failure Probability.* Paper presented at the Flood Risk Management Research − From extreme events to citizens involvement, Proceedings of European Symposium on Flood Risk Management Research. Dresden, Germany.

Kotz, S., & Van Dorp, J. R. (2004). *Beyond Beta: Other Continuous Families of Distributions with Bounded Support and Applications*. Singapore: World Scientific Press.

Kukharchyk, T. I. (2006). Flood Risk in Cities of Belarus: Specific Cases and Problems of Management. In *Flood Risk Management: Hazards, Vulnerability and Mitigation Measures*. Dordrecht, The Netherlands: Springer.

Kuklicke, C., & Demeritt, D. (2016). Adaptive and Risk-Based Approaches to Climate Change and the Management of Uncertainty and Institutional Risk: The Case of Future Flooding in England. *Global Environmental Change*, 37, 56-68.

LaRocca, S., & Guikema, S. (2011). *A Survey of Network Theoretic Approaches for Risk Analysis of Complex Infrastructure Systems*. Paper presented at the First International Symposium on Uncertainty Modeling and Analysis and Management (ICVRAM) and Fifth International Symposium on Uncertainty Modeling and Anaylsis (ISUMA), Hyattsville, Maryland.

Law, G. S. (2002). *Duration and Frequency Analysis of Lowland Flooding in Western Murfreesboro, Rutherford County, Tennessee, 1998-2000*. (Water-Resources Investigations Report 02-4266). Nashville, Tennessee: US Department of the Interior, US Geological Survey. Retrieved from https://pubs.er.usgs.gov/publication/wri024266

Leclerc, G., & Schaake, J. C. (1972). *Derivation of Hydrologic Frequency Curves*. Cambridge, Massachusetts: MIT Press.

Lekuthai, A., & Vongvisessomjai, S. (2001). Intangible Flood Damage Quantification. *Water Resources Management*, 15(5), 343-362.

Li, L., Wang, J., Leung, H., & Jiang, C. (2010). Assessment of Catastrophic Risk Using Bayesian Network Constructed from Domain Knowledge and Spatial Data. *Risk Analysis*, 30(7), 1157-1175.

Locke, E., Al-Omari, A., Kharkar, K., Passarelli, N., Tesfaye, A., & Kharkar, S. (2006). Dynamic Modeling of Wet Weather Operations at Blue Plains Advanced Wastewater Treatment Plant. In *Proceedings of the Water Environment Federation*, 2006(5), 6760-6781.

Lu, Y., Qin, X., & Xie, Y. (2016). An Integrated Statistical and Data-Driven Framework for Supporting Flood Risk Analysis under Climate Change. *Journal of Hydrology*, 533, 28-39.

Manning, M. R. (2006). The Treatment of Uncertainties in the Fourth IPCC Assessment Report. *Advances in Climate Change Research*, 2(1), 13-21.

Maryland Hydrology Panel. (2010). *Application of Hydrologic Methods in Maryland, Third Edition*. Retrieved from http://www.gishydro.eng.umd.edu/HydroPanel/hydrology_panel_report_3rd_edition_final.pdf

Mashriqui, H., Halgren, J., & Reed, S. (2014). 1D River Hydraulic Model for Operational Flood Forecasting in the Tidal Potomac: Evaluation for Freshwater, Tidal, and Wind-Driven Events. *Journal of Hydraulic Engineering*, 140(5), 04014005.

Mastrandrea, M. D., Field, C. B., Stocker, T. F., Edenhofer, O., Ebi, K. L., Frame, D. J., . . . Matschoss, P. R. (2010). *Guidance Note for Lead Authors of the IPCC Fifth Assessment Report on Consistent Treatment of Uncertainties*. Paper presented at the IPCC Cross-Working Group Meeting on Consistent Treatment of Uncertainties, Jasper Ridge, CA.

Matrosov, E. S., Woods, A. M., & Harou, J. J. (2013). Robust Decision Making and INFO-GAP Decision Theory for Water Resource System Planning. *Journal of Hydrology*, 494, 43-58.

McBean, E. A., Gorrie, J., Fortin, M., Ding, J., & Monlton, R. (1988). Adjustment Factors for Flood Damage Curves. *Journal of Water Resources Planning and Management*, 114(6), 635-646.

McCuen and Levy. (2000). Evaluation of Peak Discharge Transposition. *Journal of Hydrologic Engineering*, 5(3), 278-289.

Mearns, L., Gutowski, W., Jones, R., Leung, L., McGinnis, S., Nunes, A., & Qian, Y. (2007, updated 2014). *The North American Regional Climate Change Assessment Program Dataset*. Boulder, CO: National Center for Atmospheric Research Earth System Grid Data Portal. Retrieved from http://www.narccap.ucar.edu

Meehl, G. A., Arblaster, J. M., & Tebaldi, C. (2005). Understanding Future Patterns of Increased Precipitation Intensity in Climate Model Simulations. *Geophysical Research Letters*, 32(18).

Merz, B., Elmer, F., & Thieken, A. (2009). Significance of" High Probability/Low Damage" Versus" Low Probability/High Damage" Flood Events. *Natural Hazards and Earth System Science*, 9(3), 1033-1046.

Messner, F., & Meyer, V. (2006). *Flood Damage, Vulnerability and Risk Perception–Challenges for Flood Damage Research*. Dordrecht, The Netherlands: Springer.

Messner, F., Penning-Rowsell, E., Green, C., Meyer, V., Tunstall, S., & van der Veen, A. (2007). *Evaluating Flood Damages: Guidance and Recommendations on Principles and Methods*. Retrieved from http://repository.tudelft.nl/view/hydro/uuid:5602db10-274c-40da-953f-34475ded1755

Mishra, A. K., & Singh, V. P. (2011). Drought Modeling–a Review. *Journal of Hydrology*, 403(1), 157-175.

Moglen, G. E., & Rios Vidal, G. E. (2014). Climate Change and Storm Water Infrastructure in the Mid-Atlantic Region: Design Mismatch Coming? *Journal of Hydrologic Engineering*, 19(11), 04014026.

Müller, A. (2013). Flood Risks in a Dynamic Urban Agglomeration: A Conceptual and Methodological Assessment Framework. *Natural hazards*, 65(3), 1931-1950.

Najjar, R. G., Pyke, C. R., Adams, M. B., Breitburg, D., Hershner, C., Kemp, M., . . . Secor, D. (2010). Potential Climate-Change Impacts on the Chesapeake Bay. *Estuarine, Coastal and Shelf Science*, 86(1), 1-20.

Najjar, R. G., Walker, H. A., Anderson, P. J., Barron, E. J., Bord, R. J., Gibson, J. R., . . . O'Connor, R. E. (2000). The Potential Impacts of Climate Change on the Mid-Atlantic Coastal Region. *Climate Research*, 14(3), 219-233.

National Research Council, Committee to Assess NEXRAD Flash Flood Forecasting Capabilities at Sulphur Mountain. (2005). *Flash Flood Forecasting over Complex Terrain: With an Assessment of the Sulphur Mountian NEXRAD in Southern California*. Washington, D.C.: National Academies Press.

Neff, R., Chang, H., Knight, C. G., Najjar, R. G., Yarnal, B., & Walker, H. A. (2000). Impact of Climate Variation and Change on Mid-Atlantic Region Hydrology and Water Resources. *Climate Research*, 14(3), 207-218.

Nicholas, J., Holt, G. D., & Proverbs, D. (2001). Towards Standardising the Assessment of Flood Damaged Properties in the UK. *Structural Survey*, 19(4), 163-172.

Nirupama, N., Armenakis, C., & Montpetit, M. (2014). Is Flooding in Toronto a Concern? *Natural Hazards*, 72(2), 1259-1264.

National Oceanic and Atmospheric Administration (NOAA). (2012). *U.S. Estuary Bathymetric Data Sets*. Retrieved from http://estuarinebathymetry.noaa.gov

NOAA. (2013a). *National Hurricane Center: Storm Surge Overview*. Retrieved from http://www.nhc.noaa.gov/surge

NOAA. (2013b). *Vertical Datum Transformation*. Retrieved from http://vdatum.noaa.gov

NOAA. (2016a). *The Battery, NY - Station ID: 8518750*. Retrieved from https://tidesandcurrents.noaa.gov/stationhome.html?id=8518750

NOAA. (2016b). *Washington, D.C. - Station ID: 8594900*. Retrieved from http://tidesandcurrents.noaa.gov/stationhome.html?id=8594900

Notaro, V., Fontanazza, C., Freni, G., & La Loggia, G. (2014). Assessment of Modelling Structure and Data Availability Influence on Urban Flood Damage Modelling Uncertainty. *Procedia Engineering*, 89, 788-795.

National Weather Service (NWS). (2015). *National Weather Service Hydrologic Glossary*. Retrieved from http://w1.weather.gov/glossary/index.php?letter=f

NWS. (2016). N*ational Weather Service Hydrologic Information Center - Flood Loss Data*. Retrieved from http://www.nws.noaa.gov/hic

Oertel, M., & Schlenkhoff, A. (2008). *Flood Wave Propagation and Flooding of Underground Facilities*. Paper presented at the Proceedings of River Flow, Izmir, Turkey.

Palanca-Tan, R. (2015). Knowledge, Attitudes, and Willingness to Pay for Sewerage and Sanitation Services: A Contingent Valuation Survey in Metro Manila, Philippines. *Journal of Environmental Science and Management*, 18(2).

Pappenberger, F., Matgen, P., Beven, K. J., Henry, J. B., Pfister, L., & Fraipont, P. (2006). Influence of Uncertain Boundary Conditions and Model Structure on Flood Inundation Predictions. *Advances in Water Resources*, 29(10), 1430-1449.

Parker, D. J., Green, C. H., & Thompson, P. M. (1987). *Urban Flood Protection Benetits: A Project Appraisal Guide*. Aldershot, UK: Gower Technical Press.

Pearce, D. W., & Turner, R. K. (1990). *Economics of Natural Resources and the Environment*. Baltimore, Maryland: Johns Hopkins University Press.

Penning-Rowsell, E., Priest, S., Parker, D., Morris, J., Tunstall, S., Viavattene, C., . . . Owen, D. (2014). *Flood and Coastal Erosion Risk Management: A Manual for Economic Appraisal*. Oxon, UK: Routledge.

Penning-Rowsell, E. C., & Chatterton, J. B. (1977). *The Benefits of Flood Alleviation: A Manual of Assessment Techniques*. Farnborough, UK: Saxon House.

Penning-Rowsell, E. C., & Fordham, M. (1994). *Floods across Europe: Hazard Assessment, Modelling and Management*. Middlesex, UK: Middlesex University Press.

Penning-Rowsell, E. C., Green, C., Thompson, P. M., Coker, A., Tunstall, S., Richards, C., & Parker, D. (1992). *The Economics of Coastal Management: A Manual of Benefit Assessment Techniques*. London, UK: Belhaven Press.

Penning-Rowsell, E. C., & Wilson, T. (2003). *The Benefits of Flood and Coastal Defence: Techniques and Data for 2003*. Middlesex, UK: Middlesex University.

Perry, C. A. (2000). *Significant Floods in the United States During the 20th Century-USGS Measures a Century of Floods*. Retrieved from http://ks.water.usgs.gov/pubs/fact-sheets/fs.024-00.pdf

Pfurtscheller, C., & Schwarze, R. (2008). *Estimating the Costs of Emergency Services During Flood Events*. Paper presented at the Proceedings of the 4th International Symposium on Flood Defence, Toronto, Canada.

Pingel, N., & Watkins Jr, D. (2009). Multiple Flood Source Expected Annual Damage Computations. *Journal of Water Resources Planning and Management*, 136(3), 319-326.

Platt, R. H. (1995). *Flood Risk Management and the American River Basin: An Evaluation*. Washington D.C.: National Academies Press.

Rausand, M., & Høyland, A. (2004). *System Reliability Theory: Models, Statistical Methods, and Applications* (Vol. 396). Hoboken, NJ: John Wiley & Sons.

Remo, J. W., Pinter, N., & Mahgoub, M. (2015). Assessing Illinois's Flood Vulnerability Using Hazus-MH. *Natural Hazards*, 81(1), 1-23.

Rodriguez-Iturbe, I. (1969). Applications of the Theory of Runs to Hydrology. *Water Resources Research*, 5(6), 1422-1426.

Rosen, S. (1974). Hedonic Prices and Implicit Markets: Product Differentiation in Pure Competition. *The Journal of Political Economy*, 82(1), 34-55.

Rosenblueth, E. (1975). Point Estimates for Probability Moments. In *Proceedings of the National Academy of Sciences*, 72(10), 3812-3814.

Saint-Geours, N., Grelot, F., Bailly, J. S., & Lavergne, C. (2015). Ranking Sources of Uncertainty in Flood Damage Modelling: A Case Study on the Cost-Benefit Analysis of a Flood Mitigation Project in the Orb Delta, France. *Journal of Flood Risk Management*, 8(2), 161-176.

Sanders, D. A. (1997). Damage to Wastewater Treatment Facilities from Great Flood of 1993. *Journal of Environmental Engineering*, 123(1), 54-60.

Sauer, V. B., Thomas Jr, W. O., Stricker, V. A., & Wilson, K. V. (1983). *Flood Characteristics of Urban Watersheds in the United States*. Alexandria, Virginia. Retrieved from http://pubs.er.usgs.gov/publication/wsp2207

Scawthorn, C., Blais, N., Seligson, H., Tate, E., Mifflin, E., Thomas, W., . . . Jones, C. (2006). Hazus-MH Flood Loss Estimation Methodology. I: Overview and Flood Hazard Characterization. *Natural Hazards Review*, 7(2), 60-71.

Scawthorn, C., Flores, P., Blais, N., Seligson, H., Tate, E., Chang, S., . . . Jones, C. (2006). Hazus-Mh Flood Loss Estimation Methodology. II. Damage and Loss Assessment. *Natural Hazards Review*, 7(2), 72-81.

Schanze, J. (2006). *Flood Risk Management–a Basic Framework Flood Risk Management: Hazards, Vulnerability and Mitigation Measures*. Dordrecht, The Netherlands: Springer.

Schwirtz, M. (2012). *Sewage Flows after Storm Expose Flaws in System*. Retrieved from http://www.nytimes.com/2012/11/30/nyregion/sewage-flows-after-hurricane-sandy-exposing-flaws-in-system.html?pagewanted=all&_r=0

Scott, H., DeAngulo, J., Daniels, M., & Wood, L. (1989). Flood Duration Effects on Soybean Growth and Yield. *Agronomy Journal*, 81(4), 631-636.

Shao, W. (2010). Critical Rainfall Intensity for Safe Evacuation from Underground Spaces with Flood Prevention Measures. *Journal of Zhejiang University,* 11(9), 668-676.

Shiau, J., & Shen, H. (2001). Recurrence Analysis of Hydrologic Droughts of Differing Severity. *Journal of Water Resources Planning and Management*, 127(1), 30-40.

Smith, D. (1994). Flood Damage Estimation- a Review of Urban Stage-Damage Curves and Loss Functions. *Water SA*, 20(3), 231-238.

Smith, J. A. (1987). Estimating the Upper Tail of Flood Frequency Distributions. *Water Resources Research*, 23(8), 1657-1666.

Smith, K., & Ward, R. (1998). *Floods: Physical Processes and Human Impacts*. Chichester, New York: John Wiley and Sons Ltd.

Soetanto, R., & Proverbs, D. G. (2004). Impact of Flood Characteristics on Damage Caused to Uk Domestic Properties: The Perceptions of Building Surveyors. *Structural Survey*, 22(2), 95-104.

St. Mary's County Metropolitan Commission. (2012). *Wastewater Overflows Attributed to Hurricane Sandy*. Retrieved from http://smnewsnet.com/archives/31905

State of New Jersey Passaic Valley Sewerage Commission. (2013). *Superstorm Sandy Information*. Retrieved from http://www.nj.gov/pvsc/news/sandy

State of New Jersey Passaic Valley Sewerage Commission. (2014). *Anniversary of Superstorm Sandy*. Retrieved from http://www.nj.gov/pvsc/news/sandy

Stedinger, J. R. (1997). Expected Probability and Annual Damage Estimators. *Journal of Water Resources Planning and Management*, 123(2), 125-135.

Su, H. T., & Tung, Y. K. (2013). Incorporating Uncertainty of Distribution Parameters Due to Sampling Errors in Flood-Damage-Reduction Project Evaluation. *Water Resources Research*, 49(3), 1680-1692.

Suriya, S., & Mudgal, B. (2012). Impact of Urbanization on Flooding: The Thirusoolam Sub Watershed–a Case Study. *Journal of Hydrology*, 412, 210-219.

Takayama, T., Takara, K., Toda, K., Fujita, M., Mase, H., Tachikawa, Y., . . . Sayama, T. (2007). Research Works for Risk Assessment Technology Related to Flood in Urban Area. *Annuals of Disaster Prevention Research Institute, Kyoto University*, 49C, 39-53.

Tate, E., Muñoz, C., & Suchan, J. (2014). Uncertainty and Sensitivity Analysis of the Hazus-MH Flood Model. *Natural Hazards Review*, 16(3), 04014030.

Tawn, J. A. (1992). Estimating Probabilities of Extreme Sea-Levels. *Journal of the Royal Statistical Society*, Series C (Applied Statistics), 41(1), 77-93.

Ten Veldhuis, J., & Clemens, F. (2010). Flood Risk Modelling Based on Tangible and Intangible Urban Flood Damage Quantification. *Water Science and Technology*, 62(1), 189.

Thieken, A., Ackermann, V., Elmer, F., Kreibich, H., Kuhlmann, B., Kunert, U., . . . Piroth, K. (2008). *Methods for the Evaluation of Direct and Indirect Flood Losses*. Paper presented at the 4th International Symposium on Flood Defense: Managing Flood Risk, Reliability and Vulnerability. Toronto, Ontario, Canada.

Thorne, C. R., Evans, E. P., & Penning-Rowsell, E. C. (2007). *Future Flooding and Coastal Erosion Risks*. London, UK: Thomas Telford.

Trinh, T., Ishida, K., Fischer, I., Jang, S., Darama, Y., Nosacka, J., . . . Kavvas, M. (2016). New Methodology to Develop Future Flood Frequency under Changing Climate by Means of Physically Based Numerical Atmospheric-Hydrologic Modeling. *Journal of Hydrologic Engineering*, 21(4), 04016001.

Turner, R. K., Lorenzoni, I., Beaumont, N., Bateman, I. J., Langford, I. H., & McDonald, A. L. (1998). Coastal Management for Sustainable Development: Analysing Environmental and Socio-Economic Changes on the UK Coast. *Geographical Journal*, 164(3), 269-281.

U.S. Army Corps of Engineers Hydrologic Engineering Center (USACE HEC). (2014). *HEC-RAS 4.1.0* [Computer Software]. Retrieved from http://www.hec.usace.army.mil/software/hec-ras

U.S. Bureau of Reclamation (USBR), & U.S. Army Corps of Engineers (USACE). (2012). Probability of Failure of Mechanical or Electrical Systems on Dam Gates. In *Best Practices in Dam and Levee Safety Risk Analysis*. A Joint Publication by U.S. Department of Interior, Bureau of Reclamation, and U.S. Army Corps of Engineers. Retrieved from http://www.usbr.gov/ssle/damsafety/risk/BestPractices/Chapters/VII-4-20150504.pdf

United Nations. (2000). *Guidelines on Sustainable Flood Prevention*. Hague, the Netherlands Retrieved from http://www.unece.org/fileadmin/DAM/env/water/publications/documents/guidelinesfloode.pdf

US Departmen of Homeland Security. (2016). *Critical Infrastructure Sectors*. Retrieved from https://www.dhs.gov/critical-infrastructure-sectors

US Department of Agriculture Soil Conservation Service. (1970). *Floodwater Damage Estimates; Residential and Commercial Property*. (EWP Technical Guide No. 21 Supplement 1). Fort Worth, Texas.

USACE. (1992). *Guidelines for Risk and Uncertainty Analysis in Water Resources Planning, Vol. I, Principles with Technical Appendices* (Report 92-R-1). Fort Belvoir, VA. Retrieved from http://www.iwr.usace.army.mil/Portals/70/docs/iwrreports/92r1.pdf

USACE. (1993). *Engineering and Design - Hydrologic Frequency Analysis*. (Engineer Manual 1110-2-1415). Washington, D.C.. Retrieved from http://www.publications.usace.army.mil/Portals/76/Publications/EngineerManuals/EM_1110-2-1415.pdf

USACE. (1995). *Flood Proofing Regulations*. (Engineer Pamphlet 1165-2-314). Washington D.C.: Department of the Army, U.S. Army Corps of Engineers. Retrieved from http://www.publications.usace.army.mil/Portals/76/Publications/EngineerPamphlets/EP_1165-2-314.pdf

USACE. (1996). *Engineering and Design Risk - Based Analysis for Flood Damage Reduction Studies*. (EM 1110-2-1619). Washington, D.C.. Retrieved from http://www.publications.usace.army.mil/Portals/76/Publications/EngineerManuals/EM_1110-2-1619.pdf

USACE Hydrologic Engineering Center. (1989). *EAD Expected Annual Flood Damage Computation User's Manual*. (CPD-30). Davis, CA. Retrieved from http://www.hec.usace.army.mil/publications/ComputerProgramDocumentation/CPD-30.pdf

USACE Hydrologic Engineering Center. (2008). *HEC-FDA Flood Damage Reduction Analysis User's Manual, Version 1.2.4.* (CPD-72). Davis, CA. Retrieved from http://www.hec.usace.army.mil/software/hec-fda/documentation/CPD-72_V1.2.4.pdf

United States Geological Survey (USGS). (2013). *National Elevation Dataset*. Retrieved from http://ned.usgs.gov

USGS. (2016a). *USGS 01570500 Susquehanna River at Harrisburg, PA*. Retrieved from http://waterdata.usgs.gov/nwis/nwismap/?site_no=01570500&agency_cd=USGS

USGS. (2016b). *USGS 01583500 Western Run at Western Run, MD*. Retrieved from http://waterdata.usgs.gov/nwis/nwismap/?site_no=01583500&agency_cd=USGS

Veronesi, M., Chawla, F., Maurer, M., & Lienert, J. (2014). Climate Change and the Willingness to Pay to Reduce Ecological and Health Risks from Wastewater Flooding in Urban Centers and the Environment. *Ecological Economics*, 98, 1-10.

Wagenaar, D. (2012). *The Significance of Flood Duration for Flood Damage Assessment*. (Master thesis), Delft University of Technology, Delft, the Netherlands. Retrieved from http://www.citg.tudelft.nl/over-faculteit/afdelingen/watermanagement/secties/waterhuishouding/leerstoelen/waterbeheer/onderzoek/alle-projecten/afstudeeronderzoeken/afgeronde-afstudeeronderzoeken/000-wagenaar-dj/the-significance-of-flood-duration-for-flood-damage-assessment

Water Resources Council. (1983). *Economic and Environmental Principles and Guidelines for Water and Related Land Resources Implementation Studies*. Washington, D.C.: Water Resources Council. Retrieved from https://archive.org/details/CAT83790902

Williams, S. J. (2013). Sea-Level Rise Implications for Coastal Regions. *Journal of Coastal Research*, 63(1), 184-196.

Winsemius, H., Van Beek, L., Jongman, B., Ward, P., & Bouwman, A. (2013). A Framework for Global River Flood Risk Assessments. *Hydrology and Earth System Sciences*, 17(5), 1871-1892.

Yerramilli, S. (2012). A Hybrid Approach of Integrating HEC-RAS and GIS Towards the Identification and Assessment of Flood Risk Vulnerability in the City of Jackson, MS. *American Journal of Geographic Information System*, 1(1), 7-16.

Yevjevich, V. (1967). *An Objective Approach to Definitions and Investigations of Continental Hydrologic Droughts*. Fort Collins, Colorado: Colorado State University.

Yu, A. (2010). *Infrastructure Disruption and Interdependencies During Flood Events*. (Analyzing Infrastructures for Disaster-Resilient Communities Practitioner Report #5). Retrieved from http://www.chs.ubc.ca/dprc_koa/pdf_files/PR_No5_Flood%20Events.pdf

Yue, S. (2001). A Bivariate Gamma Distribution for Use in Multivariate Flood Frequency Analysis. *Hydrological Processes*, 15(6), 1033-1045.

Yue, S., Ouarda, T., Bobée, B., Legendre, P., & Bruneau, P. (1999). The Gumbel Mixed Model for Flood Frequency Analysis. *Journal of hydrology*, 226(1), 88-100.

Zhang, Y. (1982). Plotting Positions of Annual Flood Extremes Considering Extraordinary Values. *Water Resources Research*, 18(4), 859-864.

Zimmerman, R. (2004). *Decision-Making and the Vulnerability of Interdependent Critical Infrastructure*. Paper presented at the 2004 IEEE International Conference on Systems, Man and Cybernetics, Hague, the Netherlands.

Zio, E., & Sansavini, G. (2011). Component Criticality in Failure Cascade Processes of Network Systems. *Risk Analysis*, 31(8), 1196-1210.